DEPARTMENT OF ELECTRICAL AND COMPUTER ENGINEERING

DEVELOPMENT OF ROBUST AND EFFECTIVE COORDINATION METHODOLOGIES FOR POWER SYSTEMS

DOCTOR OF PHILOSOPHY DISSERTATION

LAZAROS ZACHARIA

2020

DEPARTMENT OF ELECTRICAL AND COMPUTER ENGINEERING

DEVELOPMENT OF ROBUST AND EFFECTIVE COORDINATION METHODOLOGIES FOR POWER SYSTEMS

LAZAROS ZACHARIA

A Dissertation Submitted to the University of Cyprus in Partial Fulfillment of the Requirements for the Degree of Doctor of Philosophy

February 2020

VALIDATION PAGE

Doctoral Candidate: Lazaros Zacharia

Doctoral Dissertation Title: Development of Robust and Effective Coordination Methodologies for Power Systems

The present Doctoral Dissertation was submitted in partial fulfillment of the requirements for the degree of Doctor of Philosophy at the ***Department of*** *Electrical and Computer Engineering and was approved on the 18th of February 2020 by the members of the* ***Examination Committee.***

Examination Committee:

Research Supervisor: _____

(Dr. Elias Kyriakides, Associate Professor)

Research Co-Supervisor: _____

(Dr. Marios Polycarpou, Professor)

Committee Member: _____

(Dr. Georgios Ellinas, Professor)

Committee Member: _____

(Dr. Ioannis Krikidis, Associate Professor)

Committee Member: _____

(Dr. Vladimir Terzija, Professor)

Committee Member: _____

(Dr. George Korres, Professor)

DECLARATION OF DOCTORAL CANDIDATE

The present doctoral dissertation was submitted in partial fulfillment of the requirements for the degree of Doctor of Philosophy of the University of Cyprus. It is a product of original work of my own, unless otherwise mentioned through references, notes, or any other statements.

…….. **[**Full name of Doctoral candidate]

…….. **[**Signature]

ΠΕΡΙΛΗΨΗ

Καθώς τα συστήματα ηλεκτρικής ισχύος προχωρούν προς την υλοποίηση των "ευφυών δικτύων", καινούριες προκλήσεις εμφανίζονται λόγω των μεγάλων αλλαγών που υπόκεινται τα δίκτυα αυτά. Μία από τις μεγαλύτερες προκλήσεις που καλούνται τα συστήματα ηλεκτροδότησης να αντιμετωπίσουν είναι η εμφάνιση διαταραχών μεταξύ περιοχών του δικτύου. Οι διαταραχές αυτές προκύπτουν ουσιαστικά από την αδύνατη διασύνδεση διαφορετικών περιοχών του συστήματος, όπου οι συμβατικές μέθοδοι ελέγχου αποτυγχάνουν στην εξ' ολοκλήρου απόσβεσή τους. Αυτό συμβαίνει κυρίως λόγω της ανεπαρκούς πληροφόρησης για την κατάσταση ολόκληρου του συστήματος και της χρήσης μόνο τοπικών σημάτων. Η ικανότητα παρατήρησης αυτών των διαταραχών κατέστη δυνατή μόνο μετά την εμφάνιση των Μετρητών Φασιθετών στα συστήματα ηλεκτρικής ισχύος. Οι συσκευές αυτές έχουν τη δυνατότητα παροχής συγχρονισμένων μετρήσεων σε σχεδόν πραγματικό χρόνο, συμβάλλοντας καθοριστικά στην υλοποίηση συστημάτων παρατήρησης και ελέγχου ευρείας περιοχής. Ο σκοπός του ελέγχου ευρείας περιοχής (ΕΕΠ) είναι να χρησιμοποιήσει με τέτοιο τρόπο τις συγχρονισμένες μετρήσεις, ώστε να εξαγάγει σήματα ανάδρασης με σκοπό την επιτυχή και πλήρης εξάλειψη όλων των διαταραχών μεταξύ των περιοχών. Ως εκ τούτου η ανάγκη για δημιουργία και χρήση ΕΕΠ υψηλής επίδοσης έχει γίνει εμφανής τα τελευταία χρόνια.

Παρόλα αυτά, το κοινό πρόβλημα το οποίο παρατηρείται σε υφιστάμενες μεθόδους σχεδιασμού ΕΕΠ, είναι η παράλειψη της δημιουργίας εύρωστων ελεγκτών οι οποίοι θα μπορούν να έχουν υψηλή επίδοση σε διάφορες συνθήκες που μπορούν να προκύψουν. Επίσης, αγνοείται σχεδόν παντελώς το γεγονός ότι το σύστημα δεν λειτουργεί σε ιδανικές συνθήκες, ότι νέα δυναμικά στοιχεία εμφανίζονται συνεχώς στο σύστημα, καθώς και το ότι υπάρχουν αβεβαιότητες στις παραμέτρους του συστήματος οι οποίες χρησιμοποιούνται από τον διαχειριστή του συστήματος. Ως εκ τούτου, η συγκεκριμένη διδακτορική διατριβή έχει ως πρωταρχικό στόχο την ανίχνευση και επιτυχή αντιμετώπιση των σημαντικών παραγόντων που μπορούν να επηρεάσουν την λειτουργία του ΕΕΠ. Η επίτευξη αυτού του στόχου κατέστη δυνατή με την δημιουργία ρεαλιστικών προσομοιώσεων οι οποίες είναι ιδιαίτερα αναλυτικές κατά την διάρκεια δυναμικών συνθήκων και παρέχουν ένα περιβάλλον κατάλληλο για δοκιμή της επίδοσης του ΕΕΠ. Στη συγκεκριμένη διδακτορική διατριβή, ο ΕΕΠ δοκιμάστηκε κάτω από διάφορες συνθήκες όπως σφάλματα στις μετρήσεις, καθυστέρηση και απόρριψη δεδομένων, ύπαρξη αβεβαιότητας στις αποθηκευμένες παραμέτρους των γραμμών και των γεννητριών του συστήματος, μη αναφορά τοπολογικών

αλλαγών του συστήματος και ύπαρξη δυναμικών φορτίων. Το αποτέλεσμα της έρευνας έδειξε ότι η λειτουργία του ΕΕΠ επηρεάζεται από την καθυστέρηση και απόρριψη δεδομένων, τη μη αναφορά τοπολογικών αλλαγών του συστήματος καθώς και από την ύπαρξη δυναμικών φορτίων στο σύστημα. Επιπλέον, η συνεχής εισδοχή Ανανεώσιμων Πηγών Ενέργειας (ΑΠΕ) στο δίκτυο αποτελεί έναν από τους πιο γνωστούς παράγοντες που μπορούν να επηρεάσουν την ευστάθεια του συστήματος και επομένως είναι ένα παράγοντας ο οποίος επίσης πρέπει να αντιμετωπιστεί. Η διδακτορική διατριβή αυτή παρουσιάζει μεθοδολογίες για την επιτυχή αντιμετώπιση όλων των θεμάτων. Συγκεκριμένα, για να αποφευχθεί η καθυστέρηση και η απόρριψη δεδομένων, έχουν υλοποιηθεί γρήγορες μέθοδοι γραμμικής πρόβλεψης οι οποίες διατηρούν υψηλή την ακρίβεια του ΕΕΠ ακόμα και σε μεγάλες καθυστερήσεις. Στην περίπτωση των ΑΠΕ, μια καινούρια μεθοδολογία ΕΕΠ ιεραρχικής διαβάθμισης έχει προταθεί σε αυτή την διατριβή, για τον επιτυχή συντονισμό όλων των γεννητριών και ΑΠΕ με σκοπό την πλήρης εξουδετέρωση όλων των διαταραχών. Η ύπαρξη άγνωστων τοπολογικών αλλαγών επιλύθηκε με την συνένωση της Παρατήρησης Ευρείας Περιοχής (ΠΕΠ) μαζί με τον ΕΕΠ η οποία υλοποιήθηκε μέσα σε προσομοιωτές πραγματικού χρόνου. Οι επιπτώσεις της ύπαρξης δυναμικών φορτίων, αντιμετωπίστηκαν μέσω της κατασκευής και χρήσης ΕΕΠ υψηλής επίδοσης. Τέλος, μειονεκτήματα της αρχικής μεθόδου που χρησιμοποιήθηκε έχουν εντοπιστεί και επιλυθεί κατάλληλα.

Ο δεύτερος στόχος της διδακτορικής διατριβής είναι η υλοποίηση προχωρημένων και καινοτόμων μεθόδων ΕΕΠ. Οι εν λόγω μέθοδοι κατασκευάστηκαν χρησιμοποιώντας ρεαλιστικές προσομοιώσεις πραγματικού χρόνου για μεγαλύτερη ακρίβεια καθώς και για δοκιμή σε σχεδόν πραγματικές συνθήκες. Στόχος των καινοτόμων μεθοδολογιών είναι ο σωστός και επιτυχής συντονισμός της λειτουργίας των τοπικών ελεγκτών όλων των γεννητριών. Πιο συγκεκριμένα, καινοτόμες μέθοδοι ΕΕΠ δημιουργήθηκαν με σκοπό τον καλύτερο έλεγχο του ρυθμιστή στροφών, του συστήματος διεγέρσεως και του σταθεροποιητή, ελέγχοντάς τους με τα κατάλληλα σήματα έτσι ώστε να μπορούν να αντιμετωπίσουν επιτυχώς όλες τις τοπικές διαταραχές αλλά και όλες τις διαταραχές μεταξύ των περιοχών του συστήματος. Η σύγκριση των προτεινόμενων μεθόδων με αντίστοιχες συμβατικές πραγματοποιήθηκε χρησιμοποιώντας την μέθοδο Prony. Επίσης, στα πλαίσια αυτής της διδακτορικής διατριβής, μια προχωρημένη μέθοδος για τον προσαρμοστικό έλεγχο των τοπικών ελεγκτών από τον ΕΕΠ έχει προταθεί. Η συνένωση όλων των καινοτόμων μεθόδων οδηγεί στην εμφάνιση ενός προχωρημένου ελεγκτή ευρείας περιοχής ο οποίος παρέχει υψηλή επίδοση κυρίως για την εξάλειψη όλων των διαταραχών μεταξύ περιοχών, ενισχύοντας έτσι σημαντικά την ευστάθεια του συστήματος ηλεκτρικής ισχύος ακόμα και σε ακραίες συνθήκες.

ABSTRACT

Inter-area oscillations have become one of the major challenges that modern power systems have to confront, since their appearance is increasing due to the vast changes and constant expansion of the power systems. The appearance of inter-area oscillations creates many issues such as the degradation of the power quality, the limitation of the transmission system capacity and in several occasions, it can even lead the system to instability. Typical local controllers utilized for damping any undesirable oscillations, fail to compensate them due to the lack of global observability. The utilization of Phasor Measurement Units (PMUs) into the power systems and the provision of synchronized measurements has made possible the observation of inter-area oscillations. Wide Area Control (WAC) aims to utilize effectively the near real-time information provided by the PMUs in order to provide feedback control and coordination signals to the system, having as an objective the compensation of all the inter-area oscillations along with the enhancement of the system's damping performance. Therefore, the necessity for the successful development of highly effective wide area controllers is becoming more apparent recently.

However, an aspect which is commonly disregarded during the WAC design phase is that the robustness of the wide area controller has to be ensured and must not be compromised under any conditions. In addition to this, the simulated conditions, usually utilized for the evaluation of the WAC performance, do not consider that the system is not ideal, it almost never operates in steady-state conditions, new dynamic components are making their appearance into the grid and that there are uncertainties considering known parameters of the system. Therefore, the first objective of this Ph.D. dissertation is to identify the most crucial factors which can affect the WAC operation and then propose methods to mitigate their effect, having as a goal to obtain a highly robust wide area controller. The former was made possible by developing realistic simulation environments (especially when dynamic conditions take place), suitable for testing WAC methodologies. The performance of the wide area controller was tested under the presence of measurement errors (steady-state and dynamic), data delays/dropout, system parameter uncertainties (transmission line and generator data), unreported topology changes and dynamic loads. The investigation revealed that the WAC performance is mainly affected from the data delays/dropout, the unreported topology changes and the presence of dynamic loads. Apart from these, a widely known reason for the degradation of the system stability is the increasing penetration of the Renewable Energy Sources (RESs), since they reduce the system's inertia and change its

dynamic characteristics. This Ph.D. dissertation proposes methods for the compensation of all the identified threads. Considering the data delays/dropout, fast model-free linear predictors are developed, which improve considerably the damping performance of the system even at the presence of severe delays. For the case of the renewables, a novel wide area controller is introduced which is able to utilize and coordinate appropriately both synchronous generators and RESs, enhancing that way the damping performance of the system, even under a high penetration of renewables. In order to mitigate the effect of the unreported topology changes, a combination of Wide Area Monitoring (WAM) and WAC schemes is developed in a real-time simulation environment, while the impact of the dynamic loads is addressed by implementing high performance coordination methods. Apart from the identified threats, drawbacks of the conventional controller are addressed as well in order to enhance significantly its robustness.

The second objective of this Ph.D. dissertation is the development of a highly effective wide area controller, by proposing novel coordination techniques. These methodologies are implemented and tested in real-time conditions (through a real-time simulator) which in combination with the aforementioned realistic simulation environments can result into the most suitable testbed for testing and validating WAC methods. Therefore, advanced schemes are proposed for the proper coordination of the synchronous generator local controllers, which are evaluated by comparing their performance to conventional methods through Prony analysis. More specifically, novel techniques are developed for enhancing the operation of the exciter, the governor and power system stabilizer (PSS). It should be noted that for the case of the governor and PSS coordination, a methodology is implemented which can be used either in coordinating all the governors of the system or in coordinating simultaneously both the governor and PSS of each generator through a common WAC signal. Furthermore, an adaptive tuning method for regulating adaptively the level of the WAC contribution to all the local controllers is also developed and applied to the novel coordination techniques in order to enhance even more their performance. The combination of all the advanced methodologies along with the application of the adaptive tuning method result to the appearance of an advanced wide area controller, which has high performance in damping effectively all the local and inter-area oscillations even under extreme conditions (i.e. high penetration of dynamic loads). The integration of the advanced wide area controller with the WAM application is realized and evaluated in almost actual conditions, through the utilization of a novel laboratory setup.

ACKNOWLEDGMENTS

This Ph.D. dissertation is dedicated to the memory of my supervisor Dr. Elias Kyriakides. He truly was a great mentor and an exceptional human being. It has been a privilege to work with such an extraordinary researcher and a unique individual. May he rest in peace.

This research project was performed under the supervision of Dr. Elias Kyriakides, Associate Professor at the Department of Electrical and Computer Engineering of the University of Cyprus. First and foremost, I would like to express my most profound gratefulness and endless appreciation to my advisor, Prof. Kyriakides, for his professional and patient guidance with his open-mindedness and unparalleled kindness during the Ph.D. project period. His kind support and tremendous help, as well as his insightful comments and ideas and his enthusiasm about research were essential for overcoming any obstacle and for achieving the goals during this Ph.D. project. It was a great honor for me to work with Prof. Kyriakides and the encouragement that he gave me will be of great supportiveness for my career and throughout my whole life. His unique character will always be a source of inspiration and guidance.

Furthermore, I am thankful to my co-advisor Prof. Marios Polycarpou for all his unconditional support and unparalleled professionalism, especially after the sudden loss of Prof. Elias Kyriakides. I would also like to thank Prof. Georgios Ellinas for his participation in the committee and for all his time in organizing the committee.

Special thanks to Prof. Ioannis Krikidis, Prof. Vladimir Terzija and Prof. George Korres for their participation in the committee. The time and effort that they spent to review the dissertation is really appreciated, while their comments have been really helpful for improving the quality of this dissertation.

I would like to express my sincere thanks to all my colleagues at the KIOS Research Center for the lovely environment and the endless friendship. A special thanks to all the team members of Dr. Elias Kyriakides and especially to Dr. Markos Asprou and Dr. Lenos Hadjidemetriou, for the very effective collaboration and the sharing of research experience during all these years.

Furthermore, I want to express the most important and the sincerest gratitude to my parents for their exceptional and unconditional love, their constant support throughout my life and for believing in me. Many thanks to my beloved sisters and childhood friends for their love and support. Finally, I would like to express my heartfelt gratitude to my beloved

fiancée for being always there for me, for the understanding, the unconditional love and her constant support through my studies.

Lazaros Zacharia

TABLE OF CONTENTS

LIST OF TABLES

LIST OF FIGURES

CHAPTER 1
INTRODUCTION

Power systems continually increase in size and complexity due to various reasons. The main drivers responsible for these continuous changes are the growing demand, the expansion in previously unserved regions, the deregulation of the energy market, the integration of Renewable Energy Sources (RESs), and the interconnection of power systems between different areas [1].

To support all these new features, along with satisfying the environmental concerns, the concept of smart grid has emerged. The smart grid concept aims at the development of an intelligent power system that is expected to be characterized by high reliability and stability. However, due to all the aforementioned vast changes that the power system is currently experiencing, new challenges have appeared which can lead to undesirable disturbances and even threaten the system's stability.

1.1 Motivation and objectives

One of the major challenges that the power system has to confront is the appearance of inter-area oscillations in the power system. Inter-area oscillations along with the local oscillations represent the two electromechanical oscillations which can occur in the power system. In contrast to the local modes which tend to be in a higher frequency range (1-2 Hz due to large inertia of generators), inter-area modes are characterized by low frequencies (0.1-1 Hz) [2]. Inter-area oscillations are typically encountered in large power systems, where there is a power exchange between different areas (groups of generators) via long distance transmission lines (weak tie-lines) and they occur when one group of generators starts to swing against the generators of another group following a disturbance [3]. Especially in the cases where there is a large amount of power transfer between the areas through weak tie-lines, the inter-area oscillations can be initiated even by a small disturbance occurring anywhere in the interconnected systems [4].

Ignoring the existence of these oscillations and leaving them uncompensated in the power system can be a very dangerous practice since they add stress to the equipment, they

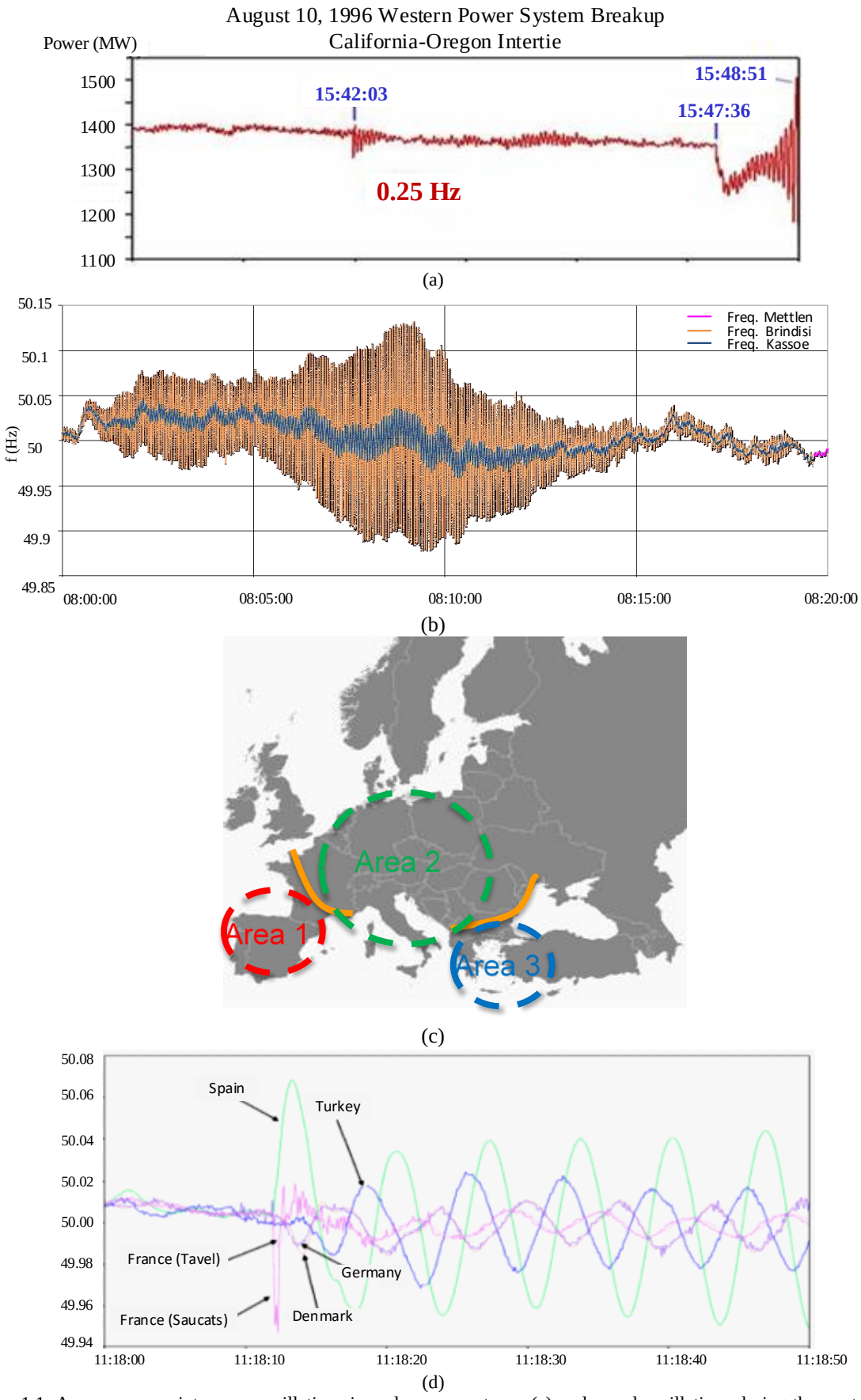

Fig. 1.1. Appearance on inter-area oscillations in real power systems: (a) undamped oscillations during the western North American Power System breakup of 1996, (b) frequency oscillations along the North-South axis of Continental Europe power system on 19th February 2011, (c) separation of the Continental Europe power system into three coherent groups and (d) representative frequency oscillations of each group after the line tripping on 1st December 2016.

degrade the power quality, they can limit the transmission system's capacity and they can even deteriorate the power system's stability [4], [5], [6]. The latter was actually the reason that the well-known breakup and blackout event occurred in the western North American Power System on August 10, 1996 (Fig. 1.1(a)). More specifically, the appearance of undamped oscillations has let to the breakup of the system into four islands resulting that way to the loss of 30,390 MW of load affecting 7.49 million customers and ending up to an estimated cost to the economy of at least 2 billion dollars [7]. More recent incidents of inter-area oscillations are analyzed extensively in the reports of ENTSO-E (European Network of Transmission System Operators for Electricity) [8], [9]. The first one occurred on 19th February 2011 and reappeared almost in the same form on 24th February 2011. More specifically, sudden inter-area oscillations have appeared within the Continental Europe (Fig. 1.1 (b)), without the occurrence of any known disturbance or forced outages beforehand. The ENTSO-E has correlated this event with changes of the generation pattern (due to the change of the hour) and with the very low total load of the system at that time [8]. A second and more serious inter-area oscillation incident was recently reported by the ENTSO-E in 2017. On 1st December 2016, a line connecting the French with the Spanish system had opened unexpectedly, triggering that way an oscillatory event in the Continental Europe electricity system. This has led to the separation of the system into three areas (Fig. 1.1(c)) where Area 1 was oscillating almost in phase with Area 3 and in anti-phase with Area 2. Note that Fig. 1.1(d) presents the frequency oscillation of representative countries from the three areas during the oscillatory event.

The traditional way to damp any oscillation occurring in the power system is to utilize either the generators' local controllers (such as Power System Stabilizers (PSSs), exciters, governors, etc.) or any power electronic converter based Flexible AC Transmission System (FACTS) device which might exist in the grid [10], [11]. Although these local controllers can be very successful in damping effectively all the local oscillations [12], they cannot ensure the complete compensation of the inter-area oscillations, mainly due to their lack of global observation [13]. The drawback of such a decentralized architecture is that each local controller tries to damp the local oscillations based only on local information, ignoring the operation of the other local controllers [10]. For this reason even advanced controllers such as the PSSs and FACTSs fail to damp effectively all the inter-area oscillations, since these oscillations are not always controllable and/or observable through local signals [14]. This happens mainly due to the linearization-based design of the PSSs and FACTSs, which ignores important dynamics that are directly connected with the inter-area

oscillations [4]. In addition, as it was pointed out in the ENTSO-E report [8], a drastic change in the system can result to a change of the modes, which in turn makes well-tuned PSS and FACTS controllers unable to sustain satisfactory performances. Therefore, the lack of global information and the absence of a common system objective are the main reasons for the inability of widely-used local controllers to damp effectively all the inter-area oscillations [10].

Due to the abovementioned issues, the necessity to develop new practices and methodologies, which will be able to firstly detect and then to compensate the inter-area oscillations, has emerged during the last few years [15]. The detection of the inter-area modes was not possible, until the advent of the synchronized measurement technology [16]. More specifically, the deployment of Phasor Measurement Units (PMUs) in the transmission level and their capability in providing synchronized, quasi real-time measurements from remote locations has made the observation of inter-area modes achievable. In addition, the widespread deployment of PMUs in power systems has laid the foundations for the development of Wide Area Monitoring and Control (WAMC) applications. Wide Area Monitoring (WAM) is the near real-time monitoring of the power system operating condition based on the PMU measurements and the state estimator. The exploitation of the synchronized measurements in order to provide feedback control and coordination to the system, with the aim of compensating all the inter-area modes, has led to the introduction of the Wide Area Control (WAC) concept [17]. The important advantage gained by utilizing a wide area controller into the power system is that it establishes a common system objective and a correlation among the independent local controllers [4]. It should be noted here that the integration of WAM and WAC schemes to the existing supervisory control and data acquisition (SCADA) system poses a lot of challenges. For instance, the receiving of PMU measurement through the SCADA system should be ensured by activating the appropriate protocols (i.e. IEEE C37.118). It is worth mentioning that new SCADA systems support the receiving and processing of synchronized measurements, therefore the integration of WAMC schemes becomes much easier.

Although WAC has the potential to improve considerably the damping of inter-area oscillations and the overall stability of the system, its performance might be deteriorated due to various factors which take place in the system. The main issue that arises is that although different successful WAC methodologies have been proposed for compensating the inter-area oscillations, their vast majority either assumes ideal conditions in the power system or they consider the occurrence of typical (and sometimes not realistic) communication delays

[18], [19]. On top of that, an infinitesimally small portion of the available WAC methodologies, have been actually tested and evaluated in real-time conditions [20]. This has as a result to obtain methodologies which perform very well in offline simulations, but in reality they may deteriorate the damping capability of the power system (instead of improving it) and can even compromise the security of the entire system. Thus, in reports (such as in [21]) where the unsolved issues of synchrophasor applications (i.e. WAC) are collected, it is pointed out that the robustness to data quality issues (e.g. data accuracy/availability/latency) of many of these applications is yet to be determined and it worths to be investigated thoroughly. In addition to all these, it is generally known, that the system is almost always operating in dynamic conditions. During dynamic conditions, some system parameters (e.g., measurement errors) are completely different from the steady-state ones and these changes are completely disregarded by the other studies. Therefore, there is a need to develop accurate simulations for testing any proposed methodology under real-time and realistic conditions, especially during dynamic events.

Another motivation of this thesis, which is one of the main drivers responsible for the vast changes that the power system is currently experiencing, is the increasing penetration of renewables. Their growing numbers may deteriorate the stability of the entire grid mainly due to the reduction of the system's inertia (e.g., displacement of synchronous generators) and the change in the system's dynamic characteristics [22]. More specifically, the displacement of synchronous generators creates two issues: 1) machines which are equipped with PSSs are left out, reducing that way the damping performance of the system, and 2) the system electromechanical modes are affected due to the displacement, resulting that way to the insufficient performance of the remaining PSSs and FACTSs since they are tuned to be valid only for a certain range around a pre-specified operating point [4]. Even though this challenge becomes more and more visible as the power system transits into the smart grid concept, the majority of the available WAC design methodologies do not take into account the effect of the installed RESs on the performance of the wide area controller.

Concluding, realistic simulation environments, which consider also the penetration of new energy sources in the power system, are important components for obtaining a robust wide area controller. Their accurate representation is required specifically when dynamic conditions take place, where the WAC contribution is essential. Towards the WAC robustification, it is therefore necessary to identify firstly all the potential threats which can affect the operation of the wide area controller (and can even lead the system to instability), and then to propose/develop methods for their compensation. This task must be

accomplished while keeping always in mind that the wide area controller has to ensure high performance in damping both local and inter-area oscillations at all times. Until now, data delays/dropouts are the most known reasons responsible for the degradation of the WAC damping capability [18]. However, under realistic conditions, other factors can be identified to affect the wide area controller's performance resulting that way to the failure of compensation methods which are proposed to deal only with the impact of the data delays and the elimination of the inter-area oscillations. This happens mainly because these methods are developed under the consideration of ideal conditions.

Summarizing, the main objectives of this Ph.D. dissertation are:

- to identify all the factors which can affect the performance of the wide area controller through the development and utilization of realistic simulation environments,
- to implement robust WAC schemes by proposing methods for compensating effectively all the identified threats and,
- to advance the wide area controller by improving its performance with regards to the damping of local and inter-area oscillations.

The fulfilment of the main objectives of this Ph.D. dissertation can increase substantially the robustness of the wide area controller, can enhance the damping capability of the power system (improving also the small signal stability), and can allow the increased penetration of renewables without compromising the system's stability.

1.2 Contribution of this work

The power system of the future has to be characterized by high reliability and stability, in order to be able to cope with the new challenges. WAC is the key application which can reinforce the system and compensate major threats to its stability, such as the appearance of inter-area oscillations. However, up until now the wide area controller's robustness to various conditions which can take place is not properly considered during its design and testing phase (apart from the data delays) and thus it is a relatively unknown and unexplored area, preventing that way its widespread utilization. For the development of a robust wide area controller, it is essential to identify firstly all the factors that can impact negatively its performance. For this reason, it is absolutely necessary to acquire and consider

realistic simulation environments which will have accurate representation of the power system behavior especially during transient conditions, where the WAC contribution is essential. The robustness can then be enhanced by implementing methods to compensate all the identified factors that can affect the operation of the wide area controller.

For advancing the WAC performance, novel methodologies need to be developed in order to derive suitable control signals for the proper coordination of all the local controllers of the system. The aim is to increase the local controllers' performance in damping effectively all the local and inter-area oscillations, by overcoming their lack of global observability, resulting to the operation of the grid which has a common system objective. It is important to note here that the simultaneous compensation of both local and inter-area oscillations must be considered, as the mitigation of only one of the two can impact negatively the other. The structure of the proposed scheme should be hierarchical, where the local controllers are located at the primary level and the WAC exists at the secondary level. This structure is desirable in order to have redundancy at the event of losing the higher level, by ensuring minimum damping performance through the controllers of the lower level.

The main objective of this Ph.D. dissertation is the development of a robust and highly effective wide area controller, by mitigating all its weaknesses and by proposing novel coordination techniques. This thesis has resulted to significant contributions to the field of WAC applications, which are briefly analyzed below:

- the implementation of realistic and accurate simulation environment suitable for testing WAC methodologies [23] (as well as other synchrophasor applications), which are developed according to available Standards and published studies as presented in Chapter 3,

- the investigation and identification of all the factors (such as realistic measurement errors, data delays/dropout, dynamic loads, etc.) that can affect the WAC performance [23], [24] as presented in Chapter 5,

- the proposition of two model-free and fast linear predictors for compensating the data delays/dropouts of the PMU measurements [23], [25] based on autocorrelation linear predictive coding as shown in Chapter 6,

- the development of two novel methodologies for addressing the high penetration of renewables. The first method considers a cooperation between the WAC and

RESs, by making the synchronous generators “aware” of the dynamic operation of the RES and by utilizing the available reactive power of the renewables for damping any local oscillations [26]. The second methodology advances the first one, in order to make the generators “aware” of the RES oscillations and vice versa, the RESs “aware” of the generator oscillations, through WAC signals [27]. These methodologies are proposed in Chapter 7,

- the proposition of methods to overcome the shortcomings of the wide area controller in order to enhance its robustness and reduce its measurement dependency [23], [28] as presented in Chapter 8,

- the development of two novel and advanced methodologies for enhancing the WAC damping performance through the proper coordination of the synchronous generator local controllers (exciter, governor and PSS) [28] as presented in Chapter 8,

- the integration and validation of WAM and WAC applications in real-time conditions as proposed in Chapter 8,

- the implementation of a novel laboratory setup for testing WAMC systems in almost actual conditions, through the use of a realistic real-time Hardware-In-the-Loop (HIL) configuration as shown in Chapter 8.

1.3 Dissertation outline

The work presented in this Ph.D. dissertation consists of nine chapters. Chapters 3-8 describe in detail all the contributions of this thesis. The remainder of this Ph.D. dissertation is as follows.

Chapter 2 discusses the state-of-the-art of all the subjects presented in this thesis as well as all the advancements that differentiate this Ph.D. dissertation from other relevant works.

The procedure to obtain analytical and realistic simulation environments for testing WAC methodologies is presented in Chapter 3. These simulation models are necessary for identifying all the threats which can affect the WAC performance. More specifically, the implementation of realistic conditions is achieved by considering available standards and published studies. An emphasis in this chapter is given to simulate as accurate as possible

the power system dynamic conditions, which are the most crucial part for the wide area controller.

Chapter 4 presents the conventional wide area controller along with the reasons for adopting this controller. In addition, all the disadvantages of the adopted method are analyzed in detail, in order to compensate them in the next chapters along with all the identified factors of Chapter 5. The overall objective is to advance the conventional wide area controller to be enhanced in terms of robustness and effectiveness. Finally, the mathematical background of the Prony analysis is presented, which is considered in this thesis as an evaluation method of the WAC performance.

An investigation for identifying the factors which can affect the damping capability of the wide area controller is shown in Chapter 5. Here the factors under consideration are presented, simulated and examined. Actually, these factors represent the conditions which can commonly occur any time in a power system and can compromise the WAC operation. More specifically, this chapter considers: the measurement errors (steady-state and dynamic), the data delays/dropout, the system parameter uncertainties, the unreported topology changes, and the existence of dynamic loads. The results of this investigation highlight the weaknesses of the wide area controller and reveal the areas where research must concentrate on in order to overcome those weaknesses.

The development of a methodology and its advancement for compensating effectively the data delays/dropouts are proposed in Chapter 6. Both methodologies are based on the Autocorrelation Linear Predictive Coding (LPC) and the aim here is to obtain model-free, faster and less complex predictors, overcoming in this way the drawbacks of conventional predictors (e.g. accuracy, processing time).

Chapter 7 presents the implementation of two methodologies for addressing the impact of the high penetration of renewables on the system's stability, through the use of a wide area controller. The first method proposes a cooperation scheme of the WAC with the RESs. This became feasible by making the synchronous generators "aware" of the dynamic operation of the RESs through the WAC signals. From the renewables' side, their controller is modified to utilize properly their available reactive power in order to damp out any local oscillations. The second methodology proposes the development of a hierarchical WAC scheme that coordinates all the synchronous generators and renewables of the system in order to improve considerably the dynamic stability of the system even under high

penetration levels of renewables. Although the second methodology advances the first one, the two methods have a different approach since the former does not consider the renewables to be coordinated by the wide area controller, while the latter integrates the RESs into the WAC scheme.

Chapter 8 proposes methods to overcome the disadvantages of the conventional wide area controller of Chapter 4, as well as novel methodologies to advance its performance. The latter aims to develop new WAC signals for the effective coordination of the synchronous generator's local controllers such as the exciter, the governor and PSSs. In addition, it presents the WAM and WAC integration in a common framework and their evaluation in real-time and realistic conditions. The implementation of a novel laboratory setup is also illustrated, where actual equipment and a real-time simulator are connected in a Hardware-In-the-Loop configuration, resulting to the development of a testbed suitable for testing and evaluating WAMC systems.

Finally, Chapter 9 concludes this Ph.D. dissertation, where the main contributions, the impact, and the future work are presented.

CHAPTER 2
LITERATURE REVIEW

This chapter presents a literature overview regarding the existing work on WAC design methodologies and on the components/factors which will be examined later on to identify their impact on the wide area controller performance.

2.1 Wide Area Control

2.1.1 Wide Area Control structure

The rapid deployment of wide-area measurements in the power system, led to the introduction and implementation of several design methods for the development of wide area controllers. Various methodologies and WAC structures have been proposed until now, for ensuring the effective damping of the inter-area oscillations and for enhancing the small-signal stability. The control structures can be classified into quasi-decentralized, centralized and hierarchical control architectures [29]. These are proposed with the aim to update the current decentralized control architecture where local controllers (which utilize only local information) are considered. Quasi-decentralized structure refers to the case where the local controllers receive some global information only regarding the state of the power system, while the majority of the data are collected and processed locally [30]. The disadvantage of this control structure is that it cannot ensure the complete compensation of all the inter-area oscillations due to its limited global information. The centralized control scheme consists of only one central controller (e.g., located in the control center) which utilizes global measurements in order to derive direct control inputs for all the active parts of the power system (such as generators and RES). In this way, this control structure bypasses and cancels out the operation of all the local controllers (such as the PSSs) of the power system [31]. The major drawback here is that this control scheme is highly depended on the communication infrastructure and any failure or delay can have catastrophic consequences on the operation of the power system. Hierarchical control refers to a multilevel control structure, where controllers of a higher level coordinate the controllers in the lower level and so on [32], [33]. This is the most desirable architecture since it utilizes the global information in order to damp effectively all the inter-area oscillations and at the event of losing a higher level, the system can still operate by utilizing the controllers of the lower level [34].

In this Ph.D. dissertation, a two-level hierarchical control structure ([32]) has been adopted and advanced. At the primary level, the current decentralized control architecture exists, which comprises by all the local controllers (e.g., PSSs, FACTSs, exciters, governors) of the power system. The secondary level considers a wide area controller, which aims to utilize the available wide area measurements for the development of suitable coordination signals in order to enhance the performance of the system's local controllers and compensate effectively all the inter-area oscillations. These control signals intend to overcome the shortcomings of the local controllers and more specifically their lack of global observability and to dominate the control whenever the system security is threatened. The main benefit of having WAC signals in the power system is the effective and simultaneous compensation of the system's local and inter-area oscillations. Note that at the event of a failure of the communication infrastructure or unavailability of the wide area controller, the local controllers' operation will ensure minimum damping performance and preserve the stability of the system.

2.1.2 Wide Area Control design

Apart from the classification of the proposed methodologies according to the adopted control structure (quasi-decentralized, centralized and hierarchical), they can also be separated into methodologies which are based on a model of the system or on predefined typical operating conditions. More specifically, in [35] a wide area controller has been implemented according to an adaptive measurement-based identification of the model and the utilization of a lead-lag structure. Furthermore, [18] proposes the utilization of a network control system model for the WAC design, according to linear matrix inequality techniques. The authors in [36] use an expectation model to develop the WAC signals, which derives from system order reduction and it considers time delay distribution. In [37], the WAC development is based on the Takagi-Sugeno fuzzy approach which takes into account various operating conditions of the system. Another method that is based on operating conditions is presented in [12], where the design parameters of an approximated proportional-derivative controller (PD) are selected according to the system's operating point. In the same context, the authors in [38] are utilizing a Linear Quadratic Gaussian (LQG) control which is a linearized controller around an operating point. In addition, a two-level controller for the PSSs coordination, based on optimal control and on order reduction techniques for fast convergence is shown in [29]. Finally, a control design method, which does not consider any simplified model or typical operating conditions of the system, is proposed in [39]. This work suggests the implementation of a hierarchical WAC, based on

wide area signals from all the generators and the reformulation of the power system into a suitable, closed form.

The main drawback of the methodologies where the WAC is designed according to several typical operating conditions is that the system conditions are changing continuously. Therefore, by utilizing fixed parameters for the WAC tuning, which do not correspond to the actual conditions of the system, has as a result to reduce the WAC damping performance [35]. This procedure becomes even more challenging and unreliable with the increasing penetration of intermittent RESs into the system [40]. Based on this, the disadvantage of utilizing wide area controllers which are implemented according to linear control techniques (i.e. the LQG approach of [38]) is that they are valid and effective only in a certain range around a predefined operating condition. In contrast, the advantage they offer is the increased computational speed. Model-based methodologies are highly depended on the detail of the adopted system's model. Simplified models provide coordination signals promptly, but they lack in terms of accuracy. Conversely, complex models have long processing times, but they derive near-optimal control signals. In both cases, the system stability can be jeopardized, due to either accuracy issues or long delays.

The methodology adopted and advanced in this Ph.D. dissertation utilizes models of the power system components (e.g. synchronous generators, power network, renewables) in order reformulate the system into a closed form, suitable for decoupling each generator's dynamics from the remaining generators and from other components as well. Therefore, this method considers only the component models which are necessary for the WAC application so that it will derive an expression of the system that comprises all the required information without increasing its complexity.

2.1.3 Coordination of system components

In the literature, various methodologies have been presented for the development of a wide area controller. The proposed WAC schemes are segregated mainly according to the components of the power system that the wide area controller is intended to coordinate. More specifically, the components which are commonly considered in the available literature for coordination are the generator local controllers (exciter, governor and PSS), the High-Voltage Direct Current (HVDC) lines, the renewables and the FACTS devices. The proposed schemes are either proposing the WAC of a specific component type or a combination of the above components.

Exciter:

Considering the coordination of synchronous generators, the existing methodologies propose the WAC of its local controllers, i.e. exciter, governor and PSS. The published schemes consider the coordination of either one or more types of local controllers. In the case of the exciter, a supplementary WAC signal is derived and applied to its input (in addition to the one provided by the PSS, when they are also included in the power system), having as a goal to increase its small-signal damping capability [41], [29]. More specifically, in [10] and [42] the authors have shown the significant improvement on the system's damping capability when the wide area controller is included in addition to the PSS devices. In the same context, in [33], WAC signals are derived for the simultaneous coordination of three synchronous generators and three renewables. It is important to clarify that the synchronous generator WAC signal is actually applied to the input of the exciter along with the reference and the PSS signals. In [43] and [12] the WAC signals are applied in the same way, deriving from wide area damping controllers based on H∞ control and time-delayed control (TDC) respectively. Finally, the authors in [14] present the development of a wide area controller based on network predictive control (NPC) for the coordination of only one synchronous generator through its exciter. The disadvantage of this scheme is that it does not ensure the effective compensation of all the local and inter-area oscillations and furthermore, in the case where the system modes change it can decrease its damping performance.

Governor:

The majority of the published WAC methodologies propose the coordination of the exciter only (directly or indirectly, through the PSS). This is mainly due to the faster response of the excitation systems compared to the governor and the availability of the PSSs feedback signal on the input of the exciter (e.g. [11], [33], [41]). However, the coordination of the governor can be proven beneficial for the damping of local and especially inter-area oscillations, since it is directly related with the control of the generators' frequency [39]. Although the WAC of the governor is not very popular, published works exist on this matter. It is important to note here that none of the available studies suggests the coordination of the governor system only. In particular, it has been found that its coordination is combined always along with the exciter's coordination. In [44], a hierarchical controller is implemented to derive WAC signals for the governor and exciter, while preserving its performance in the presence of delays through the use of a smith predictor. Similarly, in [45]

a two-level voltage and rotor-speed regulator is suggested, which is consisted by exciters and speed governors on the primary level and a centralized controller on the secondary level.

Power System Stabilizer:

The WAC of PSS is a very popular approach to increase the power system's small signal stability. This is mainly due to its capability of generating an electric torque component, which aims to compensate the local part of the low frequency oscillations [11]. Nevertheless, studies exist that suggest the coordination of the PSS by providing a supplementary signal on its output signal. This is the case for [13] where the model-free adaptive control approach is used to derive an adaptive WAC signal which is applied to the exciter along with the PSS output signal. However, in this thesis this practice is considered to be a coordination of the exciter rather than the PSS since the signal affects directly the operation of the former. In [46], wide-area power system stabilizers (WPSSs) are proposed in order to suppress the inter-area oscillations. The WPSS aims to upgrade the conventional PSSs in such a way so that its parameters will change according to the stochastically changing operational point of the system. Furthermore, in [47] PSS-based controllers are presented for regulating renewable plants, which among other capabilities, can receive wide area control signals in order to contribute to the system's small signal stability. As it is reported in [48], when the PSSs are considered it is also desirable to utilize additional remote signals to the PSS in order to form global PSS (GPSS). However, these methodologies have complexity issues when they are applied to large power systems, they are usually designed based on the linearization of the system around a specific operating point and they fail to operate effectively under large transient phenomena.

High-Voltage DC lines:

HVDC systems are becoming interesting and important components of the future power systems. This is mainly due to their low electrical losses over long distances compared to the respective AC systems [4]. HVDC lines are utilized either to deliver power from renewable sources to the main power system or to transfer large amounts of power between AC systems. Due to their power electronic-based technology, they are flexible to be controlled according to the needs of the system. For this reason, the HVDC lines are constantly gaining attention in participating into the WAC schemes, along with PSSs and FACTSs. To damp the targeted inter-area oscillation, the HVDC line modulates accordingly its active power. However, the weakness of coordinating an HVDC line to damp a specific

mode is the fact that it ignores the impact that this action has on the other inter-area modes that may exist [4]. In [49] the authors present the design of a wide area controller for the Pacific DC Intertie (PDCI). PDCI is a ± 500 kV HVDC line of 846 miles long, located into the North American Western Interconnection. The idea of properly controlling the PDCI in order to damp a specific problematic mode dates back to the 1970s [50]. Although it has been shown that the damping of the specific mode was successfully increased, it has been noticed that other modes were destabilized [51]. This issue has been overcome through the large utilization of PMU measurements as feedback. In the same context, in [52] a project is presented where an HVDC located in southern China is utilized to improve the compensation of the inter-area modes. Furthermore, in [19] a wide area controller is developed based on the loop shaping method for the modulation of the active power of a HVDC line according to synchronized measurements. Finally, an interesting method is proposed in [53]. This work considers the design of a wide area controller for the future grid of Great Britain. More specifically, the proposed WAC will be used to derive supplementary control on HVDC links (which aim to connect Scotland with North of Wales) for increasing the system's small-signal stability.

Flexible AC Transmission System:

The participation of FACTSs into the WAC scheme is also a very effective option for the successful compensation of the inter-area oscillations. Like the HVDC lines, these are power electronic converter based devices meaning that they can be flexible for coordination by a wide area controller. Therefore, various works have been published proposing wide area control designs for regulating the FACTS operation. A WAC approach which utilizes static VAR compensators (SVCs) into its architecture is presented in [54]. Here, a non-linear Kalman filter is considered along with PMU measurements in order to estimate the inter-area modes to be compensated. In [55], a wide area predictive controller is introduced for coordinating lines equipped with thyristor controlled series compensation (TCSC) devices. A combination of controlling the exciters of the synchronous generators along with static compensators is presented in [10]. The wide area controller here is implemented according to neural network based structures. In the same context, WAC schemes for the simultaneous coordination of exciters and SVCs are proposed in [56] and [57], which are derived from multimachine power system models that consider the presence of the SVCs as well.

Renewable Energy Sources

During the last decades, the system stability is threatened mainly due to the large penetration of intermittent sources (renewables) in the system, which displace conventional controllable energy sources such as the synchronous generators. Based on this transition, the system's inertia and dynamics are changing [22]. The majority of WAC design methodologies do not take into account the effect of the installed RESs on the performance of the wide area controller. However, the consideration of the effect of RESs while utilizing WAC or their integration in the WAC design is vital for the implementation of the smart grid, since the smart grid of the future is expected to have a high penetration of renewables. The current practice by the system operator (especially at low penetration levels), is to utilize the RESs as negative loads and not as components able to contribute to the overall stability [58]. Therefore, the WAC concept provides the opportunity and capability of including the renewables (along with the synchronous generators) in a common coordination scheme in order to contribute to the effective damping of all the power oscillations. Amongst other benefits, the successful compensation of the inter-area modes can even enable the very high penetration of RESs into the grid [59]. In [33], a hierarchical control scheme is proposed, which consists of centralized and local Power Oscillation Dampers (PODs) and PSSs in order to coordinate all the wind farms and generators of the system. Furthermore, [60] presents a WAC design based on particle swarm optimization, for improving the performance of the power system through the control of wind farms. In [61], an observer-driven reduced copy (ORC) is utilized along with a linear quadratic regulator to damp inter-area oscillations, when two generators are replaced by Doubly-Fed Induction Generator (DFIG) wind farms in the IEEE 68-bus test system. In the same context, the ORC approach is used in [62] as well, for the DFIG coordination under intermittent observation. In [59], the design of a wide area controller is proposed for the coordination of DFIGs according to a line modal potential energy (LMPE) method combined with extended state observer (ESO)-H∞ control. The development of a wide area controller based on combination of energy functions and machine learning methods is shown in [41], for the simultaneous control of synchronous generators and DFIGs. All the aforementioned methods consider only DFIG wind farms. A work which utilizes an average model of the wind farms' voltage-source converter for control (instead of a DFIG model) is presented in [63], where the coordination of multiple wind farms with other power system devices is illustrated.

Despite the extensive literature on the WAC of components such as the exciter, governor, PSS, HVDC and FACTS, it has been identified that further improvement of the

WAC methodologies can be achieved. The main disadvantage identified is that the proposed methodologies on this matter are not evaluated under realistic conditions in order to ensure their robustness. More specifically, the proposed methodologies are either tested under the effect of some factors which can potentially affect their performance (e.g. data delays only [46], unrealistic measurement errors [12], unrealistic constant delays [59]) or under ideal conditions [13]. For this reason, this Ph.D. dissertation illustrates the implementation of realistic simulation environments for testing WAC methods, it identifies potential threats to their performance and it proposes novel and highly effective coordination methodologies.

From the available literature regarding the RESs coordination through WAC, it can been concluded that this is a challenging area and a lot of effort must be given here. Based on the already published studies on this matter, two issues have been identified. First of all, all the works assume that almost ideal conditions are occurring in the power system, where at most they consider that either simplified data delays or typical packet dropouts occur (e.g., [41], [61]). In addition to that, the performance of the proposed techniques is evaluated by considering a relatively small penetration of renewables into the system. What is more, the overwhelming majority of proposed methodologies are intended for DFIG coordination only, while in some cases they consider it along with the control of synchronous generators. However, DFIG is only a subcategory of the wind turbines and it is not clear if the proposed methods can be applied to other types of RESs as well. This Ph.D. dissertation has addressed these issues by implementing a universal methodology for the WAC of RESs, which is tested under high penetration levels of renewables and realistic conditions.

2.1.4 Wide Area Control regulation

It is a common practice to regulate the coordination signals provided by the wide area controller (e.g., [11], [39], [63]) in order to avoid high control efforts and large contribution levels. Generally, this is accomplished by adding a constant gain at the output of the WAC. This regulation constant is tuned by the designer according to the system's behavior and it can be far from the optimal since its value should change according to the contingency's nature. A similar approach is followed for the tuning of the Automatic Generation Control (AGC), where the constant control gains are determined either through case study simulations or by trial-and-error [64]. However, in contrast to the WAC case, methodologies have been proposed for the online tuning of the AGC. More specifically, in [64] a dynamic tuning of the control gains is presented, which considers also the effect of

the wind farms' penetration in the system. In [65] an adaptive AGC is proposed with self-tuning gain capabilities in order to avoid the over-regulation caused by the system operators.

2.1.5 Coherency

One of the main drawbacks of developing a wide area controller is the increasing complexity when moving to larger power systems, since the number of its input/output signals rises substantially. Increasing the inputs and outputs from a certain point and above can affect negatively the WAC performance and it can jeopardize the system's stability. Although this is a well-known issue, the vast majority of the published studies neither proposes methods to address it nor they evaluate their methods under these conditions.

According to [66] and [45], this issue can be overcome through the use of the coherency concept. Coherency is the phenomenon of the power system where at the event of a contingency, certain generators have similar time-domain behavior [67], [68]. Based on this, it is reported in [66] that the coherency concept can be used in order to reduce the number of the required PMUs for the wide area control. Particularly, in [66] one PMU is used at each coherent group (since they have similar responses) in order to derive a common WAC signal for all the generators of the group. However, this is not practical in reality, since the coherent groups change according to the location of the fault and therefore synchronized measurements are needed from all the generator buses. Nevertheless, coherency can be used to reduce the measurement dependency of the wide area controller. In [45] it is noted that coherency can be considered as a means to reduce the number of the signals to be utilized and therefore the remaining unknown signals can be approximated. The latter is based on the fact that the variables of coherent generators are proportional. Furthermore, in [69] an online coherency-grouping algorithm is utilized to identify the required wide area signals. These signals are then used to implement and find the locations of the wide area controllers to be installed. However, this can be valid only for systems where the coherent groups are clearly separated and connected through long transmission lines. Once again, the problem that arises is when systems that are more complex are considered, where the coherent groups can vary depending on the disturbance. An interesting work is presented in [70], where the input and output signals of the wide area controller are selected according to a data-clustering algorithm.

The majority of the published studies on this matter, consider that the coherent groups are the same for different contingencies and easy to distinguish. In reality, the coherent groups in large and complex systems change according to the type and location of

the fault. In addition, real-time grouping algorithms might result into more than one partition regarding the total number of the coherent groups [67]. In this Ph.D. dissertation the coherency concept is been used to reduce the number of the required PMU signals as well as the derived coordination signals, leading to a WAC architecture which can be considered into larger power systems.

2.2 Data Delays and Data Dropout

Communication networks are utilized to transfer the synchronized measurements from the PMUs to the WAMC applications and the coordination signals from the WAC to all the local controllers of the system. However, communication networks are far from ideal and this is one of the main obstacles towards the implementation of real-time applications. The reason is that communication networks are characterized by communication delays and data dropout. These are found to be the most known factors responsible for the degradation of the WAC damping capability ([71]) which can even lead the system to instability [72], [73]. Communication delays take place during data exchange between devices (e.g., PMUs and Phasor Data Concentrator (PDC)) in a shared medium and they are mainly introduced by the long distance transportation of feedback signals, the medium type, the data buffering and the time required to send each bit. Some studies consider communication delays as constant or time-varying (e.g., [44], [74], [54], but in reality they are random due to the various communication channels. In addition to the communication delays, the operational/processing delays occurring from the parts composing the real-time applications (e.g., PMUs, PDCs), is also a significant issue [75]. More specifically, [49] and [76] provide an analytical explanation of the delay types, which are segregated into:

1) PMU Delay: This is defined as the difference between the time the timestamp of a packet is set and the time the packet is at the output of the PMU. This delay type is directly depended to the PMU operation (e.g. reporting rate, filtering).

2) Communication Delay: This is the time required for the measurement to travel from the PMU to the PDC. This delay has the most variability mainly due to the conditions of the communication network (e.g. traffic, medium length, routers, switches, etc.).

3) Control Processing Delay: The time period needed by the application to process the measurements and derive the control signals.

4) Command Delay: The time required for the coordinated component to react to the feedback control signal.

Data dropout is an unpredictable phenomenon and it can occur due to the appearance of noise/uncertainties in the communication network, transmission errors and data congestion, which lead to buffer overflow [61]. For this reason, most of the network protocols have transmission-retry mechanisms where the data are re-transmitted after a certain time period. If this period expires, the data will be dropped. Like network delays, data dropout can degrade the performance of the system [18]. Apart from the data dropouts due to network issues, data drop phenomena can occur due to cyber-attacks such as the denial of service (DOS) which can terminate the flow of measurements for several instants [77].

Various studies have been proposed to address the impact of network delays and data dropouts on the WAC performance. A common and attractive solution to tackle the problems derived from communication networks is to use predictors in the wide-area controller design. In [61] and [62], a methodology to compensate the data dropouts of the communication network is presented, based on the Observer-driven Reduced Copy (ORC) approach. More specifically, these studies utilize the ORC method to predict the behavior of the system when data dropout occurs, based on model linearization and model reduction but they ignore the stochastic nature of the delays. Furthermore, in [44] and [56], a Smith predictor was utilized to preserve the performance of the controller within specified limits and eliminate the negative effects of large data delays. The idea of the Smith predictor is to use a model of the system in order to provide a delay-free signal to the controller and cancel the delayed output of the plant. Thus, as the model becomes more accurate, the output of the Smith predictor is closer to the desirable signal. However, approaches such as the Smith predictor, Padé approximations [29] and phase lead-lag filters [78] are commonly used to compensate unrealistic constant delays [55]. A network delay compensation technique based on phase lead and on Modified Extended Kalman Filter (MEKF) is proposed in [37] and [79]. MEKF disadvantage is that its performance is highly depended on the initial state, on the order of the model and on the parameters of the Kalman filter. Lastly, in [17] and [14], the impact of communication delays is compensated through the use of network predictive control (NPC), which uses a general predictive control method to generate a set of future control signals and then it picks the correct control signal based on the delay, in order to compensate it. However, as it is reported in [55], the presence of data dropouts degrades significantly the performance of the NPC-based wide area controller.

The drawbacks identified in the already published studies are the following:

- Most of the published works consider constant delays with a known upper bound and neglect the existence of data dropouts ([46], [59], [54], [20]).
- Studies that consider random delays, assume unrealistic ranges and probability distributions without justifying their selection [14], [12].
- The majority of the methods utilize either a simplified expression of the measurement errors [61] or they do not consider them at all [79].
- Some works do not consider that there are also delays on the feedback control signal (from the WAC back to the local controllers) and therefore, they concentrate only on dealing with the delays between the PMUs and the wide area controller [18], [20].
- The proposed predictors are model-based methodologies.

Validating the proposed delay compensation techniques under realistic measurement errors is crucial, since the latter can affect the operation of the former. On the other hand, delays should be implemented to have realistic ranges and probability distributions according to available reports. In addition, data delays must be compensated along with data dropout phenomena since both occur in actual communication networks. Furthermore, it is important to consider all the delays (measurement infrastructure and feedback delays) since the negligence of any delay type while developing a compensation methodology can adversely impact the operation of WAC in real conditions. Lastly, model-based predictors have the significant disadvantage of being highly depended on the adopted model of the system. This issue appears when larger systems are considered, where more detailed models are required and thus the complexity and processing time increases rapidly. This Ph.D. dissertation addresses all these issues by proposing novel model-free and fast predictors to compensate effectively data delays and dropouts.

2.3 Measurement Errors

The availability of the PMU synchronized measurements is crucial for the WAC operation, since the observation of inter-area oscillations is only possible through their utilization. However, just like any other real-time monitoring and control applications [80], WAC can be fully and successfully performed when accurate and timely measurements are

provided by the measurement system. Furthermore, as pointed out in [21], it is absolutely necessary to investigate thoroughly the robustness of various synchrophasor applications (such as the WAC) to data quality issues such as the data accuracy. In most cases, the already published WAC methodologies are considering that ideal measurements arrive to the controller, which are not affected by measurement errors. Other studies are utilizing unrealistic measurement errors to evaluate the proposed methods without justifying their choice [12]. However, even in the rare case where they do consider non-ideal realistic measurements, they take into account only the PMU steady-state measurement errors.

PMU measurements generally have small steady-state errors due to their high accuracy (especially compared to conventional measurement devices). Nevertheless, they are still prone to precision errors mainly due to the uncertainty introduced by the measurement chain and more specifically by the instrument transformers [81], [82]. Instrument transformers are utilized to provide isolation from the high-voltages and to step down the high voltage and current levels, to a level compatible with the measurement device that is connected to them [83]. In [82] a study took place considering the impact of the uncertainty of both measurement devices and instrument transformers on the accuracy of the Weighted Least Squares (WLS) state estimator. It has been illustrated here that by obtaining weights of the measurements based on the uncertainty of the whole measurement chain, the performance of the state estimator can be improved considerably. Furthermore, [84] and [85] present methodologies for the instrument transformer calibration through the estimation of the unknown ratio errors according to synchronized measurements. The authors in [86] investigated the improvement in the accuracy of the phasor measurements, when optical instrument transformers are considered instead of the traditional ones. Lastly, methods for the evaluation of the PMU measurement uncertainty are described in [87].

Even by considering that only PMU steady-state errors occur and ignoring the instrument transformers measurement errors, this assumption is completely unrealistic. This is because the PMU measurement errors increase significantly during dynamic conditions, as it is reported in the IEEE Synchrophasor Standard C37.118.1-2011 [88]. This Standard is an updated version of the IEEE Synchrophasor Standard C37.118-2005 in order to incorporate the PMU dynamic compliance requirements as well. Therefore, it is important for methodologies that are intended for dynamic conditions (such as the WAC) to be tested under a realistic environment, where all the aspects which change during transient events are properly considered.

2.4 Dynamic Loads

Although various methodologies have been proposed for the successful development of WAC, the prevailing majority is validated considering the existence of only constant loads in the system (mainly constant power [11] and sometimes constant impedance [79] loads), which do not have any time, voltage or frequency dependence. Conversely to this assumption, several loads in the power system are in reality dynamic and highly nonlinear. Therefore, the proposed WAC methodologies should be evaluated under the existence of non-linear loads (static and dynamic), which can potentially be a threat to the stability of the system. In [54], the development of a wide area controller intended for the coordination of SVCs based on a non-linear Kalman filter and PMU measurements has been proposed. The evaluation of the proposed scheme considered the inclusion of composite load models into the system, which are separated into a constant impedance load and to two simplified induction motor loads for including a dynamic behavior as well. Furthermore, in [44] the development of a two-level hierarchical controller combined with a Smith predictor is presented. Its performance in this case has been validated by including a nonlinear load, which consists of an induction motor and a voltage depended static load (load dynamics are not included).

Dynamic load models are developed in order to represent accurately the behavior of thousands of loads which are connected on the high-voltage feeders [89]. However, accurate load modelling can be a very challenging procedure since the loads change based on their nature (e.g. industrial, residential) and according to the hour/month/year [90], [91]. Due to this reason, some load models can appear to be accurate enough for some systems, while for others they are inadequate. Overall, it is unclear how much is the actual impact of the non-linear loads on the WAC performance, especially when large-scale test systems are considered. In addition, various static and dynamic load models are available, which can have different effects on the WAC operation. Therefore, this Ph.D. dissertation examines the effect of the high penetration of various non-linear load models on the WAC operation and proposes novel methodologies that preserve their high performance even under these conditions.

CHAPTER 3
DEVELOPMENT OF ANALYTICAL AND REALISTIC SIMULATIONS

The goal of this chapter is to present the steps followed to develop realistic simulation environments, required for testing WAC methodologies. The accurate representation of the system's behavior is required specifically when dynamic conditions take place where the WAC contribution is essential. As aforementioned, the motivation here is to utilize these environments to identify potential threats which can affect the performance of the wide area controller in actual conditions, in order to be able to develop and propose techniques for their compensation. The overall objective is to implement a robust and highly effective WAC methodology, capable of coordinating appropriately all the types of local controllers, under any circumstances and disturbances.

3.1 IEEE Dynamic Tests Systems

It is absolutely necessary to acquire a dynamic simulation environment, which is able to perform accurate Electro-Magnetic Transient (EMT) simulations intended for transient analysis. This can be achieved by utilizing dynamic test systems. However, the available IEEE test bed systems are only used for steady-state studies, since they consider ideal sources and no dynamic parts. In [92] all the necessary modifications for reforming the most known IEEE test systems into dynamic test systems are presented. More specifically, a slight modification of the topology was applied in order to utilize sixth-order generator models along with their local controllers (all provided in [93]) instead of the ideal sources. The work in [92] used the PowerWorld and PowerFactory software for the development of the dynamic test systems, while in this Ph.D. dissertation the Matlab/Simulink is considered which is more suitable for the development of new control techniques.

Therefore, the IEEE 9-bus and 39-bus test systems are implemented from the very beginning in Matlab/Simulink based on the system and generator data provided by [92] and [93]. As generator local controllers, the exciter DC2A and the general purpose governor are considered, while for the needs of Chapter 8 PSSs are also included in the test systems. The topologies of the IEEE 9-bus and 39-bus test systems are illustrated in Fig. 3.1, while Fig. 3.2 depicts the block diagrams of the adopted exciter and governor.

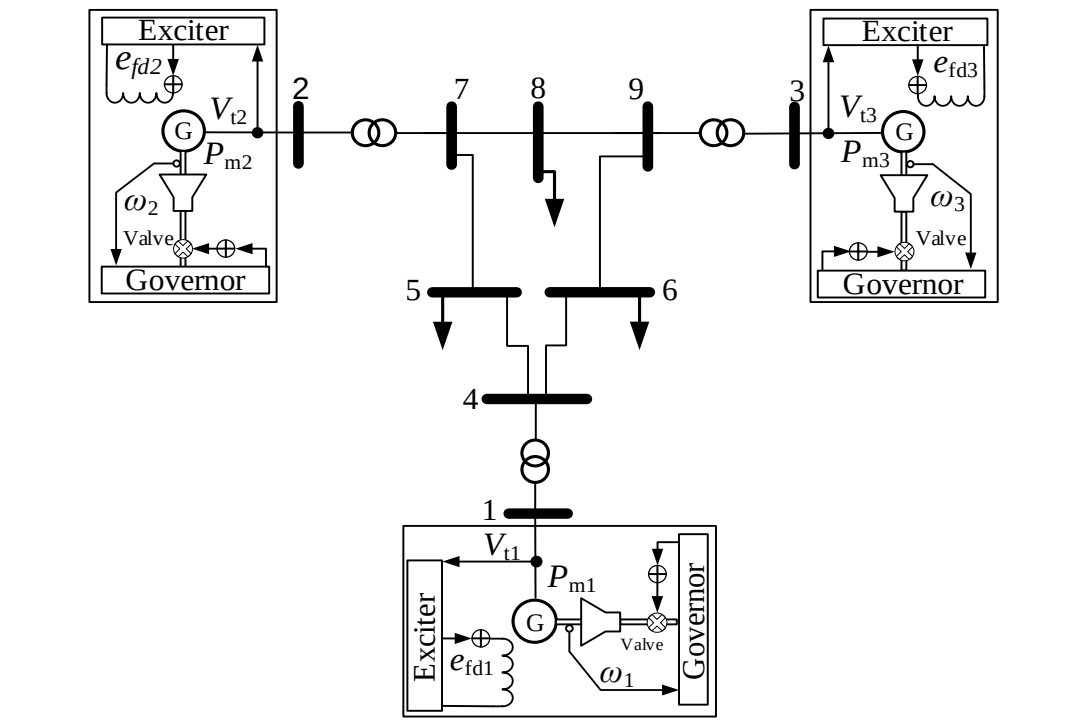

(a)

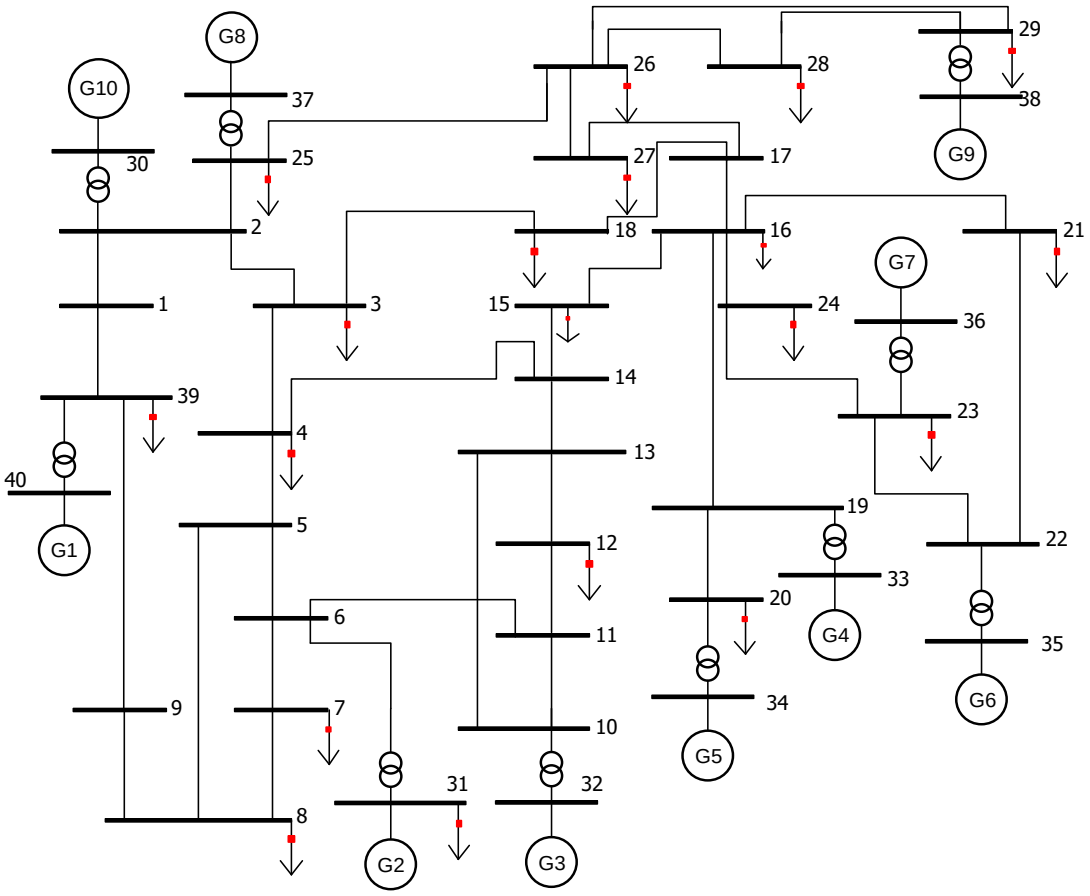

(b)

Fig. 3.1 Topologies of (a) the 9-bus and (b) the 39-bus (b) IEEE Dynamic Test Systems.

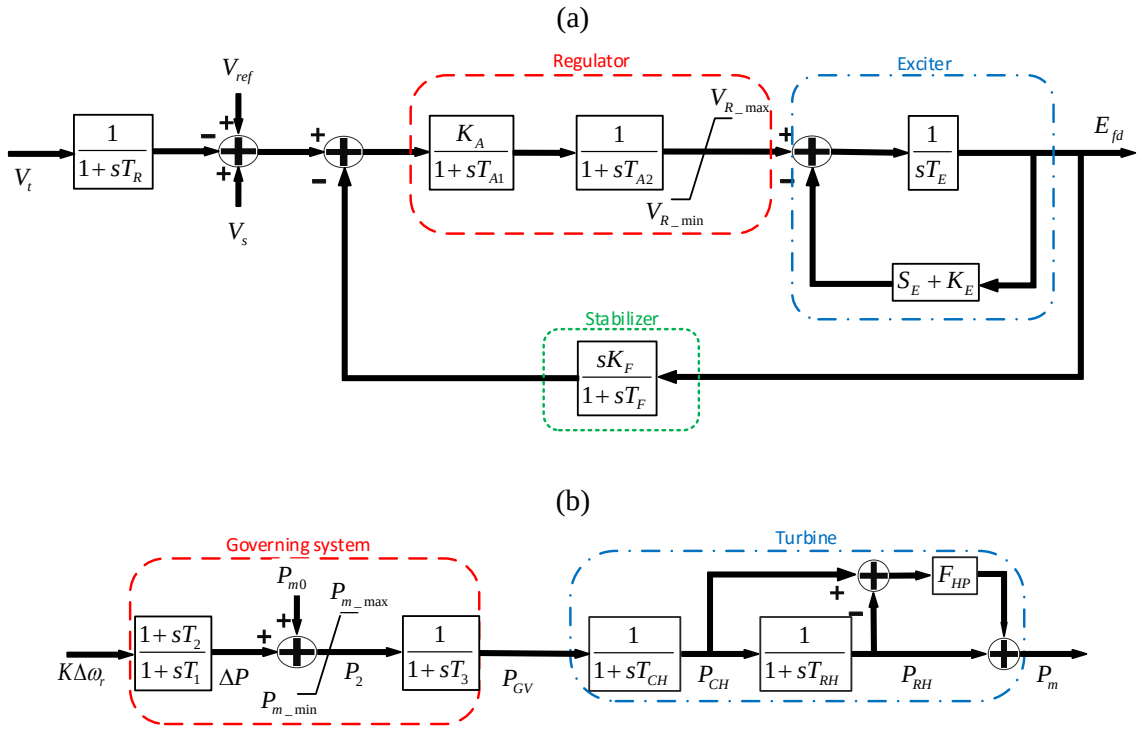

Fig. 3.2 Block diagrams of (a) DC2A exciter and (b) general purpose governor.

3.2 Realistic Measurement Error Formulation

In Chapter 2, it has been pointed out that the measurement chain requires the instrument transformers which are responsible for providing isolation from the high-voltage system and for bringing down the voltages and currents to standard instrumentation level (e.g., PMU-compatible level) [83]. Instrument transformers consist of Voltage Transformers (VTs) and Current Transformers (CTs). One would expect that the output of the instrumentation channel (composed by instrument transformer, control cables, filters, etc.) would be an exact replica of the actual high voltage and current waveforms, downscaled by a constant factor. However, in reality the signals are affected by relatively high precision errors that exist in the instrumentation channels. A typical schematic diagram which represents the measurement chain is presented in Fig. 3.3. As shown, the actual (ideal) voltage and current measurements pass firstly through the instrument transformers and then through the PMU. Therefore, the errors affecting the wide area signals are separated into the ones introduced by the sensing elements and the ones from the measurement devices. According to [82], these errors occur either due to random effects or due to systematic effects (existence of a constant “uncertainty” source). In this thesis, it is assumed that instrument

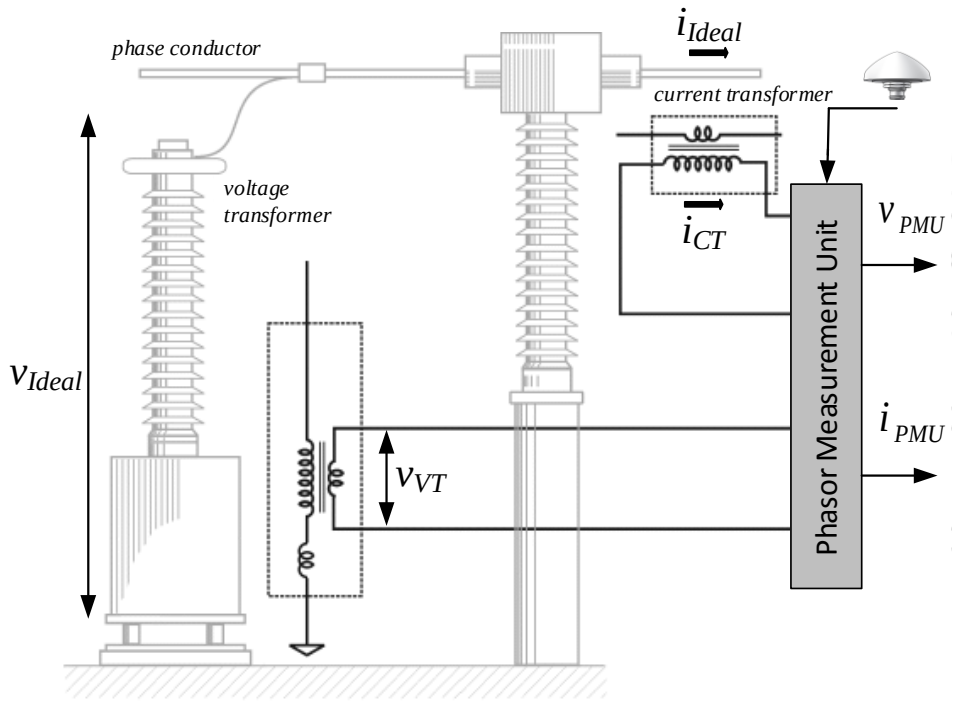

Fig. 3.3 Schematic diagram of the measurement chain, illustrating the connection of the voltage (VT) and current (CT) transformers to the PMU.

transformers and PMUs are properly calibrated to compensate all sources of systematic errors [94] and thus only random errors are considered.

According to [86], the overall measurement error can be taken as the aggregation of the individual errors from the instrument transformers and the PMU, since the measurements of the former are transferred directly to the latter. In the case that no information about the probability distribution of the errors is available, a uniform distribution with the maximum errors (provided by the manufacturer) as upper and lower limits can be used [87]. As a result, the following expressions for the actual measurements provided by the PMUs, in terms of their ideal network values can be derived as:

$$v_{PMU} = v_{Ideal}(1+e^{v}_{PMU})(1+e^{v}_{VT}) \tag{3.1}$$

$$\theta^{v}_{PMU} = \theta^{v}_{Ideal} + e^{\theta_V}_{PMU} + e^{\theta_V}_{VT} \tag{3.2}$$

$$i_{PMU} = i_{Ideal}(1+e^{i}_{PMU})(1+e^{i}_{CT}) \tag{3.3}$$

$$\theta^{i}_{PMU} = \theta^{i}_{Ideal} + e^{\theta i}_{PMU} + e^{\theta_i}_{CT} \tag{3.4}$$

$$f_{PMU} = f_{Ideal} + e^{f}_{PMU} \tag{3.5}$$

where e_{PMU}, e_{VT} and e_{CT} stand for the measurement errors of the PMU, the VT and the CT respectively. The angle θ is the phase of the measured quantity. Equations (3.1) and (3.3)

TABLE 3.1: INSTRUMENT TRANSFORMER MAXIMUM ERRORS

Type	Accuracy Class	Max Magnitude Error (%)		Max Phase Error (degrees)	
VT	0.5	$e_{VT}^{v\max}$	± 0.5	$e_{VT}^{\theta_V \max}$	± 0.333
CT	0.5	$e_{CT}^{i\max}$	± 0.5	$e_{CT}^{\theta_i}$	± 0.5

TABLE 3.2: PMU STEADY-STATE MAXIMUM ERRORS ACCORDING TO [97], [82]

Max Voltage Magnitude (%)		Max Current Magnitude (%)		Max Phase Angle (degrees)		Max Frequency (Hz)	
$e_{PMU}^{v\max}$	± 0.02	$e_{PMU}^{i\max}$	± 0.03	$e_{PMU}^{\theta\max}$	± 0.57	$e_{PMU}^{f\max}$	± 0.005

reflect the magnitude of the measured quantities, while (3.2) and (3.4) their phase. Equation (3.5) refers to the frequency (*f*) measurements.

TABLE 3.1 and TABLE 3.2 summarize all the data regarding the maximum measurement errors of the instrument transformers and the PMUs respectively, which are considered as the maximum limits of the uniform distributions utilized to simulate the errors in (3.1)-(3.5). For the instrument transformers, the measurement errors change according to the adopted accuracy class. Without any loss of generality, the accuracy class of 0.5 has been considered which is the most commonly used. In addition, the maximum error of current transformers ($e_{CT}^{i\max}$) changes according to the loading conditions of the transformer, with respect to its rated current. Therefore, the maximum measurement errors at 100% loading conditions are adopted. Note that the measurement errors utilized for the instrument transformers are all according to available standards and more specifically, the IEC 61869-2 is used for the CTs [95] and the IEC 61869-3 for the VTs [96]. Furthermore, it is worth mentioning that the PMU data of TABLE 3.2 which correspond to steady-state conditions (as reported in the data sheet of [97] and in [82]), comply with the steady-state requirements of the IEEE Synchrophasor Standard C37.118.1-2011 [88]. The latter is actually an updated version of the IEEE Synchrophasor Standard C37.118-2005.

However, in the case of the PMU measurement errors, things are more complicated. Although it is generally accepted that PMUs are offering significantly higher accuracy (and therefore, low measurement errors), things are very different during dynamic conditions. This fact is actually the most common mistake that the vast majority of published studies does, where they utilize only the PMU steady-state measurement errors even when transient events occur. In reality, when dynamic conditions take place in the power system (e.g., due to a fault), the steady-state PMU measurement errors cease to be valid as it is reported in the IEEE Synchrophasor Standard C37.118.1-2011 [88]. Therefore, the dynamic compliance

requirements of IEEE Synchrophasor Standard C37.118.1-2011 are utilized in this work in order to identify the appropriate dynamic measurement errors to be considered. Note that these dynamic measurement errors are essential for the implementation of a realistic simulation during transient events.

All the details regarding the utilization of the dynamic compliance requirements to derive the dynamic measurement errors are descripted analytically in the following steps:

1) According to the application, identify the PMU class to be utilized. The reason for this is because the dynamic compliance guidelines are provided for two performance class PMUs: the P-class (intended for protection applications) and the M-class (intended for analytic measurement applications). WAC requires the existence of the latter class in the system and therefore, the requirements for the M-class PMUs are considered in this work.

2) Select the type of the disturbance to be applied and visualize the measurement signals directed to the PMUs, during the event. This step is necessary in order to identify which one amongst the dynamic compliance tests is closer to their shape and therefore utilize the respective dynamic compliance requirements in the simulation. In the IEEE Synchrophasor Standard C37.118.1-2011 [88], three dynamic compliance tests are reported, namely: the modulation signal test, the frequency ramp test, and the input step change test.

3) According to the dynamic compliance tests find the dynamic compliance requirements and further, the dynamic measurement errors. More specifically, dynamic compliance requirements include the limits of the Total Vector Error (TVE), the frequency error (FE), and the rate of change of frequency error (RFE). Note that TVE is a quantity which comprises both the amplitude and phase errors as specified in [88] and its general form is shown in Fig. 3.4. Actually, it represents the difference of the PMU-measured synchrophasor compared to the true value of the synchrophasor. According to [88], in steady-state conditions TVE is limited to 1% meaning that the maximum magnitude and phase errors are 1% and 0.573°, respectively.

4) Set the resulted dynamic measurement errors to take place when the disturbance occurs. If the time interval to return back to the steady-state errors is not reported in [88] (as in the case of the modulation signal test) then keep the dynamic error

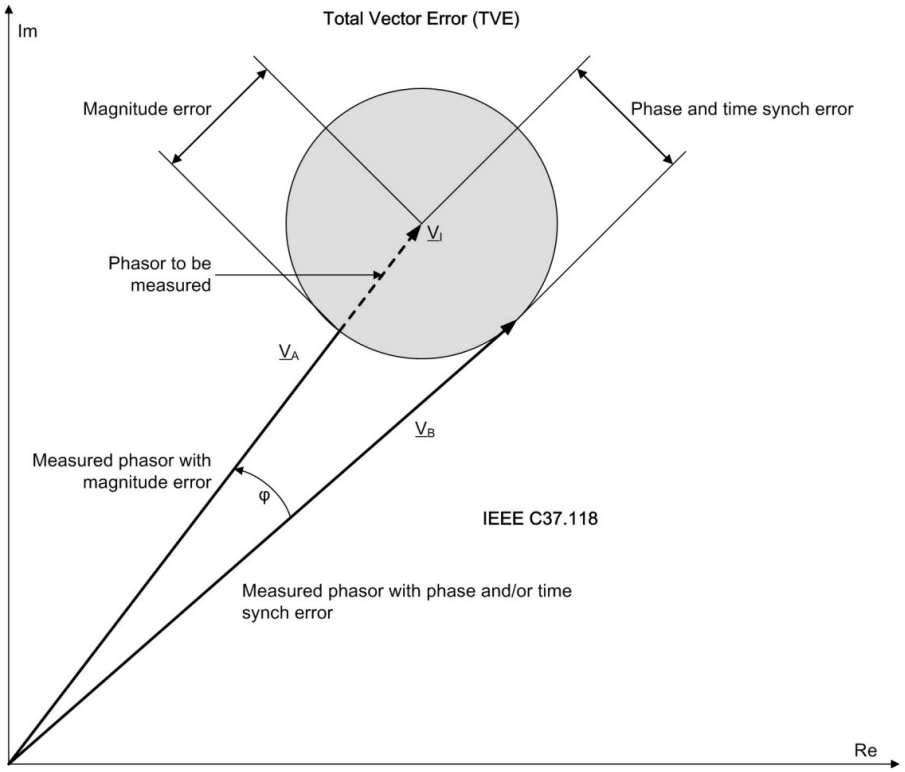

Fig. 3.4 Representation of TVE in its general form [142].

effective until the magnitude deviation of the measured signal compared to its pre-fault value is lower than 0.1 pu. In rest simulation, utilize the PMU steady-state maximum errors according to the data sheet of [97], which complies with the steady-state TVE, FE and RFE reported in [88].

3.3 Development of Data Delays and Data Dropout

The WAC operation includes unavoidable data delays and dropout phenomena that can degrade its damping capability [56], [17]. Data dropout is an unpredictable phenomenon, which results due to transmission errors/noise, buffer congestion or even from cyber-attacks [61], [55]. Generally, a delay in the synchrophasor communication is defined as the interval from the time the signal has a certain value, to the point where it is utilized by the intended application. According to the IEEE Synchrophasor Standard C37.118.2-2011 and Fig. 3.5 the delays of the measurement infrastructure are separated into the measurement process delays, the communication delays, and the application delays [98], [99]. The measurement process delays include the sampling procedure, the filtering and the data processing/alignment delays. In [88], the PMU measurement process delay (or measurement reporting latency) is defined as the maximum time interval between the time stamp of a measurement and the time when the same measurement is available at the PMU output. Typical ranges provided in [99] indicate that measurement process delays are largely

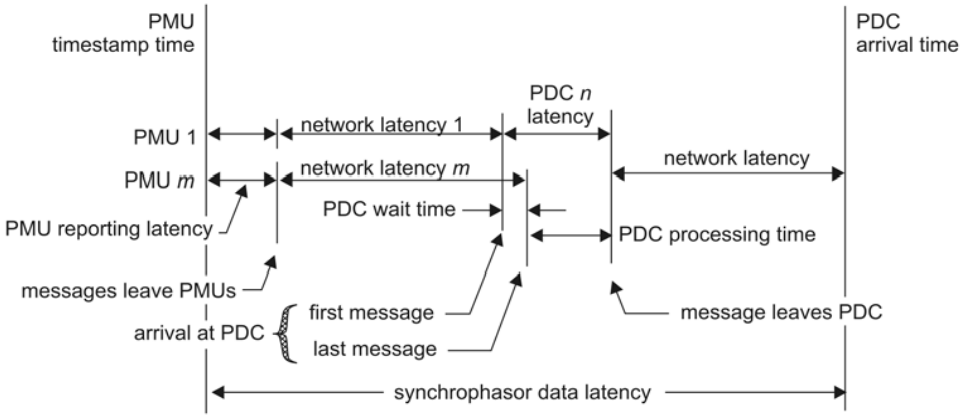

Fig. 3.5 Breakdown of the synchrophasor data delays [102].

depended on the delays of sampling window and the filtering process. Communication delays can be further separated into propagation delays, transmission delays and data queuing delays [55]. The communication delays are due to the distance, the medium type, the error correction, the data buffering and the time required to send each bit. Especially buffering and error correction can be time-consuming procedures. Lastly, the application delays refer to the processing latency of the end device (e.g. PDC) and the application methods (such as WAM and WAC).

Most of the studies are mistakenly considering the communication infrastructure to be responsible for the long delays that might occur but in reality, in most of the cases, it is the measurement process delays that have the greatest share. This is especially the case when a dedicated communication infrastructure exists (e.g. fiber optics) for the needs of the power system. Measurement process and communication delays will be further on referred to as measurement infrastructure delays. A relative approximation to calculate the range of the measurement infrastructure delays is provided in [99]. More specifically, it is reported that typical delays from a PMU to the PDC are between 20-50 ms and each level above adds additional delays in the range of 30-80 ms. Therefore, a two-level communication infrastructure (e.g., PMU to regional PDC and regional PDC to central PDC) will have overall delays in the range of 50-130 ms.

Furthermore, some available studies do not consider that delays occur on the feedback control signal as well (from the WAC to the local controllers) and therefore, they concentrate only on dealing with the delays between the PMUs and the wide area controller (e.g., [17] and [18]). However, especially the inclusion and compensation of the feedback delays is equally important since it can adversely impact the operation of WAC and thus it can jeopardize the stability of the whole system. Note here that the feedback delays are

consisted by the application delays (processing of the end device and the application methods) and the communication delays that are associated to the transfer of the WAC signals back to the system. Since both, measurement infrastructure delays and feedback delays utilize the communication infrastructure, data dropouts must be considered to occur along with these delays. As aforementioned in Chapter 2, generally data delays have a random nature. Thus, probability distributions must be used to simulate their stochastic behavior. In this Ph.D. dissertation the measurement infrastructure delays and feedback delays are modeled according to three Probability Distribution Functions (PDFs), namely: the uniform [36], Beta [100] and Gamma [101] distributions. More specifically, the measurement infrastructure delays are simulated as uniform distributions since various sources of delay exist in the communication path from the PMUs until the WAC. Beta and Gamma distributions are considered to model the feedback delays, as they are typical PDFs for simulating packet-based networks.

A realistic representation of the communication infrastructure requires also the existence of a PDC. More specifically, apart from the PDC processing/alignment delays (which are included into the overall measurement infrastructure delays), the PDC "absolute wait time" concept has been applied in this Ph.D. dissertation, as it is specified in the IEEE Synchrophasor Standard C37.244-2013 [102]. This concept is illustrated in Fig. 3.6 and it represents the maximum time that various measurement-based tools (such as the PDC) can wait for the synchronized measurements to arrive after the expected timestamp. In the case where data arrive after the "absolute wait time" expires, the PDC utilizes the previously received measurements and it discards any delayed data received afterwards. Therefore, long

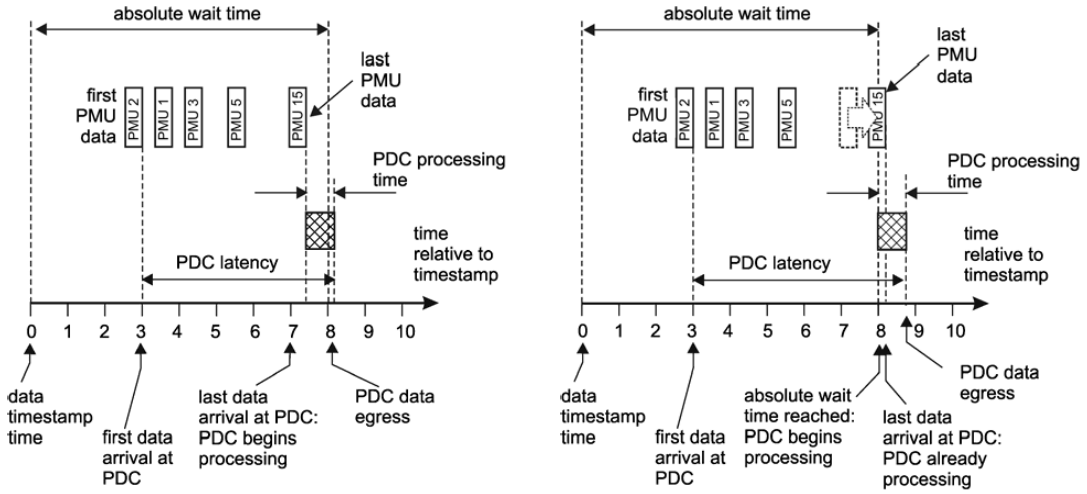

(a) (b)

Fig. 3.6 Illustration of the "absolute wait time" concept of a PDC for the cases of (a) no data drop and (b) data drop [102].

delays or lost measurements, both lead to data dropouts. In this way, the packet disorder is avoided.

3.4 Renewable Energy Sources

For illustrating the effect of the high penetration of renewables into the power system, it is essential to utilize a detailed model of the power system along with a very accurate model of the RES local controller for more realistic operation. A fully converted RES consists of a wind turbine with any type of a three-phase electric generator, a generator side converter, and a Grid Side Converter (GSC) based on power electronics technology as shown in Fig. 3.7. The generator side converter is responsible for the optimal power extraction from the wind turbine according to the wind speed, while the GSC properly injects the produced power into the grid.

The GSC controller developed for the purpose of this work (Fig. 3.7) is mainly based on: a robust synchronization method [103] for estimating the phase angle (θ') of the grid voltage $v_{abc}=[v_a\ v_b\ v_c]^T$ at the Point of Common Coupling (PCC), an accurate current controller [104] for regulating the injected currents $i_{abc}=[i_a\ i_b\ i_c]^T$ (inner loop), and a PQ controller [105] for generating the reference currents $i_{ref}=[i_a^*\ i_b^*\ i_c^*]^T$ (outer loop). More specifically, for the synchronization method, the DNαβ PLL has been used ([103]) which is very robust against asymmetric voltage sag and harmonic distorded conditions. This method uses a pre-filtering stage based on a decoupling network (designed in multiple synchronous reference frames) that allows the dynamic decomposition of the voltage components. The

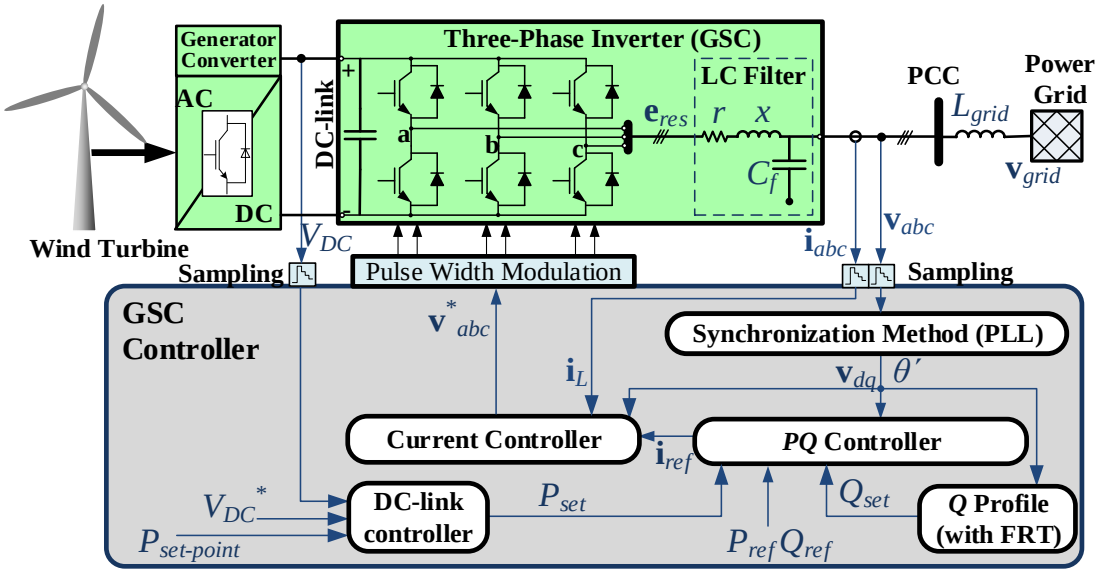

Fig. 3.7 An example of a fully converted RES with the generator converter, the GSC and its controller.

positive sequence voltage ($\mathbf{v}_{dq}$= [v_d v_q]) is then used to estimate the grid voltage at the PCC. The grid voltage and the amplitude of the positive sequence voltage are crucial for the PQ and current controller.

The outer loop of the GSC controller is mainly based on the DC-link controller, a *Q*-profile scheme (enhanced with Fault Ride Through (FRT) capabilities) and a *PQ* controller.

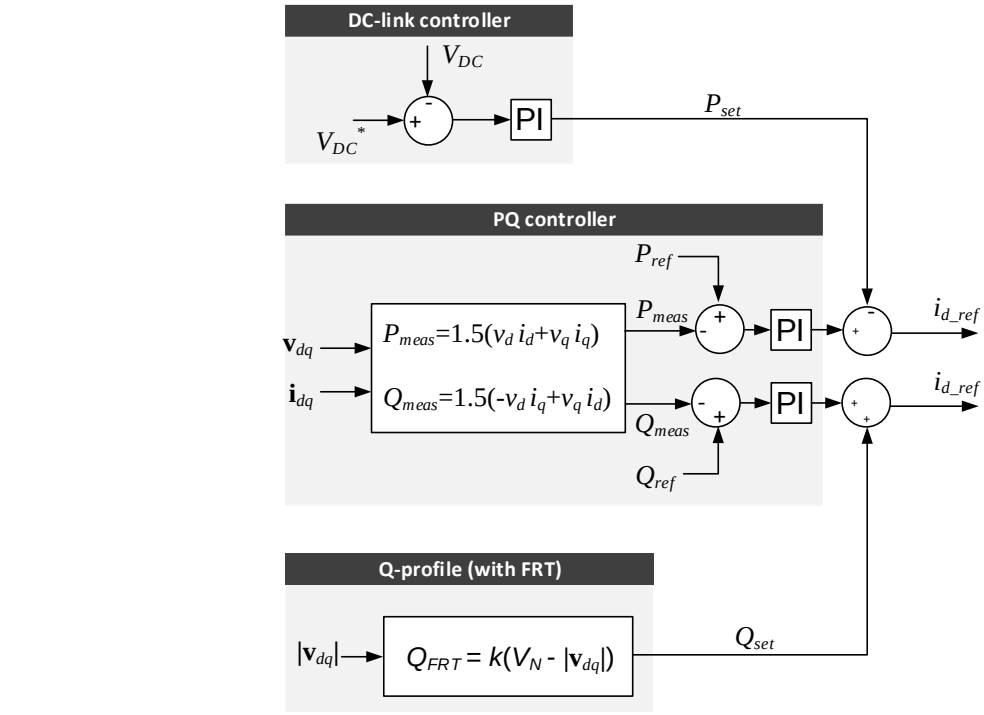

(a)

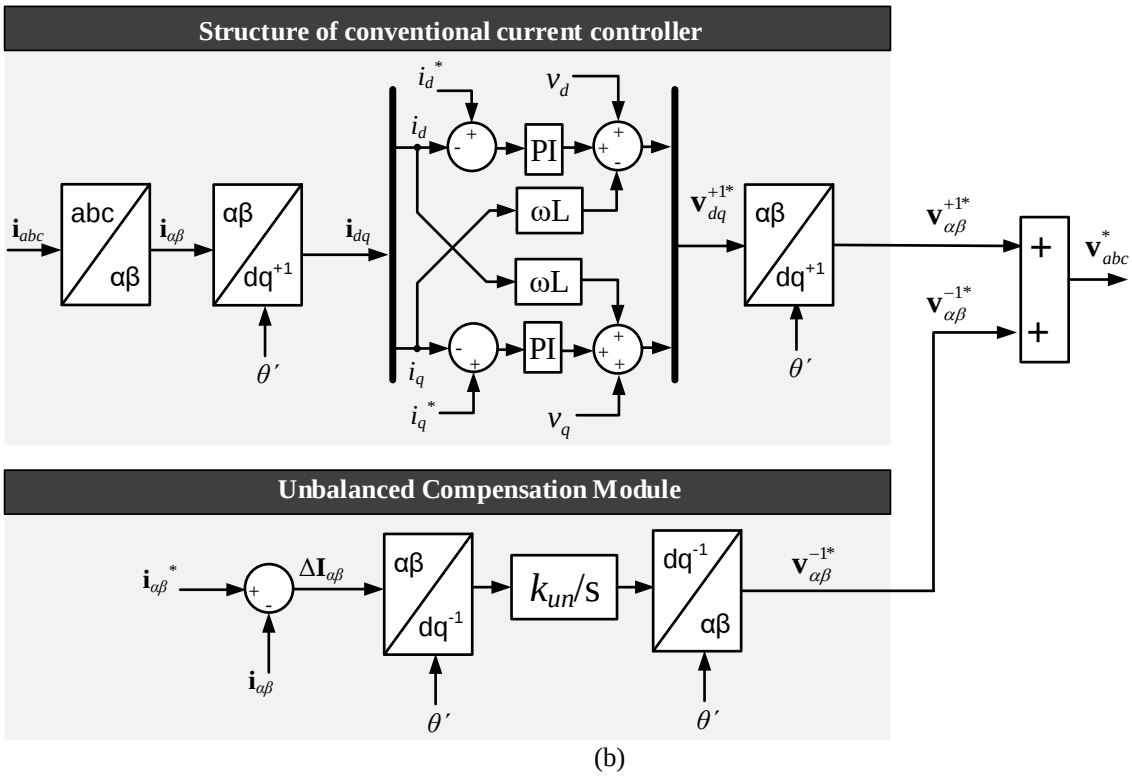

(b)

Fig. 3.8 Illustration of the (a) outer and (b) inner loop of the GSC controller.

The DC-link controller aims to maintain the DC voltage (V_{DC}) at the reference value (V_{DC}*) and as a result it injects the produced power by the RES to the grid. On the other hand, the *Q*-profile regulates the reactive power injection (according to Q_{ref}) in order to make the renewable capable of providing voltage support to the power system during grid faults according to modern grid regulations for interconnecting RES [106]. Finally, the *PQ* controller generates the reference current that will be fed to the current controller in order to regulate the active and reactive power injection. The overall structure of the outer loop is illustrated in Fig. 3.8a.

The inner loop of the controller (Fig. 3.8b) is actually a current controller that calculates the voltage reference for the pulse width modulation (PWM) unit, ensuring that way the proper current injection by the inverter. The current controller of [104] is based on a conventional current controller, designed in a synchronous reference frame (*dq*-frame). The utilization of *dq*-frame allows the use of a simple Proportional Integral (PI) controller for controlling the current injection. Further, for enabling the appropriate operation of the RES under asymmetric voltage sag, the current controller is also enhanced with an Unbalanced Compensation Module, based on an Integral controller (I), which makes the GSC able to inject positive sequence current during faulty conditions.

3.5 Dynamic Load models

Load modelling refers to the mathematical expression of the load's behavior under steady-state and transient conditions. Load models are mainly used to recreate the system's conditions for analysis or to predict its response during specific disturbances. However, there is an imperative need from both the research community and industry for accurate load modelling, since loads are constantly evolving and changing [107]. The main issue is that still there is not a standard load model available, which can be used in the analyses, contingency assessments and power system models [89]. For example, a certain load model can be found adequate for specific dynamic analyses of the power system, but inaccurate for other purposes. Therefore, several load models have been proposed according to the load composition and behavior [108], [109]. Here, the static and dynamic load models utilized to study the impact of the non-linear loads on the WAC performance are presented. It is important to mention that in this thesis, "static load" refers to time-invariant voltage-depended loads.

3.5.1 Exponential Load Model

The exponential load model is actually one of the most commonly used static load models, which means that its active and reactive power is a time-invariant function of the voltage and/or the frequency [110]. The important feature of this model is that it can be set to represent all the main load characteristics, namely: constant power, constant current, and constant impedance. This can be achieved by setting the active and reactive exponents (n_p and n_q) in (3.6) and (3.7) equal to 0, 1 and 2 respectively.

$$P = P_0 \left(\frac{V}{V_0} \right)^{n_p} \tag{3.6}$$

$$Q = Q_0 \left(\frac{V}{V_0} \right)^{n_q} \tag{3.7}$$

where V, P and Q stand for the positive sequence voltage, the active power and the reactive power of the load respectively. Note also that V_0, P_0 and Q_0 are the initial values of these quantities.

3.5.2 Exponential Dynamic Load Model

To include time dependency in the static exponential load model (in other words, dynamics) the following model is considered, which is actually based on the dynamic load model proposed in [111].

$$P(s) = P_0 \left(\frac{V}{V_0} \right)^{n_p} \frac{1}{1+T_p s} \tag{3.8}$$

$$Q(s) = Q_0 \left(\frac{V}{V_0} \right)^{n_q} \frac{1}{1+T_q s} \tag{3.9}$$

where T_p and T_q are the recovery time constants for the active and reactive power, respectively.

3.5.3 ZIP Load Model

ZIP load model is expressed by a second order polynomial, which is depended on the constant impedance (Z), constant current (I) and constant power (P) characteristics, as Fig. 3.9(a) illustrates [112]. Therefore, it can be implemented by utilizing three exponential load models where each one will have exponents going from 2 to 0, respectively. It is also

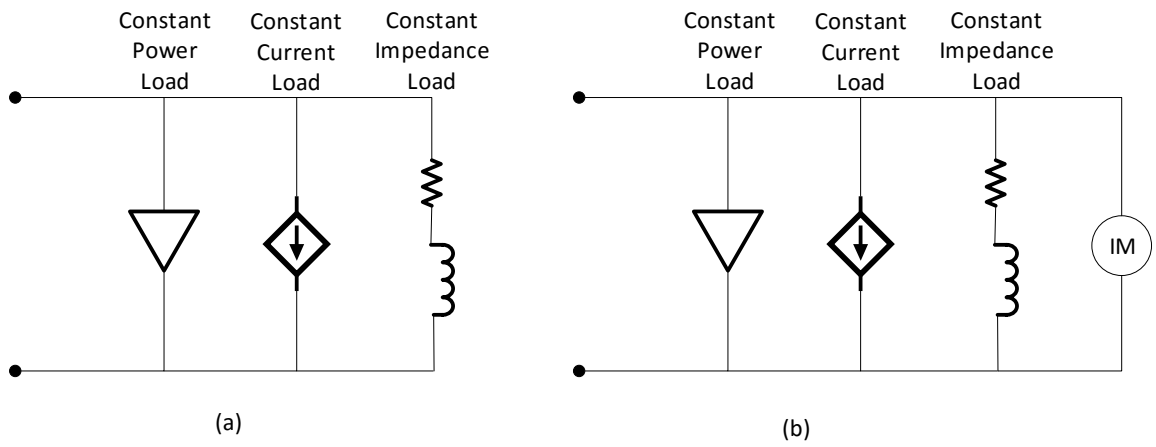

Fig. 3.9 Illustration of the dynamic load models for the cases of: (a) ZIP and (b) ZIP-IM

noteworthy that this model utilizes relative participation coefficients (p_i and q_i) which are usually in the range of [0 1] and always have a total sum equal to unity [107]. These coefficients are considered in order to obtain a model which is a mixture of the three main characteristics.

$$P=P_0\left[p_1\left(\frac{V}{V_0}\right)^2+p_2\left(\frac{V}{V_0}\right)+p_3\right] \tag{3.10}$$

$$Q=Q_0\left[q_1\left(\frac{V}{V_0}\right)^2+q_2\left(\frac{V}{V_0}\right)+q_3\right] \tag{3.11}$$

3.5.4 ZIP-Induction Motor Load Model

As it can be seen from (3.10) and (3.11), the ZIP model is actually a static voltage-depended model. The dynamic load model (shown in Fig. 3.9(b)) can be obtained by combining the static ZIP model in parallel with an induction motor (ZIP-IM) [89]. More specifically, the fourth order model of the induction machine is utilized as the dynamic part of the load. Therefore, (3.10) and (3.11) change into the following form:

$$P(s)=P_0\left[p_1\left(\frac{V}{V_0}\right)^2+p_2\left(\frac{V}{V_0}\right)+p_3\right]+P_{IM} \tag{3.12}$$

$$Q(s)=Q_0\left[q_1\left(\frac{V}{V_0}\right)^2+q_2\left(\frac{V}{V_0}\right)+q_3\right]+Q_{IM} \tag{3.13}$$

where P_{IM} and Q_{IM} are the active and reactive power consumption of the induction motor.

CHAPTER 4
WIDE AREA CONTROL DESIGN AND PERFORMANCE EVALUATION

This chapter presents the methodology for the implementation of a conventional wide area controller as proposed in [39], which will be utilized further on to identify the factors that affect its performance and to be enhanced in terms of robustness and effectiveness. In addition, several disadvantages of the adopted methodology will be presented here as well, having as a goal to address them in the next chapters. Furthermore, this chapter shows the mathematical background of the evaluation method considered for assessing the WAC performance in this work.

4.1 Models Necessary for the Wide Area Control Design

The model of the synchronous generator is vital for the WAC implementation, since a hierarchical wide area controller is primarily controlling the generators through their local controllers. Amongst the various models of the generators, the fourth order model, expressed in the local *d-q* frame is found sufficient for WAC design [113]. Equations (4.1) and (4.2) describe the relationship between the stator currents (i_d and i_q), the internal voltages (e_d and e_q) and the field (e_{fd}) voltages, while (4.3) and (4.4) represent the swing equation of the i^{th} generator [114]:

$$T'_{doi}\dot{e}'_{qi} = -e'_{qi} - (x_{di} - x'_{di})i_{di} + e_{fdi} \tag{4.1}$$

$$T'_{qoi}\dot{e}'_{di} = -e'_{di} + (x_{qi} - x'_{qi})i_{qi} \tag{4.2}$$

$$\frac{2H_i\omega_{pui}}{\omega_s}\frac{d^2\delta_i}{dt^2} + \frac{D_i\omega_{pui}}{\omega_s}\frac{d\delta_i}{dt} = P_{mi} - P_{ei} \tag{4.3}$$

$$P_{ei} = v_{di}i_{di} + v_{qi}i_{qi} \tag{4.4}$$

where T'_{do} and T'_{qo} stand for the open circuit constants, while x_d, x_q, x'_d and x'_q are the generator's synchronous and transient reactances, all expressed on the local *d-q* frame. P_m and P_e represent the mechanical and electrical power. ω is the rotor speed, while ω_s is the synchronous speed. Lastly, H, D and δ stand for the generator's inertia constant, its damping coefficient and power angle, respectively. All the quantities are in per unit, except the time constants which are in seconds and the power angle in radians.

In addition, it is important to have equations which connect the terminal voltage and stator currents of the generator to its internal voltages, since the PMU can provide measurements concerning only the former two. Equations that contain the terminal voltage of the generator expressed on the *d-q* axis (v_d and v_q), are the following stator dynamic equations:

$$v_{di} = e'_{di} - r_{si} i_{di} + x'_{qi} i_{qi} \tag{4.5}$$

$$v_{qi} = e'_{qi} - r_{si} i_{qi} - x'_{di} i_{di} \tag{4.6}$$

where r_s stands for the stator resistance in per unit.

Generators utilize local controllers (i.e., exciter and governor controllers) to compensate local disturbances, but when inter-area oscillations occur, their lack of global observability makes them unable to react effectively. Therefore, WAC aims to enhance their operation by providing suitable coordination signals to their local control inputs. Thus, it is important to know the types of the local controllers used in the system, in order to identify correctly their local control inputs. This work considers the exciter DC2A and the general purpose governor [93], [114]. Their respective local control inputs, which the wide area controller will interact with, are the excitation signal (e_{fd}) and the steam valve output (P_{GV}). The governor, in contrast to the exciter (which is directly attached to the generator), connects to the generator through the turbine. Thus, the following model of the turbine is additionally needed for deriving the governor's WAC signals, since it connects the governor's P_{GV} with the generator's mechanical power (P_m):

$$P_m = \frac{1}{1 + sT_{CH}} \frac{1 + sT_{RH} F_{HP}}{1 + sT_{RH}} P_{GV} \tag{4.7}$$

where T_{CH} represents the delay due to the steam chest/inlet piping, T_{RH} stands for the delay of the re-heaters and F_{HP} is the total turbine power developed in the high-pressure cylinder. The delays are expressed in seconds and the power in per unit.

Finally, the model of the power network is required as well. The interconnection of the transmission system can be represented by two current equations, depending on whether the system's nodes are generator or generator-free buses ((4.8) and (4.9) respectively). Index *m* refers to the total number of the system's buses. G', B' stand for the real and imaginary elements the bus admittance matrix elements.

$$\frac{-1}{jx_{di}^{'}}(e_{di}^{'}+(x_{qi}^{'}-x_{di}^{'})i_{qi}+je_{qi}^{'})e^{j(\delta_i-\pi/2)}+\sum_{k=1}^{m}(G_{ik}^{'}+jB_{ik}^{'})v_k e^{j\theta_k}=0 \quad (4.8)$$

$$\sum_{k=1}^{m}(G_{ik}^{'}+jB_{ik}^{'})v_k e^{j\theta_k}=0 \quad (4.9)$$

4.2 Formulation of Wide Area Control Signals

The reasons that led to the selection of the wide area controller of [39] to be examined and advanced in this Ph.D. dissertation are firstly its important advantage of decoupling each generator's dynamics from the remaining generators (introducing that way a method to distinguish the perturbation terms from the local terms) and secondly the development of nonlinear decoupling control based on input-output linearization control. The main idea of the methodology in [39] is firstly to reformulate the power system into a closed form and then to perform a change of variables in order to obtain a new state space representation of the power system. These new dynamic equations will have as state variables the terminal voltages of the generators, expressed in their local *d-q* frame (v_d and v_q). Actually, the main goal of the methodology is to develop coordination signals which explicitly cancel out all the interactions (perturbation terms) between the generators of the system, thus increasing the damping performance of the local controllers. Note that the measurement signals required by this methodology are the generator's terminal voltage, its frequency and its power angle.

The following three steps summarize the method's procedure:

1) The voltages of the generator-free buses are expressed in terms of the generators' terminal voltages (v_d and v_q) through (4.8)-(4.9).

2) The internal voltage (e_d and e_q) and stator current (i_d and i_q) of each generator are expressed in terms of its terminal voltage (v_d and v_q) by utilizing (4.5), (4.6) and (4.8).

3) The derived expressions of the internal voltage and stator current are replaced in the generator model and swing equation ((4.1)-(4.4)).

The result of applying these steps are the i^{th} generator's dynamic equations for the terminal voltage and rotor speed:

$$\dot{v}_{di}=a_{1i}v_{di}+a_{2i}v_{qi}+p_{1i}e_{fdi}+\psi_{di} \quad (4.10)$$

$$\dot{v}_{qi} = b_{1i} v_{di} + b_{2i} v_{qi} + p_{2i} e_{fdi} + \psi_{qi} \tag{4.11}$$

$$\frac{2H_i \omega_{pui}}{\omega_s} \frac{d\omega_i}{dt} + \frac{D_i \omega_{pui}}{\omega_s} \frac{d\delta_i}{dt} = P_{mi} - G_{ii}{}^{f} (v_{di}^2 + v_{qi}^2) - \psi_{\omega i} \tag{4.12}$$

where a_1, a_2, b_1, b_2, p_1, p_2 are parameters which depend on the elements of the admittance matrix and the parameters of the generators, resulting from the reformulation of the power system into a closed form. ψ_d, ψ_q and ψ_ω are the coupling perturbation terms (or inter-generator interactions) from other generators on the i^{th} generator, which mainly depend on the terminal voltages of the former. Detailed expressions of all these terms are provided in [39].

Furthermore, the formulation of the wide area control signals derives from the replacement of v_d, v_q and ω in the dynamic equations by their error compared to their steady-state values (dv_d, dv_q and de_ω). This change of variables is required in order to cancel out the WAC contribution when the system is in steady-state. The main idea is to differentiate the resulting dynamic expressions until the local controllers' inputs (e_{fd} and P_{GV}) appear in the equations (application of input-output linearization). Then, these control inputs are decomposed into local and global signals, where the global signal expressions (which actually derive from the wide area controller) are chosen to explicitly cancel out all the perturbation terms of the dynamic equations (ψ_d, ψ_q and ψ_ω). Looking at (4.10)-(4.12), one can note directly the existence of the excitation signal (e_{fd}); but not the steam valve output (P_{GV}). In this case, the turbine model of (4.7) is required to be utilized, in order to bring forth the P_{GV} in (4.12) through P_m.

In addition, from (4.10) and (4.11), it is evident that the exciter's local control input appears in both dynamic equations. Thus, their combination is utilized to find a common global control input, which cancels both perturbation terms (ψ_d and ψ_q). This is achieved through $dv_t^2 = dv_d^2 + dv_q^2$, which is essentially an expression for the terminal voltage deviation

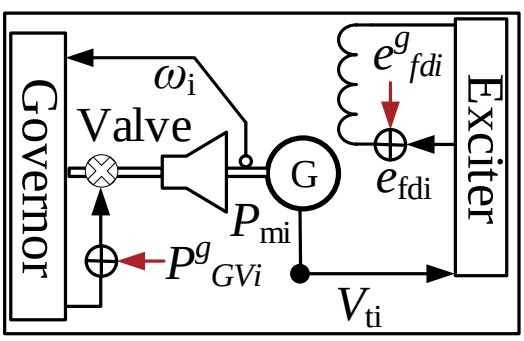

Fig. 4.1 Application of conventional WAC signals for coordination of exciter and governor local controllers.

(dv_t) in terms of its *d*-*q* components. The following set of equations shows the resulting wide area control signals for the coordination of the exciter and governor. Fig. 4.1 illustrates the application of the coordination signals of (4.13)-(4.14), on the respective local control inputs. An analytical description of their development, along with full expressions of all the reported parameters is presented in [39].

$$e_{fdi}^{g} = -\gamma_i \frac{(\psi_{dv_d}^{i} dv_{di} + \psi_{dv_q}^{i} dv_{qi})}{p_{1i} dv_{di} + p_{2i} dv_{qi}} \tag{4.13}$$

$$p_{GVi}^{g} = -\gamma_i \frac{T_{CH} \dot{\psi}_{\omega}^{g} + \psi_{\omega}^{g}}{F_{HP}} \tag{4.14}$$

where γ_i is a constant parameter, required for the regulation of the WAC contribution.

4.3 Disadvantages Identified

Although the WAC design procedure of [39] is a well-defined and effective methodology (due to the reformulation of the power system into a suitable, closed form and the model-based decoupling nonlinear control), it still has some severe drawbacks which need to be addressed. First of all, as it is aforementioned, the adopted methodology requires the generators' terminal voltages (v_t), their frequencies (f) and their power angles (δ). In [39], it is assumed that all three quantities can be provided by the measurement infrastructure, but this statement is valid only for the terminal voltage and frequency, since most of the commercial PMUs cannot measure the rotor angle directly.

The second drawback concerns the assumption that all the generator buses have PMUs installed and able to provide all the required measurements. However, until now this is not a realistically feasible scenario due to the high cost of the PMUs, which are placed only on selected buses in order to make the system observable. The third drawback that arises is due to scalability issues of the methodology. In large power systems, the required PMU number (and therefore the number of the WAC inputs) will increase substantially. This will have as a result for the output signals of the method to increase as well, since one PMU installed at a generator bus corresponds to two feedback control signals (exciter and governor) which need to be derived for its coordination.

The last issue is about the fact that the adopted method considers a constant weighting factor (γ_i) for the tuning of the WAC contribution (refer to (4.13)-(4.14)), which is set by the WAC designer. However, the optimal value of this parameter varies from system to system

and according to the nature of the contingency. For example, in the case studies of Chapter 5 considering the IEEE 9-bus and 39-bus dynamic test systems, γ_i is equal to 0.25 and 0.15 respectively for all the WAC signals. In the same manner, γ_i is selected to be equal to 0.15 in [39], where it is stated that it has been found through trial-and-error approach. Therefore, by selecting a constant weighting factor, which corresponds "well" for the majority of the disturbances, does not ensure high WAC performance at all times.

Methods to address each one of the aforementioned disadvantages are developed in the context of this Ph.D. dissertation in order to advance the robustness and applicability of the adopted methodology to a new level.

4.4 Prony analysis

For evaluating the WAC damping capability in this thesis, the Prony analysis has been adopted. Prony analysis is a widely known, measurement-based method suitable for ringdown analysis and small-signal properties' estimation [2], [115]. More specifically, this method is actually a parametric identification procedure, which aims to fit a linear combination of damped exponential terms to a uniformly sampled signal as Fig. 4.2 denotes [116]. The aim of the analysis is to find the frequency, damping (σ), phase (φ) and magnitude (A) of each term i composing the original time-domain signal, according to the selected model order (p) [117]. The advantages of utilizing this method are that it is not a model-depended procedure (therefore, there is no need for accurate modelling of the power system) and it provides accurate mode estimation since it utilizes the actual response of the system [118]. Its only drawback is that it can be affected by the presence of noise in the measurements and thus proper preprocessing of the signal is required [119] The following equation shows the linear approximation ($\hat{y}$) of the original signal (y) by exponential terms:

$$y \approx \hat{y} = \sum_{i=1}^{p} A_i e^{\sigma_i t} \cos(2\pi f_i t + \varphi_i) \tag{4.15}$$

Prony analysis is extensively used in the studies of well-established organizations, such as in the recent reports of ENTSO-E for analyzing the inter-area oscillations [9]. Furthermore, it has been considered in the available literature mainly to identify the dominant modes of the system [116]. In [120], the Prony analysis is considered as a distributed optimization problem in order to derive a distributed algorithm for the estimation of the electromechanical modes in large power systems. A methodology for identifying the dominant low-frequency modes of the system according to their energy content is proposed

in [118]. Another mode identification procedure, which utilizes a modified Prony method and the selection of the model order, is presented in [117].

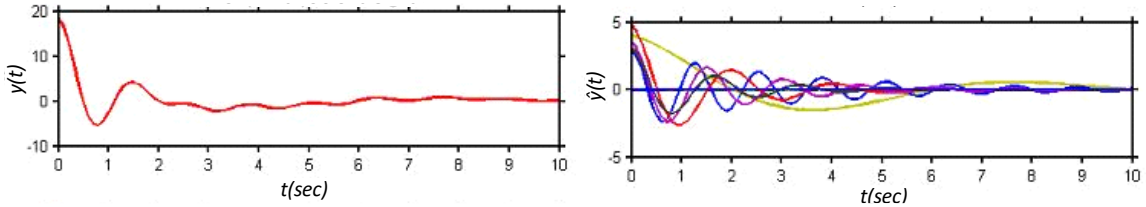

Fig. 4.2 Examples of: (a) the original signal y and (b) the damped exponential terms (resulted from the Prony analysis) utilized to construct the approximation $\hat{y}$.

Therefore, the procedure followed in this thesis is that at the end of every simulation, measurements are collected from the system, they are preprocessed and then they are fed to the Prony method for extracting the damping ratio (ζ) and frequency (f) of all the dominant modes (local and inter-area). The dominant modes are estimated through their energy content [118] and their constant appearance independently of the selected model order [117]. Note that a higher damping ratio means a better WAC performance.

4.5 Conclusions

This chapter has presented the step-by-step procedure to derive the conventional wide area controller which will be adopted in the next chapters for: (1) identifying the potential threats to the WAC performance and (2) advancing the WAC robustness and effectiveness. The wide area controller of [39] was chosen for this task (instead of other methods) due to two main reasons. The first one considers the decoupling of each generator's dynamics from the remaining generators, while the second one involves the development of nonlinear decoupling control signals based on input-output linearization control method. Furthermore, the disadvantages of the adopted method were also identified here, having as an objective to compensate them accordingly in the following chapters. These include the assumption of acquiring the generator's rotor angle as a synchronized measurement, the assumption of having PMUs installed on all the generator buses, its scalability issues and finally, the utilization of a constant weighting factor for the tuning of the WAC contribution. For evaluating the performance of the wide area controllers in the following chapters, the Prony analysis tool has been introduced here which will provide the damping ratios of the dominant modes.

CHAPTER 5
INVESTIGATION OF POTENTIAL FACTORS INFLUENCING THE WAC PERFORMANCE

In this chapter, potential threats which might be able to affect the WAC operation are presented, simulated and examined. More specifically, the factors considered here are: the measurement errors (steady-state and dynamic), the data delays/dropouts, the system parameter uncertainties, the unreported topology changes and the dynamic load penetration. The objective of this section is to assess the damping capability of the WAC in the presence of each factor, in order to identify which ones have to be compensated for enhancing significantly its robustness. It is important to be mentioned here that in order for the wide area controller to operate successfully, it must be able to compensate both local and inter-area oscillations at all times. Therefore, for their graphical illustration, the terminal voltage of the generators is utilized to visualize the local signal, while the speed difference of two distant generators is considered to follow the inter-area oscillation damping.

5.1 Effect of Measurement Errors on WAC Performance

This subchapter aims to illustrate the effect that the presence of measurement errors can have on the wide area controller performance. The impact of the measurement errors (due to the measurement chain of Fig. 3.3) on the WAC operation will be evaluated through simulations based on the IEEE 39-bus dynamic test system. The measurement errors are simulated by utilizing (3.1)-(3.5) in combination with the PMU steady-state and dynamic errors according to the prevailing system conditions. Since the rotor angle is also one of the required measurements, the synchrophasor-based expression proposed in Chapter 8 is adopted here, in order to have all the WAC inputs deriving from measurement chain. Therefore, the error in δ results actually from the propagation of all the measurement errors considering the magnitude/phase measurements of the voltages and currents which are utilized to estimate δ.

As aforementioned the vast majority of the published studies that do consider measurement errors, take into account only the steady-state PMU errors, ignoring their substantial increase during transient conditions [88] and the existence of instrument transformers in the measurement chain. As a first step, these specific unrealistic errors are

considered here and in [24] in order to evaluate the impact of the commonly used PMU steady-state errors on the WAC operation. For this purpose, a disturbance is applied at t=3 s and more specifically, a line trip of the line connecting buses 6 and 11. The simulation results are illustrated in Fig. 5.1, where the generator 10 (G10) terminal voltage is utilized to follow the local damping, while the speed difference of generators G7 and G10 detects the compensation of inter-area oscillations. According to Fig. 5.1, it can be noted that the inclusion of PMU steady-state measurement errors has a negligible effect on the WAC damping capability. This result is reasonable, since the PMUs have small steady-state errors as TABLE 3.2 denotes. It is worth mentioning here that "ideal damping" refers to the case where none of the under investigation factors takes place.

However, as it was analytically presented in subchapter 3.2 and in [23], the consideration of PMU steady-state measurement errors only is far from the actual conditions which take place in the measurement chain. For this reason, the VT and CT errors (TABLE 3.1) need to be included as shown in (3.1)-(3.5). Furthermore, it is essential to apply also

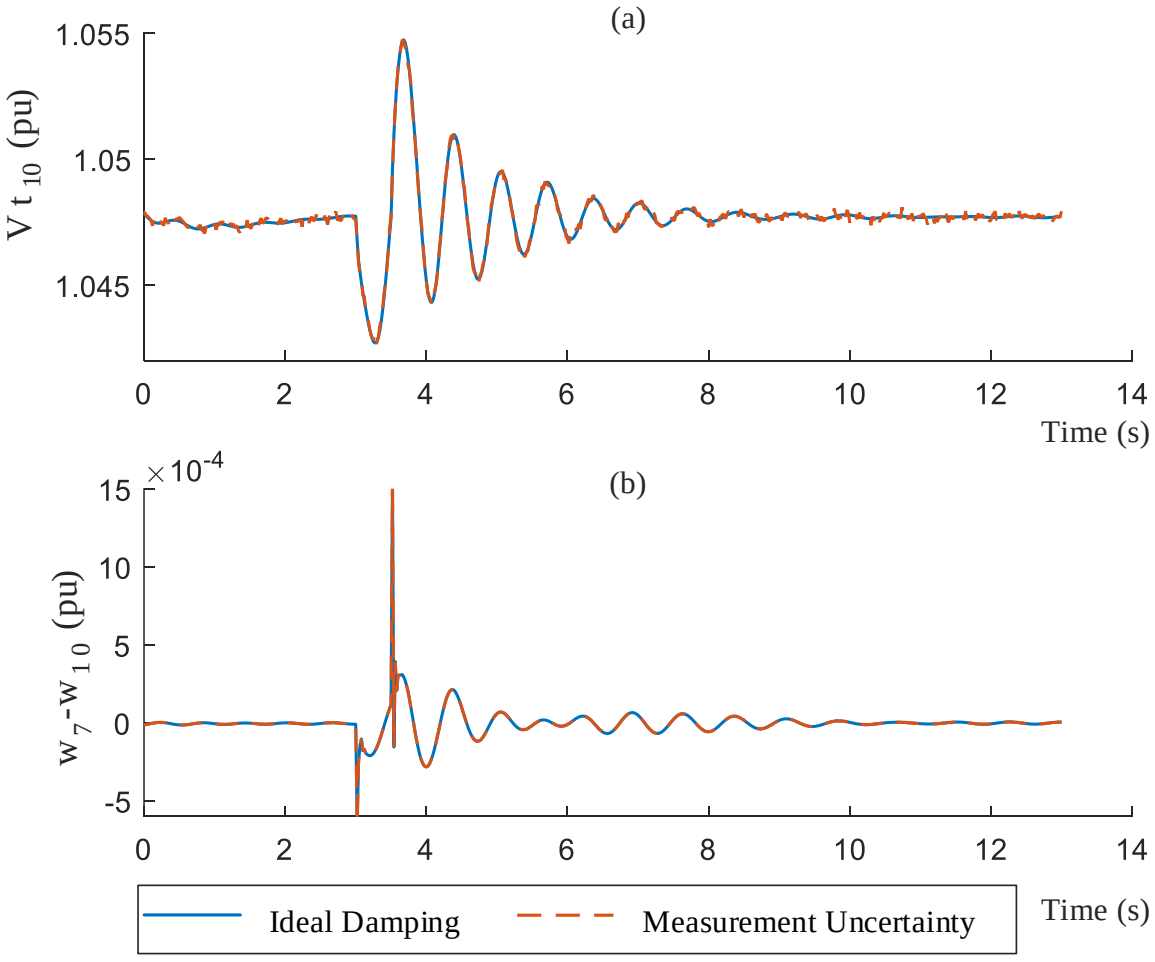

Fig. 5.1 System performance comparison between ideal damping and WAC with PMU steady-state measurement errors for the cases of: (a) local oscillation of the terminal voltage of G10, and (b) inter-area oscillation between G7 and G10.

appropriately the PMU dynamic measurement errors, since they increase substantially during transient conditions. For the latter, a step-by-step procedure is presented in subchapter 3.2 which must be followed here. The PMU performance class utilized in the WAC applications is the M-class that is intended for analytic measurement applications. Thus, the M-class dynamic requirements will be utilized to find the dynamic measurement errors [88].

Next, the disturbance to be applied needs to be selected, in order to visualize the input measurement signals to the PMU from the instrument transformers (v_{VT}, i_{CT}). This step is required, since different fault types produce different measurement signals, meaning that for each fault type appropriate dynamic errors will need to be applied according to the most suitable dynamic compliance requirements of [88] (i.e. modulation signal test, the frequency ramp test, and the input step change test). The adopted WAC methodology has been modified to require only voltage and current measurements from all the generators of the system, through the synchrophasor-based expression for the rotor angle (Chapter 8). Therefore, it is necessary to visualize these signals under the event of the selected disturbance. The contingency considered here is a 5-cycle three-phase grounded fault occurring on the line connecting bus 15 to bus 16 of the IEEE 39-bus dynamic test system. Fig. 5.2 presents the voltage and current of generator G2 during the fault. Note that the measured voltages and currents from all the generators of the system have a similar form to the ones of G2. The resulted signals indicate that the voltage behaves like a stepped signal after the occurrence of the fault, while the current can be viewed as a modulation signal. Therefore, the dynamic

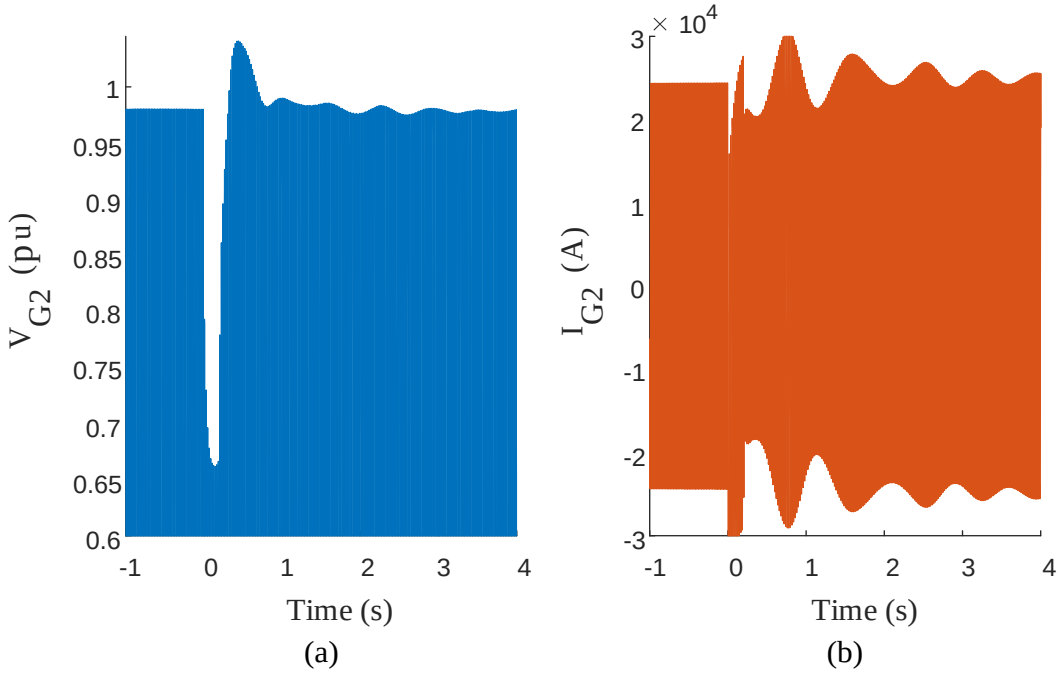

Fig. 5.2 Measurement signals from G2 during a fault: (a) voltage measurements and (b) current measurements.

TABLE 5.1: PMU MAXIMUM ERRORS UNDER DYNAMIC CONDITIONS ACCORDING TO [88] AND FIG. 5.3.

Signal Type	Max TVE (%)	Magnitude (%)		Phase Angle (degrees)		Frequency (Hz)		Time Interval (s)
Voltage	8	$e_{PMU}^{v\max}$	± 5.4	$e_{PMU}^{\theta v\max}$	± 3.3	$e_{PMU}^{f\max}$	± 0.3	0.07
	12	$e_{PMU}^{v\max}$	± 6.2	$e_{PMU}^{\theta v\max}$	± 4.58	$e_{PMU}^{f\max}$	± 0.3	0.07
Current	3	$e_{PMU}^{i\max}$	± 1.6	$e_{PMU}^{\theta i\max}$	±1.44255	$e_{PMU}^{f\max}$	± 0.3	3

compliance requirements for the input step change and the modulation signal tests need to be utilized as the dynamic measurement errors of all the voltage and current measurements, respectively. TABLE 5.1 presents the PMU maximum errors under dynamic conditions, according to the amendment of the IEEE Synchrophasor Standard C37.118.1-2011 [121]. Note that the time interval to return back to the steady-state errors (after the disturbance) is found through the response time requirement of [121] for the input step change test. In the case of the modulation signal test, the respective time interval is not defined in the Standard and therefore, it is taken as the duration until the magnitude deviation of the measured signal compared to its pre-fault value is lower than 0.1 pu. Regarding the TVE of the input step change test, the IEEE Synchrophasor Standard C37.118.1-2011 states that for a 10% change in the magnitude the TVE reaches 6%. Therefore, in this work since the voltage magnitude change is larger than 10% (Fig. 5.2), both 8% and 12% TVEs are considered.

However, the issue that arises here is how to obtain the appropriate measurement errors by knowing only the TVE, since the Standard defines the magnitude and phase errors only for the case of maximum TVE of 1%. TVE is an expression that indicates the difference between the theoretical (ideal) value of the PMU measurement compared with the actual one, all expressed in Cartesian coordinates. Thus, TVE comprises both the magnitude and phase errors and to obtain them the following expression needs to be considered for a range of measurement errors:

$$TVE(n) = \sqrt{\frac{(\hat{u}_r(n) - u_r(n))^2 + (\hat{u}_i(n) - u_i(n))^2}{(u_r(n))^2 + (u_i(n))^2}} \tag{5.1}$$

where $\hat{u}_r$ and $\hat{u}_i$ represent the real and imaginary parts of the actual measurement respectively, while u_r and u_i are the real and imaginary parts of the theoretical value, all defined at the instants of time n.

By solving (5.1) for the measurement error ranges of [0-7]% for the magnitude and [0-7]° for the angle the result of Fig. 5.3 is obtained. Note that for convenience and without

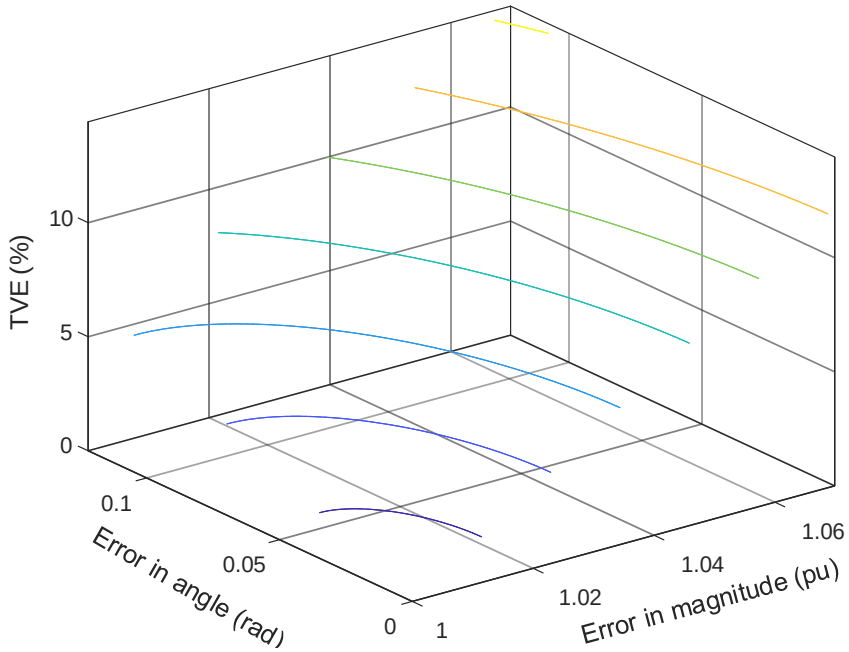

Fig. 5.3 TVE in percentage for phase errors [0-0.12] rad and magnitude errors of [0-7]%.

any loss of generality the ideal magnitude is taken to be 1 pu, while the ideal angle is 0°. Therefore, the measurement errors of TABLE 5.1 have been found through Fig. 5.3, while keeping in mind that the TVE is mainly dominated by phase errors for phase errors greater than 0.5°. The latter is defined in the IEEE Synchrophasor Standard C37.242-2013 [83].

The system's response has been evaluated under the scenarios where no WAC exists in the system (No WAC), the ideal error-free damping, when only the steady-state measurement errors (SSME) are considered, and the scenarios where the dynamic measurement errors (DME 1 and DME 2) occur during the disturbance (according to the data of TABLE 5.1). Note that DME 1 corresponds to the 8% TVE, while DME 2 represents the application of the 12% TVE. In both scenarios, the TVE on the current phasor measurements is kept to 3 % according to the dynamic compliance requirements for the modulation signal test.

Fig. 5.4 depicts the simulation results for the terminal voltage of G2 (v_2) and the speed difference between G7 and G10 (w_7-w_{10}). Based on these, it can be seen that the overall measurement error introduced by the measurement chain (in the case of both the steady-state only and the appropriate dynamic PMU measurement errors during the fault) has negligible effect on the performance of the wide area controller in compensating local and inter-area oscillations. This result can be further supported by the Prony analysis results of TABLE 5.2, where it is evident that the damping ratio is extremely close for each case for all the respective modes. The outcome of this case study illustrates clearly that if all the necessary

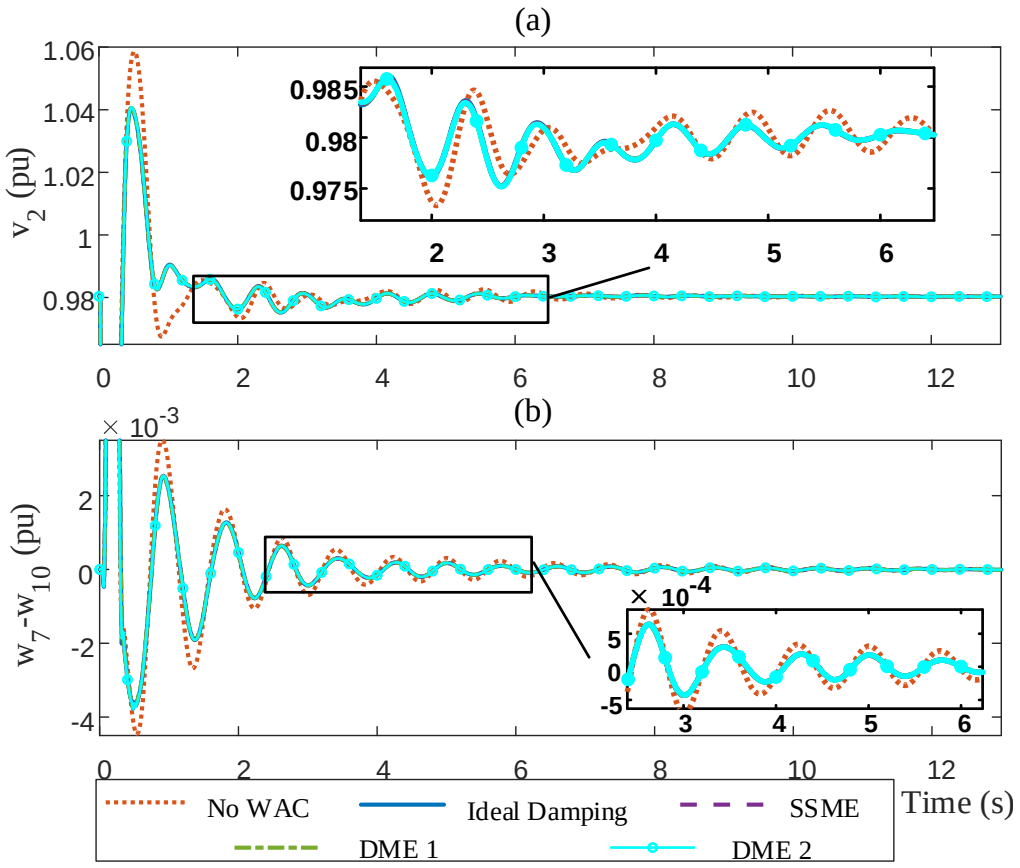

Fig. 5.4 Comparison of system's response between No WAC, Ideal Damping, WAC with steady-state measurement errors (SSME), WAC with dynamic measurement errors (DME 1) where TVE for voltage and current is equal to 8% and 3%, and WAC with dynamic measurement errors (DME 2) where TVE for voltage and current is equal to 12% and 3%. (a) Local oscillation of the terminal voltage of G2 and (b) the inter-area oscillation between G7 and G10.

TABLE 5.2: PRONY ANALYSIS FOR THE MEASUREMENT ERRORS

Type	**No WAC**		**Ideal Damping**	
	ζ(%)	*f*(Hz)	ζ(%)	*f*(Hz)
Local mode	5.58	1.2	18.25	1.2
Inter-area mode	29.9	0.71	38.3	0.69
Type	**SSE**		**DME 1**	
	ζ(%)	*f*(Hz)	ζ(%)	*f*(Hz)
Local mode	17	1.2	15.88	1.2
Inter-area mode	38.3	0.69	36.5	0.69
Type	**DME 2**			
	ζ(%)	*f*(Hz)		
Local mode	15.88	1.2		
Inter-area mode	36.5	0.69		

inputs are originated from PMUs, they can be used directly to the wide area controller without compromising the stability of the system.

5.2 Impact of Data Delays/Dropout and Measurement Errors

The objective of this subchapter is to study the WAC behavior when realistic delays and dropouts occur in the system. As mentioned in Chapter 3, the data delays utilized in this

Ph.D. dissertation are separated into the measurement infrastructure delays (measurement process delays plus communication delays) and the feedback delays (application delays plus feedback communication delays) for obtaining more realistic results. The former refers to the measurement delay from the PMUs to the wide area controller, while the latter stands for the control signal delay from the WAC system to the system's local controllers. As Fig. 5.5 denotes, the simulation here considers a two-level measurement infrastructure, where local PDCs exist on the first level and a regional PDC along with the WAC application are placed on the second level. Therefore, according to IEEE Synchrophasor Standard C37.118.2-2011 [99], the cumulative lower bound of the overall delay here is 50 ms. More specifically, it is reported in this standard that typical delays from a PMU to the Phasor Data Concentrator (PDC) are between 20-50 ms and each level above adds additional delays in the range of 30-80 ms. Thus, for the two-level communication infrastructure the overall delays should be in the range of 50-130 ms. However, as an upper bound instead of the 130 ms, a 250 ms delay is selected according to the relatively high delays reported in [79], in order to consider the worst case scenario in the simulation. Note also that the minimum delay of 50 ms agrees also with the measurement reporting latency compliance of [88] which is 5/(PMU reporting rate) for the M class PMUs. In this work, the reporting rate is chosen to be 100 phasors/second.

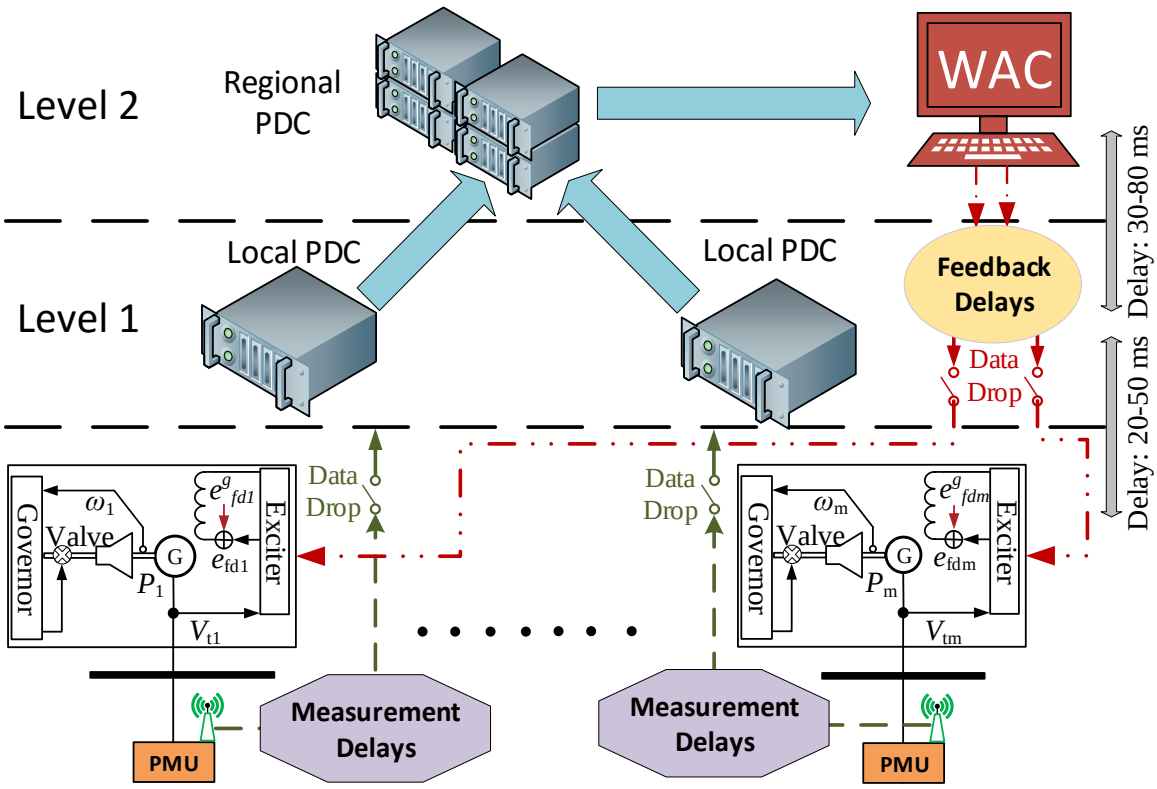

Fig. 5.5 Measurement infrastructure delays included for the data transfer between the PMUs, the local PDCs (Level 1) and the regional PDC/WAC (Level 2), and feedback delays from the WAC to the local controllers.

As it was aforementioned, the PDC concept is considered in this study in order to forward the PMU data to the wide area controller. The reporting rate of the PDC can be selected based on the range of the measurement infrastructure delays. More specifically, the minimum rate at which it can operate (in order to take into account the data delays of the measurements) is 50 ms. The problem that arises here is that at 50 ms very few measurements will be on time. Therefore, the "absolute wait time" concept of Chapter 3 (illustrated in Fig. 3.6) has been applied in the PDC. According to this, the time interval that the PDC can wait for the measurements to arrive is considered to be 20 ms. This is an extra time added to the minimum reporting rate (50 ms). Therefore, the "wait time" (and thus the maximum reporting rate of the PDC) is equal to 70 ms. In the case where all the measurements are received before the "wait time" expires, the PDC forwards them directly to the WAC. Data dropout occurs when the measurements are delayed more than 70 ms or if they are lost.

For simulating the measurement infrastructure delays and the feedback delays, three different Probability Distribution Functions (PDFs) are utilized in the delay models, where the effect of each PDF separately as well as their combinations are examined. It is worth noting here that the latter is actually one of the contributions of this subchapter and [23], as the usual case is to test the impact when a single PDF is used to simulate both, measurement infrastructure delays and the feedback delays. The PDFs considered in this Ph.D. dissertation are the uniform [36], Beta [100] and Gamma [101] distributions. Therefore, the first step is to examine the WAC performance when each PDF is used to simulate both, measurement infrastructure delays and feedback delays while data dropouts are neglected. Fig. 5.6 shows examples of the delay variations for the three PDFs. Note that the simulation considered the same test system and disturbance (hence the same dynamic measurement errors are utilized here) as the ones of subchapter 5.1. According to the results of Fig. 5.7 and TABLE 5.3, the inclusion of data delays reduces the performance of the wide area controller in compensating both local and inter-area oscillations. The significant decrease of the damping capability can be realized when the Prony analysis damping ratios of TABLE 5.3 are compared with the damping ratio of the "ideal damping" in TABLE 5.2. Looking at Fig. 5.7, it is worth noting that especially in the case of the uniform distribution, the WAC has been affected to the point where it is unable to damp effectively the power system oscillations. This is also evident when the local and inter-area damping ratios of the uniform distribution are considered (TABLE 5.3), which are lower than the No WAC scenario of TABLE 5.2. Therefore, dealing with the data delays is of a primary importance in order to ensure the smooth operation of the wide area controller.

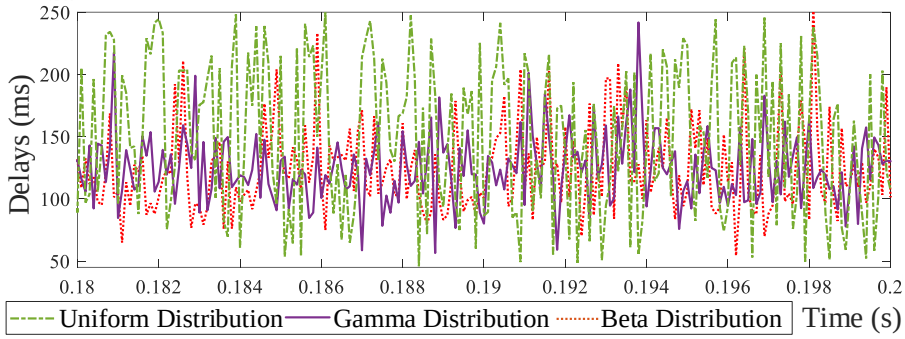

Fig. 5.6 Examples of the Uniform, Gamma and Betta communication delays.

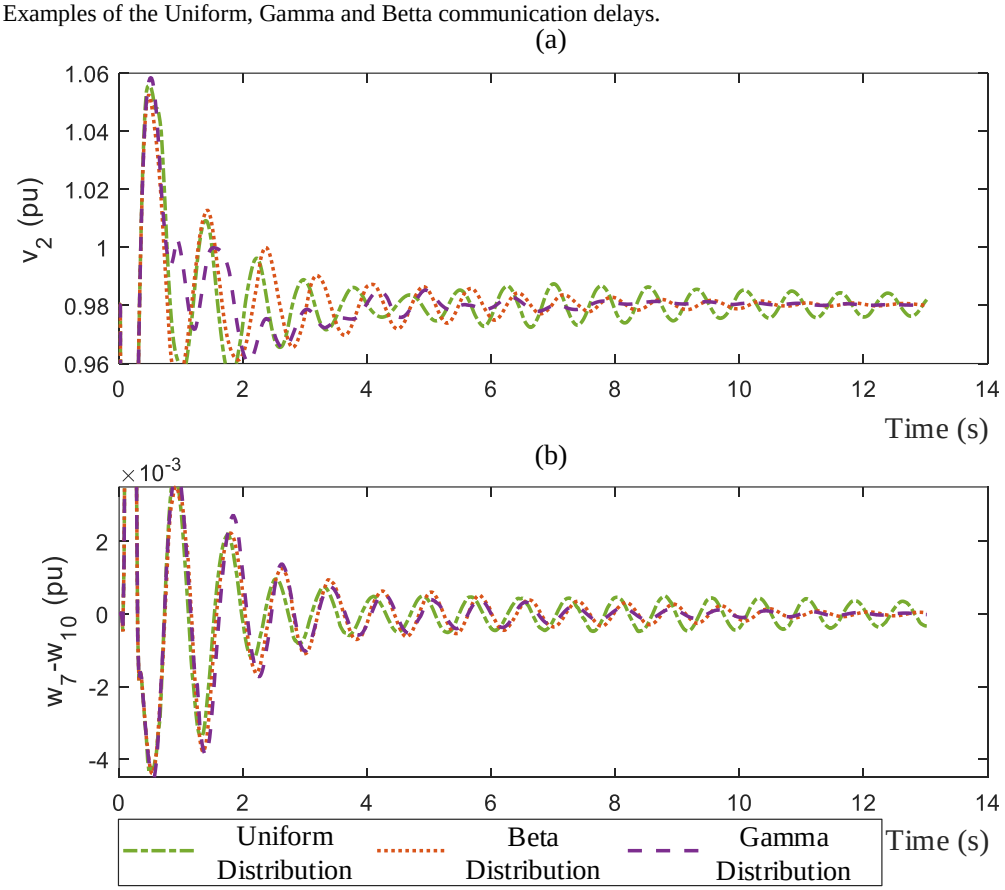

Fig. 5.7 Comparison of WAC performance when Uniform, Beta and Gamma delays occur, considering: (a) the local oscillation of the terminal voltage of G2, and (b) the inter-area oscillation between G7 and G10.

TABLE 5.3: PRONY ANALYSIS FOR THE DATA DELAYS

Type	Uniform Distribution		Beta Distribution		Gamma Distribution	
	ζ(%)	*f*(Hz)	ζ(%)	*f*(Hz)	ζ(%)	*f*(Hz)
Local mode	3.3	1.3	6.6	1.2	7.93	1.2
Inter-area mode	22.8	0.68	23.9	0.72	28.2	0.65

In terms of considering realistic conditions in the simulation, it is more appropriate to utilize one PDF to simulate the measurement infrastructure delays and a different one for the feedback delays, as suggested by the authors in [23]. More specifically, TABLE 5.4 summarizes the examined cases and the adopted parameters of the PDFs in each case. The

TABLE 5.4: EXAMINED CASES AND PDF PARAMETERS

Case	Measurement Delay Model	Feedback Delay Model
I	Uniform (max=250, min=50)	Gamma (x=30, y=3)
II	Uniform (max=250, min=50)	Beta (c=18, d=188)*

where x and y are the shape and scale parameters of the Gamma PDF, while c and d represent the first and second shape parameter for the Beta PDF.
*Note that the Beta PDF is in seconds, while Uniform and Gamma are in ms.

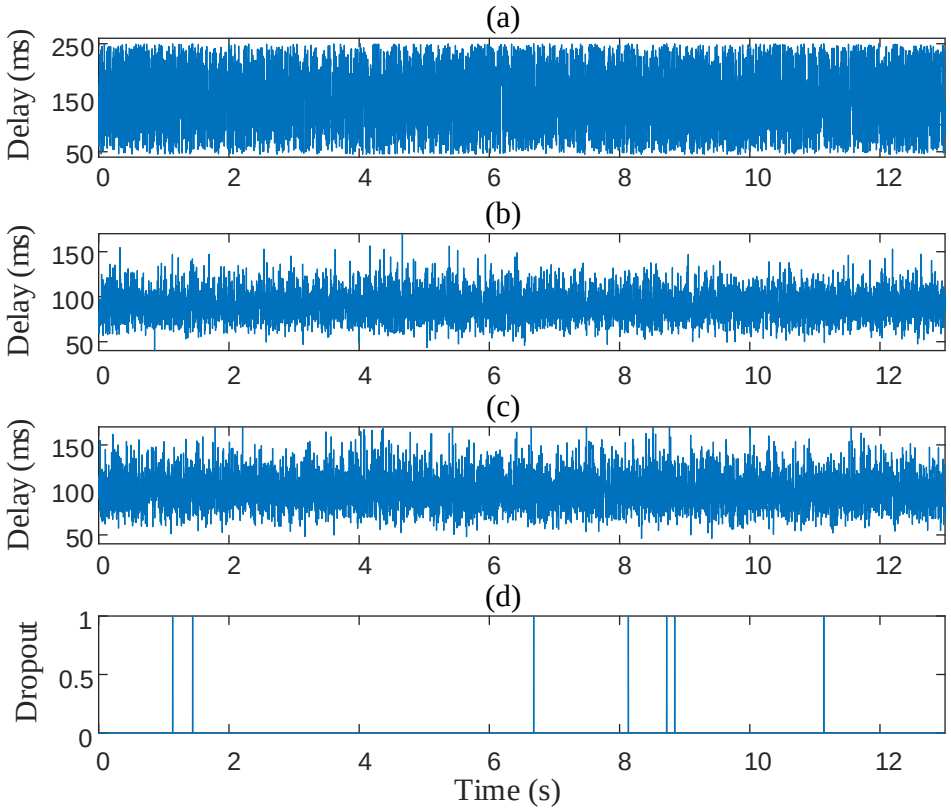

Fig. 5.8 (a) Uniform measurement delays, (b) Gamma feedback delays, (c) Betta feedback delays, and (d) data dropouts.

uniform distribution is utilized for modelling the measurement infrastructure delays, since various sources of delay exist in the communication path from the PMUs until the WAC. Beta and Gamma are used to model the feedback delays, as they are typical PDFs for simulating packet-based networks. Since both, measurement infrastructure delays and feedback delays utilize the communication infrastructure, data dropouts are considered to occur along with these delays. Fig. 5.8 illustrates examples of the measurement infrastructure delays (for one PMU) and feedback delays (for one control signal), along with the data dropouts considered in the simulation. Note that each PMU measurement and each feedback control signal experience different measurement infrastructure delays and feedback delays (respectively) by selecting different seed for the PDFs utilized in each case.

It is important to be mentioned that the innovation here is the investigation of the WAC behavior when realistic data delays and measurement errors occur simultaneously. Conversely, the majority of the works which investigate the effect of data delays on WAC

are either utilizing a simplified steady-state expression for the measurement errors or they do not consider them at all. However, in reality the data delays take place along with the overall errors of the measurement chain (which change during dynamic conditions). Therefore, the consideration of both in the simulation is essential for obtaining results that are more realistic. It is worth mentioning here that since there is no measurement procedure into the path of the feedback signal, a small Gaussian noise is considered along with the feedback delays to simulate the channel noise.

For the implementation of this case study, the same test system and disturbance as were described in subchapter 5.1 are considered. Therefore, the same dynamic measurement errors are applied here too. In this sense, the measurements in this case are affected by measurement errors, delays and dropouts. The negative effect of the delays and dropouts on the WAC performance is confirmed graphically and numerically through Fig. 5.9, Fig. 5.10 and TABLE 5.5. As shown, in all the examined cases, the data delays/dropouts can

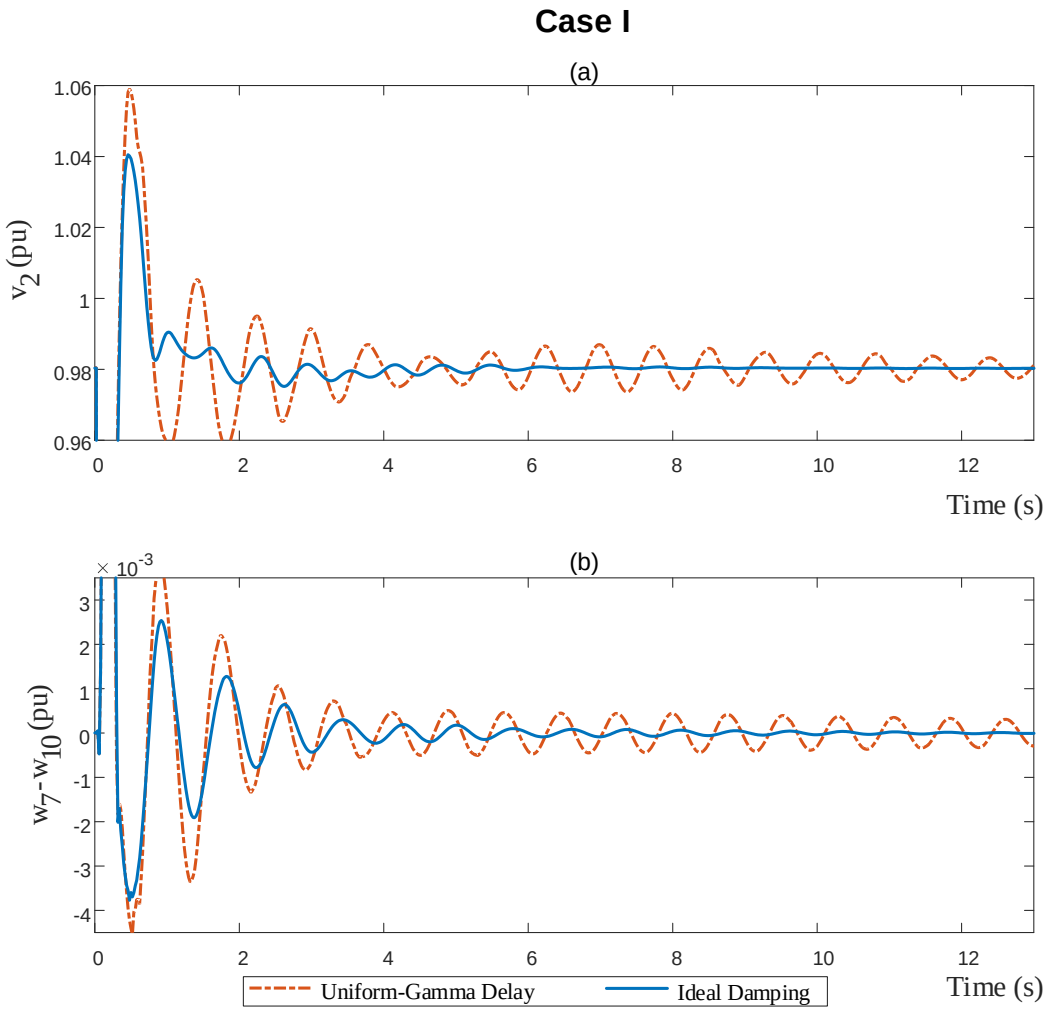

Fig. 5.9 Comparison of WAC performance when ideal conditions occur and when the Uniform-Gamma delays of Case I take place considering: (a) the local oscillation of the terminal voltage of G2, and (b) the inter-area oscillation between G7 and G10.

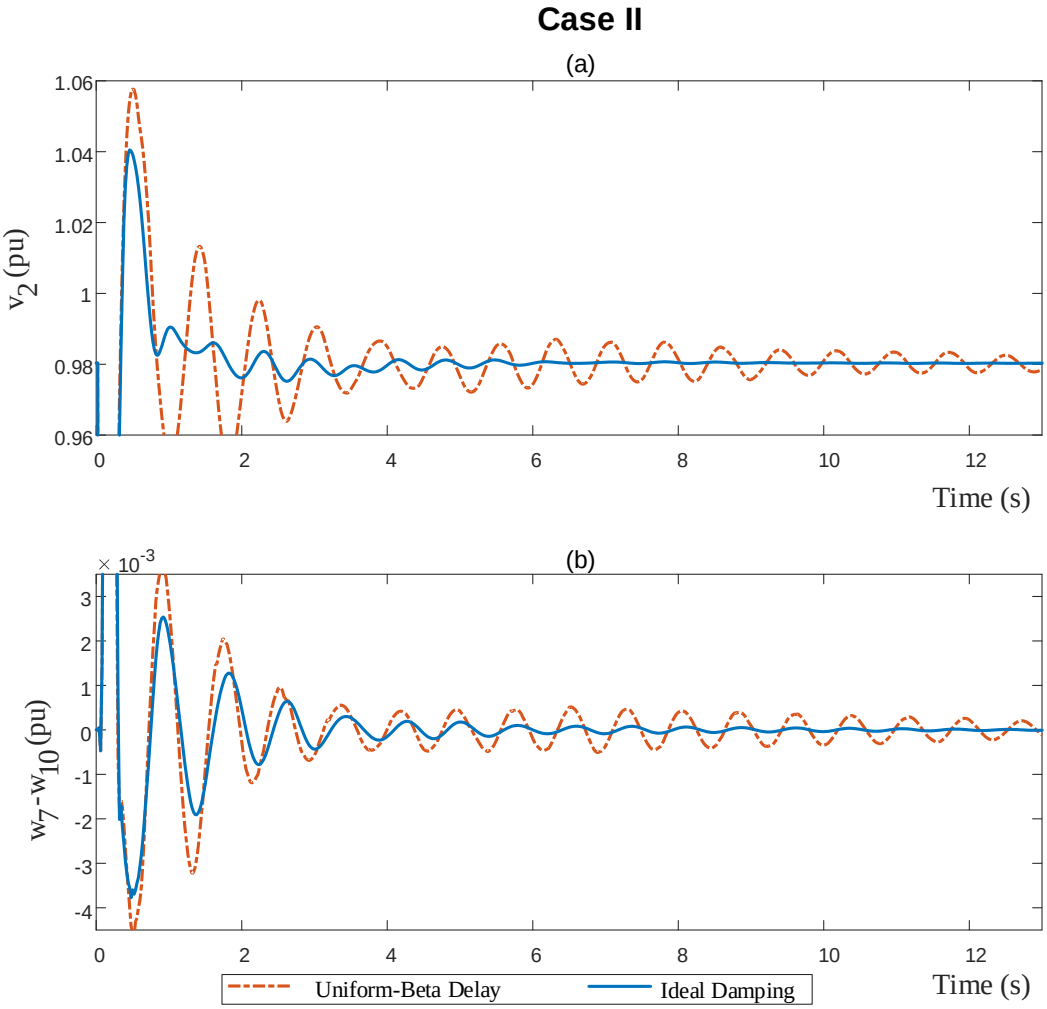

Fig. 5.10 Comparison of WAC performance when ideal conditions occur and when the Uniform-Beta delays of Case II take place considering: (a) the local oscillation of the terminal voltage of G2, and (b) the inter-area oscillation between G7 and G10.

TABLE 5.5: PRONY ANALYSIS RESULTS FOR THE DATA DELAYS OF CASES I-II

CASE I				
Type	**Ideal Damping**		**Uniform-Gamma Delay**	
	ζ(%)	*f*(Hz)	ζ(%)	*f*(Hz)
Local mode	18.25	1.2	2.93	1.3
Inter-area mode	38.3	0.69	21.2	0.69
CASE II				
Type	**Ideal Damping**		**Uniform-Beta Delay**	
	ζ(%)	*f*(Hz)	ζ(%)	*f*(Hz)
Local mode	18.25	1.2	2.61	1.4
Inter-area mode	38.3	0.69	21.5	0.70

deteriorate the damping capability of the wide area controller, leading the system even to instability. More specifically, Fig. 5.9 and Fig. 5.10 illustrate clearly that the WAC is unable to damp the local and inter-area oscillations in the presence of delays/dropouts. Note that this is also evident through the Prony analysis results of TABLE 5.5, where the damping ratios of the local and inter-area modes of Cases I-II are found to be lower than the No WAC

scenario of TABLE 5.2. Therefore, all the results indicate that the inclusion of a data delay compensator is essential for the WAC operation.

5.3 System Parameter Uncertainty

Commonly, various data considering the system parameters (such as the generator and the transmission line parameters) that are stored in the databases of the control centers, can be found to be different from the actual ones. The parameters of the transmission lines are usually calculated based on ideal conditions and manufacturer data, ignoring the various factors that can affect them such as mutual coupling of parallel lines, soil resistivity, and ambient temperature [122]. In addition to that, unreported and frequently neglected changes such as the connection or substitution of a line with an underground cable make the actual parameters to deviate even more compared to the stored ones. Studies have indicated that the difference between stored values and the actual ones can be as high as 30% of their nominal values [123]. For this reason, various methodologies have been proposed for estimating the transmission line parameters either through the use of PMU measurements [124] or by considering a combination of synchronized and conventional measurements [125]. For incorporating also the errors of instrument transformers and PMUs, in [126] a methodology is proposed for estimating the bounds of the obtained transmission line parameters. Since the WAC methodology presented in Chapter 4 requires the Y-matrix (through (4.8)-(4.9)) it is therefore important to identify the effect of considering erroneous line parameters instead of the actual ones when deriving the coordination signals, especially when this kind of errors can even affect the state estimator's performance [127].

Apart from the transmission line parameters, one can realize from the analysis presented in subchapter 4.2 that the derived coordination signals, are highly depended on the synchronous generator parameters. This is clearly visible when equations (4.1)-(4.6) are considered, but it is not very obvious in the case of the derived WAC signals of (4.13) and (4.14), where the generator parameters are actually included into the coupling perturbation terms (ψ_d, ψ_q, ψ_ω). In [128] it is noted that the data provided by the manufacturers can differ from the actual ones. This happens primarily because the manufacturer parameters are estimated through off-line experiments and do not correspond to the actual state of the generator when it operates, and secondarily because they refer to typical design guidelines of a range of available products.

Therefore, in this subsection, the wide area controller's performance has been tested in the presence of uncertainties on the transmission line and synchronous generator parameters stored in the algorithm. This information is useful especially for the electric

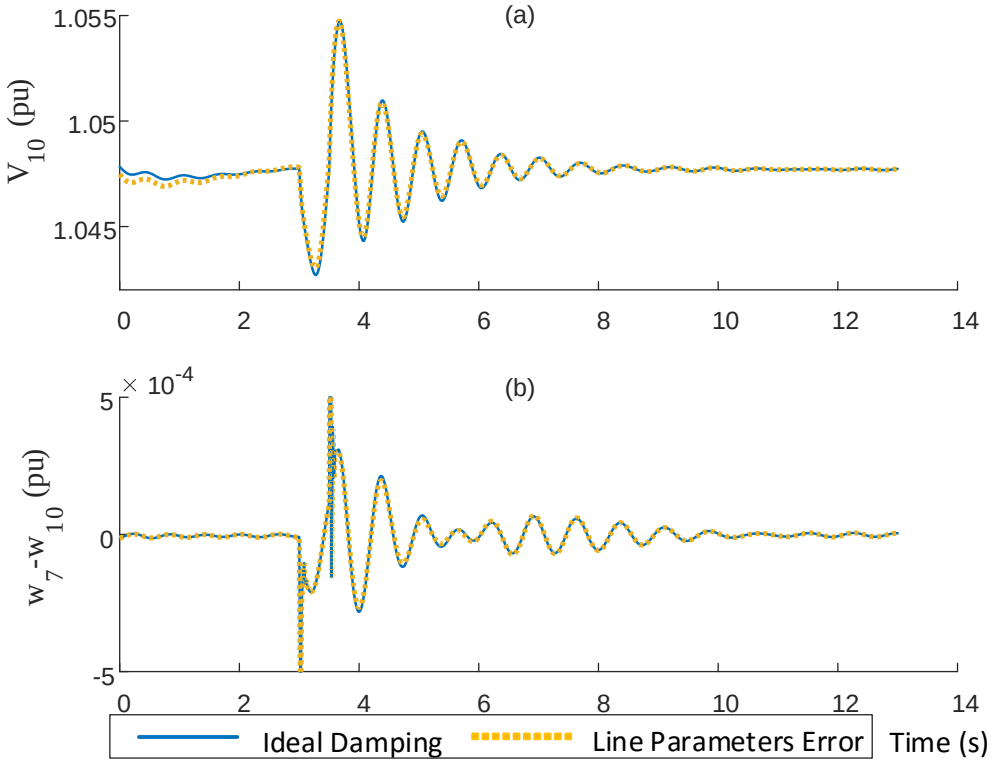

Fig. 5.11 WAC performance comparison between ideal damping and line parameters error for: (a) the local oscillation of the terminal voltage of G10, and (b) the inter-area oscillation between G7 and G10.

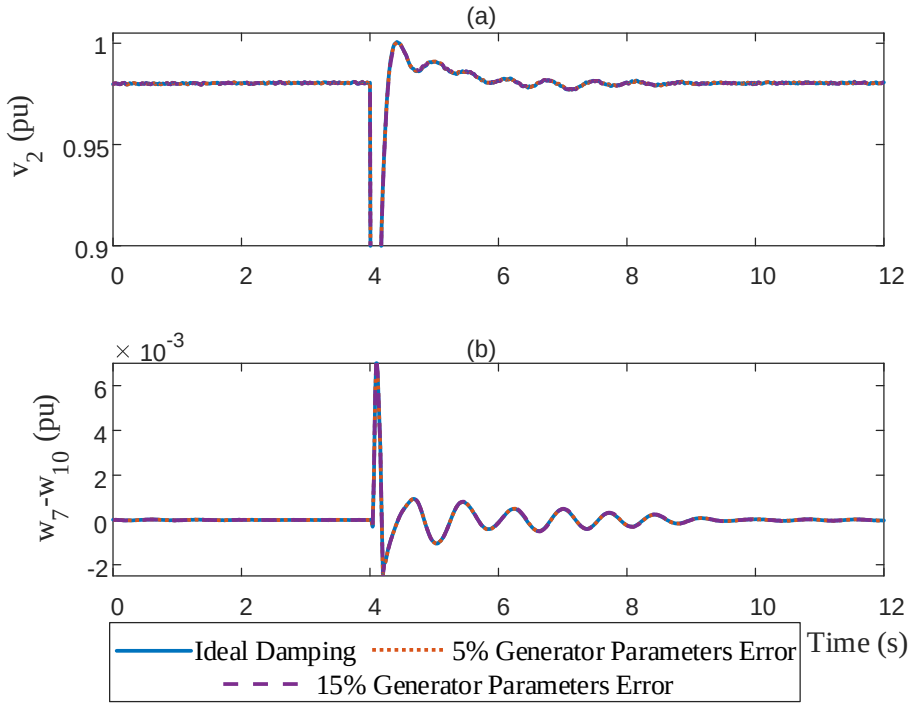

Fig. 5.12 WAC performance comparison between ideal damping and generator parameters error for: (a) the local oscillation of the terminal voltage of G2, and (b) the inter-area oscillation between G7 and G10.

utilities, to learn about the consequences on the WAC operation when an inaccurate model and parameters of the system are utilized. To investigate here and in [24] the impact of having an error in the line parameters, the parameter values of ten lines in total (five in one area and five in another area) of the system are increased by 30% from their nominal value. This change is applied to the resistance, reactance and capacitance of the line. The disturbance considered here is a line trip of the line connecting buses 6 and 11 at t=3 s. The simulation results are illustrated in Fig. 5.11, where it can be noted that the existence of line parameter errors does not have any impact on the WAC performance.

On a separate case study, the synchronous generator data are modified to deviate by 5%, which is approximately the greatest deviation reported in [128], and by 15% in order to consider a more extreme scenario. The synchronous generator parameters affected in this case are the open circuit time constants (T'_{do} and T'_{qo}), the synchronous reactances (x_d and x_q), and the transient reactances (x'_d and x'_q). As a disturbance, a 5-cycle three-phase grounded fault is applied on bus 3. The simulation results of Fig. 5.12 have indicated that in this case as well, the WAC operation remains unaffected by the generator data errors and thus there is a minor effect on its damping performance.

5.4 Unreported Topology Changes

It is a common practice to design the wide area controller in advance, based on a specific topology of the power system. The topology is usually incorporated into the system's model utilized for the WAC development. In the case of the adopted methodology of [39] the topology exists in the bus admittance matrix elements (G' and B') of (4.8) and (4.9). However, various (unknown to the WAC) topology changes may occur in the system. These can be separated into planning changes, such as substitution or addition of a line in order to reinforce the power system, and operation changes (e.g., line trips due to circuit breakers at the event of faults). Topology changes may not be so often but when they take place, the power flow of the whole system is affected. More specifically, in [129], it has been shown that the removal of any line from the system can result to a change of the modes. This change can affect the stability of the system in the case where the wide area controller is not capable of properly compensating the shifted modes. Thus, as shown in [24] it is interesting to investigate the wide area controller's performance when such events occur. To do this, the line connecting bus 21 to bus 22 is removed from the beginning of the simulation, while the WAC is not aware of this change, and afterwards the event of a line trip and reclose (line connecting bus 6 to bus 11) takes place. The specific line is selected to be removed because

TABLE 5.6: PRONY ANALYSIS FOR UNREPORTED TOPOLOGY CHANGES

Type	Ideal Damping		Unreported Topology Changes	
	ζ(%)	f(Hz)	ζ(%)	f(Hz)
Local mode	-	-	-	-
Inter-area mode	27.1	0.13	16.9	0.13

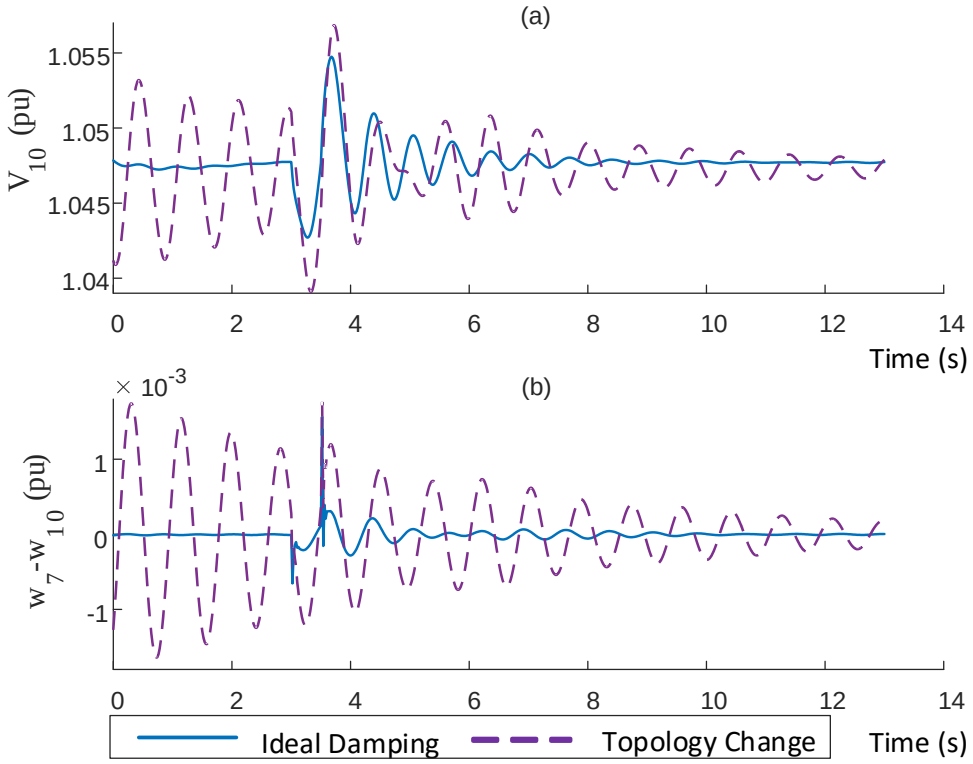

Fig. 5.13 WAC performance comparison between ideal damping and topology changes for: (a) the local oscillation of the terminal voltage of G10, and (b) the inter-area oscillation between G7 and G10.

it is one of the lines which are heavily loaded, according to the power flow results of the IEEE 39-bus test system. The system's response under these conditions is illustrated in Fig. 5.13. As shown the unreported topology changes have a severe impact on the WAC operation from the beginning of the simulation, indicating that the WAC is unable to bring the system to stability before the disturbance takes place. More specifically, as TABLE 5.6 denotes, the line trip results to the appearance of an inter-area oscillation, which is enhanced and shifted due to the unreported topology change. This happens because the wide area controller considers a different topology of the system compared to the actual one and therefore it derives false WAC signals, leading that way to the appearance of oscillations.

5.5 Dynamic Loads

The vast majority of the proposed Wide Area Control (WAC) methodologies is tested and evaluated under the assumption that the system consists only of constant power loads. However, in reality the power system is dominated by the existence of non-linear loads, which can potentially affect the operation of the wide area controller and deteriorate the

system's stability. Therefore, this study is focused on examining the impact of various and commonly used non-linear load models (static and dynamic) on the WAC performance, such as the exponential, exponential dynamic, ZIP and ZIP-Induction Motor (ZIP-IM) load models. For the simulation of all four dynamic load models, the mathematical expressions presented in subchapter 3.5 are considered. The damping capability of the wide area controller is evaluated here under the penetration of the aforementioned dynamic load models through three case studies. For all the case studies, the IEEE 39-bus dynamic test system is utilized, where a three-phase grounded fault is considered to occur on the line connecting bus 2 to bus 3. Note that the IEEE 39-bus dynamic test system comprises ten generators and nineteen loads. The total load demand of the system is 6097 MW and 1408 MVAr.

5.5.1 Case Study I: Impact of static and dynamic loads on WAC operation

TABLE 5.7 presents the parameters of all the non-linear load models, which are utilized in the simulation, along with their references. The procedure considers the increasing introduction of the aforementioned load models, by substituting the existing constant power loads in the IEEE 39-bus system with the respective dynamic ones. The evaluation is accomplished by comparing the system's response when the loads are modelled as 1) constant power loads (Ideal), 2) exponential loads (Exp), 3) exponential dynamic loads (DynExp), 4) ZIP loads and, 5) ZIP-IM loads. This case study begins by changing one-by-one the existing constant power loads with non-linear loads, until the WAC damping performance is affected. Fig. 5.14 (a) and (b) present the local and inter-area oscillations when 30% (6/19) of the constant power loads are represented as non-linear. Note that the wide area controller is unable to damp the local and inter-area oscillations in the presence of six and more exponential dynamic load models (DynExp), leading that way the system to instability. In the case of the ZIP-IM load model, six induction motors resulting to a total demand of 600 MW (100 MW each) have been utilized.

As shown in Fig. 5.14, the consideration of the ZIP and ZIP-IM load models has minor impact on the WAC performance, while the introduction of the exponential load models affects only the local stability. This is still the case even when almost all the constant power loads have been represented by these load models. Therefore, it can be concluded from the results that the inclusion of dynamics (i.e. time delays for the load recovery) in the

TABLE 5.7: PARAMETERS UTILIZED IN THE EXAMINED LOAD MODES

Exp		**ZIP**		**ZIP-IM**	
Source	[112]	Source	[107]	Source	[89]
n_p	0.25	p_1	0.64	p_1	0.1406
n_q	7.9	p_2	0.15	p_2	0.4963
		p_3	0.21	p_3	0.3631
		q_1	2.45	q_1	-0.1395
		q_2	-6.19	q_2	0.7082
		q_3	4.74	q_3	0.4313
				P_{IM} (MW)	100
				Q_{IM} (MVAr)	50
DynExp					
Source	[112]	Source	[90]	Source	[130]
n_p	0.25	n_p	1.7408	n_p	0.3425
n_q	7.9	n_q	5.2577	n_q	2.4951
T_p	135	T_p	1089.8	T_p	131.78
T_q	89	T_q	60.823	T_q	124.11

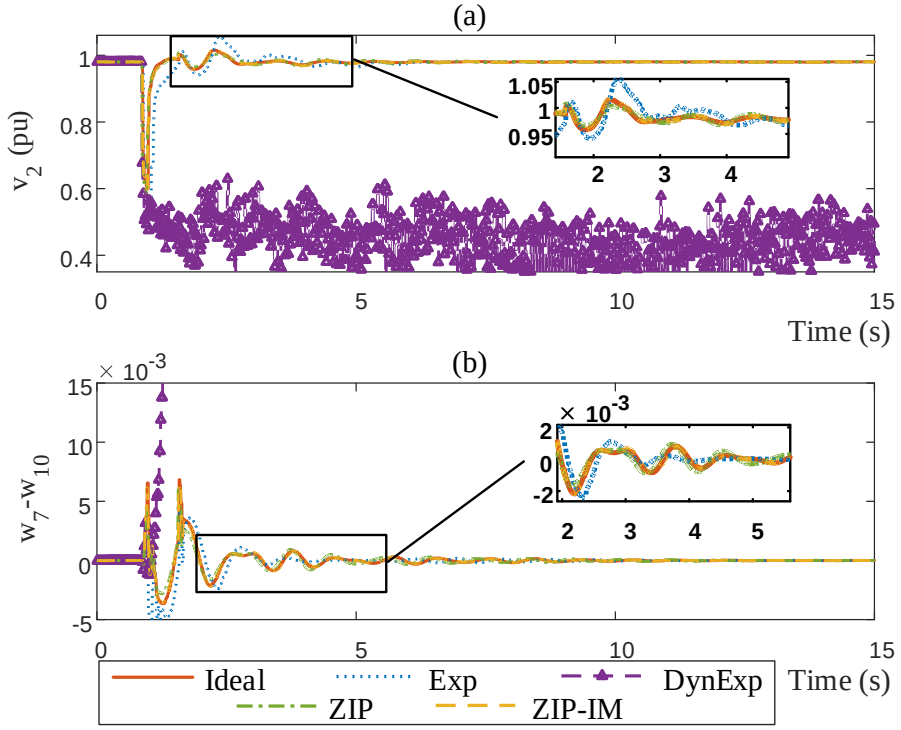

Fig. 5.14 WAC performance under the existence of constant power (ideal), exponential (Exp), exponential dynamic (DynExp), ZIP and ZIP-IM load models: (a) local oscillation of G2, and (b) inter-area oscillation of G7-G10.

exponential load model, can worsen the WAC damping capability. Thus, in the remaining subchapter, more attention is given on examining the impact of the exponential dynamic load model on the wide area controller.

5.5.2 Case Study II: Validation of the exponential dynamic load effect on WAC performance

In order to validate that the exponential dynamic load has actually a negative effect on the WAC performance, the parameters of [90] and [130] have been utilized as well in the same model (TABLE 5.7). From Fig. 5.15, one can realize that indeed the consideration of

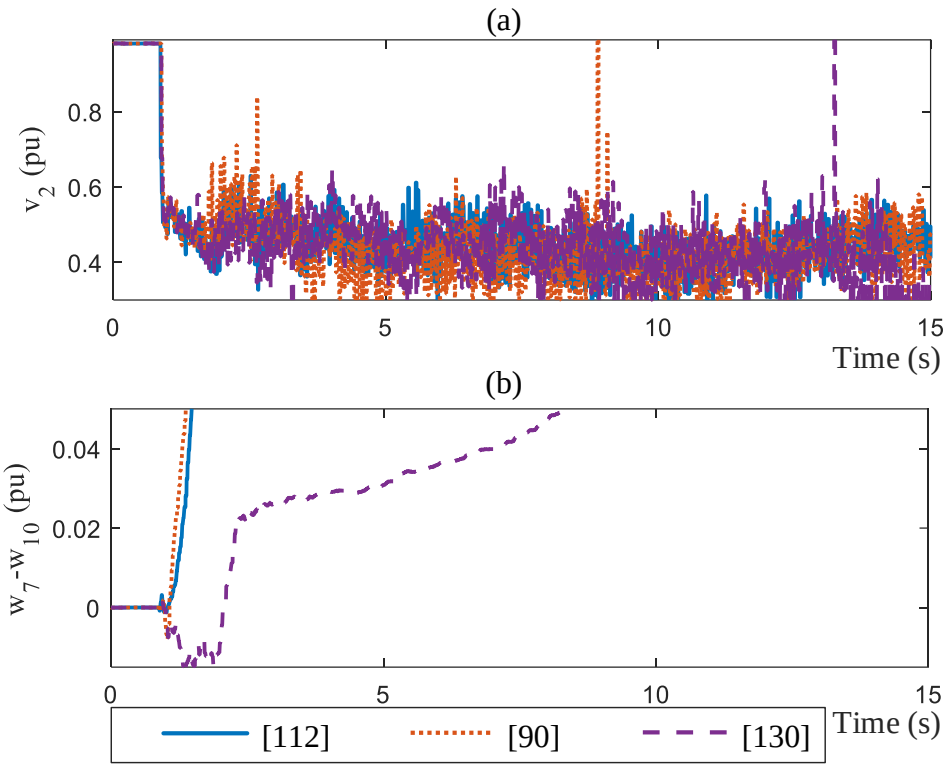

Fig. 5.15 Comparison of WAC operation based on parameters from [112], [90] and [130] for the exponential dynamic load model, considering: (a) local voltage of G2, and (b) speed difference between G7 and G10.

exponential dynamic loads into the simulation deteriorates the operation of the wide area controller to the point where the system goes to instability. It should be noted that for all the examined scenarios the penetration of dynamic loads in the system is maintained to 30% of the total system loads. Therefore, regardless the parameters used, the WAC performance is severely affected by the existence of dynamic loads into the system.

5.5.3 Case Study III: Load Characteristics and Dynamics

As it is aforementioned in subchapter 3.5, the advantage of utilizing the exponential load model is that by selecting its exponents to be 0, 1 or 2 it can have constant power, constant current or constant impedance characteristics. However, the examined exponents of [112], [90] and [130] (TABLE 5.7) are somewhere between these values (mainly n_p), representing a hybrid behavior. Therefore, Fig. 5.16 demonstrates the effect that loads with constant power/current/impedance characteristics can have on the wide area controller, combined with the dynamics (T_p and T_q) of [112]. As shown, all of them have a limited impact on the WAC performance, with the dynamic constant power loads affecting more the local oscillation damping due to its dynamic behavior. These results show that the consideration in the test cases of constant power/current/impedance load models, even when realistic dynamics are included, can be insufficient for validating WAC methodologies. Therefore, exponential dynamic loads with a hybrid behavior and realistic dynamics should

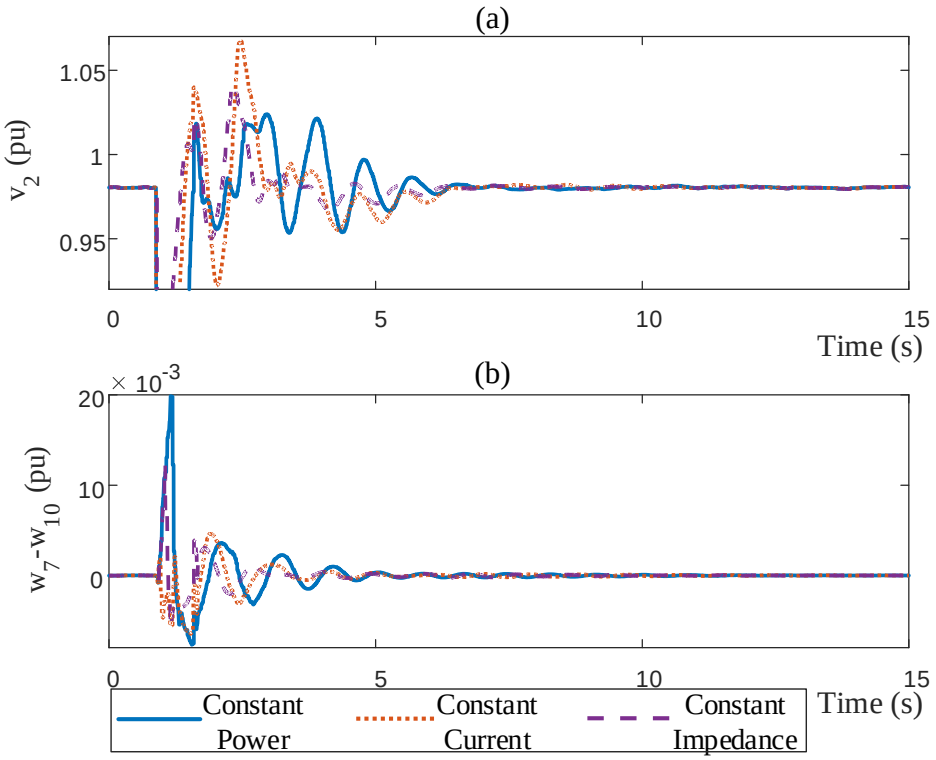

Fig. 5.16 Effect of constant power, constant current and constant impedance load models on the WAC damping capability of: (a) local oscillations of G2, and (b) inter-area oscillation of G7-G10.

be considered for testing and validating the damping capability of the WAC methods under real conditions.

5.6 Conclusion

The aim of this chapter was to examine the impact of various factors/conditions (commonly occurred in the power system) on the damping performance of the wide area controller. This is necessary in order to identify which factors are actual threats to the WAC operation and therefore, develop methods for their effective compensation leading that way to a robust wide area controller. More specifically, the factors considered here are: the measurement errors (steady-state and dynamic), the data delays/dropouts, the system parameter uncertainties, the unreported topology changes and the dynamic load penetration. Note that a lot of effort has been given so that all the under investigation threats are implemented to be as close to reality as possible, according to available Standards and published studies.

Summarizing the outcomes of this chapter, the investigation which took place has revealed that the WAC performance is mainly affected from the data delays/dropouts, the unreported topology changes and the presence of dynamic loads (specifically, the exponential dynamic loads) into the system. Therefore, methodologies to compensate the impact of these threats should be developed further on. In addition, it is clarified that realistic

measurement errors and the uncertainty of the system parameters (transmission lines and generators) have negligible effect, thus an effort must be given in addressing the identified issues. It is to be noted that apart from the data delays/dropouts, the unreported topology changes and the dynamic loads, the renewable penetration into the system is a widely known reason for the degradation of the system stability, mainly due to the reduction of the system's inertia and the change in the system's dynamic characteristics. Therefore, it will also be considered as a factor which must be addressed as well, in order to enhance even more the robustness of the wide area controller.

CHAPTER 6
DATA DELAY COMPENSATION TECHNIQUES BASED ON LINEAR PREDICTION

The previous chapter has concluded that data delays/dropouts are one of the main factors which can have a severe impact on the WAC damping capability. In addition, the state-of-the-art presented in subchapter 2.2 has indicated that in order to compensate the system's data delays and data dropouts, the development of predictive methodologies is considered as the most attractive solution. The predictors proposed in the available literature are implemented according to various techniques such as the Smith Predictor [56], MEKF [37], Holt's linear exponential smoothing [81], NPC [14], etc.

However, three main disadvantages have been identified in the already proposed methods, which actually derive from the two components on which they all depend on: the measurements and the adopted model. Firstly, all the methodologies are tested considering either a simplified expression of the measurement errors (PMU steady-state errors only) or they completely ignore them. Validating the proposed delay compensation techniques under realistic measurement errors of the overall measurement chain is crucial, since the presence of measurement errors (especially large ones during dynamic conditions) can deteriorate the operation of the prediction methods. Secondly, most of the published works consider either constant delays with a known upper bound or they utilize random delays while assuming unrealistic ranges and probability distributions. In addition, amongst the available literature, some studies exist which neglect the existence of data dropouts or the feedback delays. Finally, the proposed predictors are model-based methodologies, which means that their accuracy and processing time are directly and inversely proportional (respectively) to the adopted model. Therefore, when larger systems are considered, more detailed models are required and thus the complexity and processing time increase rapidly.

To overcome this issue, predictors which are based only on measured data are implemented. An example is shown in [131] where an adaptive time delay compensator is implemented based on several lead-lag filters (each one is appointed to a different time interval). As clearly stated in [131], this methodology suffers from various disadvantages. More specifically, it fails in the case of frequent delay changes or in the presence of large delays, which can lead the system to instability. Furthermore, the implementation of a

prediction based hierarchical delay compensation (PHDC) method is presented in [132], which is developed by considering Linear Prediction (LP). The utilization of LP is also adopted for increasing the simulation accuracy of distributed real-time simulators as shown in [133]. Although the measurement-based predictors of [131] and [132] show promising results, they both suffer from processing time issues (when they are applied in larger systems) since they derive several predictions at each iteration for each feedback control signal and they select the appropriate one at the local controller's (actuator) level. In addition, both methodologies totally disregard the existence of data dropouts in the network which if they are not properly addressed, they can even lead the system to instability.

6.1 Autocorrelation Linear Predictive Coding

In order to deal with the dependence on the system's model and to overcome the aforementioned issues of the measurement-based predictors, this chapter presents two methodologies (the second one is actually an advancement of the first one) developed while having as a goal the implementation of model-free, faster and less complex predictors, which depend only on the measured data. The cornerstone of both methodologies is the utilization of the Autocorrelation Linear Predictive Coding (LPC), which its main use is in the speech processing applications (such as speech coding, synthesis and recognition). The overall idea is that any future signal sample ($\hat{u}_{M+1}$) can be approximated as a linear combination of its present value ($\hat{u}_M$) and a finite number of past samples (u_i). This can be achieved by determining the coefficients of the linear predictor (a_i) in a way so that they will minimize the prediction error in a least squares sense:

$$\hat{u}_{M+1} = -(a_2 u_M) - (a_3 u_{M-1}) - \ldots - (a_{N+1} u_{M-N+1}) \tag{6.1}$$

$$\min_{\{a_i\}} E\left[\left| u_M - \sum_{i=1}^{N} a_i u_{M-i} \right|^2\right] \tag{6.2}$$

or (6.2) expressed in a matrix form:

$$\min \left\| U\tilde{a} - b \right\| \tag{6.3}$$

where

$$\tilde{a} = \left[a_2 \ldots a_{N+1} \right]^T$$

$$b = \left[u_2 \ldots u_M \; 0 \ldots 0 \right]^T$$

$$U = \begin{bmatrix} u_1 & u_2 & \ldots & u_i & \ldots & u_M & 0 & \ldots & 0 \\ 0 & u_1 & u_2 & \ldots & u_i & \ldots & \ddots & \ddots & \vdots \\ \vdots & \ddots & \ddots & \ldots & \ldots & \ldots & \ldots & \ddots & 0 \\ 0 & \ldots & 0 & u_1 & \ldots & \ldots & \ldots & \ldots & u_M \end{bmatrix}^T$$

N represents the size of the coefficient vector $\tilde{\alpha}$ and the window length which holds the present and a finite number of the past signal samples, required for the prediction. The number N of the LPC coefficients to be used during the prediction process actually depends on the number of considered samples (u_i). Too many or inadequate samples can lead to wrong prediction results. Therefore, it is important to identify the suitable size of the vector, which will be used for the prediction. This can be done in offline simulations through a testing process, based on available measurements (e.g., historical data). Note also that it is desirable to have as less samples as possible, in order to reduce the complexity of the algorithm but enough to provide accurate predictions. For the IEEE 9-bus and 39-bus dynamic test systems considered in this chapter, 20 samples (thus N=20) are found to be sufficient for accurate predictions. The only disadvantage of the LPC methodology is that it requires up to 1 second for setting and correcting its coefficients, therefore during that period the derived predictions are ignored.

6.2 Linear Predictor Based on Prediction Error

The first LPC-based predictor of this chapter, developed for compensating the data delays/dropouts, has as main characteristic the utilization of the prediction error as feedback [25]. This is required in order to overcome the main disadvantage of the LPC method, which is the existence and continuous increase (as the time passes) of an error that results to the deviation of the predicted value from the actual one. Fig. 6.1 illustrates all the components consisting the proposed linear predictor. Following, the content and operation of each block is fully analyzed:

1) Autocorrelation LPC: This block provides the coefficients of the N^{th}-order forward linear predictor based on the least square minimization of (6.2) (or (6.3)), which are required to predict the future measured value according to (6.1).

2) Prediction: At this step the algorithm solves (6.1), by using as inputs the autocorrelation LPC coefficients and a vector holding past and present values of the measured signal.

3) Prediction error feedback: Here, the error of the previous prediction is computed based on the predicted and actual value (in the case where the latter arrives after the intended time and saved in a buffer) of the measured signal and it is added to the next prediction for more accurate results:

$$\tilde{u}_{k+1} = \hat{u}_{k+1} + e_{prd} \tag{6.4}$$

$$e_{prd} = \hat{u}_k - u_k \tag{6.5}$$

where e_{prd} is the prediction error, $\hat{u}_k$ represents the predicted value at time step k, u_k stands for the actual value of the signal at time step k and $\tilde{u}_{k+1}$ is the corrected prediction at step k+1.

4) Compensation: This block is used to compensate data delays, whenever they occur, by providing the predicted value of the measured signal as an output when the delay exceeds the specified "wait time". In addition, a reliability step is incorporated in this block where the predicted value is evaluated and if it is found unreliable, the mean of the last twenty values of the measured signal (based on the buffer) is used instead as output, in order to correct the following future predictions. The reliability of the prediction is calculated by comparing the prediction ($\tilde{u}_{k+1}$) with the actual value of the measured signal of the previous step u_k (if available) and if their difference is beyond a certain threshold (in this case 0.001), then the prediction is deemed as unreliable. This is based on the

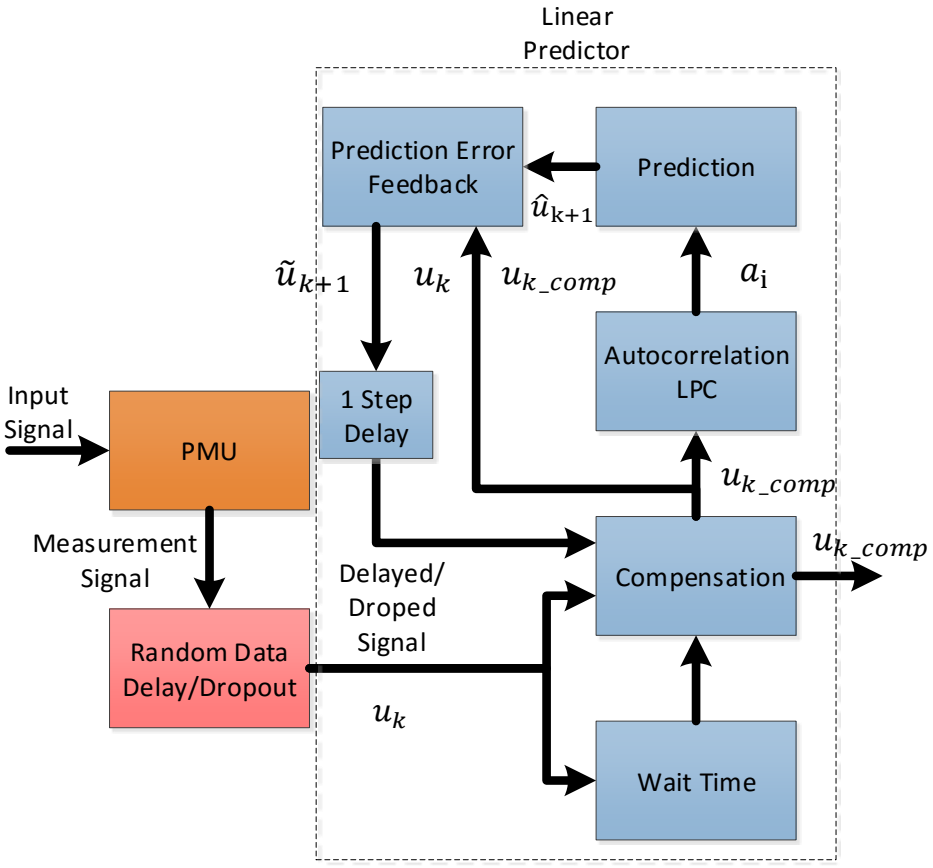

Fig. 6.1 Schematic diagram of the proposed Linear Predictor based on prediction error

observation that the measured signal values are close to each other. In the case where an unreliable prediction is used, the subsequent predictions will be affected as well, leading to wrong future predictions.

Initially, the performance of the proposed linear predictor is tested under relatively small delays in the range of [12-28] ms. Nevertheless, the delays are taken as random, following a Gaussian distribution with a mean value of 20 ms and variance 7. The "wait time" of the linear predictor is taken to be 15 ms, in order to make sure that at each time step (20 ms) the compensated signal will be available. This scheme was tested in the IEEE 9-bus dynamic test system, where delays were applied on the voltage and rotor speed deviation ($d\omega$) measurements of the synchronous generators. The disturbance considered here is actually a load increase of the load located at bus 6. The proposed predictor is compared to the ideal delay-free signal and the case where no delay compensation occurs and thus the application utilizes the previous value of the signal whenever the "wait time" expires. It should be noted here that this study did not consider the existence of WAC and therefore the obtained signals are compared only graphically. The results are illustrated at Fig. 6.2, indicating that the proposed scheme can compensate effectively all the data delays, while

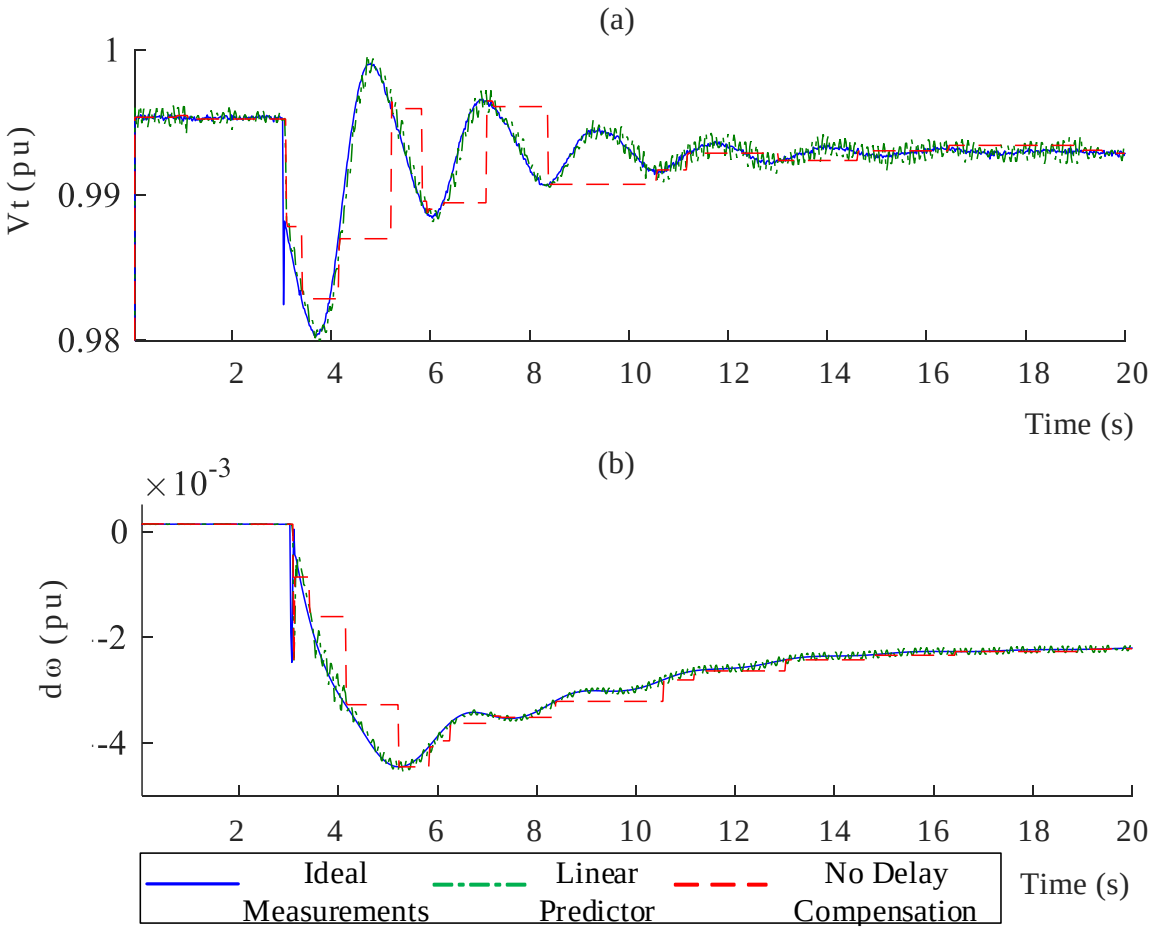

Fig. 6.2 Performance of linear predictor based on prediction error for the cases of: (a) terminal voltage, and (b) rotor speed deviation of generator G1.

the uncompensated signal loses important information especially during the transient conditions. However, these results only show that the proposed linear predictor has the potential to compensate effectively larger delays, since the adopted ones are relatively small and furthermore an unrealistic PDF has been used.

Next, the proposed linear predictor has been tested in the IEEE 39 bus dynamic test system, in a common architecture with the wide area controller, under the occurrence of uniform random delays with a mean value of 100 ms and ±100 ms, as upper and lower limits ([0-200] ms). Once again, the "wait time" is equal to 15 ms and the WAC time step is 20 ms. The considered disturbance here is a 5-cycle three-phase fault on the line connecting bus 3 to bus 4. Note that as Fig. 6.3 illustrates, linear predictors are placed both on the wide area controller and on the generator local controllers, in order to compensate the measurement infrastructure delays and the feedback delays, respectively. Furthermore, the linear predictor was evaluated when ideal measurements and when steady-state errors of the whole measurement chain are considered. The Prony analysis results of TABLE 6.1 show that the proposed scheme improves considerably the damping performance of the system, compared to the scenario where the measurement delays are left uncompensated. In addition, it is interesting to point out here that conversely to the outcome of subchapter 5.1, the measurement errors can actually affect the WAC performance indirectly, through their

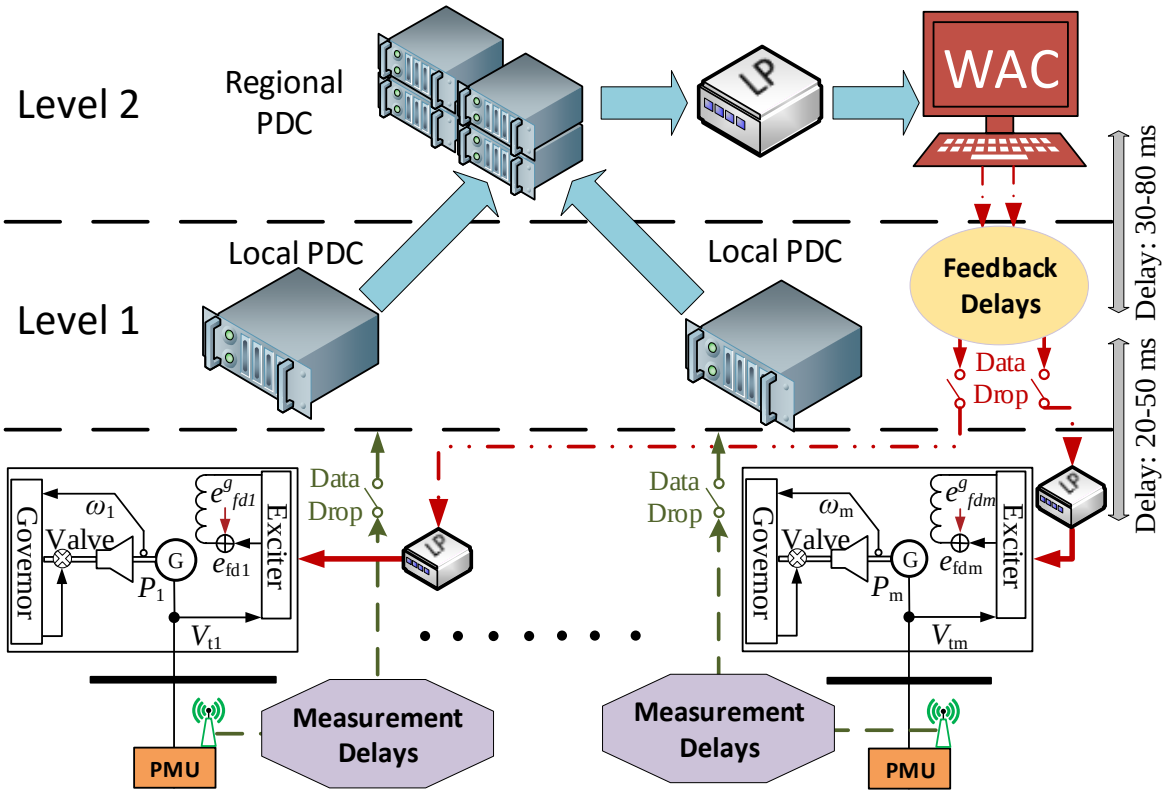

Fig. 6.3 Placement of linear predictors (LPs) on the inputs of the wide area controller and the generator local controllers for compensating all the measurement infrastructure delays and the feedback delays.

impact on the operation of the predictor. This remark further enhances the need of utilizing realistic simulation environments for the development and application of robust WAC methodologies. Fig. 6.4 presents also the graphical simulation results for the local (v_2) and inter-area oscillations (w_7-w_{10}), which verify the impact of the delays on the WAC operation, the substantial improvement through the use of the linear predictor and the impact of the measurement errors on the linear predictor performance.

TABLE 6.1: PRONY ANALYSIS RESULTS FOR LINEAR PREDICTOR BASED ON PREDICTION ERROR

Type	Ideal Damping		Uniform Distribution Delay	
	ζ(%)	*f(Hz)*	*ζ(%)*	*f(Hz)*
Local mode	6.8	1.3	4.28	1.3
Inter-area mode	32.2	0.75	16	0.65
Type	Linear Prediction Based on Prediction Error (without Measurement Errors)		Linear Prediction Based on Prediction Error (with Measurement Errors)	
	ζ(%)	*f(Hz)*	*ζ(%)*	*f(Hz)*
Local mode	6.58	1.4	5.69	1.2
Inter-area mode	22.5	0.76	18.2	0.75

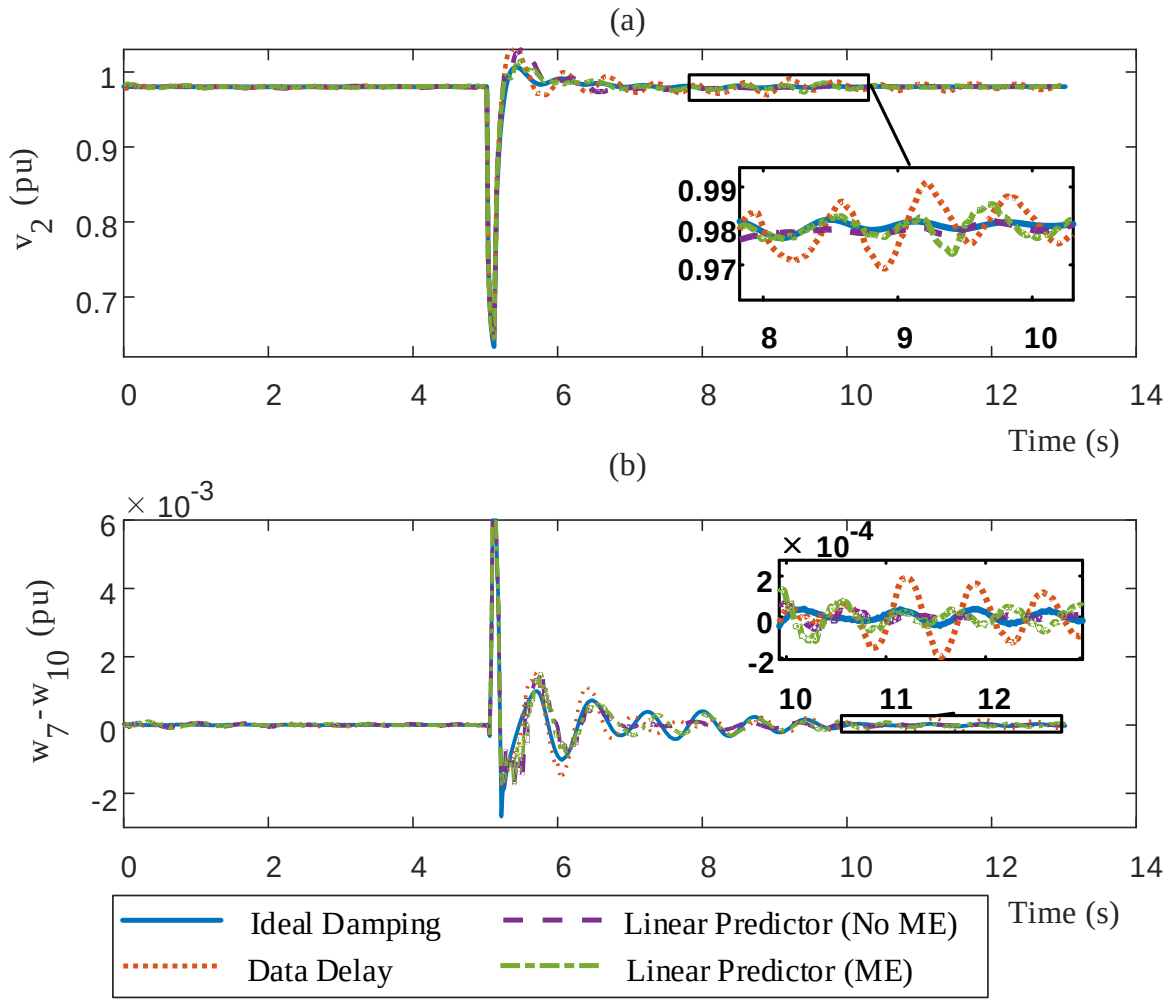

Fig. 6.4 WAC performance for (a) the terminal voltage of G2 and (b) the inter-area oscillation of G7-G10 between: ideal damping, measurement delays, linear predictor without measurement errors (No ME), linear predictor with measurement errors (ME).

6.3 Linear Predictor Based on Prediction Error Power

The data delays ([0-200] ms), the "wait time" (15 ms) and the same PDF for simulating all the delays (measurement infrastructure delays and feedback delays) which are considered previously do not correspond to the actual system conditions. Moving to the application of more realistic data delays, "wait time" and PDF combinations (as these were introduced in subsections 3.3 and 5.2), although the linear predictor proposed in the previous subsection provided sufficient results in compensating effectively all data delays, it has become necessary to improve the methodology even more. The main issue was that its performance is highly depended on the prediction error which results from the previous prediction step and then it is added to correct the next prediction. More specifically, this technique needs the actual value of the signal to arrive promptly at some point in order to identify and correct the prediction error. However, under large delays and successive data dropouts the prediction error may not correspond to the actual one, due to the unavailability of the true value of the signal, which can lead to wrong predictions. In addition to this, the aforementioned linear predictor has shown to be vulnerable to the presence of measurement errors and its performance reduces even more when dynamic measurement errors take place. To improve the resulted predictions in this case and to reduce the linear predictor's dependence on the measurement and prediction errors, the following expressions have been utilized:

$$\hat{u}_{M+1} = -(a_2 u_M) - (a_3 u_{M-1}) - \ldots - (a_{N+1} u_{M-N+1}) + (k_2 P_M) + (k_3 P_{M-1}) + \ldots + (k_{N+1} P_{M-N+1}) + e_{prd} \quad (6.6)$$

$$k_i = \frac{-\Delta_{i-1}}{P_{i-1}} \quad (6.7)$$

where k_i are the reflection coefficients which result from the Autocorrelation LPC procedure and P_i stands for the prediction error power of each of the previous predictions. Δ_{i-1} is actually the cross-correlation of the forward prediction error and the unit delayed backward prediction error. Note that in the case where u_j data arrive before the "wait time" expires (and therefore the predicted value is not utilized), the prediction error power of the j^{th} step is set to $P_j = 0$. It is important to mention here that whenever a new signal sample arrives (either the actual or the predicted one) the LPC procedure estimates the new linear predictor coefficients a_i and the reflection coefficients k_i according to (6.2) and (6.7).

The proposed linear predictor (PropLP) is evaluated under realistic conditions. More specifically, it is considered to compensate the impact of the data delays in Cases I and II,

as these were presented in subchapter 5.2 and TABLE 5.4. Therefore, the same PDF combinations and delay ranges used for simulating the measurement infrastructure delays and the feedback delays in subchapter 5.2 are adopted here as well, along with their data dropouts. Note that as a disturbance, a 5-cycle three-phase grounded fault occurs on the line connecting bus 15 to bus 16 of the IEEE 39-bus dynamic test system. The specific fault is chosen in order to consider also here the realistic (steady-state and dynamic) measurement errors of subchapter 5.1. Furthermore, it is worth mentioning that as previously (Fig. 6.3)

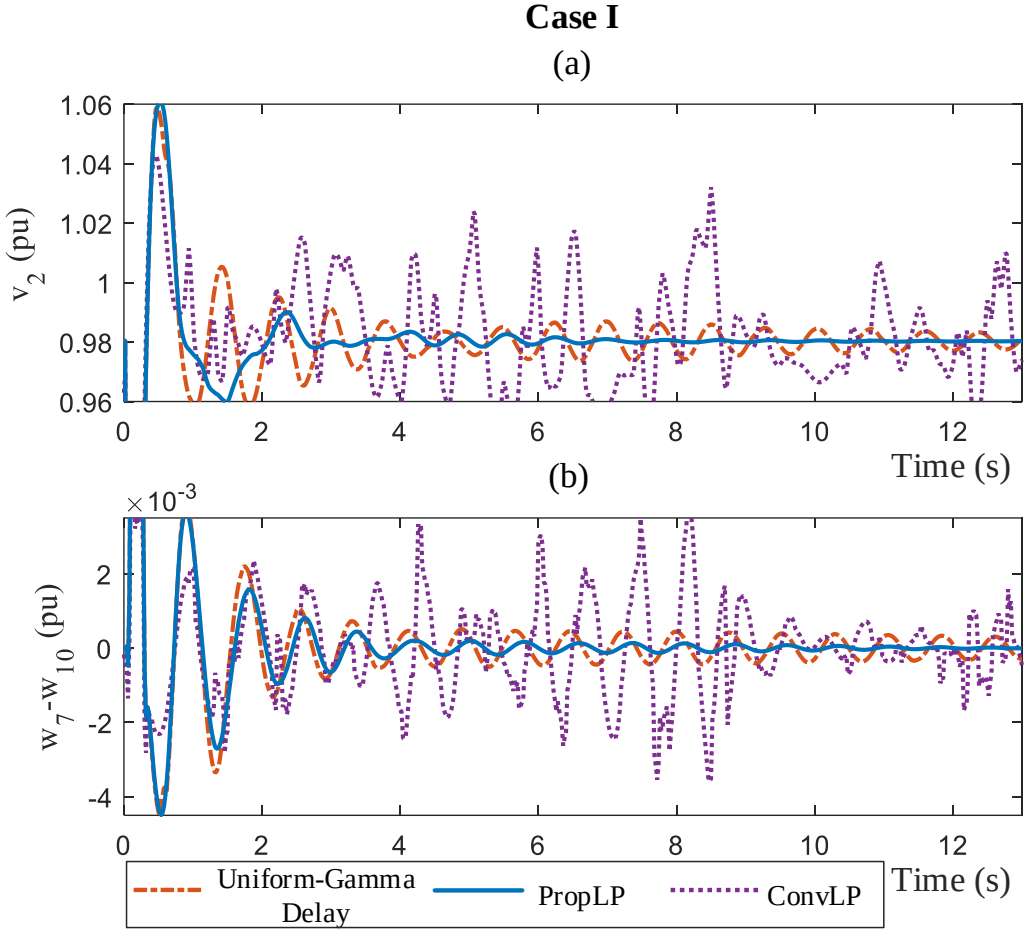

Fig. 6.5 Comparison of WAC performance for the delays of Case I, when no delay compensation exists and when the conventional and proposed predictors are utilized, considering: (a) the local oscillation of the terminal voltage of G2, and (b) the inter area oscillation between G7 and G10.

TABLE 6.2: PRONY ANALYSIS RESULTS FOR THE DATA DELAYS OF CASES I-II, CONVENTIONAL LINEAR PREDICTOR AND PROPOSED LINEAR PREDICTOR

CASE I						
Type	**Uniform-Gamma Delay**		**ConvLP**		**PropLP**	
	ζ(%)	f(Hz)	ζ(%)	f(Hz)	ζ(%)	f(Hz)
Local mode	2.93	1.3	1.08	1.3	11.7	1.2
Inter-area mode	21.2	0.69	Instability		30.3	0.75
CASE II						
Type	**Uniform-Gamma Delay**		**ConvLP**		**PropLP**	
	ζ(%)	f(Hz)	ζ(%)	f(Hz)	ζ(%)	f(Hz)
Local mode	2.61	1.4	2.95	1.4	11.5	1.2
Inter-area mode	21.5	0.70	13.9	0.67	31.7	0.62

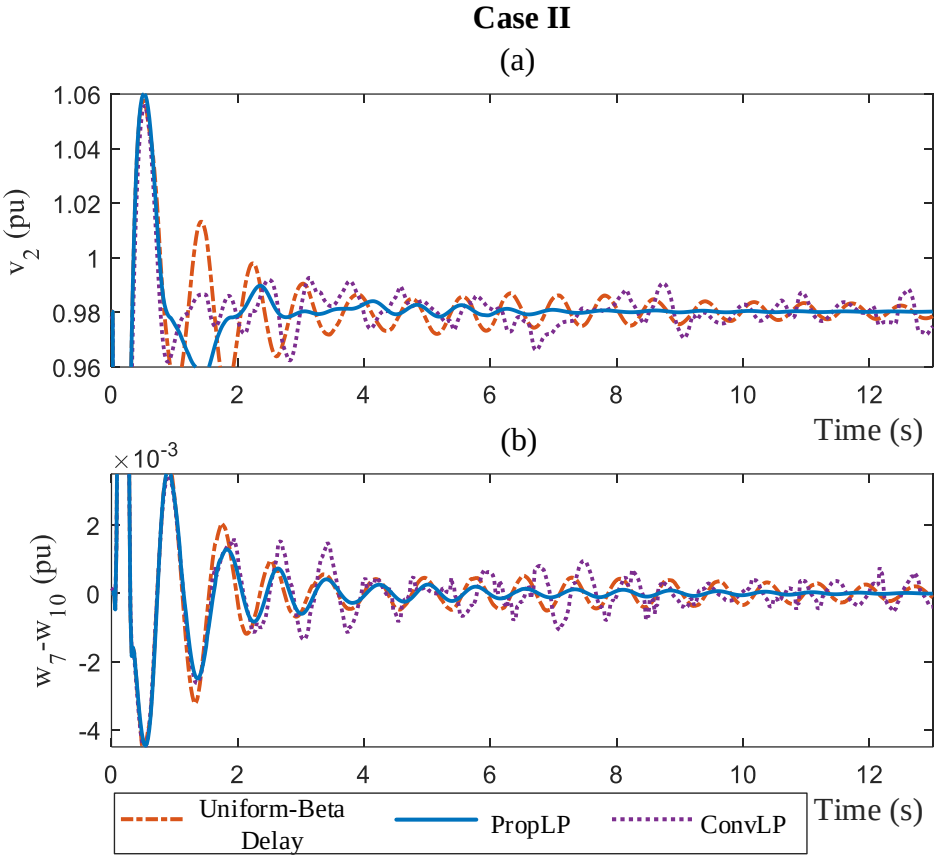

Fig. 6.6 Comparison of WAC performance for the delays of Case II, when no delay compensation exists and when the conventional and proposed predictors are utilized, considering: (a) the local oscillation of the terminal voltage of G2, and (b) the inter area oscillation between G7 and G10.

linear predictors are placed on both, the wide area controller and the generator local controllers for compensating all the measurement infrastructure delays and the feedback delays, respectively.

Apart from the proposed linear predictor, a conventional LP (ConvLP) according to (6.1) is also considered into the simulations. This is done in order to present the significant improvement of the WAC performance when the proposed scheme is utilized. Fig. 6.5, Fig. 6.6 and TABLE 6.2 illustrate the simulation results for the compensation of the local and inter-area oscillations in Cases I and II. As shown, the inclusion of the proposed linear predictor in the WAC scheme improves considerably the damping performance of the system, compared to the case where the data delays/dropouts are left uncompensated. More specifically, the consideration of the proposed predictors in the simulation makes the wide area controller capable of bringing the system back to stability. Conversely, the utilization of the conventional LP is unable to compensate effectively the data delays/dropouts, leading the system to instability. The latter is especially notable when the delays of Case I occur (Fig. 6.5). This remark is also confirmed through the Prony analysis results of TABLE 6.2. Here, it can be seen that the WAC combination with the proposed linear predictor achieves

high damping ratios, while the damping ratios drop significantly in the cases of the conventional predictor or when no delay compensation is considered at all.

Accuracy information regarding the approximation of the non-delayed signal for all the three examined cases (No LP, ConvLP and PropLP) are provided in TABLE 6.3. In particular, the mean square error (MSE), calculated as shown in (6.8), is tabulated. As it is illustrated the MSE of the ConvLP is much larger than the other two cases. This is because the prediction error feedback (e_{prd}) is not considered at all in (6.1), in order to improve the future predictions. In contrast, as clearly shown in (6.6), the PropLP considers the prediction error power along with the prediction error feedback in the calculation of the future predictions, resulting to better results.

$$MSE = \frac{1}{L}\sum_{i=1}^{L}\left(Y_i - \tilde{Y}_i\right)^2 \tag{6.8}$$

where L is the total number of the data points considered, Y_i stands for the non-delayed signal and $\tilde{Y}_i$ represents either the delayed signal in the case where there is no delay compensation (No LP) or the compensated signal when a linear predictor is used (ConvLP/PropLP). All these results indicate both the effectiveness of the proposed linear predictor and the necessity of including an accurate linear predictor into the WAC architecture. Furthermore, it is important to be mentioned that the proposed linear predictor is tested in the cases of presence

TABLE 6.3: MEAN SQUARE ERROR OF THE DELAYED SIGNAL, THE CONVENTIONAL LP AND THE PROPOSED LP

Measurement	**No LP**	**ConvLP**	**PropLP**
v	0.0036	0.9403	0.0025
δ	0.0084	0.3009	0.0074

TABLE 6.4: COMPARISON OF PREDICTION METHODS

Prediction Method	Smith Predictor [56]	MEKF [37]	Lead-Lag Filter [87]	Linear Predictor [132]	Proposed Predictor
Model Size Independency	✗	✗	✓	✓	✓
Feedback Control Delay Compensation	✓	✗	✓	✓	✓
Data Dropouts Compensation	✗	✓	✗	✗	✓
Dynamic Delay Consideration	✗	✓	✓	✓	✓
Measurement Error Consideration	✗	✗	✗	✗	✓

and absence of measurement errors, where it was illustrated that its performance remains unaffected.

Finally, TABLE 6.4 summarizes the characteristics of some of the aforementioned model-based and measurement-based methodologies for data delay compensation compared to the proposed linear predictor. Note that none of these methods considers the existence of measurement errors (which can potentially affect the prediction) and that only one includes the compensation of the data dropouts. Furthermore, as it is illustrated, some methods do not compensate the feedback delays, while others ignore the random nature of the delays. The proposed scheme is actually a model-free, faster and less complex predictor which is tested under realistic conditions (random data delays/dropouts and dynamic measurement errors) and it has been proved to be able to compensate successfully all the measurement infrastructure delays and feedback delays.

6.4 Conclusion

This chapter proposed the development of two model-free and fast predictors for compensating effectively all the data delays/dropouts, in order to ensure at all times the availability of measurements to the wide area controller input. Both methods are implemented based on the Autocorrelation LPC concept and require only measurement signals as inputs, while no information of the system's model is needed. The results indicate that by including the proposed linear predictors into the WAC scheme, the performance of the latter is substantially improved even at the event of severe delays which if left undamped they could lead the system to instability. The first linear predictor is developed based on the utilization of the prediction error as feedback. The proposed scheme has been tested in the presence of small and large random delays, following a Gaussian and a Uniform PDF respectively. The results illustrate that the proposed scheme improves considerably the wide area controller damping performance, compared to the scenario where the measurement delays are left uncompensated. Furthermore, as it was shown by testing the linear predictor-WAC combination in the presence and absence of steady-state measurement errors, the measurement errors could actually affect the WAC performance indirectly, through their impact on the operation of the linear predictor. This result actually illustrates the necessity of utilizing realistic simulations for the design and evaluation of robust WAC methodologies, where factors which do not seem to have a direct impact on their performance (thus they are commonly neglected) could be identified to affect their operation through indirect means.

Therefore, in order to overcome the disadvantages of the first linear predictor, an advanced linear predictor is then proposed. The latter is implemented in such a way so that it will reduce the high dependence of the previous method on the prediction error feedback and to compensate the impact of the measurement errors on its operation. To achieve these, a linear predictor is implemented which is based on the prediction error power along with the prediction error, leading that way to a more robust solution. The proposed scheme is evaluated in the presence of realistic measurement errors, along with measurement infrastructure delays, feedback delays and data dropouts. More specifically, combinations of three different PDFs (uniform, Beta and Gamma) are considered to model the measurement infrastructure delays and the feedback delays of two case studies. The results indicate that the proposed scheme outperforms conventional methods which can even lead the system to instability, increasing that way significantly the damping capability of the wide area controller. Actually, by using the advanced linear predictor, the WAC becomes capable of bringing the system back to stability.

Overall, it has been illustrated in this chapter that the existence of an effective prediction scheme, capable of compensating the measurement infrastructure delays, the feedback delays and the data dropouts, is crucial for maintaining the system's stability.

CHAPTER 7
INTEGRATION OF WIDE AREA CONTROL WITH RENEWABLE ENERGY SOURCES

RESs are characterized mainly by their ability to produce green energy (required to satisfy the environmental concerns) and by their intermittent nature due to the varying environmental conditions. As mentioned before the main problem that arises from the increasing penetration of renewables into the grid, is that the whole system is changing and reforming. More specifically, its inertia is reduced due to the displacement of synchronous generators by RESs, which in turn alters the dynamic characteristics of the system [22]. In addition, one of the results of this system transitioning is the change of the modes affecting that way negatively the performance of well-tuned PSS and FACTS controllers.

The majority of the proposed WAC methodologies does not consider the existence of renewables into the system and the current practice by the system operator is to consider them as negative loads [58]. However, the WAC concept offers the opportunity and capability to utilize effectively the RESs, in order to contribute to and increase the overall stability and damping of the system. The effective compensation of the inter-area modes can enable the very high penetration of renewables increasing that way even more the stability of the system through WAC-RES schemes. Therefore, in this chapter, two methodologies are proposed with the first one illustrating the steps of making the wide area controller aware of the RESs behavior (leading that way to a cooperation scheme), while the latter presents the procedure of integrating the RESs into the WAC architecture. It is worth mentioning that the developed methodologies of this chapter can be considered for any type of renewable without any limitation, in contrast to the majority of the already published techniques which are intended only for DFIG wind farms.

7.1 Cooperation of Wide Area Control with Renewable Energy Sources

The aim of this subchapter is to make the wide area controller able to cooperate with the renewables in order to increase the damping capability of the power system, as shown in [26]. The word “cooperation” here means that no WAC signals are derived for the coordination of the RESs. To achieve this, one must realize firstly that the actual benefit in

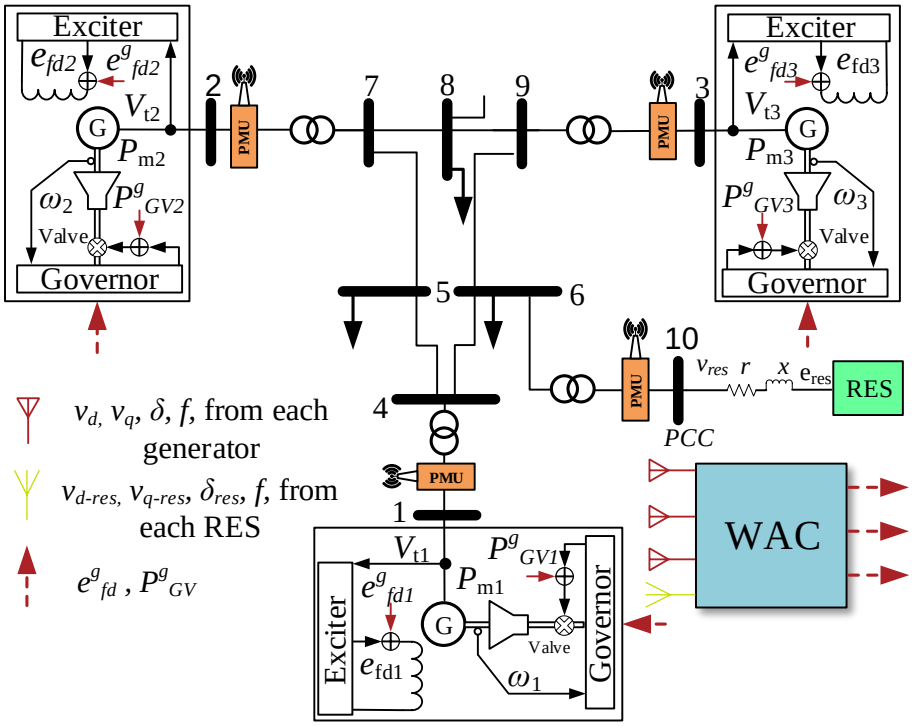

Fig. 7.1 Proposed cooperation scheme of WAC and RES. Solid lines represent PMU signals, while dashed lines represent WAC signals.

utilizing the WAC control signals is that they convey and provide to each local controller all the necessary information regarding the behavior of the rest of the generators. This is accomplished through the decoupling (Chapter 4) of each generator's dynamics from the remaining generators and based on the latter the coordination signals are derived. In the same context, it would be very beneficial for the generator operation to become "aware" of the RES oscillations as well, resulting that way to a cooperation scheme between the two components. This can be achieved through the utilization of WAC signals. More specifically, the first step towards this end is to obtain wide area measurements from the renewables, similar to the ones collected from the generators, in order to include also the RES response into the WAC formulation of subchapter 4.2. For this reason, apart from the availability of synchronized measurements from each generator bus, PMUs are assumed to be connected at the PCC of each RES (Fig. 7.1) in order to provide their terminal voltage (v_{res}), current (i_{res}), and frequency.

The problem that arises here is that the power angle is also required when applying the methodology. However, in the case of RESs there is no power angle (in contrast to the generators). To overcome this obstacle and make the methodology applicable for renewables as well, a virtual power angle for RES (δ_{res}) is introduced that represents the angle between the terminal voltage v_{res} and the virtual voltage e_{res}. The virtual voltage is the fundamental voltage phasor at the output of the GSC, as shown in Fig. 7.1. Note that since this voltage

contains high-frequency switching noise (this noise is eliminated by the LC filter), it cannot be measured directly and therefore, its estimation is required. The computation of δ_{res} is based on the terminal voltage phasor v_{res} =[$v_{res\text{-}d}$ $v_{res\text{-}q}$]^T and the injected current phasor i_{res} =[$i_{res\text{-}d}$ $i_{res\text{-}q}$]^T, expressed into the local *dq*-frame, according to (7.1)-(7.3). More specifically, (7.1) and (7.2) are used to calculate the corresponding components of the e_{res} =[$e_{res\text{-}d}$ $e_{res\text{-}q}$]^T and as a result the virtual δ_{res} can be obtained by (7.3).

$$e_{res-d} = v_{res-d} + ri_{res-d} - xi_{res-q} \tag{7.1}$$

$$e_{res-q} = v_{res-q} + ri_{res-q} + xi_{res-d} \tag{7.2}$$

$$\delta_{res} = \arctan\left(\frac{e_{res-d}}{e_{res-q}}\right) \tag{7.3}$$

It is to be noted that r and x represent the series resistance and reactance of the LC filter between the inverter and the PCC, as shown in Fig. 7.1. The capacitor (C_f) of the LC filter (illustrated in Fig. 7.6) can be neglected here since it damps only the high order harmonics.

By obtaining the appropriate wide area measurements from the RESs, the proposed procedure considers a modification of the first step of the methodology presented in subchapter 4.2 so that the generator-free and renewable-free buses are expressed now in terms of the generators and RESs terminal voltages (v_d, v_q and $v_{res\text{-}d}$, $v_{res\text{-}q}$, respectively). This step is important in order to make each generator "aware" of the oscillations caused by the rest of the generators and RESs. More specifically, through this procedure the terminal voltages of the renewables are included now into the perturbation terms (ψ_d, ψ_q and ψ_ω). The rest of the steps remain as they were described in subchapter 4.2 for deriving the generators' WAC signals. By utilizing this scheme, the RES local controller does not require any modification in order to become able to receive any WAC signals and thus the wide area controller derives signals intended only for the coordination of the synchronous generators.

For enhancing the damping operation of the system and furthermore, to enable the renewables to locally contribute to the voltage oscillation damping, some modifications are proposed in this subsection on the reactive control strategies of RES. The Fault Ride Through (FRT) support by RES is only activated when the voltage at the PCC is violating the limits of the Dead Band Zone (DBZ), defined as ±10% variation around the nominal voltage (Fig. 7.2). The grid regulations [106], define the reactive current (I_{Q1}) that should be injected by the RES as given by,

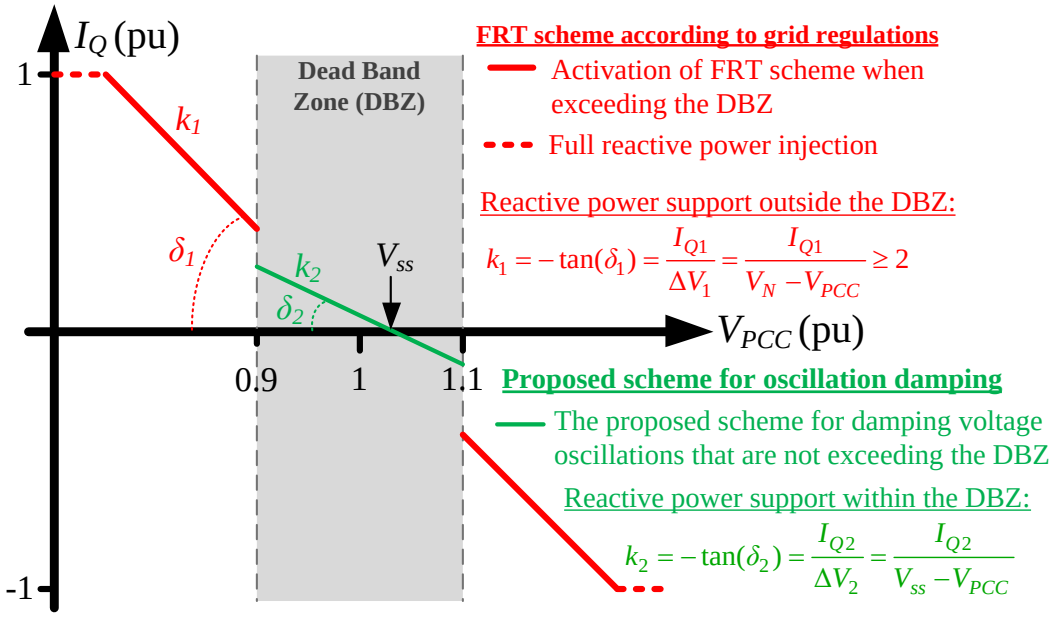

Fig. 7.2 Reactive support scheme of RES. The current grid regulatios are illustrated in red color, while green color stands for the proposed scheme for enabling RES to contribute into the oscillation damping.

$$I_{Q1} = k_1 \Delta V_1 = k_1 (V_N - V_{PCC}) \tag{7.4}$$

where V_N=1 pu and V_{PCC} stands for the voltage at the PCC. The parameter k_1 should be equal or greater than two, according to [106], in order to provide an aggressive voltage support under intense voltage sag.

However, in most cases, disturbances on large power systems can cause inter-area oscillations that may not be observed as voltage limit violations. For example, an expected voltage oscillation with maximum overshoot of 0.05 pu (and a slow oscillation frequency of 0.1-1 Hz due to the large inertia of the generators) and with an extended duration (5-10 s) will not activate the reactive support of RES. Hence, the renewable cannot support the grid for damping such oscillations. Therefore, a reactive support scheme is proposed here in order to enable the local contribution of RES for damping power system oscillations. The proposed scheme can be applied to the grid tied inverter of the renewable in order to regulate the reactive support in the presence of such inter-area oscillations where the voltage oscillates but without exceeding the DBZ. More specifically, the proposed reactive support by the RES when a voltage oscillation occurs (that does not violate the DBZ shown in Fig. 7.2), is realized by injecting the following reactive current (I_{Q2}):

$$I_{Q2} = k_2 \Delta V_2 = k_2 (V_{SS} - V_{PCC}) \tag{7.5}$$

where k_2 is a parameter that determines how intense is the reactive support during inter-area oscillations and should be less than two (small voltage oscillations). For the purposes of this subchapter, k_2 is set to one. Further, V_{ss} represents the steady-state voltage of the RES at the PCC prior the inter-area oscillation and can be calculated according to the first order low-pass filter of (7.6).

$$V_{SS} = \frac{\omega_f}{s + \omega_f} V_{PCC} \tag{7.6}$$

Note that the cutoff frequency of frequency ω_f of the filter is set to $2\pi \cdot 0.05$ rad/s in order not to be affected by the inter-area oscillations with a frequency range of 0.1-1 Hz. The proposed scheme for reactive support introduces a virtual voltage inertia on the RES that resists to small changes of the voltage at the PCC by injecting or absorbing reactive power. Thus, it can locally enable the renewable to contribute to the compensation of the inter-area oscillations and can smoothly cooperate with the proposed WAC scheme.

The proposed WAC and RES cooperation has been implemented and applied to the IEEE 9-bus dynamic test system, where a 20 MVA RES is integrated at bus 6 of the system through a step-up transformer (Fig. 7.1). Note that if not stated otherwise, the output of the renewable is set at 10 MW while constant wind conditions are assumed. The performance

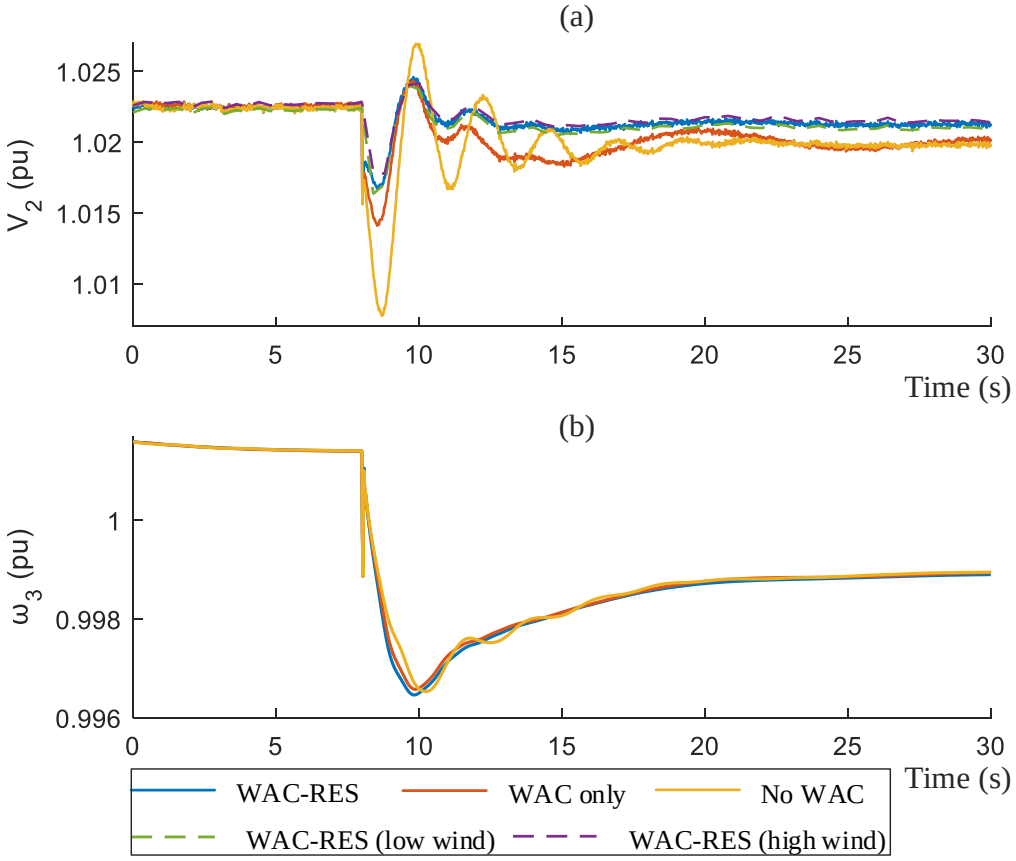

Fig. 7.3 System response for the No WAC, WAC only and WAC-RES scenarios at the event of load change, considering also high and low wind conditions for the WAC-RES scenario. (a) terminal voltage of G2 and (b) rotor speed of G3.

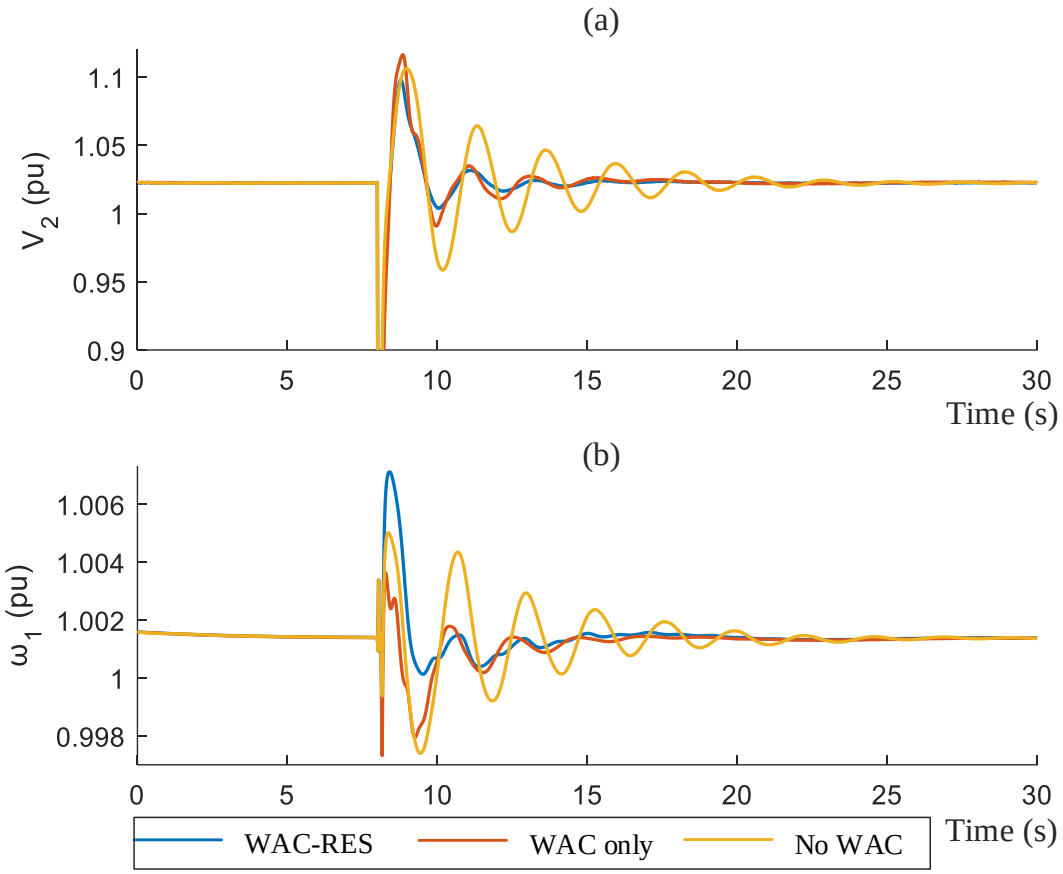

Fig. 7.4 System response for the No WAC, WAC only and WAC-RES scenarios at the event of symmetric fault for the cases of: (a) terminal voltage of G2 and (b) rotor speed of G1.

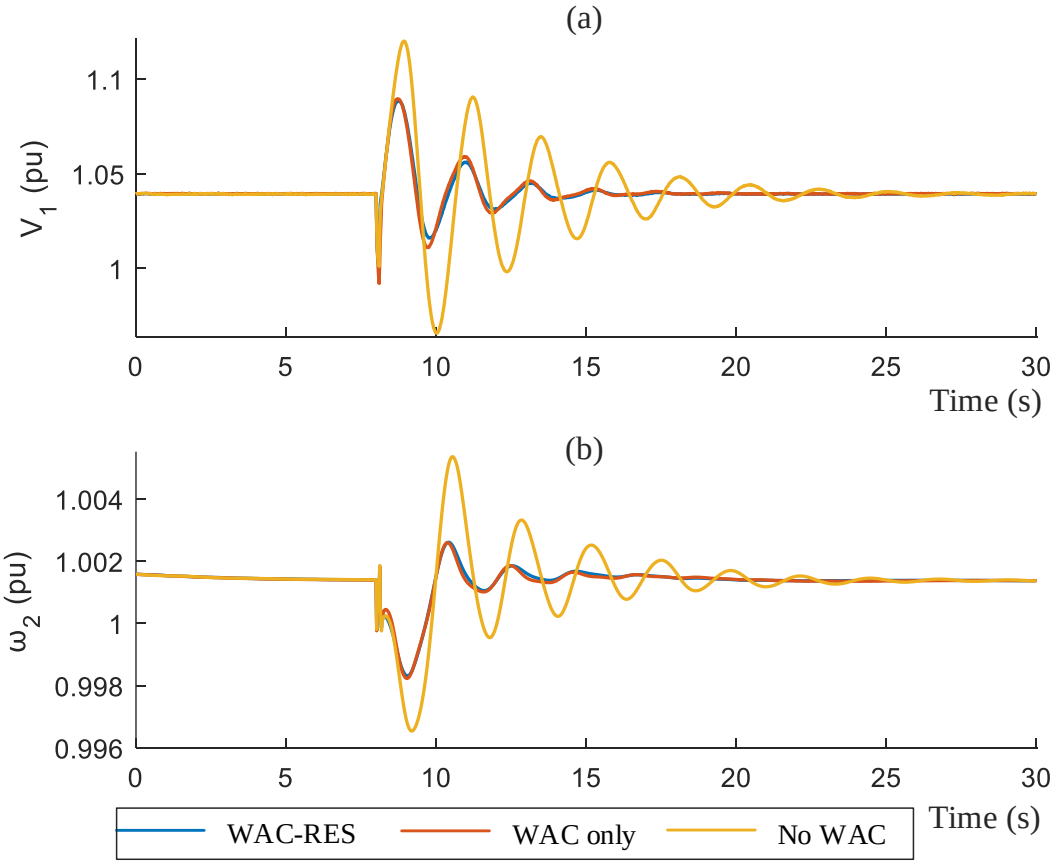

Fig. 7.5 System response for the No WAC, WAC only and WAC-RES scenarios at the event of asymmetric fault for the cases of: (a) terminal voltage of G1 and (b) rotor speed of G2.

and robustness of the proposed WAC-RES scheme was verified by various simulation case

studies. These include load change, symmetric faults and asymmetric grid faults, based on the IEEE 9-bus test system. For the load change case study, a 50% increase of the load located at bus 6 (by 45 MW and 15 MVAr) took place which represents a 14% increase of the initial total load. The symmetric fault case study considered a 5-cycle three-phase grounded fault, while for the asymmetric fault case, a 5-cycle single-phase to ground fault occurred. All the examined faults take place on the line connecting bus 6 with bus 9.

The performance of the proposed WAC-RES cooperation scheme (WAC-RES) was compared to the normal operation scenario where no WAC exists (No WAC) in the system and the scenario where WAC exists in the system but it does not cooperate with the RES (WAC only). It is worth mentioning here that only graphical results are presented here, as this is a preliminary work of the methodology developed in the next subchapter. The results of applying the load change, the symmetric fault and the asymmetric fault are illustrated in Fig. 7.3, Fig. 7.4 and Fig. 7.5 respectively. More specifically, Fig. 7.3 shows substantial increase of the WAC damping performance especially when the terminal voltage of G2 is considered, even at high and low wind conditions. It is noted that in high wind conditions, the RES produces 15 MW, while in low wind conditions it produces only 5 MW. Considering the symmetric (Fig. 7.4) and asymmetric faults (Fig. 7.5), it can be seen that the inclusion of WAC is essential, as the system is severely affected by the appearance of intense oscillations. By comparing the WAC only and WAC-RES scenarios, it is noted that at both cases a smaller but still a significant improvement is achieved through the utilization of the cooperation scheme. It is worth noting here that this is improvement is obtained by considering only one renewable into the system.

Summarizing, this cooperation scheme became feasible by making the generators "aware" of the RES oscillations through the WAC signals. In addition, the damping capability of the system is increased by modifying the RES local controller to properly utilize the available reactive power of the renewable in order to damp out any local oscillations. The advantage of this control scheme is that there is no need to derive WAC signals for the control of RESs and therefore their integration into the WAC scheme is not required to improve the dynamic stability of the system.

7.2 Integration of Renewables into the Wide Area Control Scheme

The work presented in the previous subsection has illustrated that by providing to the synchronous generators the information considering the renewable's behavior and by

modifying also the RES's local controller to provide support at the presence of small signal oscillations, has improved the system's stability. Therefore, naturally one would wonder what is going to be the achievable improvement on the system's damping performance, when instead of considering a cooperation between the WAC and RESs, an actual integration of the two components took place along with increased penetration levels of the latter. Due to this reason, this subsection proposes the implementation of a two-level hierarchical controller, which integrates both synchronous generators and RESs in its design. The proposed WAC scheme is developed by advancing the methodology presented in [39], in order to derive coordination signals not only for the generators but for the RESs as well. Furthermore, the ultimate goal is to illustrate that the correct coordination of generators and RESs, through the WAC, improves the damping performance of the entire system instead of decreasing it, even under a high penetration of renewables [27]. It should be mentioned that in this work, detailed models of the power system are combined with a very accurate model of the RES local controller (subchapter 3.4) for a more realistic operation.

7.2.1 Integration of RESs in the WAC scheme

This study considers the effect of the high penetration of large scale fully converted renewables, where the only requirement for their integration into the proposed WAC scheme is to slightly adjust the GSC controller. Like in the case of the synchronous generator's local

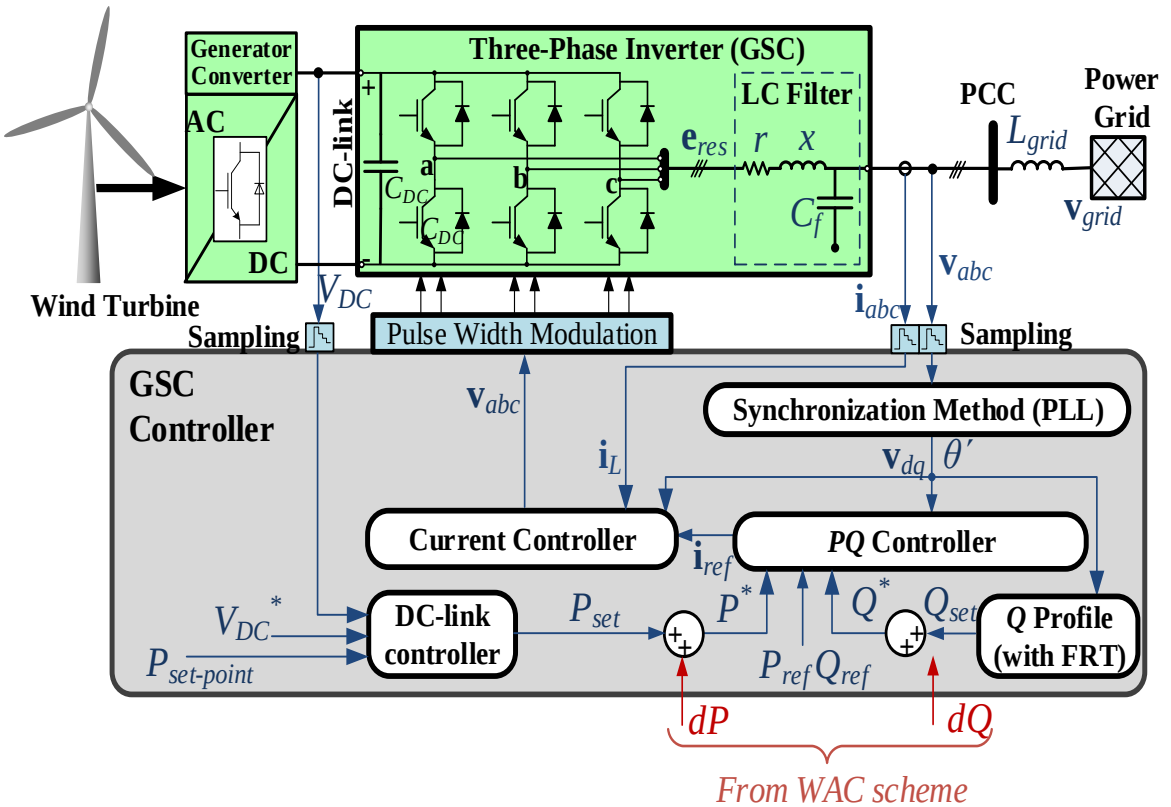

Fig. 7.6 A fully converted RES with the generator converter, the GSC and its controller, and the slight modifications for considering WAC signals.

controllers (subchapter 4.1), to make possible their WAC coordination it is important to identify the appropriate local control inputs which the wide area controller will interact with. Considering the RESs, these signals are the reference inputs of the GSC's PQ controller, as shown in Fig. 7.6. More specifically, the GSC needs to be able to receive the remote signals for the active (*dP*) and reactive power (*dQ*) in order to adjust the injected active and reactive power by the renewable according to the proposed WAC scheme. The signals *dP* and *dQ* are derived by the wide area controller and they aim to decouple the oscillations caused by other generators and RESs, resulting that way to a proper damp of local and inter-area oscillations under intense power disturbances.

The integration of the RESs into the WAC scheme is actually based on the availability of all the necessary synchronized measurements, required for the wide area controller operation. Due to this reason, the analysis presented in the previous subchapter considering the RES virtual power angle estimation ((7.1)-(7.3)) has been utilized here as well. In the same context, the suggested modification (proposed previously) of the first step of the methodology presented in subchapter 4.2, is also used here. In other words, the proposed procedure begins by expressing all the generator-free and renewable-free buses in terms of the generators and RESs terminal voltages (v_d, v_q and $v_{res\text{-}d}$, $v_{res\text{-}q}$, respectively). This step is important in order to make each generator "aware" of the oscillations caused by the remaining generators and RESs and vice versa, each RES to be "aware" of the oscillations caused by the remaining RESs and generators. The rest of the steps remain as they were described in subchapter 4.2, to derive the generators' WAC signals, while for the RESs these steps are different. More specifically, in the case of renewables, equation (7.7) needs to be added to the power system network model ((4.8)-(4.9) of subchapter 4.1), which actually represents the current equation for the i^{th} RES bus.

$$(i_{res-di} + ji_{res-qi})e^{j(\delta_i - \pi/2)} + \sum_{k=1}^{m}(G_{ik}^{'} + jB_{ik}^{'})v_k e^{j\theta_k} = 0 \qquad (7.7)$$

Based on (7.7), the injected current phasor ($i_{res\text{-}d}$ and $i_{res\text{-}q}$) of each RES is expressed in terms of its terminal voltage ($v_{res\text{-}d}$ and $v_{res\text{-}q}$) respectively. This leads to (7.8)-(7.9), where indices *n* and *l* refer to the total number of generator and RES buses, respectively. G^f and B^f are terms based on the elements of the admittance matrix, which result from the application of the first step of the proposed methodology. Note that respective expressions (which depend on terminal voltages of generators and renewables), will result when the formulation of the generator WAC signals is considered.

$$i_{res-di} = -G_{ii}^{f} v_{res-di} + B_{ii}^{f} v_{res-qi} - \sum_{k=1}^{n} (G_{ik}^{f} v_{dk} - B_{ik}^{f} v_{qk}) \cos\delta_{ki} - (G_{ik}^{f} v_{qk} + B_{ik}^{f} v_{dk}) \sin\delta_{ki}$$
$$- \sum_{\substack{j=1 \\ j \neq i}}^{l} (G_{ij}^{f} v_{res-dj} - B_{ij}^{f} v_{res-qj}) \cos\delta_{ji} - (G_{ij}^{f} v_{res-qj} + B_{ij}^{f} v_{res-dj}) \sin\delta_{ji} \quad (7.8)$$

$$i_{res-qi} = -G_{ii}^{f} v_{res-qi} - B_{ii}^{f} v_{res-di} + \sum_{k=1}^{n} (G_{ik}^{f} v_{dk} - B_{ik}^{f} v_{qk}) \sin\delta_{ki} + (G_{ik}^{f} v_{qk} + B_{ik}^{f} v_{dk}) \cos\delta_{ki}$$
$$+ \sum_{\substack{j=1 \\ j \neq i}}^{l} (G_{ij}^{f} v_{res-dj} - B_{ij}^{f} v_{res-qj}) \sin\delta_{ji} + (G_{ij}^{f} v_{res-qj} + B_{ij}^{f} v_{res-dj}) \cos\delta_{ji} \quad (7.9)$$

where, $\delta_{ji} = \delta_j - \delta_i$

The next step is to replace (7.8) and (7.9) into the model of the RES. For this reason, the RES virtual model (which has been defined in (7.1) and (7.2)) is utilized. Furthermore, all the terminal voltages of generators and renewables existing in the resulting expressions are substituted by their error compared to their steady-state values (corresponding dv_d, dv_q and dv_{res-d}, dv_{res-q}), thus deriving expressions of the de_{res-d} and de_{res-q}. This change of variables is required for canceling out the WAC contribution when the system is operating in steady-state conditions.

Similar to the generators' case, in order to formulate the RES WAC laws, it is important to identify the suitable local signals, which the wide area controller will utilize to interact with the RES local controller. Based on the RES virtual model of (7.1) and (7.2), these are the e_{res-d} and e_{res-q}. Thus, by decomposing de_{res-d} and de_{res-q}, into local and global control signals, the RES coordination signals are found by selecting the global part to explicitly cancel out the perturbation terms ψ_{res_d} and ψ_{res_q}. These terms are actually equal to the superposition terms of (7.8) and (7.9), respectively, where dv_d, dv_q and dv_{res-d}, dv_{res-q} are considered. This leads to the following expressions for the RES WAC signals:

$$de_{res\_di}^{g} = -r_i \psi_{res\_d}^{i} + x_i \psi_{res\_q}^{i} \quad (7.10)$$

$$de_{res\_qi}^{g} = -r_i \psi_{res\_q}^{i} - x_i \psi_{res\_d}^{i} \quad (7.11)$$

where,

$$\psi_{res\_d}^{i} = -\sum_{k=1}^{n} (G_{ik}^{f} dv_{dk} - B_{ik}^{f} dv_{qk}) \cos\delta_{ki} - (G_{ik}^{f} dv_{qk} + B_{ik}^{f} dv_{dk}) \sin\delta_{ki}$$
$$- \sum_{\substack{j=1 \\ j \neq i}}^{l} (G_{ij}^{f} dv_{res-dj} - B_{ij}^{f} dv_{res-qj}) \cos\delta_{ji} - (G_{ij}^{f} dv_{res-qj} + B_{ij}^{f} dv_{res-dj}) \sin\delta_{ji}$$

$$\psi^{i}_{res\_q} = \sum_{k=1}^{n}(G^{f}_{ik}v_{dk} - B^{f}_{ik}v_{qk})\sin\delta_{ki} + (G^{f}_{ik}v_{qk} + B^{f}_{ik}v_{dk})\cos\delta_{ki}$$
$$+\sum_{\substack{j=1 \\ j\neq i}}^{l}(G^{f}_{ij}v_{res-dj} - B^{f}_{ij}v_{res-qj})\sin\delta_{ji} + (G^{f}_{ij}v_{res-qj} + B^{f}_{ij}v_{res-dj})\cos\delta_{ji}$$

The result of the aforementioned analysis is that the wide area controller can now provide the $de^{g}_{res\text{-}d}$ and $de^{g}_{res\text{-}q}$ control signals of (7.10)-(7.11) to the renewables' controller in order to regulate their operation for damping the power system oscillations. However, as mentioned previously, according to the GSC controller of Fig. 7.6, the most suitable signals for the wide area controller to interact with are the references for the active and reactive power. Therefore, the $de^{g}_{res\text{-}d}$ and $de^{g}_{res\text{-}q}$ signals (according to the virtual RES model) need to be converted into the compatible signals (dP and dQ) by the wide area controller and then to be sent into the RES local controller (Fig. 7.6).

To overcome this compatibility issue, firstly the wide area controller needs to compute the new expressions for the virtual internal RES voltage according to (7.12) and (7.13), as these result from the application of the WAC signals of (7.10)-(7.11).

$$e^{new}_{res-di} = v_{res-di} + r_i i_{res-di} - x_i i_{res-qi} + de^{g}_{res\_di} \tag{7.12}$$

$$e^{new}_{res-qi} = v_{res-qi} + r_i i_{res-qi} + x_i i_{res-di} + de^{g}_{res\_qi} \tag{7.13}$$

Thus, the resulting active and reactive power flow between the grid tied inverter and the LC filter can be calculated as follows:

$$P_{dq\_i} = \frac{3}{2}(e^{new}_{res-di}\, i_{res-di} + e^{new}_{res-qi}\, i_{res-qi}) \tag{7.14}$$

$$Q_{dq\_i} = \frac{3}{2}(e^{new}_{res-qi}\, i_{res-di} - e^{new}_{res-qi}\, i_{res-qi}) \tag{7.15}$$

Furthermore, the new active and reactive power of RES at the PCC (P_{new} and Q_{new}) obtained from applying the WAC signals are given in (7.18)-(7.19), which derive by subtracting the LC filter losses of (7.16)-(7.17) from the power of (7.14)-(7.15).

$$P_{losses\_i} = \frac{3}{2}(i^2_{res-di} + i^2_{res-qi})r_i \tag{7.16}$$

$$Q_{losses\_i} = \frac{3}{2}(i^2_{res-di} + i^2_{res-qi})x_i \tag{7.17}$$

$$P_{new\_i} = P_{dq\_i} - P_{losses\_i} \tag{7.18}$$

$$Q_{new\_i} = Q_{dq\_i} - Q_{losses\_i} \tag{7.19}$$

Finally, the required coordination signals (*dP* and *dQ*) are derived according to (7.20)-(7.21), where P_{res} and Q_{res} represent the current active and reactive power output of RES.

$$dP_i = P_{new\_i} - P_{res\_i} \tag{7.20}$$

$$dQ_i = Q_{new\_i} - Q_{res\_i} \tag{7.21}$$

It is to be noted that the lower bound of *dP*, can be as much as the WAC needs it to be. However, its upper bound is limited by the available active power, which the RES can provide. The resulting *dP* and *dQ* signals derived by the WAC scheme can now be sent to

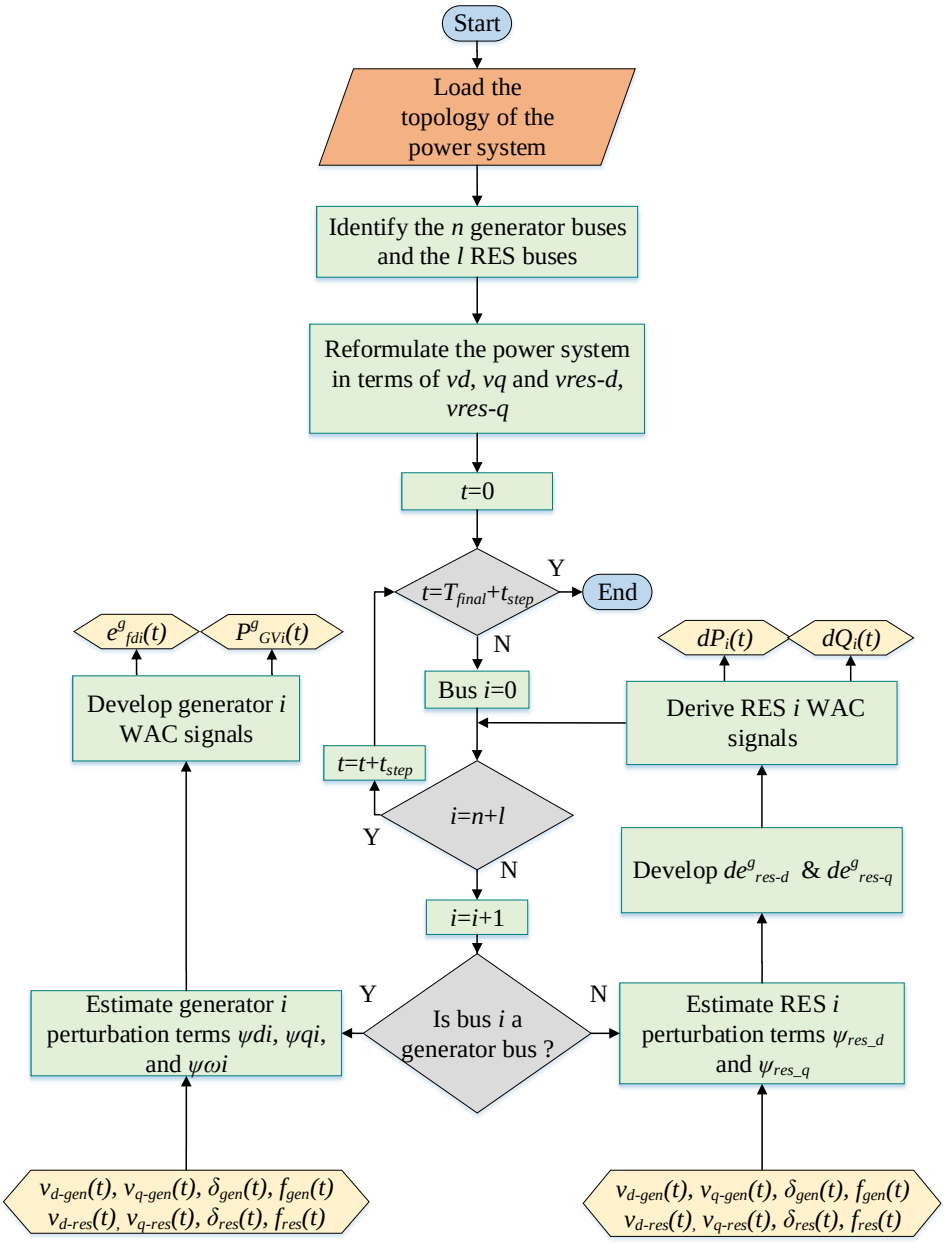

Fig. 7.7 Flow diagram of proposed methodology, illustrating the procedure followed to derive the WAC signals intented for the coordination of synchronous generators and renewables.

the respective renewables in order to ensure that both generators and RESs can properly contribute to the power oscillation damping. The flowchart of Fig. 7.7 summarizes the overall procedure of the proposed scheme for the development of coordination signals for generators and RESs. Note that T_{final} represents the total time of the simulation and t_{step} the reporting rate of the PMU (20 ms).

The objective now is to validate the performance of the proposed control scheme. To achieve this, various simulation case studies were performed, based on the two dynamic test systems. Note that to verify the performance of the proposed WAC-RES integration (WAC-RES), a comparison was made with the normal operation scenario where no WAC exists in the system, (No WAC) and the scenario where WAC exists in the system, but it considers only the generators (not the RESs) for coordination in its design (WAC only).

7.2.2 Validation through the IEEE 9-bus dynamic test system

For the evaluation of the proposed scheme, the IEEE 9-bus dynamic test system has been initially utilized here where various simulation case studies were performed. To illustrate the performance of the proposed methodology, a significant penetration of large-scale renewables is considered. More specifically, three 20 MVA RESs are integrated at buses 5, 6 and 8 through step-up transformers, as shown in Fig. 7.8.

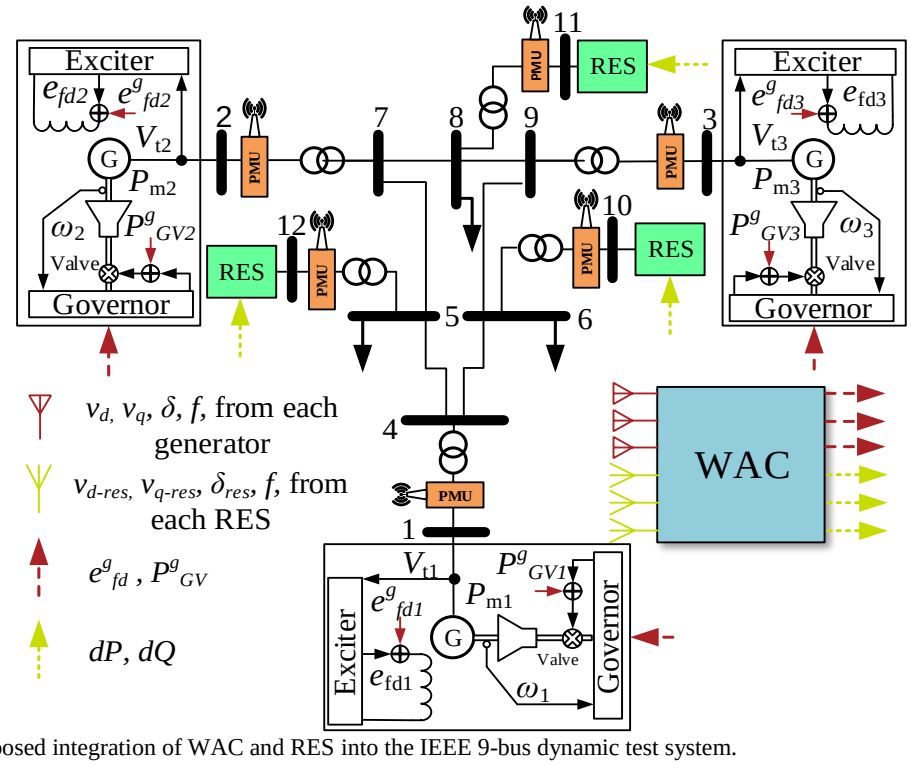

Fig. 7.8 Proposed integration of WAC and RES into the IEEE 9-bus dynamic test system.

Case Study 1: Constant Loads

To present the increased performance of the proposed WAC, in this first case study a symmetric fault occurs. More specifically, a 5-cycle three-phase fault (grounded) is considered in the simulation (which occurs on the line connecting bus 4 and bus 6 at t=8 s) along with constant loads. TABLE 7.1 lists the Prony analysis results for the dominant local and inter-area modes of the system. From TABLE 7.1, it can be noted that in the case of both local and inter-area oscillations, the proposed WAC-RES scheme provides significant additional damping compared to the WAC only and No WAC scenarios. Furthermore, Fig. 7.9(a) presents the frequency oscillation of G2, where it is evident that the proposed scheme surpasses all the other scenarios.

Case Study 2: Dynamic Loads

In order to further verify the stability improvement of the proposed method, the aforementioned symmetric fault is utilized again for the case where dynamic non-linear loads are included in the test system. Specifically, the constant loads located at buses 6 and 8 (Fig. 7.8) are substituted by their corresponding dynamic loads (considering the same initial active and reactive power). The model of the dynamic non-linear load adopted in this case study is the exponential dynamic load model, as it has been introduced in subchapter 3.5 ((3.8) and (3.9)). The model parameters considered here are [n_p n_q]=[0.39 1.72] and [T_p T_q]=[363s 0.1s] in order to achieve an intense dynamic behavior from the two loads. As illustrated by Fig. 7.9(b) and TABLE 7.1, the No WAC and the WAC only scenarios lead the system to instability when the fault occurs. On the contrary, the WAC-RES scenario damps effectively all the local and inter-area oscillations. Consequently, in this case study, only the proposed scheme is capable of restoring the system's stability, outperforming the other two scenarios.

Case Study 3: DFIG and Dynamic Loads

The objective of the third test is mainly to study the impact of considering two dynamic loads and a DFIG wind turbine (in addition to the fully converted RES) in the test system. The DFIG wind turbine is included mainly to illustrate the applicability of the proposed scheme to any type of renewable. As a disturbance, a symmetric fault which takes place at bus 2 is utilized. The dynamic loads are placed once again on buses 6 and 8, but in this case study [n_p n_q]=[1.01 1.04] and [T_p T_q]=[0.1s 0.2s]. The DFIG wind turbine has substituted the fully converted renewable of bus 12. The methodology, as it is presented in

subchapter 7.2.1, can be applied directly to the GSC of the DFIG wind turbine regarding the reactive power coordination (*dQ*). The active power coordination (*dP*) cannot be used directly in this type of wind turbine due to the strong coupling between the active and reactive power of the induction generator that does not straightforwardly allow the

TABLE 7.1: PRONY ANALYSIS FOR THE IEEE 9-BUS TEST SYSTEM

Constant Loads						
Type	No WAC		WAC only		WAC-RES	
	ζ(%)	*f(Hz)*	*ζ(%)*	*f(Hz)*	*ζ(%)*	*f(Hz)*
Local mode	3.85	1.9	4.68	1.9	5.27	1.9
Inter-area mode	4.62	0.93	5.69	0.95	6.29	0.96
Dynamic Loads						
Type	No WAC		WAC only		WAC-RES	
	ζ(%)	*f(Hz)*	*ζ(%)*	*f(Hz)*	*ζ(%)*	*f(Hz)*
Local mode	Instability		Instability		4.35	1.9
Inter-area mode	Instability		Instability		6.35	0.95
DFIG and Dynamic Loads						
Type	No WAC		WAC only		WAC-RES	
	ζ(%)	*f(Hz)*	*ζ(%)*	*f(Hz)*	*ζ(%)*	*f(Hz)*
Local mode	5.27	1.9	5.85	1.9	6.1	1.9
Inter-area mode	5.3	0.93	5.57	0.94	6.08	0.94

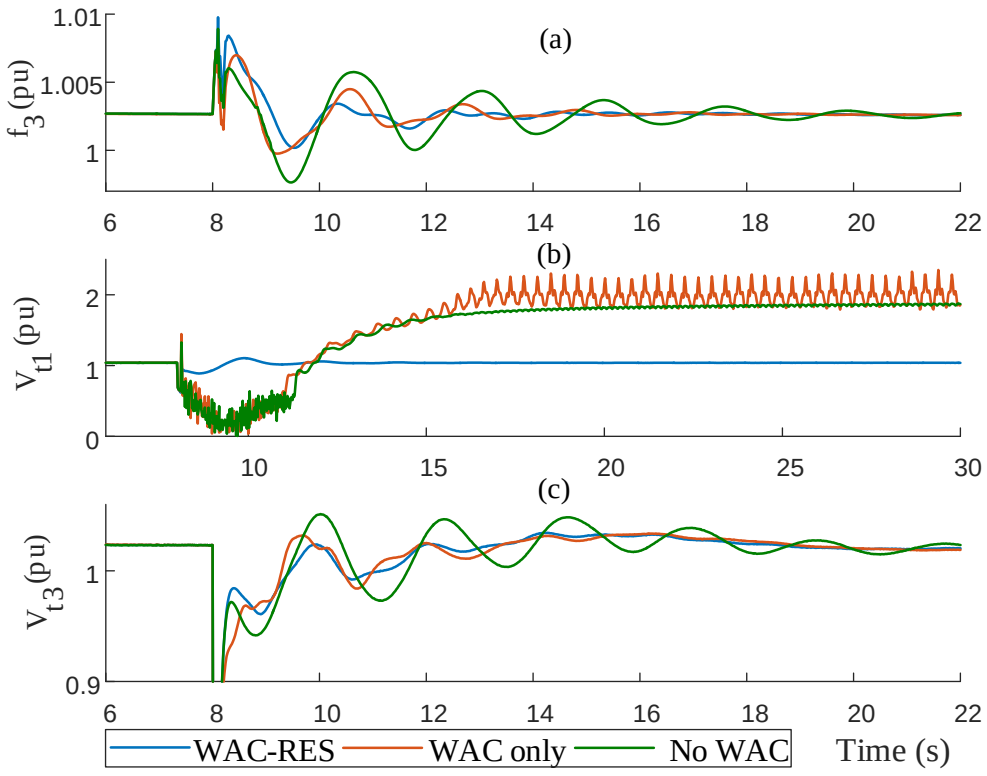

Fig. 7.9 Comparison of WAC-RES, WAC only and No WAC performances on the IEEE 9-bus test system considering: (a) the frequency oscillation of G3 for constant loads, (b) the voltage oscillation of G1 for dynamic loads, and (c) the voltage oscillation of G3 for DFIG and dynamic loads.

decoupled coordination of the DFIG. More specifically, by sending the *dP* signal to the GSC will have as a result to also affect the rotor side converter which in turn will change the active power of the rotor. As a consequence, the active power of the stator of the induction machine will change as well. Due to the coupling nature of the induction machine, the reactive power of the DFIG will also be affected. Therefore, only the *dQ* signal is sent to the GSC which allows the decoupled coordination of the reactive power without affecting the active power. Nevertheless, the Prony results of TABLE 7.1 illustrate once again that the transient performance of the system is improved with the proposed WAC-RES scheme. More specifically, in Fig. 7.9(c) one can note that the WAC-RES compensation of local oscillations excels all the other scenarios.

7.2.3 Validation through the IEEE 39-bus dynamic test system

For further validation of the proposed scheme's performance, the latter has been also applied in a larger test system. More specifically, the IEEE 39-bus dynamic test system has been utilized here. To apply a high penetration of renewables in this test system, five 250 MVA RESs are considered to be installed on buses 8, 14, 24, 25 and 27 through step-up transformers, as Fig. 7.10 denotes.

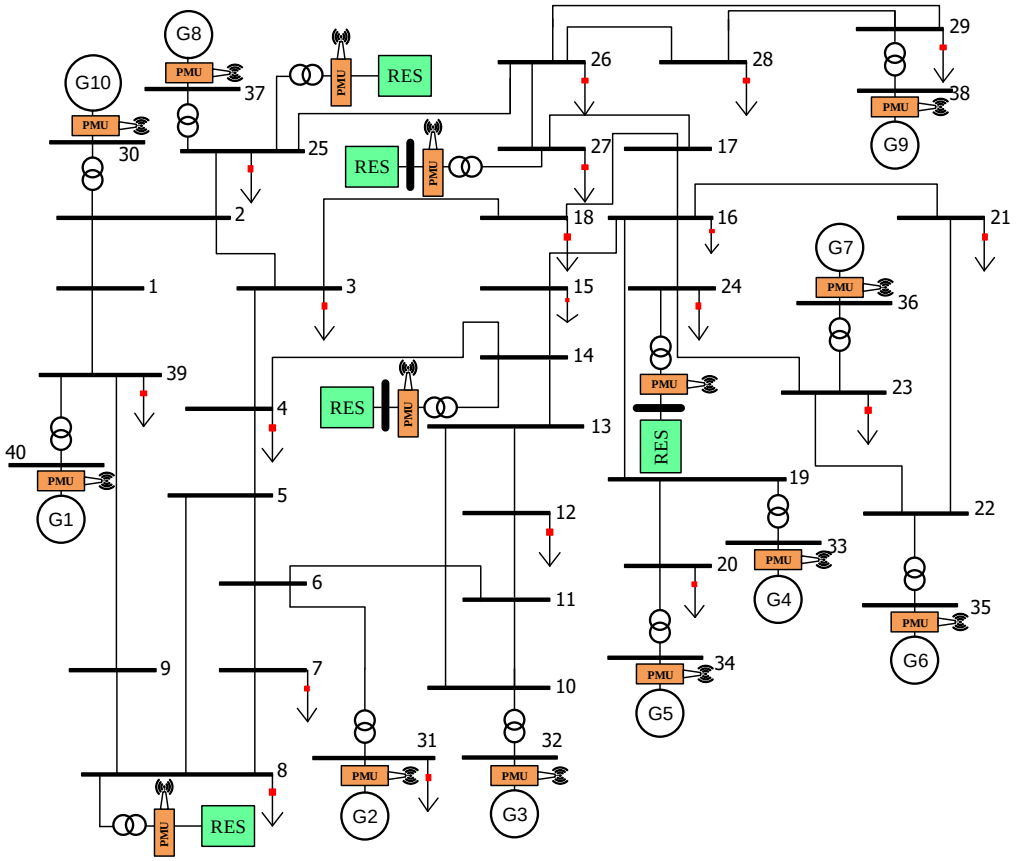

Fig. 7.10 Proposed integration of WAC and RES into the IEEE 39-bus dynamic test system.

Case Study 1: Load Change

To evaluate the performance of the proposed scheme in this system as well, firstly a total load increase of 640 MW and 200 MVAr (11% increase of the initial load) occurs on the loads of buses 3 and 16 at t=3 s. As shown in TABLE 7.2 and Fig. 7.11(a), the proposed method surpasses the other two scenarios regarding the effective damping of both local and inter-area oscillations.

Case Study 2: Symmetric Fault

Next, a 5-cycle three-phase grounded fault has been applied on the line connecting bus 3 and bus 4, at t=3 s. TABLE 7.2 presents the Prony analysis results of this case study, where it can be seen that the WAC-RES scenario provides (once again) better damping of the system's oscillations (Fig. 7.11(b)). An interesting point here is that although the No WAC scenario has a local mode damping that is approximately half of the proposed method's performance, it has a comparable damping ratio to the latter regarding the compensation of the inter-area modes.

Case Study 3: Asymmetric Fault

Finally, the application of an asymmetric fault has been investigated. More specifically, a two-phase ungrounded fault takes place on the line connecting bus 3 and bus 4, at t=3 s. TABLE 7.2 illustrates clearly that in the case of an asymmetric fault, the proposed scheme still has a better damping of both, local and inter-area oscillations, compared to the WAC only and No WAC scenarios. An example of the local oscillation damping is illustrated in Fig. 7.11(c), which presents the frequency response of G10.

7.3 Conclusion

This chapter proposed two novel and universal methodologies, not only for addressing the impact of the high penetration of RESs but for improving also the system's stability through the use of WAC schemes. The first method presents a cooperation scheme between the wide area controller and the renewables, having as a goal the improvement of the system's stability. The advantage of this methodology is that it improves the dynamic stability of the system without deriving coordination signals for the WAC of RESs and therefore their integration into the wide area controller architecture is avoided. This became feasible by making the synchronous generators "aware" of the dynamic operation of the RES, through the use of WAC signals which are implemented based on synchronized

TABLE 7.2: PRONY ANALYSIS FOR THE IEEE 39-BUS TEST SYSTEM

Load Change						
Type	No WAC		WAC only		WAC-RES	
	ζ(%)	*f(Hz)*	*ζ(%)*	*f(Hz)*	*ζ(%)*	*f(Hz)*
Local mode	8.49	1.4	9.82	1.5	11.3	1.4
Inter-area mode	20.8	0.66	22.3	0.66	27.4	0.67
Symmetric Fault						
Type	No WAC		WAC only		WAC-RES	
	ζ(%)	*f(Hz)*	*ζ(%)*	*f(Hz)*	*ζ(%)*	*f(Hz)*
Local mode	3.29	1.4	5.22	1.4	6.23	1.3
Inter-area mode	12	0.79	10.6	0.85	12.3	0.83
Asymmetric Fault						
Type	No WAC		WAC only		WAC-RES	
	ζ(%)	*f(Hz)*	*ζ(%)*	*f(Hz)*	*ζ(%)*	*f(Hz)*
Local mode	5.45	1.4	5.72	1.5	6.56	1.5
Inter-area mode	15.1	0.77	16.3	0.77	19.2	0.75

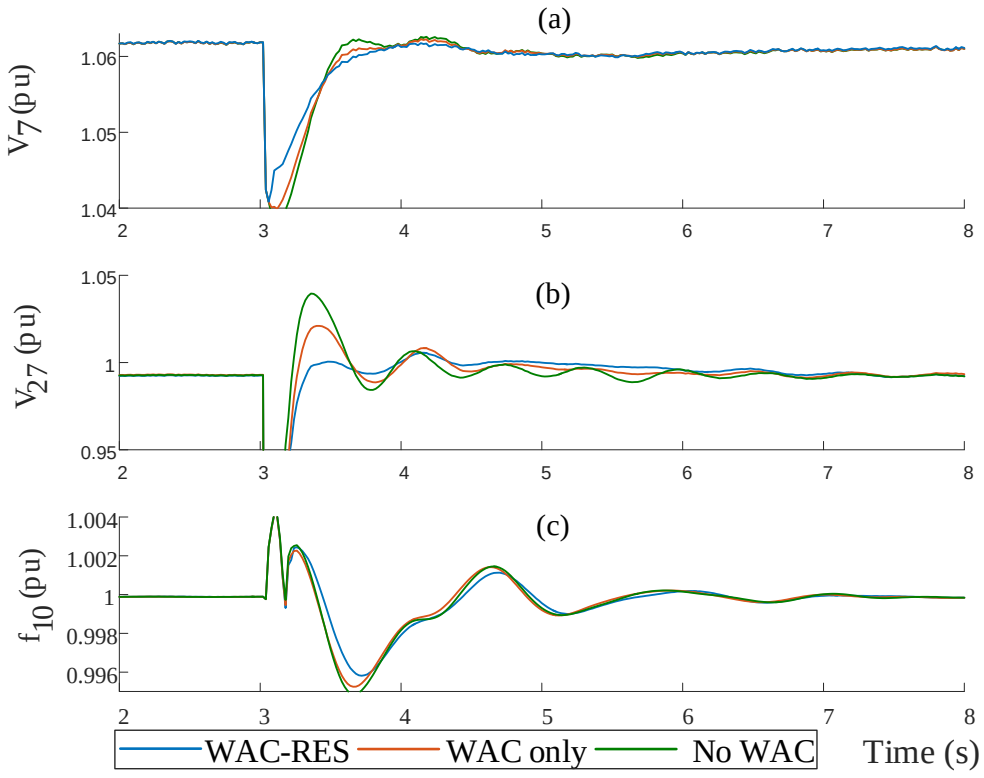

Fig. 7.11 Comparison of WAC-RES, WAC only and No WAC performances on the IEEE 39-test system considering: (a) the terminal voltage oscillation of G7 during load change, (b) the voltage oscillation of bus 27 during a symmetric fault, and (c) the frequency oscillation of G10 during an asymmetric fault.

measurements from generators and renewables. In addition, the damping capability of the system is increased by modifying the RES local controller to properly utilize the available reactive power of the renewable in order to damp out small oscillations which do not exceed the DBZ. The performance of the proposed method is evaluated by case studies based on the

IEEE 9-bus test system, where various disturbances were investigated, such as load increase, symmetric and asymmetric grid faults. The simulation results indicate that the power system oscillations are effectively compensated by utilizing the proposed cooperation scheme.

The second methodology advances the first one, in order to make both the generators "aware" of the RES oscillations and vice versa, the RESs "aware" of the generator oscillations. It actually proposes a hierarchical WAC scheme that coordinates all the generator and renewable local controllers in order to improve considerably the power system dynamic stability under a high penetration of renewable energy sources. Note that adjustments where applied to the obtained RES WAC signals so that minor modifications will be required on the RES local controllers to become compatible. Various case studies under different contingencies based on the IEEE 9-bus and 39-bus dynamic test systems, are used to evaluate the performance of the proposed control scheme. In all cases, the simulation results indicate that the proposed WAC coordination of generators and RESs improves the damping performance of the entire system under a high penetration of renewables.

In order to present the improved damping performance of the proposed schemes, all the results of this chapter are obtained in comparison with the normal operation scenario where no WAC exists in the system and the scenario where WAC exists in the system but it does not consider the RESs for cooperation/integration schemes. Although, the second methodology advances the first one, the two methods have a different approach since the former does not consider the renewables to be coordinated by the wide area controller, while the latter integrates the RESs into the WAC scheme. Note that both methodologies are implemented in such a way so that they can be applied to any type of renewable.

CHAPTER 8
NOVEL COORDINATION METHODOLOGIES FOR ADVANCING THE WIDE AREA CONTROL PERFORMANCE IN REAL-TIME ENVIRONMENTS

Although methodologies have been implemented for compensating the data delays/dropouts and the penetration of renewables into the system, there is still work to be done in order to obtain a highly effective and robust wide area controller. Therefore, this chapter presents the implementation of novel methodologies for advancing and enhancing the WAC performance, along with methods for addressing the remaining threats and the drawbacks of the adopted wide area controller (as they were identified in Chapter 4). In this context, the combination of the WAM with an advanced wide area controller is illustrated. In addition, it is important to emphasize that the final component remaining for ensuring the robustness and effectiveness of a WAC method is to utilize real-time simulation environments. To achieve this it is necessary to apply the methodology in real-time conditions, which in combination with the aforementioned realistic simulation environments can result into the most suitable testbed for testing and validating WAC methodologies. Furthermore, this chapter illustrates the implementation of a novel laboratory setup for evaluating the WAMC performance in almost actual conditions, by utilizing the real-time simulator and real equipment. Therefore, it is necessary to begin this chapter with an introduction to the real-time simulation environments.

8.1 Real-Time Simulation

8.1.1 Introduction and State-of-the-art

Chapter 3 has illustrated the steps considered in this Ph.D. dissertation for deriving realistic simulation environments, suitable for testing WAC methodologies (as well as other synchrophasor applications) which are developed according to available Standards and published studies. As it has been illustrated in previous chapters, these simulation environments are especially needed for evaluating the performance of the wide area controller under realistic conditions and for identifying/mitigating threats to its operation. However, the consideration of these environments is still not enough for ensuring that the

proposed WAC methodologies will be successfully implemented and further that they will be able to operate effectively in actual conditions. This is mainly due to the fact that the WAC is an application which needs to be executed in near real-time. The latter is actually a very challenging task and to overcome this issue, advanced design and testing methods are necessary [134].

More specifically, real-time simulators are required to validate the performance of the wide area controller (as well as other real-time methodologies) under highly accurate and real-time environments. The increased accuracy and real-time capability of these simulators combined with the realistic simulation environments (presented in Chapter 3) results into an ideal testbed, suitable for evaluating new methodologies under close to reality conditions. It is important to be mentioned here that the industry considers the utilization of real-time simulators as a widely known and recognized validation procedure of engineering concepts, which is a necessary step before moving to real field tests since it reduces delays, risks and costs. This is mainly due to the real-time validation procedure which provides realistic insights into practical design and implementation challenges [135]. Overall, the real-time simulators provide three simulation options for validating proposed methodologies:

1) SIL: The first one is the Software-In-the-Loop (SIL) simulation where the proposed method is integrated and tested into a real-time model of the system [136]. Fig. 8.1a presents an example of the SIL connection.

2) HIL: The second option is the Hardware-In-the-Loop (HIL) simulation, which provides the capability of connecting physical devices to the real-time simulation model. This kind of simulation is actually used for the development and test of highly complex control, protection and monitoring systems [137]. More specifically, HIL simulation is an alternative to traditional testing, where the real system is replaced by its equivalent real-time model and it is used to interface with other physical equipment (Fig. 8.1b).

3) PHIL: Finally, the advancement of the HIL option is the Power Hardware-In-the-Loop (PHIL). HIL is considered when low-voltage and low-current physical devices are connected to the real-time model, while PHIL provides the actual power flow required by higher power devices. As shown in Fig. 8.1c, this is achieved through the use of a power amplifier between the real-time simulator

and the higher power equipment, meaning that actual power system components (e.g. PVs, relays) can also be included into the loop [138].

Although, this is a crucial part for the evaluation of the WAC performance there is still a very limited work published in the literature. More specifically, the majority of research studies ignore the fact that the real-time simulation is a necessary step for the actual evaluation of these kind of applications. In [120] distributed optimization algorithms are proposed and evaluated offline using MATLAB software and also in real-time through the utilization of a real-time simulator integrated via HIL with PMUs. An analysis of the time delay effect on the WAMC applications is performed in [20], by considering a real-time digital simulator (RTDS). In this work, SIL and HIL simulations have taken place, where in the case of the latter a STATCOM device is used (PMUs are virtually modelled). The issues identified in [20] are that it considers only constant delays to occur between the PMUs and WAMC ignoring also the feedback delays, while it does not provide any means to compensate their effect. In [48], an intelligent energy-based WAC is presented which is tested firstly offline under the event of unrealistic constant delays, and then on a real-time

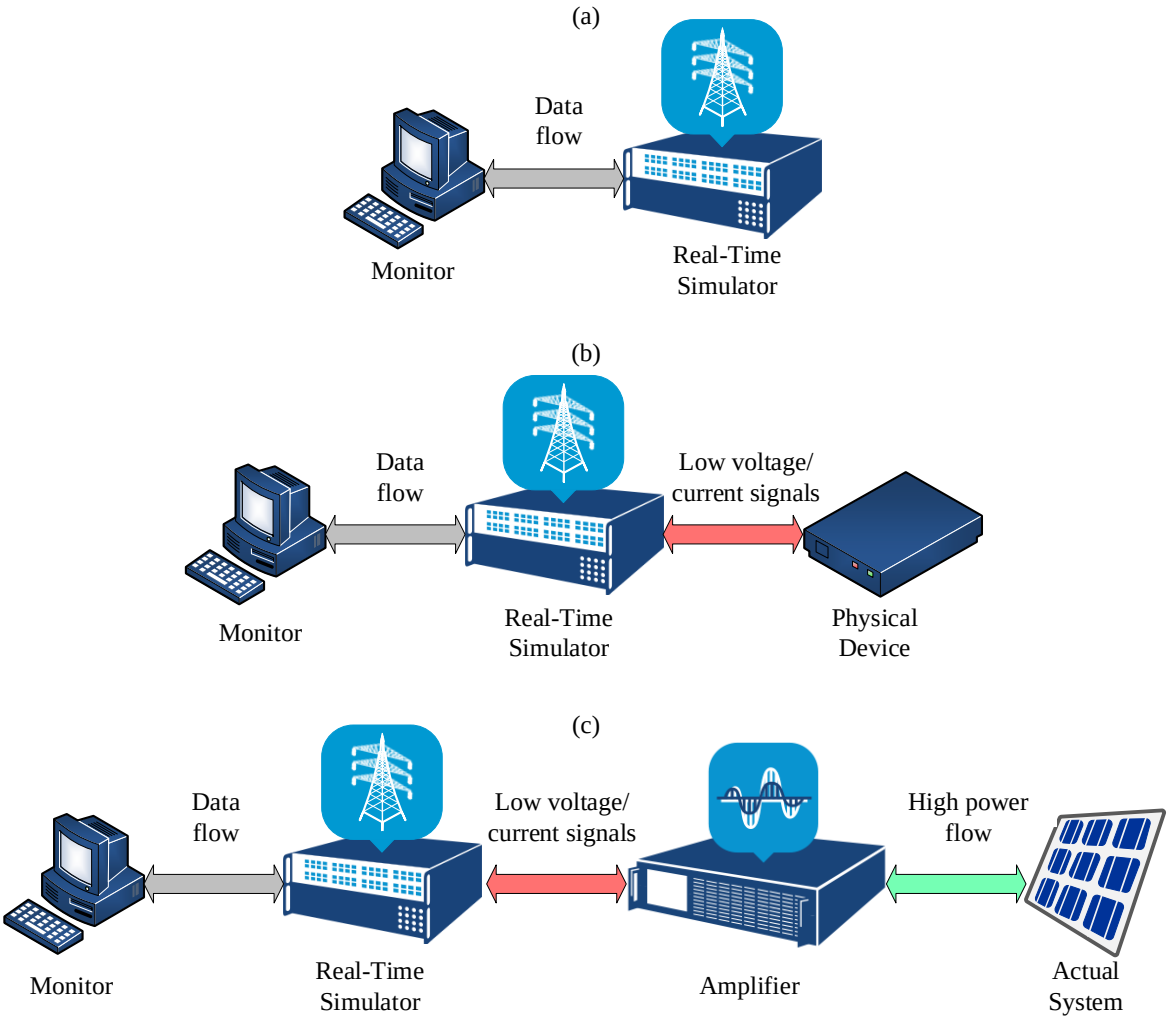

Fig. 8.1 Illustrations the three real-time simulation options: (a) SIL, (b) HIL and (c) PHIL.

simulator (OPAL HYPERSIM) in order to illustrate the real-time stability improvement. Furthermore, a real-time HIL testbench is considered in [135] for the performance assessment of three islanding detection methods and for determining the communication latencies of the implemented network. The development of a flexible and modular distributed infrastructure for smart grid studies is proposed in [136], which is based on an OPAL RT OP5600 real-time simulator. In [139], the authors present the development of a synchro-measurement application which is evaluated through the use of a RTDS, PMUs and a PDC. Finally, [134] presents an overview of how real-time simulators have been utilized in research laboratories around the world.

8.1.2 Real-time simulation models

An OPAL-RT real-time simulator is considered in this chapter for obtaining in real-time more accurate results. More specifically, the OP5700 real-time simulator (Fig. 8.2) combined with the eMEGASIM software package is utilized for simulating in real-time the power system models. The simulation models are initially implemented by blocksets from the MATLAB/Simulink SimPowerSystems toolbox and for the transition to real-time simulation models some components and solvers from the OPAL-RT ARTEMiS plug-in library are considered. The models are compiled and transferred to the real-time simulator through the use of the RT-LAB software. Note that the OP5700 has four cores, each one equipped with an Intel Xeon E5 8 Core CPU at 3.2 GHz and with 8 GB RAM.

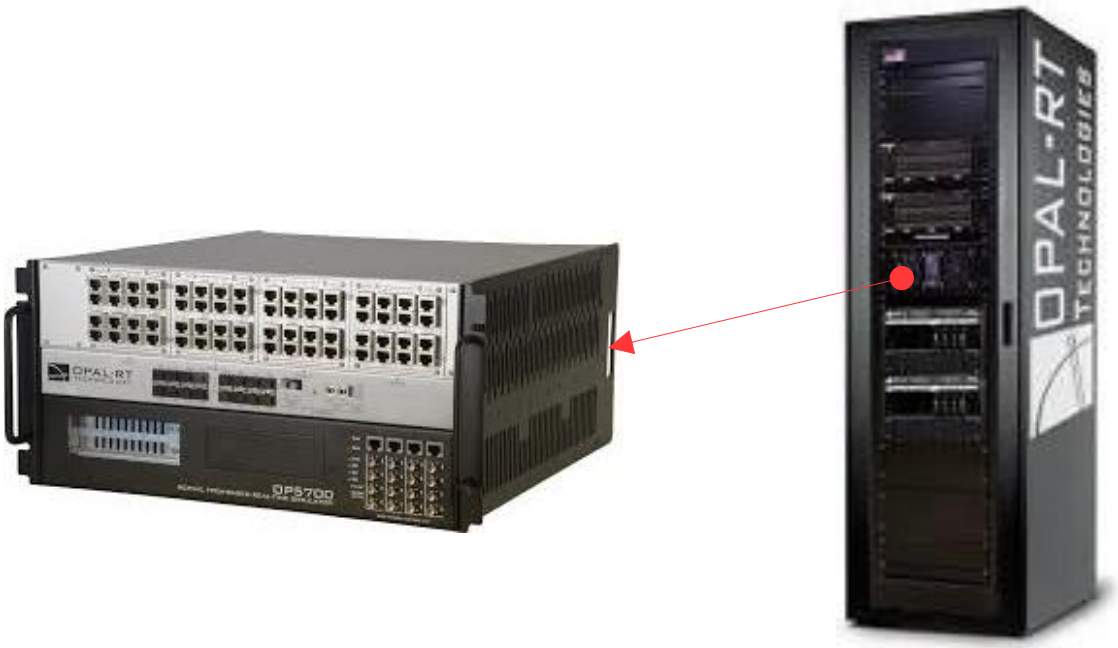

Fig. 8.2 OPAL-RT OP5700 real-time simulator

Subchapter 3.1 has presented the development of two IEEE dynamic test systems, which are modified here into real-time dynamic test systems. Note that the test systems of subchapter 3.1 are considering the commonly used Pi-model for simulating all the transmission lines. For the transition to real-time models, it is necessary to separate the power systems into the areas which are connected via long transmission lines. This is done in order to substitute Pi-models of these lines by the ARTEMiS Distributed Parameters Line (DPL) model. DPL is actually implemented based on the Bergeron's travelling wave method and it

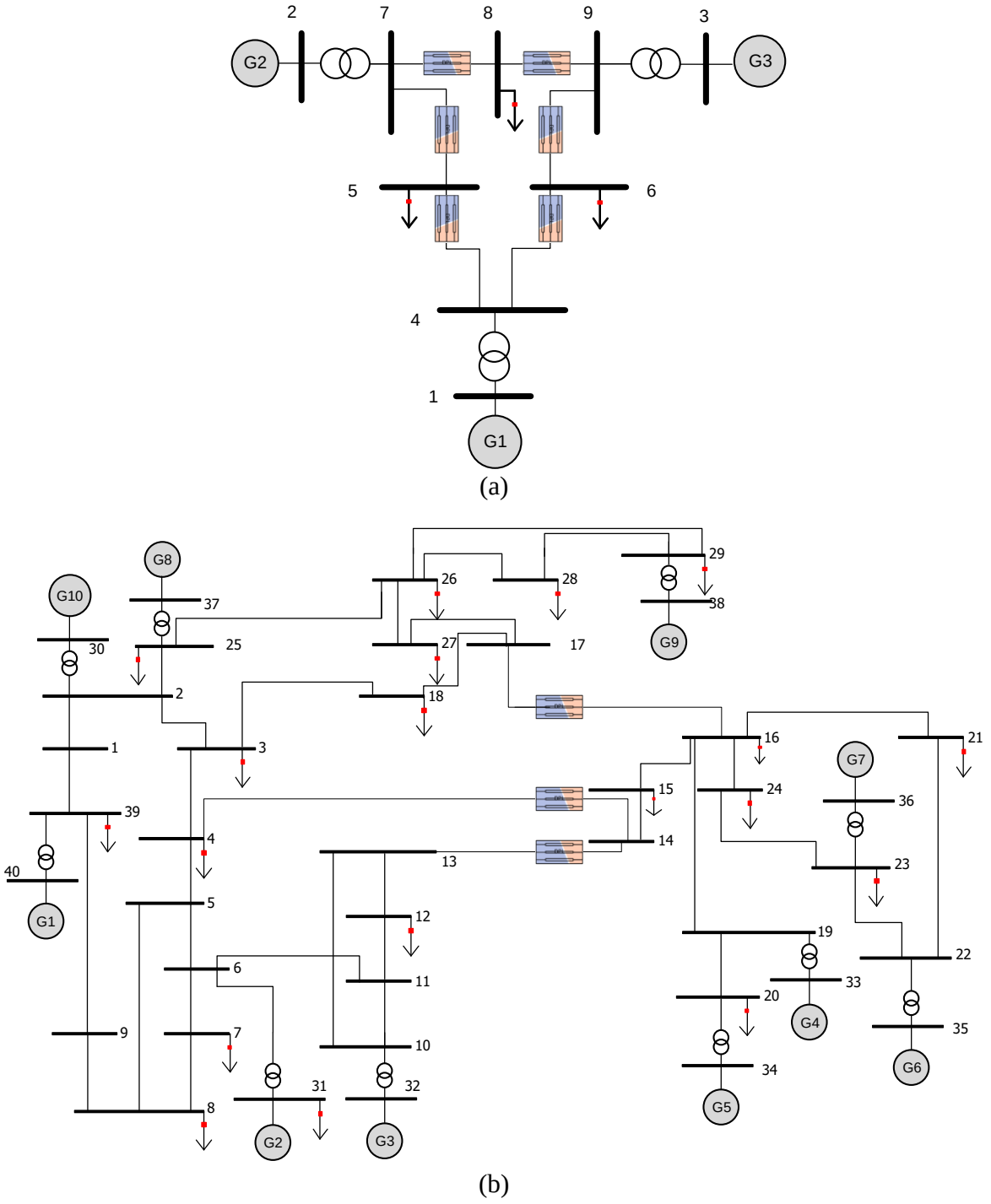

Fig. 8.3 Modification of (a) the IEEE 9-bus and (b) IEEE 39-bus dynamic test systems in order to become real-time models, through the use of ARTEMiS DPL models.

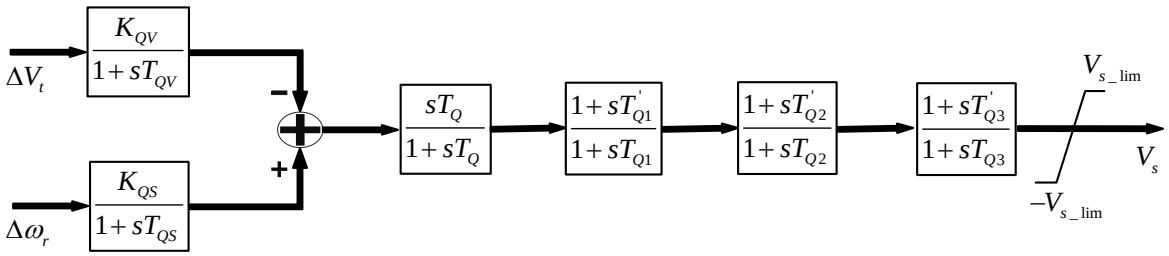

Fig. 8.4 Power system stabilizer block diagram.

allows network decoupling since it reproduces the wave propagation delay which is naturally introduced by the long transmission lines. Fig. 8.3 shows the real-time IEEE 9-bus and 39-bus dynamic test systems.

Furthermore, it is worth noting that if not stated otherwise the synchronous generators of this chapter are further equipped with PSSs. All the required data for the adopted PSS are provided in [93], while Fig. 8.4 shows its block diagram. This addition took place in order to enhance the stability of the systems and to present novel methodologies which are: 1) surpassing by far the achievable stability offered by the PSSs, and 2) they are considering the proper coordination of all the local controllers of the synchronous generator (exciter, governor and PSS).

8.2 Addressing the Wide Area Controller Drawbacks

Apart from presenting the adopted methodology for deriving a conventional wide area controller, Chapter 4 has reported also its several disadvantages which must be compensated here in order to advance the robustness and applicability of the adopted methodology to a new level. The drawbacks identified in subchapter 4.3 are: 1) the assumption that the PMUs provide also the generator's rotor angle δ as a synchronized measurement, 2) scalability issues due to the substantial increase of the required inputs and the derived output signals when moving to larger systems, 3) the utilization of a constant weighting factor for the tuning of the WAC contribution, and finally 4) the assumption of having PMUs installed on all the generator buses.

Therefore, the objective of this subchapter is to present methodologies to address each one of the identified disadvantages. Note that the real-time validation of these methods will be illustrated in the next chapters. Furthermore, it is worth mentioning that a method for compensating a threat to the WAC performance (topology changes) is also shown here, since it coincides with the approach followed for addressing one of its drawbacks. By compensating properly all the threats to the wide area controller performance and the

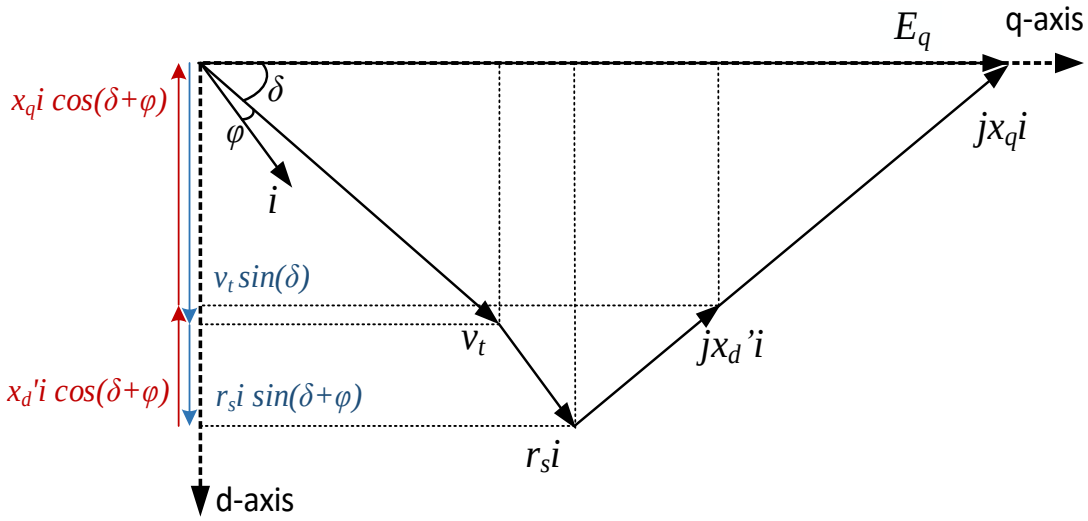

Fig. 8.5 Phasor diagram of a synchronous generator under transient conditions, without including a damper winding.

drawbacks of the adopted WAC design methodology, its robustness can significantly enhanced.

8.2.1 Estimation of rotor angle through synchronized voltage and current phasor measurements

As aforementioned, the adopted methodology of [39] requires as inputs the generators' terminal voltages, their frequencies and their power angles to be provided by PMUs. However, this is not the case in reality, as most of the commercial PMUs cannot measure the rotor angle directly. Therefore, the rotor angle δ must be estimated based solely on synchronized measurements. This step is needed in order to derive all the WAC inputs from the measurement chain of Fig. 3.3. For this purpose, the synchronous generator phasor diagram of Fig. 8.5 is utilized ([114]) in order to develop a methodology which provides accurate estimates of the rotor angle, suitable for wide area control applications.

More specifically, Fig. 8.5 illustrates the behavior of the generator under transient conditions, neglecting only the damper winding (note that the stator resistance is included as well). By utilizing the phasor diagram, one can derive an expression of the rotor angle based on known quantities. This is achieved from the decomposition of all the vectors into the *d*-*q* axes. By considering only the *d*-axis, the next equation results:

$$v_t sin(\delta) = -r_s i\, sin(\delta+\varphi) + (x_d' + x_q)\, i\, cos(\delta+\varphi) \tag{8.1}$$

where i represents the terminal current of the generator and φ is the difference between the phase angle measurements of voltage and current. Using the trigonometric identities for sine and cosine in (8.1), the following expression is derived for the rotor angle with respect to the terminal voltage magnitude of the generator:

$$\tan(\delta)=\frac{(x_d^{'}+x_q)i\cos(\varphi)-r_s i\sin(\varphi)}{v_t+(x_d^{'}+x_q)i\sin(\varphi)+r_s i\cos(\varphi)} \quad (8.2)$$

Looking at (8.2), one can realize that by knowing the generator parameters (x_q, $x^{'}_d$ and r_s), the rotor angle can be estimated only from PMU measurements. Therefore, by considering the rotor angle estimation, the synchronized measurements required by the wide area controller are now the generator's terminal voltage (magnitude and angle), its terminal current (magnitude and angle), and its frequency. It is important to clarify here that the proposed rotor angle estimation has been considered in chapters 5-7 and in this one as well, in order to have all the WAC inputs deriving from the measurement infrastructure of Fig. 3.3.

8.2.2 Complexity reduction of wide area controller

The scalability of the adopted methodology can become a serious challenge when moving to larger systems. This is mainly due to the substantial increase of the number of the required inputs which as a result increase also the number of the output signals that need to be derived at each time step. The latter is due to fact that PMU measurements from one generator bus correspond to two feedback control signals (exciter and governor) which need to be derived for the generator coordination. Note that this condition holds for the case of the renewables as well (Chapter 7). Therefore, the scalability issue is actually caused due to the measurement dependency of the WAC methodology and the necessity to derive coordination signals for each local controller of the system.

This obstacle can be overcome through the utilization of the coherency concept. Coherency refers to a phenomenon that occurs in power systems where at the event of a contingency, certain generators have similar time-domain behavior, leading that way to the separation of the system into coherent groups. The concept of coherency is especially useful at times where it is desirable to reduce the measurement dependency (and hence the required PMU number) of an application. Therefore, in this thesis according to the coherent groups obtained during a disturbance, only one PMU is used at each coherent group (since they have similar responses) in order to derive a common WAC signal for all the generators of the group. Thus, a grouping algorithm (such as the ones of [67], [140]) can be used to provide promptly the coherent groups in order to select appropriately the input and output signals of the wide area controller. By reducing the required inputs/outputs, the complexity and processing time of the WAC methodology is minimized as well. The results from applying the coherency concept will be shown in detail in subchapter 8.3.

8.2.3 Implementation of an adaptive WAC tuning method

A critical drawback of the adopted methodology, which is highlighted in Chapter 4, is the fact that the method considers a constant weighting factor (γ_i) for the tuning of the WAC contribution as shown in (4.13)-(4.14). This is actually a crucial parameter that can affect directly the performance of the wide area controller, since an incorrect tuning of the WAC contribution to the generators' local controllers, can lead the system to instability. Therefore, as it is clearly pointed out in [39] the main issue of the adopted methodology is that the contribution level of the WAC signals must be tuned a priori manually by the designer. However, the weighting factor cannot remain constant at all times, since its value must change according to the nature and the location of the contingency. Thus, the consideration of a constant weighting factor, which corresponds "well" for the majority of the disturbances, does not ensure high WAC performance at all times.

In this Ph.D. dissertation, a method to tune adaptively the weighting factor of the coordination signals is developed. The overall idea is that the contribution of the coordination signals should take into account the connectivity of the power system in order to identify the strongly connected areas. The information about the connectivity is especially needed for compensating the inter-area oscillations, since the latter results from the existence of weak tie lines in the grid. A straightforward way to estimate the electric connectivity between generators is as follows ([114]):

$$w_{ij} = e_i^{'} e_j^{'} Y_{ij}^{f} \tag{8.3}$$

where Y^f represents the magnitude of the reformulated admittance matrix, which is also known as the electric distance in a power system. It is worth mentioning here that the reformulated admittance matrix (which results from applying the first step of the adopted methodology in subchapter 4.2) is utilized in (8.3), instead of the reduced admittance matrix. Note also that the electric connectivity depends indirectly (through the internal voltages) on the generators' terminal voltages. The internal voltages are estimated through synchronized voltage and current measurements based on the stator dynamic equations shown in (4.5) and (4.6).

As shown in (8.3), to apply correctly the concept of electric connectivity as a weighting factor on the coordination signals (intended for the exciter, governor and PSS) it is essential to consider that electric connectivity does not depend on the i^{th} generator and the rest of the generators as a whole, but on each generator pair *i-j* separately. Therefore, the

weighting scheme derived from (8.3) will have the ability to regulate exclusively each inter-generator interaction between generators *i* and *j*, according to their electric connectivity. Looking at the exciter and governor WAC signal expressions of (4.13)-(4.14) one can realize that the parameters which hold the information regarding the inter-generator interaction between each *i-j* generator pair are the coupling perturbation terms (ψ_d, ψ_q and ψ_ω). As it will be shown in detail in subchapter 8.3, the coupling perturbation terms which result through the three-step procedure of Chapter 4, are actually superposition terms that sum all the *i-j* inter-generator interactions. Furthermore, it is important to be noted here that the inverse of the electric connectivity is utilized as a weight of the inter-generator interactions since it is desirable to apply high WAC contribution on sets of generators which are connected through weak tie lines and the opposite where strongly connected generators exist. The important advantage gained by considering this method is that the contribution of the WAC signals will be tuned on-line and adaptively according to the PMU measurements obtained from the generators.

8.2.4 Optimal PMU placement and topology change compensation

The final drawback of the adopted methodology which needs to be addressed is the assumption that PMUs are installed on all the generator buses. However, this is not realistically feasible yet due to the high cost of the PMUs. Therefore, priority is been given in installing PMUs only on selected buses in order to render the system observable. The latter is achieved through the use of real-time state estimators. State estimators utilize a redundant number of measurements deriving from specific buses of the system and combined with the system's topology, the states of all the buses can be computed. This means that at the event of a PMU outage, it is very likely to have enough measurements for performing successfully the state estimation. However, there is a possibility to lose a PMU with critical measurements and therefore the state estimation will not be executed. To overcome this issue, a constraint to the optimal PMU placement can be added for ensuring the N-1 criterion of PMUs (where N is the total PMU number). The consideration of PMU measurements into the state estimation can result to a near real-time Wide Area Monitoring (WAM) scheme. Through the cooperation between WAM and WAC systems, pseudo-measurements from the state estimator can be utilized to substitute any missing inputs to the wide area controller. It is important to note here that the latter has been made feasible by assuring that all the WAC inputs derive from synchronized measurements (subchapter 8.2.1). Subchapter 8.5 will present the WAM and WAC integration and its application into real-time simulation environments.

Furthermore, the investigation that took place in Chapter 5 has resulted that amongst others, the WAC performance can be affected by the unreported topology changes which might occur. Topology changes may not be so often but when they take place, the power flow of the whole system gets affected. To mitigate their effect, it is important to update in real-time the system topology that the WAC utilizes (i.e. the bus admittance matrix). For this reason, the aforementioned WAM-WAC combination can be considered here as well, since the WAM can provide in near real-time the topology of the system by utilizing the breaker status also as system states, keeping that way the wide area controller always aware of any system changes.

8.3 Wide Area Control of Governors and Power System Stabilizers with an Adaptive Tuning of Coordination Signals

All the methodologies proposed so far are more focused on providing robustness to the wide area controller by identifying potential threats or drawbacks and proposing methods to compensate them. However, one of the main objectives of this Ph.D. dissertation is to enhance the WAC damping performance through the proper coordination of the synchronous generator's local controllers. Therefore, this subchapter will present a novel methodology for obtaining WAC signals suitable for the coordination of the governors and PSSs. More specifically, the development of a methodology which can be used either to coordinate all the governors of the system (in case the system does not utilize PSSs) or to coordinate simultaneously both the governor and PSS of each generator through a common WAC signal is presented here and in [28]. Note that the common coordination of the two local controllers is achieved without any modification in the signal formulation and that this method is flexible to be applied to systems with or without PSSs. This concept cannot be applied in the case of the adopted methodology proposed in [39], since it derives coordination signals to interact only with the excitation signal and the steam valve output, bypassing in that way the operation of the PSS whenever they exist in the system. For this reason, the objective here is to derive coordination signals, which can increase the damping of local and especially inter-area oscillations by coordinating effectively all the governors and PSSs of the system. It is worth mentioning that for the exciter coordination, the conventional WAC signal of (4.13) will be considered here.

8.3.1 Development of governor coordination signals

For the formulation of the proposed governor WAC, the following model of the multi-machine power system dynamics is considered instead of the swing equation shown in (4.3)-(4.4) of Chapter 4,

$$J_i \frac{d^2\delta_i}{dt^2} = P_{mi} - e_i'^2 G_{ii}^r - \sum_{\substack{j=1 \\ j\neq i}}^{n} (C_{ij}\sin(\delta_{ij}) + D_{ij}\cos(\delta_{ij})) \tag{8.4}$$

where

$$\delta_{ij} = \delta_i - \delta_j$$

$$C_{ij} = e_i' e_j' B_{ij}^r$$

$$D_{ij} = e_i' e_j' G_{ij}^r$$

This set of equations is usually utilized for constructing Lyapunov functions intended for the transient stability assessment and to derive equations which describe the mutual motion of paired machines [114]. The important advantage of utilizing this equation instead of (4.3)-(4.4), is that there is no need to go into the three-step procedure of subchapter 4.2 for deriving the governor coordination signals [39]. The reason is that (8.4) is already in a suitable form where the local terms are separated completely from the inter-generator interactions (superposition term).

Equation (8.4) depends directly on the self- and transfer- admittances of the reduced network (G^r and B^r). The problem that arises is that the reduction of the admittance matrix down to the generator buses either assumes static and linear loads or it completely neglects them [114]. To overcome this issue and utilize a more suitable expression for the reduced admittance matrix, the reformulation (G^f and B^f) deriving from expressing the non-generator bus voltages in terms of the generators' terminal voltages is considered (step 1 of subchapter 4.2). As a reminder, in this step the admittance matrix is reformulated (into a closed form) to consider only the generator buses through the current equations of (4.8) and (4.9).

By considering (8.4), the formulation of the governor coordination signals can be illustrated. As it is aforementioned in subchapter 4.2, the variables of the equation must be substituted by their difference compared to their steady-state values (de and $d\omega$) in order to nullify the contribution of the wide area controller when the system is in steady-state. Due to the fact that the internal voltage of each generator cannot be measured directly by the

PMUs, (4.5) and (4.6) are utilized for estimating e'_d and e'_q, respectively. The result is then substituted in (8.4) through the following expression:

$$de_i'^2 = de_{di}'^2 + de_{qi}'^2 \tag{8.5}$$

One of the main novelties of this work is that the derived WAC will not interact with the local control signal P_{GV} (like in the case of [39]), but instead it will be implemented to coordinate the governing system through its input signal (rotor speed deviation $\Delta\omega_r$). For this reason, the equations of the turbine and the governing system are required. These can be derived from (4.7) and Fig. 3.2b. More specifically, the turbine equations are the following:

$$P_{mi} = (P_{CHi} - P_{RHi})F_{HPi} + P_{RHi} \tag{8.6}$$

$$T_{CHi}\dot{P}_{CHi} = P_{GVi} - P_{CHi} \tag{8.7}$$

$$T_{RHi}\dot{P}_{RHi} = P_{CHi} - P_{RHi} \tag{8.8}$$

where P_{CH} and P_{RH} represent the steam pressure and the re-heated steam pressure in per unit, respectively. In addition, the derived equations describing the governor operation are:

$$T_{3i}\dot{P}_{GVi} = P_{2i} - P_{GVi} \tag{8.9}$$

$$P_{2i} = P_{m0i} + \Delta P_i \tag{8.10}$$

$$T_{1i}\Delta\dot{P}_i = -K_i(\Delta\omega_{ri} - T_{2i}\Delta\dot{\omega}_{ri}) - \Delta P_i \tag{8.11}$$

where T_1, T_2 and T_3 are time constants (in seconds), while K is the speed regulation constant.

In order to develop the appropriate coordination signals, which will interact with the input of the governor, the input-output linearization approach has been adopted. This is a methodology which actually results to the implementation of non-linear decoupling control signals. The idea behind this technique is to differentiate the equation where the end-up variable to be controlled indirectly exists (e.g., equation (8.4) for the case of P_m), until the desirable input appears ($\Delta\omega_r$). The following expression presents the result of applying the input-output method on (8.4), until $\Delta\omega_r$ shows up:

$$\frac{d^4\omega_i}{dt^4} = \frac{1}{J_i}\left[F_{HPi}\left[-K_i \frac{((\Delta\omega_{ri}^l + \Delta\omega_{ri}^g) - T_{2i}\Delta\dot{\omega}_{ri}}{T_{1i}T_{3i}T_{CHi}} - \frac{\Delta P_i}{T_{1i}T_{3i}T_{CHi}} - \frac{\ddot{P}_{CHi}}{T_{CHi}} \right] + \dddot{P}_{RHi}(1-F_{HPi}) - \dddot{e}_i'^2 G_{ii}^f + \dddot{\psi}_{gi} \right] \tag{8.12}$$

where

$$\psi_{gi} = \sum_{\substack{j=1 \\ j \neq i}}^{n} (de_i' de_j' B_{ij}^f \sin(\delta_{ij}) + de_i' de_j' G_{ij}^f \cos(\delta_{ij})) \tag{8.13}$$

Note that to derive the expression of (8.12), the equations of the turbine ((8.6)-(8.8)) and the governing system ((8.9)-(8.11)) are utilized.

To obtain the suitable WAC signal, the input to be controlled is decomposed into a local ($\Delta\omega_r^l$) and a global part ($\Delta\omega_r^g$). The latter term represents the interaction of the wide area controller with the local controller and it is determined by selecting the global signal to cancel out the inter-generator interactions (ψ_g). This has as a result to derive a novel WAC signal intended for the coordination of the governor, through its input signal:

$$\Delta\omega_{ri}^g = -\gamma_i \frac{T_{1i} T_{3i} T_{CHi} \ddot{\psi}_{gi}}{K_i F_i} \tag{8.14}$$

8.3.2 Case study 1: Performance of the proposed governor coordination

In order to evaluate the damping capability of the proposed WAC (PropWAC) and furthermore to illustrate its enhanced performance, the proposed scheme is compared to the conventional wide area controller of [39] (hereafter referred to as ConvWAC). It is important to mention here that for the exciter coordination, the proposed scheme considers the same WAC signal as the conventional method (shown in Fig. 8.6). The aim is to illustrate clearly the performance enhancement when the WAC signal of (8.14) is utilized for the coordination of the governor instead of the conventional one of (4.14). Both methodologies are implemented and tested on the IEEE 39-bus dynamic test system, where coordination is applied to the exciter DC2A (Fig. 3.2a) and on the general-purpose governor (Fig. 3.2b) of all the generators. Note that as a benchmark, the scenario where no WAC (NoWAC) exists

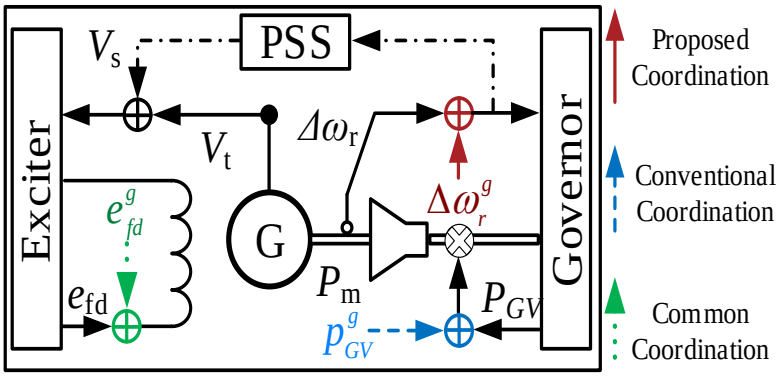

Fig. 8.6 Illustration of the proposed (red solid line) and conventional (blue dashed line) coordination signals. Green dotted line represents the common signal, which remains the same for both schemes. Dash-dotted line indicates the case where PSS is optionally installed.

in the system is considered. As a first step, the proposed scheme is evaluated using EMT offline simulations on MathWorks Simulink.

It is also worth mentioning that conversely to the conventional WAC of [39], a rate limiter is applied to all the coordination signals of the exciter and the governor. The reason behind this addition is to avoid the wearing-and-tearing of the local controllers due to the abrupt changes (resulting from the application of the WAC signals) and thus to allow the more smooth transition from the one state to the other. This is especially the case for the governor, which has a slower response compared to the exciter operation. Therefore, two different rate limits (faster/slower) are utilized on the WAC signals intended for coordinating the exciter and the governor. For considering a more realistic dynamic behavior of the system during transient conditions, the proposed governor coordination performance is evaluated in the presence of dynamic load models instead of the commonly used ideal constant-power ones. More specifically, the exponential dynamic load model is considered where the

TABLE 8.1: PRONY ANALYSIS RESULTS FOR CASE STUDY 1

Type	**NoWAC**		**ConvWAC**		**PropWAC**	
	ζ(%)	f(Hz)	ζ(%)	f(Hz)	ζ(%)	f(Hz)
Local mode	8.42	1.6	6.65	1.6	13.7	1.5
Inter-area mode	21.1	0.81	14.3	0.77	31.7	0.81

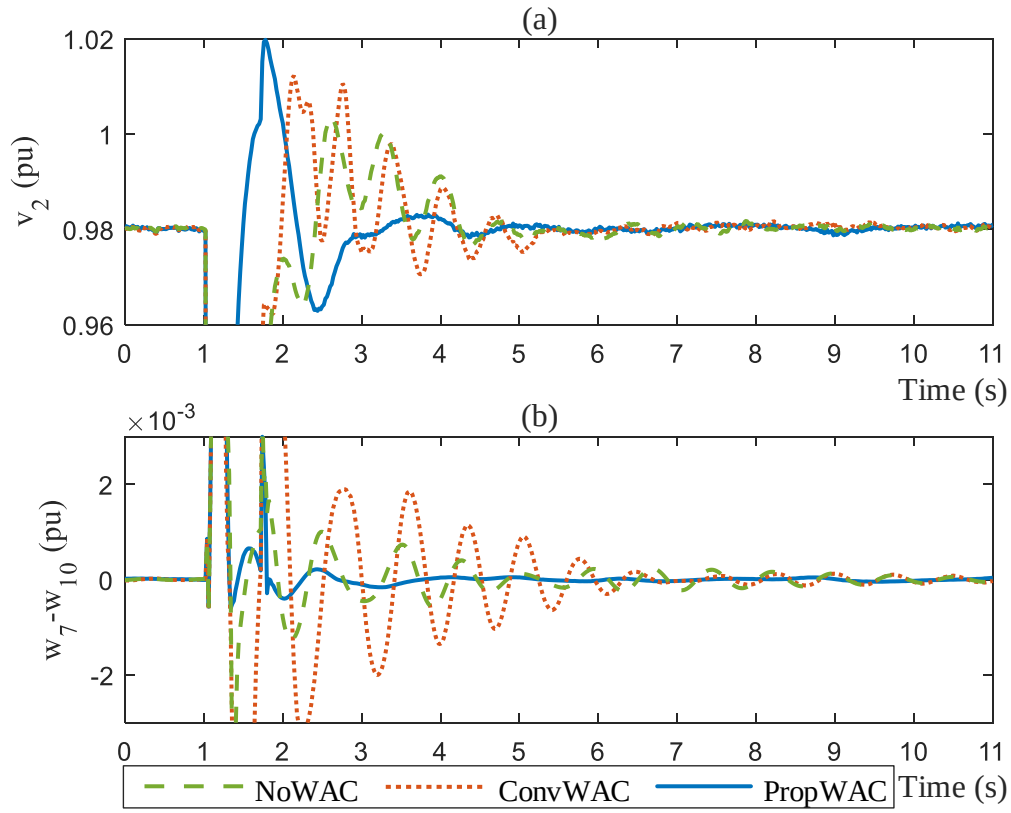

Fig. 8.7 Illustration of the performance of the NoWAC, ConvWAC and PropWAC in compensating the local (a) and inter-area (b) modes for Case Study 1.

adopted parameter values are based on the parameter estimation shown in [130] (TABLE 5.7).

All the examined scenarios (NoWAC, ConvWAC and PropWAC) are tested at the event of a 5-cycle three-phase fault on the line connecting bus 2 to bus 3 at t=1 s, followed by a line tripping at t=1.1 s and its reclosing at t=1.7 s. Note also that the static loads of buses 4, 8, 15, 21 and 27 are substituted by their respective exponential dynamic loads. Furthermore, it is important to mention here that the weighting factor (γ_i) of all the WAC signals is tuned by trial and error. Therefore, it is found that for the ConvWAC scheme γ_i=0.2 is applied to both WAC signals of (4.13) and (4.14), for all the generators of the system. In the case of the proposed scheme, γ_i=0.1 is utilized for the exciter coordination of (4.13), while γ_i=0.3 is considered for the governor coordination of (8.14).

For the graphical illustration of the simulation results, the terminal voltage of G2 (v_2) and the speed difference between G7 and G10 are considered (w_7-w_{10}). Fig. 8.7 shows that the proposed coordination outperforms the ConvWAC and NoWAC scenarios in damping both local and inter-area oscillations. More specifically, due to the presence of non-linear loads, the ConvWAC scenario provides the worst performance even compared to the NoWAC scenario. This is especially noted in the case of inter-area oscillations where a small oscillation remains undamped and which can create stability issues to the power system. This outcome can be further verified through the Prony analysis results of TABLE 8.1. Here, the increased damping ratio in the case of both local and inter-area modes indicates the considerable improvement of the WAC performance when the proposed governor coordination is considered. Furthermore, it is worth noting here, that the PropWAC provides more than double damping ratios than the ConvWAC which has the lowest ones of all three scenarios considering both local and inter-area modes.

8.3.3 Case Study 2: Coordination of governor and PSS

The significant advantage of coordinating a local controller through its input signal is that it provides the flexibility and capability of coordinating simultaneously other local controllers, which might be using the same input. This is actually the case of the governor and the PSS, which both have as input the rotor speed deviation ($\Delta\omega_r$). Therefore, as shown in Fig. 8.6 the same WAC signal of (8.14) can be used for the simultaneous coordination of both governor and PSS, in the case where PSSs exist in the system (dash-dotted line).

The coordination of the PSS (in addition to the governor) will damp faster and more effectively the inter-generator interactions. This is achieved by coordinating (through PSS) the electric torque component that is generated due to the exciter's output. The idea of utilizing simultaneously the governor and PSS to damp the perturbation terms (ψ_g) of (8.12) is to consider both the mechanical (governor) and the electrical (PSS) part of the generator for increasing the system's small-signal stability.

For evaluating the performance of the proposed scheme in the presence of PSS, the latter is added into all the generators of the system according to [93]. In this case study, a 5-cycle three-phase fault is applied on the line connecting bus 16 to bus 17, at t=1 s. Once again, the line trips for 0.6 s in order to clear the fault and then it recloses. Furthermore, exponential dynamic load models are considered to exist on buses 4, 15, 25, 27 and 29. Note

TABLE 8.2: PRONY ANALYSIS RESULTS FOR CASE STUDY 2 AND CASE STUDY 3

Type	**NoWAC**		**ConvWAC**	
	ζ(%)	*f(Hz)*	*ζ(%)*	*f(Hz)*
Local mode	15.7	1.4	11.9	1.6
Inter-area mode	17.5	0.74	18.3	0.76
Type	**PropWAC**		**AdapWAC**	
	ζ(%)	*f(Hz)*	*ζ(%)*	*f(Hz)*
Local mode	17.6	1.6	23.7	1.5
Inter-area mode	30.7	0.69	28.8	0.74

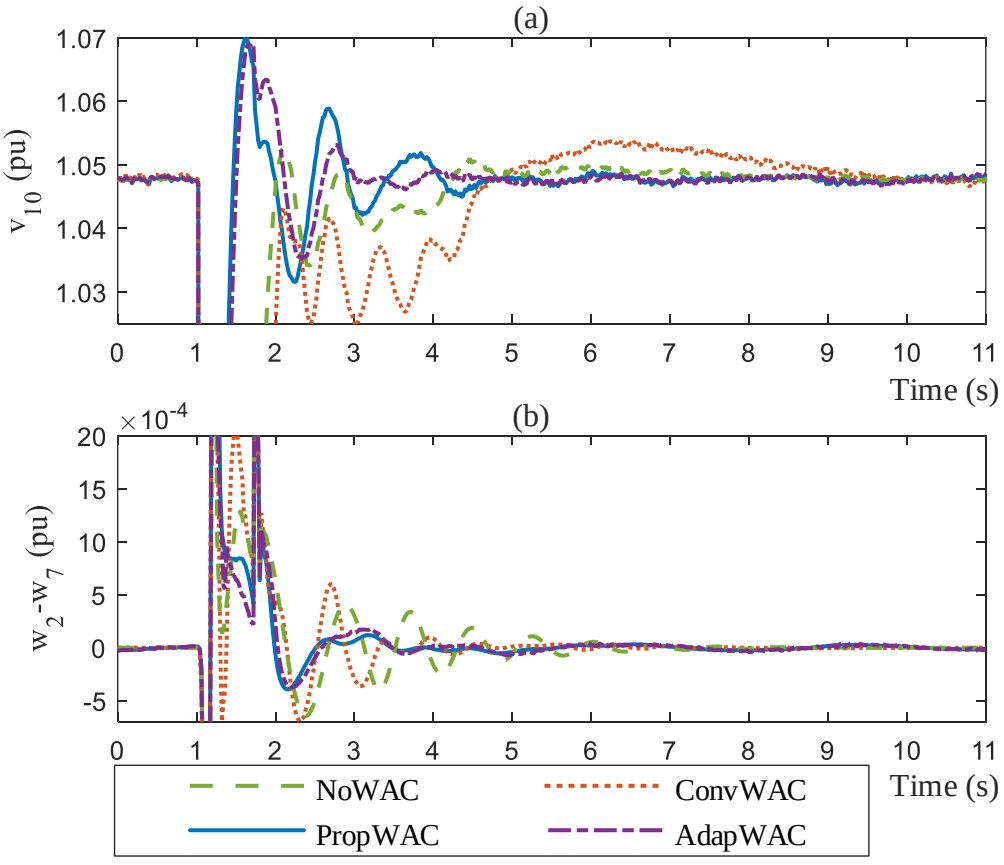

Fig. 8.8 Damping performance comparison between the NoWAC, ConvWAC, PropWAC and AdapWAC scenarios considering the compensation of the local (a) and inter-area (b) modes for Case Study 2 and 3.

that the same weighting factors as shown previously are applied here as well, along with the same rate limiters. Fig. 8.8 along with TABLE 8.2 present the graphical and numerical results of the simulation. For the graphical illustrations of the local and inter-area signals, the terminal voltage v_{10} and the speed difference w_2-w_7 are considered respectively. The simulation results of this case study illustrate that the PropWAC scheme has the best performance over the other two schemes since it achieves an effective damping of local and inter-area modes. It is also worth mentioning that from Fig. 8.8 it can be derived that the ConvWAC scenario fails to compensate promptly the local oscillation. The Prony analysis results of TABLE 8.2 present clearly that the proposed scheme provides significant additional damping of the local and inter-area modes compared to the NoWAC and ConvWAC schemes.

8.3.4 Case Study 3: Adaptive tuning of coordination signals

Based on the formulation of the proposed and conventional wide area controllers, one can argue that their performance depends highly on one crucial parameter, the weighting factor γ_i. This statement is generally true, since an incorrect tuning of the WAC contribution to the generators' local controllers, can lead the system to instability. In addition, the weighting factor cannot remain constant at all times, since its value must change according to the nature and the location of the contingency. Therefore, this case study aims to apply the adaptive tuning of (8.3) for regulating the contribution of the WAC signals in order to overcome the drawback of utilizing the constant weighting factor γ_i in the coordination signals of (4.13) and (8.14). As aforementioned, the proposed adaptive tuning method is based on weights that are calculated through the wide area measurements and the electric connectivity between the generators. For this reason, the utilization of (8.3) provides the capability of regulating exclusively each inter-generator interaction between generators *i* and *j*, according to their electric connectivity. Thus, strongly connected generator pairs will have low weights applied on their respective perturbation terms and conversely, high weights are assigned on the perturbation terms of generator pairs which are connected through weak tie lines. To illustrate the application of the proposed adaptive tuning method on the WAC signals, the proposed governor/PSS coordination of (8.14) is considered:

$$\Delta\omega_{ri}^{g} = -\frac{T_{1i}T_{3i}T_{CHi}}{K_i F_{HPi}}\frac{d^3}{dt^3}\left[\sum_{\substack{j=1\\ j\neq i}}^{n}\left(\frac{1}{w_{ij}}\left(de_i^{'}de_j^{'}B_{ij}^{g}\sin(\delta_{ij}) + de_i^{'}de_j^{'}G_{ij}^{g}\cos(\delta_{ij})\right)\right)\right] \tag{8.15}$$

Note that the superposition term of (8.15) is derived by substituting (8.13) into (8.14), which is necessary for illustrating clearly the regulation of each inter-generator interaction between generators *i* and *j*. Note that in a similar way, the weighting scheme is applied also into the perturbation terms of the exciter WAC in (4.13).

To illustrate the impact of considering the adaptive tuning concept on the WAC architecture, the results of Case Study 2 include also the system's response when the proposed adaptive method is applied to the coordination signals of the PropWAC scenario ((4.13) and (8.14)). Based on Fig. 8.8, one can note that the resulted adaptive WAC (AdapWAC) scenario provides better damping of the local oscillations, while it has almost the same performance in compensating the inter-area modes compared to the PropWAC scenario. The numerical results of TABLE 8.2 further validate the performance of the AdapWAC scenario in successfully damping all the modes.

8.3.5 Case Study 4: Adaptive tuning under high penetration of non-linear loads

In order to illustrate clearly the actual contribution of the AdapWAC scenario, a slightly different case study is also included in this section. More specifically, the same disturbance and fault-clearing on the line connecting bus 16 to bus 17 is considered, but more non-linear loads are assumed in this case study. Note that dynamic loads are placed on buses 4, 8, 15, 21, 23, 25, 27, 29 and that the same weighting factors and simulation specifications (as discussed in Case Study 1) are utilized here, while PSSs are considered into all the generators. The reason that the specific case study is considered here is due to the outcome of subchapter 5.5, where it has been concluded that the increased penetration (above 30%) of the exponential dynamic load models leads the system to instability.

The derived results are presented in Fig. 8.9 where the terminal voltage v_8 and the speed deviation w_2-w_{10} are used to view the local and inter-area oscillations, respectively. As it is illustrated, only the AdapWAC scheme is capable of damping effectively all the dominant modes and preserving the system's stability, outperforming the other schemes. This outcome illustrates that it is essential to incorporate an adaptive tuning procedure into the WAC scheme, in order to ensure the stability of the system at all times. These conclusions can be further verified through the Prony analysis results of TABLE 8.3, where it is evident that the application of the proposed adaptive tuning on the proposed WAC has increased its damping performance, while all the other scenarios fail to keep the system stable.

TABLE 8.3: PRONY ANALYSIS RESULTS FOR CASE STUDY 4

Type	NOWAC		CONVWAC	
	ζ(%)	*f(Hz)*	*ζ(%)*	*f(Hz)*
Local mode	Instability		Instability	
Inter-area mode	Instability		Instability	
Type	**PROPWAC**		**ADAPWAC**	
	ζ(%)	*f(Hz)*	*ζ(%)*	*f(Hz)*
Local mode	6.14	1.5	14.8	1.6
Inter-area mode	Instability		27.3	0.73

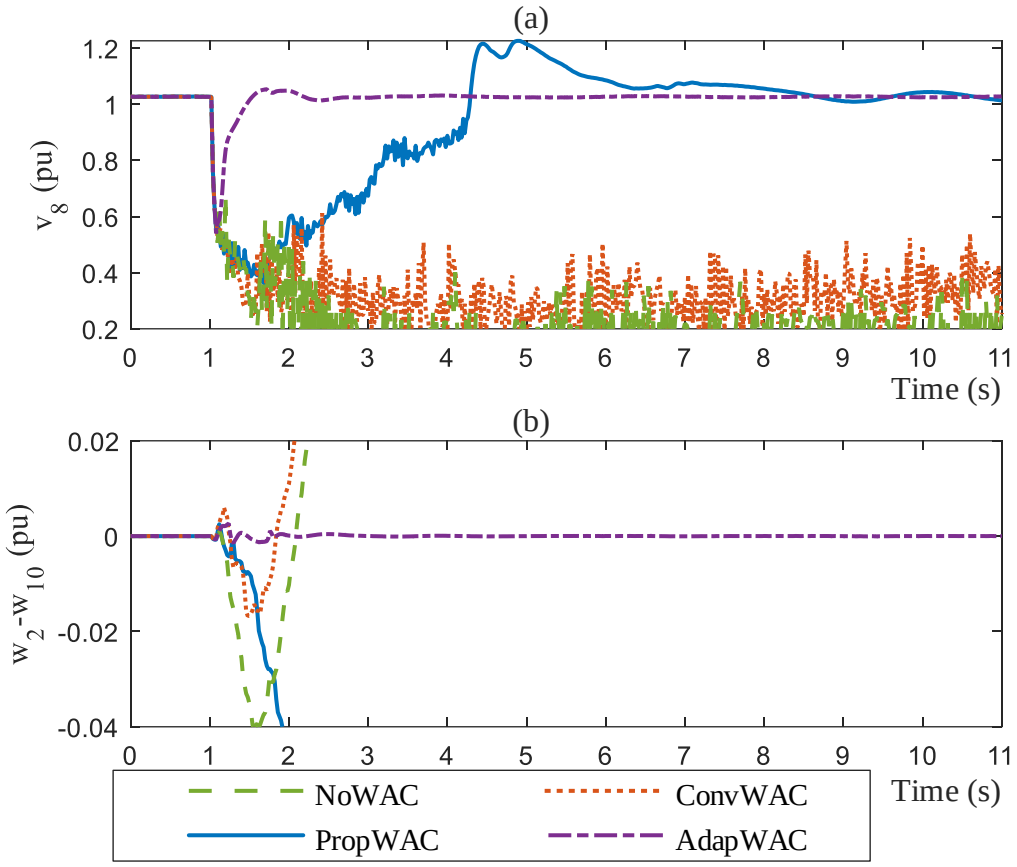

Fig. 8.9 Case Study 4 results illustrating the performances of the NoWAC, ConvWAC, PropWAC and AdapWAC scenarios in compensating the local (a) and inter-area (b) oscillations.

8.3.6 Case Study 5: Real-time simulation results for three-phase fault

Although the offline simulation results of Case Studies 1-4 have illustrated clearly the performances of the proposed coordination and the adaptive tuning methodologies, their actual evaluation can only be ensured through real-time simulation. For this reason, the OPAL-RT real-time simulator (presented in subchapter 8.1) is utilized to obtain in real-time, more accurate simulations for further validation. More specifically, the real-time model of the IEEE 39-bus dynamic test system (Fig. 8.3) is considered for the evaluation. Note that this validation procedure required three cores of the OP5700. Two cores were used for implementing the dynamic test system, while a third core was utilized for running the WAC algorithms as shown in Fig. 8.10.

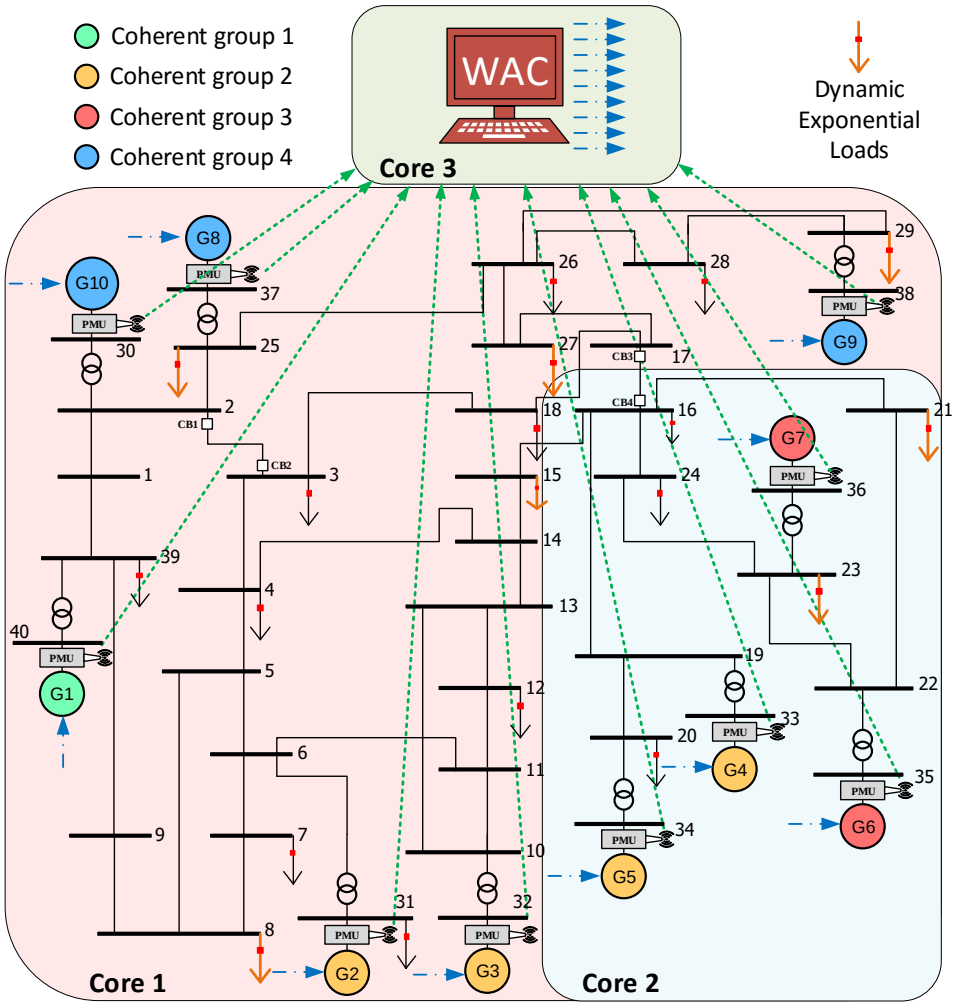

Fig. 8.10 IEEE 39-bus test system illustrating: (i) the separation of the system into 3 cores for *real-time* simulation, (ii) the coherent generators (each generator color implies a different coherent group), and (iii) the buses which consider dynamic exponential load models.

The disturbance considered into the real-time simulation is a 5-cycle three-phase fault on the line connecting bus 2 to bus 3 at t=1 s, followed by the line tripping at t=1.1 s and its reclosing at t=1.7 s. In this case study, dynamic loads were placed on buses 8, 15, 21, 23, 25, 27 and 29 as Fig. 8.10 shows. Once again, the aim is to compare the performances of all the examined scenarios (NoWAC, ConvWAC, PropWAC and AdapWAC) in real-time. For this reason, graphical (Fig. 8.11) and numerical results (TABLE 8.4) are considered. More specifically, Fig. 8.11 presents the terminal voltage v_2 and the speed deviation w_7-w_{10}. The results show clearly that the NoWAC and ConvWAC scenarios fail to keep the system stable at the event of the fault, leading it to instability. Therefore, only the PropWAC and AdapWAC scenarios are capable in this case of damping effectively all the local and inter-area oscillations. For the effective comparison between the two scenarios, the Prony analysis results are utilized. According to TABLE 8.4, one can note that the AdapWAC has increased performance compared to the PropWAC scenario in damping effectively all the oscillations and especially the inter area modes.

TABLE 8.4: PRONY ANALYSIS RESULTS OF THE REAL-TIME SIMULATION FOR CASE STUDY 5

Type	NoWAC		ConvWAC	
	ζ(%)	*f(Hz)*	*ζ(%)*	*f(Hz)*
Local mode	Instability		Instability	
Inter-area mode	Instability		Instability	
Type	PropWAC		AdapWAC	
	ζ(%)	*f(Hz)*	*ζ(%)*	*f(Hz)*
Local mode	9.68	1.8	12.28	1.8
Inter-area mode	18.2	0.8	31.5	0.72

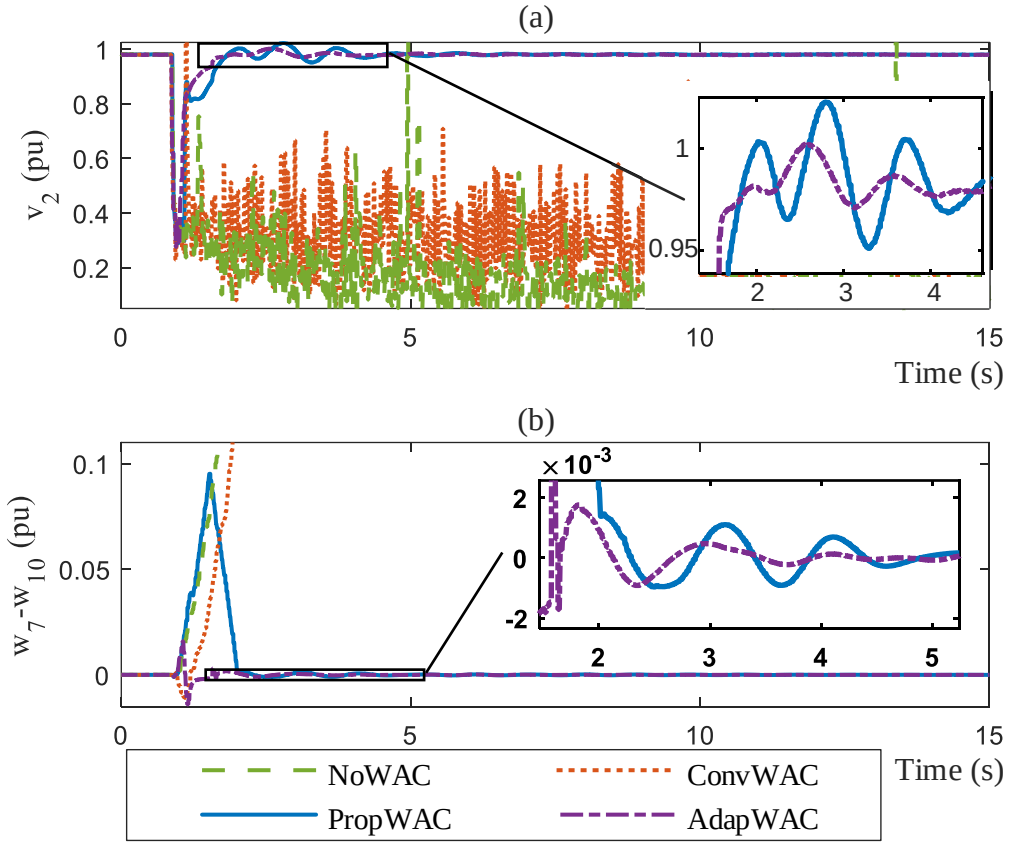

Fig. 8.11 Real-time simulation results of Case Study 5 illustrating comparison of NoWAC, ConvWAC, PropWAC and AdapWAC in compensating (a) local and (b) inter-area modes.

8.3.7 Case Study 6: Impact of measurement errors on adaptive tuning in real-time conditions

As it has been illustrated in subchapters 5.1 and 8.2.1, in order to create a realistic simulation environment it is crucial to have all the WAC inputs deriving from the measurement infrastructure of Fig. 3.3 where steady-state and dynamic measurement errors are appropriately considered. Apart from the WAC inputs, it has been shown in subchapter 8.2.3 that the adaptive tuning method of (8.3) is also heavily depended on synchronized measurements through the stator dynamic equations of (4.5) and (4.6). Therefore, it is important to evaluate the proposed methodology under the presence of realistic measurement errors. To achieve this, the procedure presented in subchapter 5.1 and in [23] is adopted here

as well. More specifically, the synchronized voltage and current measurements which are utilized for estimating the weights of (8.3) derive from (3.1)-(3.4) where the errors of TABLE 3.1, TABLE 3.2, TABLE 5.1 are considered accordingly. In that way, both the WAC inputs and the adaptive tuning are affected by realistic measurement errors.

The outcome of applying the measurement errors (further on refer to as the AdapWAC_ME scenario) is presented in Fig. 8.12. As shown, the presence of measurement errors has a small effect on the performance of the AdapWAC scenario in compensating effectively all the local and inter-area oscillations. This is further validated by comparing the Prony analysis results of the AdapWAC scenario (TABLE 8.4) with the respective results of the AdapWAC_ME scenario (TABLE 8.5), which show that only the inter-area compensation has slightly been decreased due to the presence of measurement errors.

TABLE 8.5: PRONY ANALYSIS RESULTS FOR CASE STUDY 6 AND CASE STUDY 7

Type	**ADAPWAC_ME**		**ADAPWAC_COH**	
	ζ(%)	*f(Hz)*	*ζ(%)*	*f(Hz)*
Local mode	12.28	1.8	11.65	1.9
Inter-area mode	26	0.77	26.9	0.74

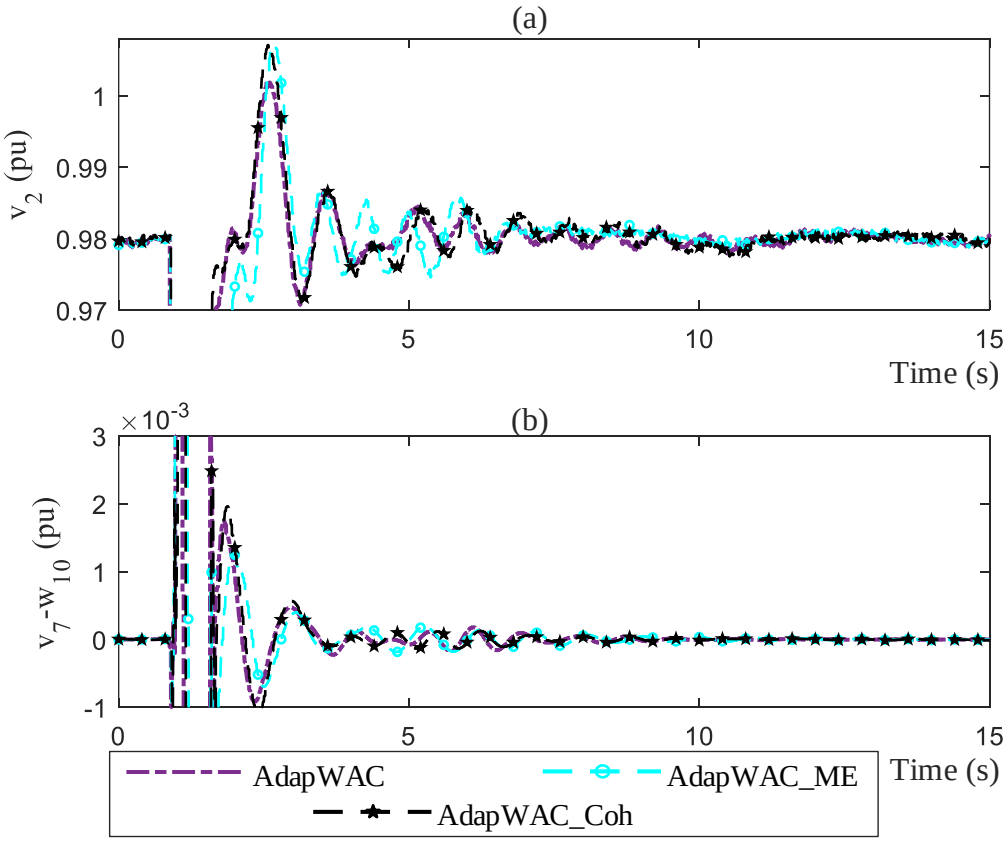

Fig. 8.12 Real-time simulation results of Case Study 6 and 7 illustrating comparison of AdapWAC, AdapWAC with measurement errors (AdapWAC_ME) and AdapWAC with coherency (AdapWAC_Coh) in compensating (a) local and (b) inter-area modes.

8.3.8 Case Study 7: Complexity reduction through coherency in real-time conditions

As aforementioned in subchapter 8.2.2, an important attribute that a WAC scheme must offer is the scalability in order to be capable of operating sufficiently in small and large power systems. By moving to larger power systems both, the number of the required inputs as well as the number of the derived output signals, increase substantially. Therefore, the scalability issue is directly connected to the measurement dependency of the WAC methodology and to the need of deriving coordination signals for each local controller of the system.

A common way to address this challenge is the utilization of the coherency concept. This is due to the observation that generators belonging to the same coherent group have similar responses and strong connections. The latter remark denotes that the perturbation terms of each generator pair of the coherent group are close to zero and thus similar coordination signals are derived from the WAC scheme for each generator of the group. Therefore, coherency is applied here to reduce the measurement dependency of the wide area controller, as well as the derived coordination signals. More specifically, the procedure followed here is that according to the coherent groups obtained during a disturbance, synchronized measurements from only one PMU are used at each coherent group (due to the similar behavior) in order to derive a common WAC signal for all the generators of the group. The application of a 5-cycle three-phase fault on the line connecting bus 2 to bus 3 and the line trip/reconnection followed, results into the separation of the system into four groups which are shown in different colours in Fig. 8.10. Therefore, synchronized measurements deriving from only one generator's PMU at each group (generators 1, 2, 7 and 10 respectively) are considered in the proposed scheme for deriving coordination signals for each coherent group. Note that the coherency grouping can be achieved through a real-time algorithm (such as the one proposed in [67]) for providing promptly the coherent groups in order to select the appropriate input and output signals of the wide area controller. The graphical illustrations (Fig. 8.12) combined with the Prony analysis results (TABLE 8.5) demonstrate that the coherency concept can be utilized successfully for the reduction of the required PMU measurements without compromising the proposed scheme's performance. Actually, the damping ratios of the local and inter-area oscillations resulted from the coherency-based WAC (AdapWAC_Coh) are very close to the ones of the AdapWAC

scenario. This is especially notable when the Prony analysis results of the AdapWAC_Coh (TABLE 8.5) are compared with the ones of the AdapWAC (TABLE 8.4).

8.3.9 Case Study 8: Real-time simulation results for generator tripping

Apart from the faulty contingencies, less severe disturbances can also take place in the power system. A common one is the event of a generator trip, which can potentially affect the wide area controller operation since the latter actually losses an actuator that is coordinated for compensating all the unwanted oscillations. Therefore, it is interesting and important to test the performances of all the examined scenarios (NoWAC, ConvWAC, PropWAC and AdapWAC) under the event of a generator trip as well. More specifically,

TABLE 8.6: PRONY ANALYSIS RESULTS OF THE REAL-TIME SIMULATION FOR CASE STUDY 8

Type	NOWAC		CONVWAC	
	ζ(%)	*f(Hz)*	*ζ(%)*	*f(Hz)*
Local mode	7.72	1.5	7.14	1.8
Inter-area mode	14.2	0.69	13.2	0.8
Type	**PROPWAC**		**ADAPWAC**	
	ζ(%)	*f(Hz)*	*ζ(%)*	*f(Hz)*
Local mode	8.19	1.8	8.34	1.9
Inter-area mode	15	0.65	15.7	0.7

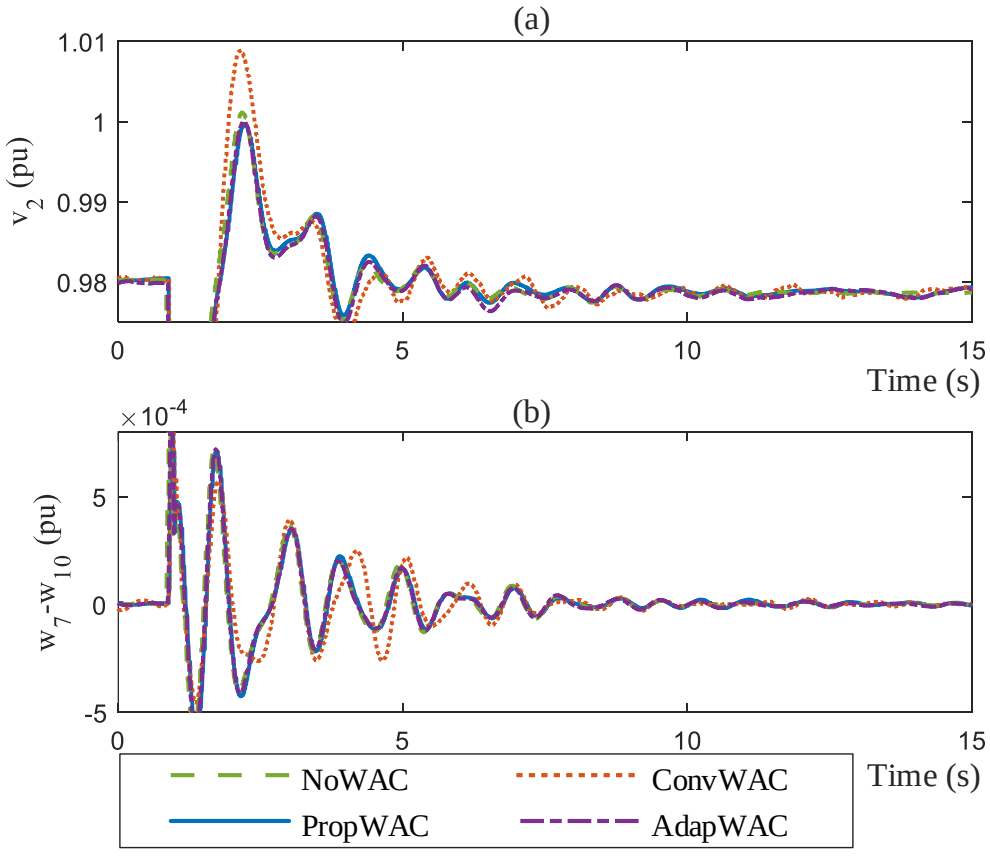

Fig. 8.13 Real-time simulation results for the G1 trip of Case Study 8 illustrating comparison of NoWAC, ConvWAC, PropWAC and AdapWAC in compensating (a) local and (b) inter-area modes.

this case study considers that at t=1 s generator G1 trips unexpectedly, while dynamic loads exist on the same buses as previously (Fig. 8.10).

Fig. 8.13 depicts the *real-time* simulation results of this case study, where it is shown that all the examined scenarios have comparable performances. As it can be noted more clearly through the Prony analysis results of TABLE 8.6, the AdapWAC scenario provides slightly better performance while the ConvWAC scenario has slightly worst damping ratios compared to all the other scenarios. The latter remark happens due to the sensitivity of the ConvWAC scenario to the presence of dynamic loads.

8.3.10 Conclusion

A novel methodology for the coordination of the synchronous generator governor and PSS is proposed to increase the damping capability of the system, especially for compensating the inter-area oscillations. The formulation of the proposed WAC signals becomes feasible by utilizing the multi-machine power system dynamic model, in order to identify and cancel out effectively all the inter-generator interactions. The simultaneous coordination of the governor and PSS is achieved through the interaction of the wide area controller with their common input signal (i.e., rotor speed deviation). Furthermore, this subchapter has presented the application of an adaptive tuning methodology to regulate the contribution of the WAC signals, overcoming the drawback of utilizing a constant non-optimal weighting factor.

The performances of the proposed governor/PSS coordination and its combination with the adaptive tuning method, is tested through EMT analysis by using the IEEE 39-bus test system, where exponential dynamic load models are assumed in various buses of the system. More specifically, for validation purposes, offline and real-time simulations (four case studies for each simulation type) took place where the OPAL-RT equipment was considered in the case of the latter. Note that the proposed scheme has been tested in the presence/absence of the PSSs. Through the utilization of graphical illustrations and the outcomes of the Prony analysis, it can be concluded that the proposed governor/PSS coordination has improved performance compared to the conventional WAC. Even better results are obtained through the use of the adaptive tuning methodology in the proposed WAC scheme, which enhances considerably the power system stability. To evaluate further the performance of the adaptive tuning, realistic measurement errors were considered into the real-time simulation. The results have indicated that measurement errors have a very small effect on the proposed scheme's performance. Finally, the coherency concept has been

successfully applied here in order to reduce the required PMU number as well as the derived WAC signals.

8.4 Novel Coordination of Excitation Systems

The previous subsection has proposed a methodology for deriving WAC signals for the effective and simultaneous coordination of the governor and PSS. However, as it was pointed out in Chapter 2, the majority of the published WAC methodologies propose the coordination of the exciter (instead of the governor) for increasing the system's damping capability. This happens mainly due to the faster response of the excitation systems. Therefore, the aim of this subchapter is to present a novel methodology for the development of coordination signals which will enhance the operation and performance of the exciter in damping local and especially inter-area oscillations. Note that the derived WAC signals are created to be completely compatible with the previously proposed governor/PSS coordination and the adaptive tuning method, in order to obtain a compact solution which will coordinate appropriately all the local controllers of the synchronous generator. It should be noted that in this subsection the performance of the proposed scheme is tested only through offline simulations since its real-time evaluation will take place in subsection 8.5.

8.4.1 Development of exciter coordination signals

According to the adopted methodology of [39] (presented in Chapter 4) the expressions shown in (4.1)-(4.2) are considered in order to identify the conventional exciter coordination, while the swing equation of (4.3)-(4.4) is utilized to estimate the steam valve output conventional coordination. This is achieved through the i^{th} generator's dynamic equations of (4.10)-(4.12). The proposed methodology presented in subchapter 8.3 has considered the multi-machine power system dynamics model (shown in (8.4)) instead of the swing equation in order to derive appropriate and more effective WAC signals for the governor and PSS coordination. Therefore, in this case as well, more suitable expressions instead of the ones presented in (4.1) and (4.2) are utilized to develop a novel exciter coordination signal. More specifically, the following model of the synchronous generator with one damper winding in the *q*-axis and the transient saliency neglected ($x'_d = x'_q$) is considered here:

$$T'_{di}\dot{e}'_{qi} = -e'_{qi} + \frac{x_{di} - x'_{di}}{x_{di}} v_{qi} + \frac{x'_{di}}{x_{di}} e_{fdi} \tag{8.16}$$

$$T_{qi}^{'}\dot{e}_{di}^{'} = -e_{di}^{'} + \frac{x_{qi} - x_{di}^{'}}{x_{qi}} v_{di} \tag{8.17}$$

where $T_d^{'}$ and $T_q^{'}$ stand for the short circuit time constants of the synchronous generator (in seconds).

By applying the three-step procedure presented in subchapter 4.2, one can note that the fourth-order model equations ((4.1)-(4.2) to be substituted by (8.16)-(8.17)) are utilized at step 3, where the derived expressions of the internal voltage (e_d and e_q) and the stator current (i_d and i_q) are replaced. In the case of (8.16)-(8.17) only the expressions for the internal voltage are required, since the stator current is removed. More specifically, the internal voltage expressions resulting from step 2 are the following:

$$\frac{e_{qi}^{'}}{x_{di}^{'}} = G_{ii}^{f} v_{di} - B_{ii}^{f} v_{qi} + \sum_{\substack{j=1 \\ j \neq i}}^{n} ((G_{ij}^{f} v_{dj} - B_{ij}^{f} v_{qj}) \cos(\delta_{ji}) - (G_{ij}^{f} v_{qj} + B_{ij}^{f} v_{dj}) \sin(\delta_{ji})) \tag{8.18}$$

$$\begin{aligned} \frac{e_{di}^{'}}{x_{qi}^{'}} &= -G_{ii}^{f} v_{qi} - v_{di} (B_{ii}^{f} + \frac{1}{x_{di}^{'}} - \frac{1}{x_{qi}^{'}}) \\ &\quad - \sum_{\substack{j=1 \\ j \neq i}}^{n} ((G_{ij}^{f} v_{dj} - B_{ij}^{f} v_{qj}) \sin(\delta_{ji}) + (G_{ij}^{f} v_{qj} + B_{ij}^{f} v_{dj}) \cos(\delta_{ji})) \end{aligned} \tag{8.19}$$

where G^f and B^f are the elements of the reformulated admittance matrix.

By substituting (8.18)-(8.19) into (8.16)-(8.17) and solving the equations to find expressions for the derivatives of v_d and v_q, the next set of equations is obtained:

$$\dot{v}_{di} = \frac{-A v_{di} + (B + \frac{x_{di} - x_{di}^{'}}{x_{di}}) v_{qi} - D + \frac{x_{di}^{'}}{x_{di}} e_{fdi} + T_{di}^{'} B \dot{v}_{qi} - T_{di}^{'} C}{T_{di}^{'} A} \tag{8.20}$$

$$\dot{v}_{qi} = -\frac{E v_{qi} + (F + \frac{x_{qi} - x_{di}^{'}}{x_{qi}}) v_{di} + I + T_{qi}^{'} F \dot{v}_{di} + T_{qi}^{'} G}{T_{qi}^{'} E} \tag{8.21}$$

where,

$$A = x_{di}^{'} G_{ii}^{f}, \quad B = x_{di}^{'} B_{ii}^{f}$$

$$C = x_{di}^{'} \sum_{\substack{j=1 \\ j \neq i}}^{n} \begin{bmatrix} (G_{ij}^{f} \dot{v}_{dj} - B_{ij}^{f} \dot{v}_{qj}) \cos(\delta_{ji}) - (G_{ij}^{f} v_{dj} - B_{ij}^{f} v_{qj}) \sin(\delta_{ji}) (\omega_j - \omega_i) \\ -(G_{ij}^{f} \dot{v}_{qj} + B_{ij}^{f} \dot{v}_{dj}) \sin(\delta_{ji}) - (G_{ij}^{f} v_{qj} + B_{ij}^{f} v_{dj}) \cos(\delta_{ji}) (\omega_j - \omega_i) \end{bmatrix}$$

$$D = x_{di}^{'} \sum_{\substack{j=1 \\ j \neq i}}^{n} ((G_{ij}^{f} v_{dj} - B_{ij}^{f} v_{qj}) \cos(\delta_{ji}) - (G_{ij}^{f} v_{qj} + B_{ij}^{f} v_{dj}) \sin(\delta_{ji}))$$

$$E = x_{qi}^{'} G_{ii}^{f}, \quad F = x_{qi}^{'} (B_{ii}^{f} + \frac{1}{x_{di}^{'}} - \frac{1}{x_{qi}^{'}})$$

$$G = x_{qi}^{'} \sum_{\substack{j=1 \\ j \neq i}}^{n} \begin{bmatrix} (G_{ij}^{f} \dot{v}_{dj} - B_{ij}^{f} \dot{v}_{qj}) \sin(\delta_{ji}) + (G_{ij}^{f} v_{dj} - B_{ij}^{f} v_{qj}) \cos(\delta_{ji}) (\omega_j - \omega_i) \\ + (G_{ij}^{f} \dot{v}_{qj} + B_{ij}^{f} \dot{v}_{dj}) \cos(\delta_{ji}) - (G_{ij}^{f} v_{qj} + B_{ij}^{f} v_{dj}) \sin(\delta_{ji}) (\omega_j - \omega_i) \end{bmatrix}$$

$$I = \sum_{\substack{j=1 \\ j \neq i}}^{n} ((G_{ij}^{f} v_{dj} - B_{ij}^{f} v_{qj}) \sin(\delta_{ji}) + (G_{ij}^{f} v_{qj} + B_{ij}^{f} v_{dj}) \cos(\delta_{ji}))$$

Since (8.20) contains the derivative of v_q and (8.21) the derivative of v_d, the system of (8.20)-(8.21) is next solved to obtain decoupled expressions for the derivatives of v_d and v_q, deriving that way the new dynamic equations for the i^{th} generator:

$$\dot{v}_{di} = \frac{-A' v_{di} + B' v_{qi} - D + \frac{x_{di}^{'}}{x_{di}} e_{fdi} - \frac{T_{di}^{'} BI}{T_{qi}^{'} E} - \frac{T_{di}^{'} BG}{E} - T_{di}^{'} C}{T_{di}^{'} A + \frac{T_{di}^{'} BF}{E}} \tag{8.22}$$

$$\dot{v}_{qi} = -\frac{\begin{bmatrix} (E' v_{qi} + F' v_{di} + I + T_{qi}^{'} G)(T_{di}^{'} A + \frac{T_{di}^{'} BF}{E}) \\ -T_{qi}^{'} FD + T_{qi}^{'} F \frac{x_{di}^{'}}{x_{di}} e_{fdi} - \frac{T_{di}^{'} BIF + T_{di}^{'} T_{qi}^{'} FBG}{E} - T_{di}^{'} T_{qi}^{'} FC \end{bmatrix}}{T_{qi}^{'} E (T_{di}^{'} A + \frac{T_{di}^{'} BF}{E})} \tag{8.23}$$

where,

$$A' = \frac{A + T_{di}^{'} B (F + \frac{x_{qi} - x_{di}^{'}}{x_{qi}})}{T_{qi}^{'} E}$$

$$B' = B + \frac{x_{di} - x_{di}^{'}}{x_{di}} - \frac{T_{di}^{'} B}{T_{qi}^{'}}$$

$$E' = E + \frac{T_{qi}^{'} FB'}{T_{di}^{'} A + \frac{T_{di}^{'} BF}{E}}$$

$$F' = F + \frac{x_{qi} - x_{di}^{'}}{x_{qi}} - \frac{T_{qi}^{'} FA'}{T_{di}^{'} A + \frac{T_{di}^{'} BF}{E}}$$

In order to formulate the novel exciter coordination signals, all the terminal voltage variables which appear (directly or indirectly) in (8.22) and (8.23) must be substituted by their difference compared to their steady-state values (dv_d and dv_q). Just like in the case of the conventional WAC design methodology (Chapter 4), this is done in order to nullify the contribution of the wide area controller when the system is in steady-state. Furthermore, as it can be noted in (8.22) and (8.23), the exciter's local control input (e_{fd}) appears in both dynamic equations. Therefore, a common coordination signal must be formulated which cancels out all the perturbation terms which exist in both equations. The perturbation terms are actually all the superposition terms that appear in the dynamic equations (namely *C*, *D*, *G* and *I*). Once again, this is achieved by utilizing the differentiation of the following expression for the terminal voltage deviation (dv_t), in which the expressions of (8.22) and (8.23) are substituted:

$$dv_t^2 = dv_d^2 + dv_q^2 \tag{8.24}$$

By concentrating all the perturbation terms into a common equation (through (8.24)), the novel WAC signal for the exciter coordination can be obtained. More specifically, the exciter's local control input is decomposed into a local ($e_{fd}{}^{l}$) and a global part ($e_{fd}{}^{g}$), where the global part represents the coordination signal derived from the wide area controller. Therefore, the novel WAC signal is determined by choosing $e_{fd}{}^{g}$ to explicitly cancel out all the perturbation terms of the dynamic equations (*C*, *D*, *G* and *I*):

$$e_{fdi}{}^{g} = \frac{x_{di}}{x_{di}^{'}} \frac{\left[\begin{array}{l} dv_{di}T_{qi}^{'}E(D + \frac{T_{di}^{'}BI}{T_{qi}^{'}E} + \frac{T_{di}^{'}BG}{E} + T_{di}^{'}C) \\ +dv_{qi}\left(\begin{array}{l} (I + T_{qi}^{'}G)(T_{di}^{'}A + \frac{T_{di}^{'}BF}{E}) - T_{qi}^{'}FD \\ -\frac{T_{di}^{'}BIF + T_{di}^{'}T_{qi}^{'}FBG}{E} - T_{di}^{'}T_{qi}^{'}FC \end{array}\right) \end{array}\right]}{T_{qi}^{'}(dv_{di}E - dv_{qi}F)} \tag{8.25}$$

8.4.2 Case study 1: Performance of the proposed exciter only coordination

As a first step, it is important to evaluate the performance of the proposed exciter coordination (PropExc) compared to the performance of the conventional exciter coordination (CovExc). For this reason, the PropExc scenario considers the application of the WAC signal of (8.25) on the exciter, while the ConvExc utilizes the conventional coordination of (4.14). As it has been noted in the case studies of subchapter 5.5, the conventional WAC is sensitive to the appearance of dynamic loads. Therefore, this case

study will compare the two methodologies under conditions where the conventional WAC has increased performance. This means that only ideal constant-power loads will be considered in the IEEE 39-bus dynamic test system. Furthermore, once again as a benchmark, the scenario where no WAC (NoWAC) exists in the system is used. The proposed scheme is evaluated using EMT offline simulations on MathWorks Simulink.

Just like in the previous subsection, the synchronous generators are equipped with PSS, the exciter DC2A and the general-purpose governor. The disturbance considered for all the examined scenarios (NoWAC, ConvExc and PropExc) is a 5-cycle three-phase fault on bus 3. For the graphical illustration of the simulation results, the terminal voltage of G2 (v_2) is used to follow the local damping, while the speed difference between G7 and G10 (w_7-w_{10}) detects the compensation of inter-area oscillations. According to the simulation results of Fig. 8.14a one can note that the proposed coordination has slightly better performance compared to the ConvExc, while both have significantly better damping of the

TABLE 8.7: PRONY ANALYSIS RESULTS FOR CASE STUDY 1

Type	NoWAC		ConvExc		PropExc	
	ζ(%)	*f(Hz)*	*ζ(%)*	*f(Hz)*	*ζ(%)*	*f(Hz)*
Local mode	4.37	1.6	5.72	1.5	5.76	1.6
Inter-area mode	15.7	0.77	13.6	0.74	16.3	0.78

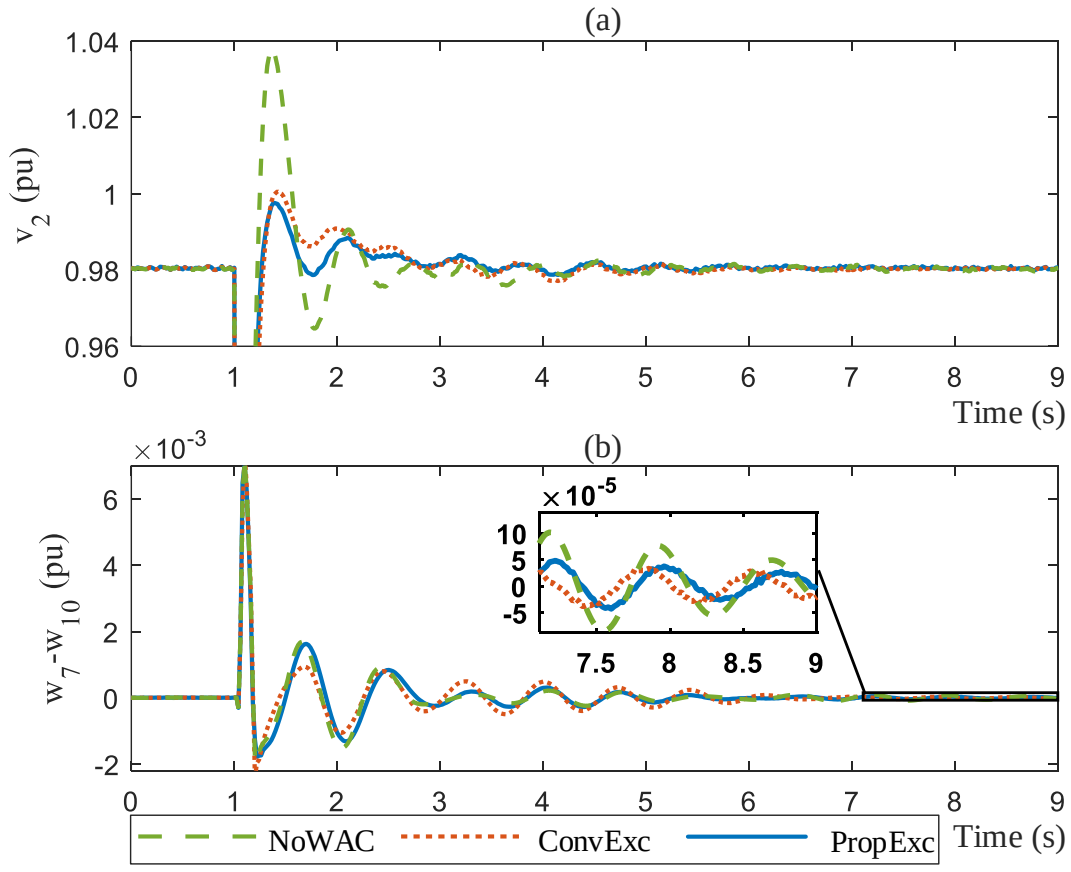

Fig. 8.14 Case Study 1 results illustrating the performances of the NoWAC, ConvExc and PropExc scenarios in compensating the local (a) and inter-area (b) oscillations.

local oscillation compared to the NoWAC scenario. Considering the results of Fig. 8.14b, it is shown that while all the scenarios have comparable performances, the PropExc scenario surpasses the other scenarios, since it provides higher damping of the inter-area oscillation from the beginning of the fault until the end of the simulation. These remarks can be further verified through the Prony analysis results of TABLE 8.7, which underlines the increased performance of the proposed scheme especially in the case of the inter-area oscillations.

8.4.3 Case study 2: Combination of novel exciter coordination with the proposed WAC of governor/PSS and adaptive tuning

The objective of this case study is to present the performance of a complete and highly effective WAC solution, enhanced by the proposed methods for the novel and adaptive coordination of all the synchronous generator local controllers (exciter, governor and PSS). For this reason, the proposed governor/PSS coordination of (8.14) and the adaptive tuning method of (8.3) are combined with the novel exciter coordination of (8.25), forming that way an advanced WAC scheme (AdvWAC). Note that the proposed adaptive tuning is applied to all the coordination signals (exciter and governor/PSS) for regulating their contribution. For evaluation purposes, the AdvWAC scenario is compared with the AdapWAC scenario of subchapter 8.3 (where novel coordination is applied only to the governor and PSS), the ConvWAC scenario and the NoWAC scenario. Note that EMT offline simulations on MathWorks Simulink are considered here as well.

In this case study, a 5-cycle three-phase fault occurs on the line connecting bus 16 to bus 17 at t=1 s, which is followed by the line tripping at t=1.1 s and its reclosing at t=1.7 s. For more realistic and intense dynamic behavior of the system during transient conditions, exponential dynamic loads are placed on buses 4, 8, 15, 21 and 27. Fig. 8.15 along with TABLE 8.8 present the graphical and numerical results of the simulation. Once again, the graphical illustrations depict the terminal voltage v_2 and the speed difference w_7-w_{10}. All the results are illustrating clearly the enhanced performance of the AdvWAC scheme compared to all the other scenarios. This is especially noted in the case of inter-area oscillations (Fig. 8.15b) where the AdvWAC scenario shows considerable higher damping capability. It is also worth mentioning that from Fig. 8.15 it can be derived that the ConvWAC scenario fails to keep the system stable, mainly due to the presence of dynamic loads. The Prony analysis results of TABLE 8.8 show that the proposed scheme outperforms even the AdapWAC scenario providing higher damping ratios in compensating effectively the local and

especially the inter-area modes. It is notable that this enhanced performance is obtained just by adding the novel exciter coordination into the AdapWAC scenario.

8.4.4 Conclusion

A novel coordination scheme for the WAC of the exciter is proposed here in order to enhance significantly the performance of the wide area controller in damping all the local and inter-area oscillations. This is achieved by obtaining new dynamic equations for the i^{th} generator, through the use of the synchronous generator model with one damper winding in the *q*-axis and the transient saliency neglected. Note that the proposed coordination is implemented to be completely compatible with the proposed governor/PSS coordination and the adaptive tuning method, forming that way an advanced WAC scheme.

TABLE 8.8: PRONY ANALYSIS RESULTS OF CASE STUDY 2

Type	NoWAC		ConvWAC	
	ζ(%)	*f(Hz)*	*ζ(%)*	*f(Hz)*
Local mode	5.72	1.5	Instability	
Inter-area mode	13.4	0.74	Instability	
Type	**AdapWAC**		**AdvWAC**	
	ζ(%)	*f(Hz)*	*ζ(%)*	*f(Hz)*
Local mode	6.45	1.6	9.09	1.5
Inter-area mode	18.5	0.66	26.9	0.74

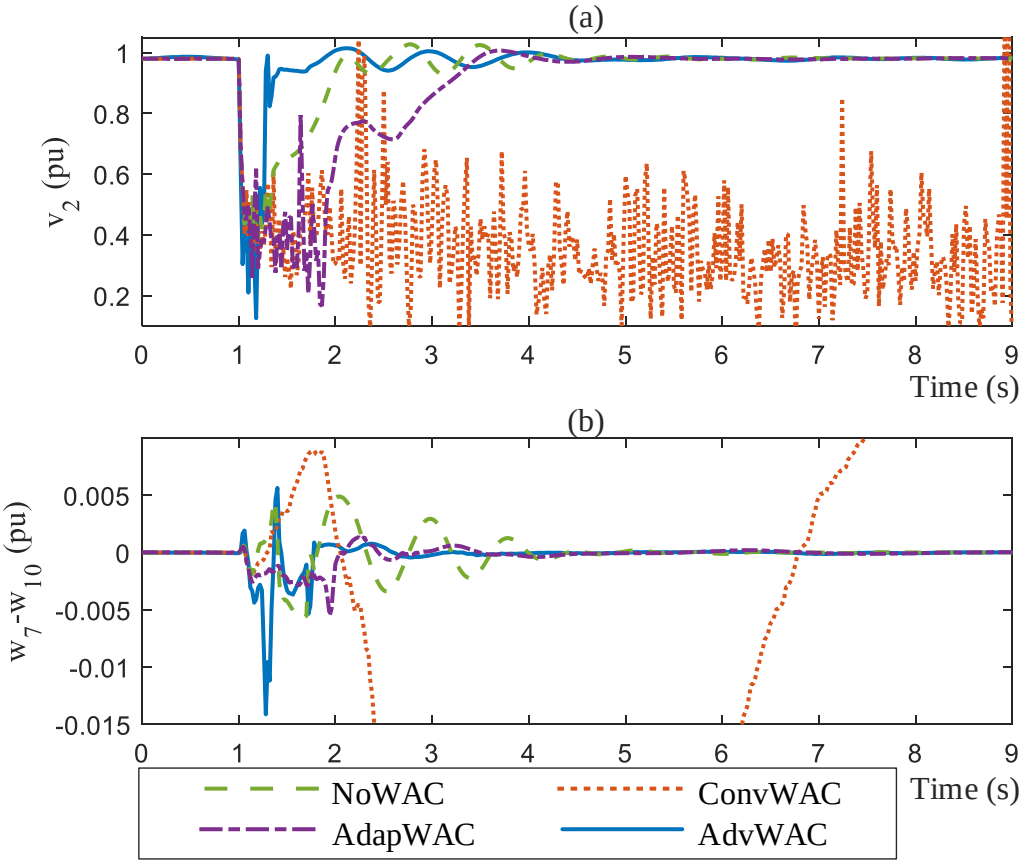

Fig. 8.15 Case Study 2 results illustrating the performances of the NoWAC, ConvWAC, AdapWAC and AdvWAC scenarios in compensating the local (a) and inter-area (b) oscillations.

The performance of the proposed scheme is evaluated through two case studies. The first case study considered the application of the proposed and conventional coordination of the exciter only (neglecting the WAC of governor/PSS) compared to the scenario where a wide area controller is not used in the system. The proposed scheme has shown improved damping ratios for compensating both local and inter-area modes, compared to the other scenarios. Even higher performance is achieved when the exciter coordination is combined with the proposed governor/PSS coordination and the adaptive tuning method, forming an advanced wide area controller. The proposed advanced WAC scheme is tested in the presence of dynamic loads, where it has been shown that it surpasses even the AdapWAC scenario of the previous subchapter.

8.5 Integration of Wide Area Monitoring and Wide Area Control in Real-Time Conditions

Subchapter 8.2.4 specifies that in order to address the remaining drawback of the adopted method considering the assumption of having PMUs installed on all the generator buses (Chapter 4) and the remaining threat of the topology changes (Chapter 5), the integration of the WAM with the WAC application is an essential step. More specifically, the WAM-WAC combination will allow the optimal PMU placement according to the needs of the system and it will update in real-time the system topology that the WAC utilizes (i.e. the bus admittance matrix). Therefore, in this subchapter, a conventional WAM method is integrated with the previously presented advanced wide area controller and their operation is evaluated in real-time realistic conditions. It is important to mention here that the state-of–the-art (published WAC) methods assure the availability of the synchronized measurements directly from the system, ignoring the existence of the WAM application. However, in order to ensure the high performance of the proposed wide area controller, it is essential to be tested and evaluated in a real-time and realistic environment which is close to the actual operating conditions.

8.5.1 Linear state estimator development

The procedure of deriving the states (i.e. voltage magnitude and angle) for all the system buses based on a redundant number of PMUs (which are allocated optimally) is called state estimation.State estimation is the core of WAM, since it processes PMU measurements from specific buses of the system along with the network topology to obtain in near real-time the states of all the buses. Therefore, a state estimator is required here in order to provide

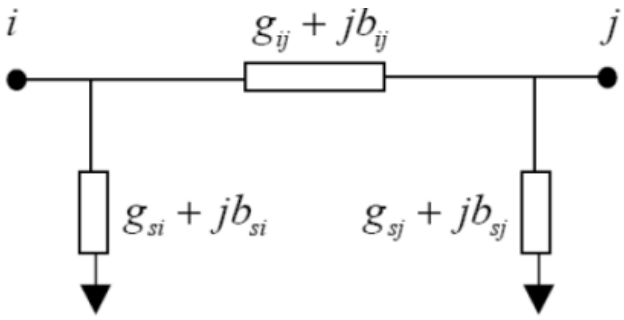

Fig. 8.16 Pi-model of transmission line connecting bus *i* to bus *j*.

all the missing inputs to the wide area controller, since the PMUs are not placed on the generator buses. Furthermore, it is worth mentioning here that the utilization of a state estimator (and thus the WAM-WAC combination) became feasible only because it is assured that all the WAC inputs derive from the synchronized measurement infrastructure (e.g. rotor angle in subchapter 8.2.1). Note that in order to realize the WAM-WAC combination, the commonly used real-time linear state estimator is adopted here which is presented in detail in [141]:

$$z = h(x) + e \tag{8.26}$$

where z is the measurement vector, $h(x)$ is the vector that contains equations relating the measurements to the system states, x is the state vector and e is the Gaussian noise of the measurements.

In order to obtain a unique estimation for the system states, an optimal PMU placement should take place (considering the minimum required number of PMUs) that makes the system observable. Since the PMU provides synchronized voltage and current phasors, the latter need to be expressed in terms of the system states (i.e. voltage phasors). By expressing the voltage phasors in a rectangular form and based on the pi-model of the transmission line (Fig. 8.16) and on the assumption that a PMU is installed on bus *i*, the following expression is derived:

$$\bar{I}_{ij} = \bar{V}_i(g_{si} + jb_{si}) + (\bar{V}_i - \bar{V}_j)(g_{ij} + jb_{ij}) \tag{8.27}$$

where I_{ij} stands for the current flow between buses *i* and bus *j*, while V_i and V_j are the voltages of buses *i* and *j* respectively, all shown in their phasor form.

Separating the real and imaginary parts of the currents and voltages in (8.27), the following linear state estimator can be derived:

$$z = Hx + e = \begin{bmatrix} V_r^{meas} \\ V_i^{meas} \\ I_r^{meas} \\ I_i^{meas} \end{bmatrix} = \begin{bmatrix} \frac{\partial V_r}{\partial V_r} & \frac{\partial V_r}{\partial V_i} \\ \frac{\partial V_i}{\partial V_r} & \frac{\partial V_i}{\partial V_i} \\ \frac{\partial I_r}{\partial V_r} & \frac{\partial I_r}{\partial V_i} \\ \frac{\partial I_i}{\partial V_r} & \frac{\partial I_i}{\partial V_i} \end{bmatrix} \begin{bmatrix} V_r \\ V_i \end{bmatrix} + e \tag{8.28}$$

where z holds all the PMU measurements, H is the Jacobian matrix and x contains the power system states (i.e. the real V_r and imaginary V_i parts of bus voltage phasor). I_r and I_i are the real and imaginary parts of the branch current phasor, respectively.

By applying the Weighted Least Square formulation, x can be found by minimizing the following expression:

$$min \;\; J(x) = [z - Hx]R^{-1}[z - Hx] \tag{8.29}$$

where R is the measurement error covariance matrix.

Finally, the state vector can be estimated by differentiating (8.29) over x and setting it to zero:

$$x = (H^T R^{-1} H)^{-1} H^T R^{-1} z \tag{8.30}$$

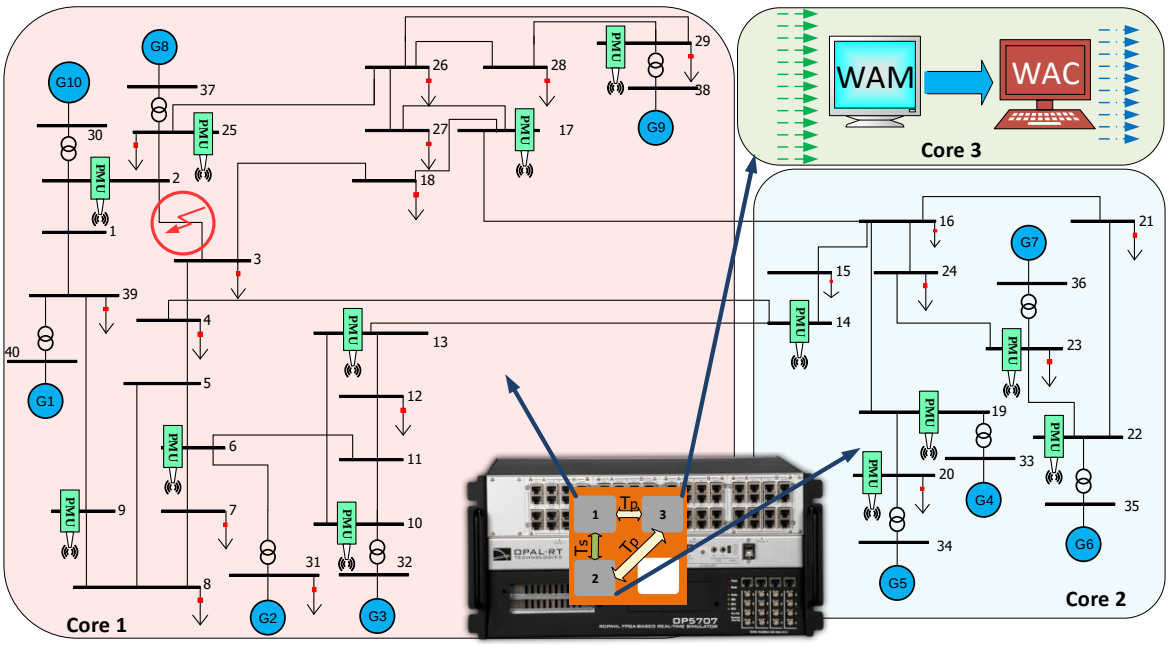

Fig. 8.17 IEEE 39-bus test system illustrating: (i) the separation of the system into 3 cores for *real-time* simulation, and (ii) the optimal PMU placement in the system.

8.5.2 WAM-WAC integration in the real-time IEEE 39-bus dynamic test system

The aim of this subchapter is to evaluate the performance of the WAM-WAC integration in real-time conditions, using the real-time IEEE 39-bus dynamic test system (Fig. 8.3). As aforementioned, the combination of WAM with WAC requires the optimal placement of PMUs in the system. Therefore, for the case of the IEEE 39-bus dynamic test system, 13 PMUs in total are needed to be installed on specific buses in order to obtain full observability. The optimal placement of the PMUs for the case of the IEEE 39-bus dynamic test system is shown in Fig. 8.17. Based on the state estimator presented previously, the WAM will provide to the wide area controller at each time step all the required voltage and current phasors for all the generator buses. The WAM-WAC integration was tested in OPAL-RT real-time simulator where three cores of the OP5700 are used. Two cores are used for running in real-time the dynamic test system with a time step of Ts=0.1 ms. Actually, each core represents an area of the IEEE 39-bus dynamic test system. In order to acquire a

TABLE 8.9: PRONY ANALYSIS RESULTS OF WAMC OPERATION INTO THE REAL-TIME IEEE 39-BUS DYNAMIC TEST SYSTEM

Type	**WAMC DEACTIVATED**		**WAMC ACTIVATED**	
	ζ(%)	*f(Hz)*	*ζ(%)*	*f(Hz)*
Local mode	Instability		7.05	1.8
Inter-area mode	Instability		13.7	0.69

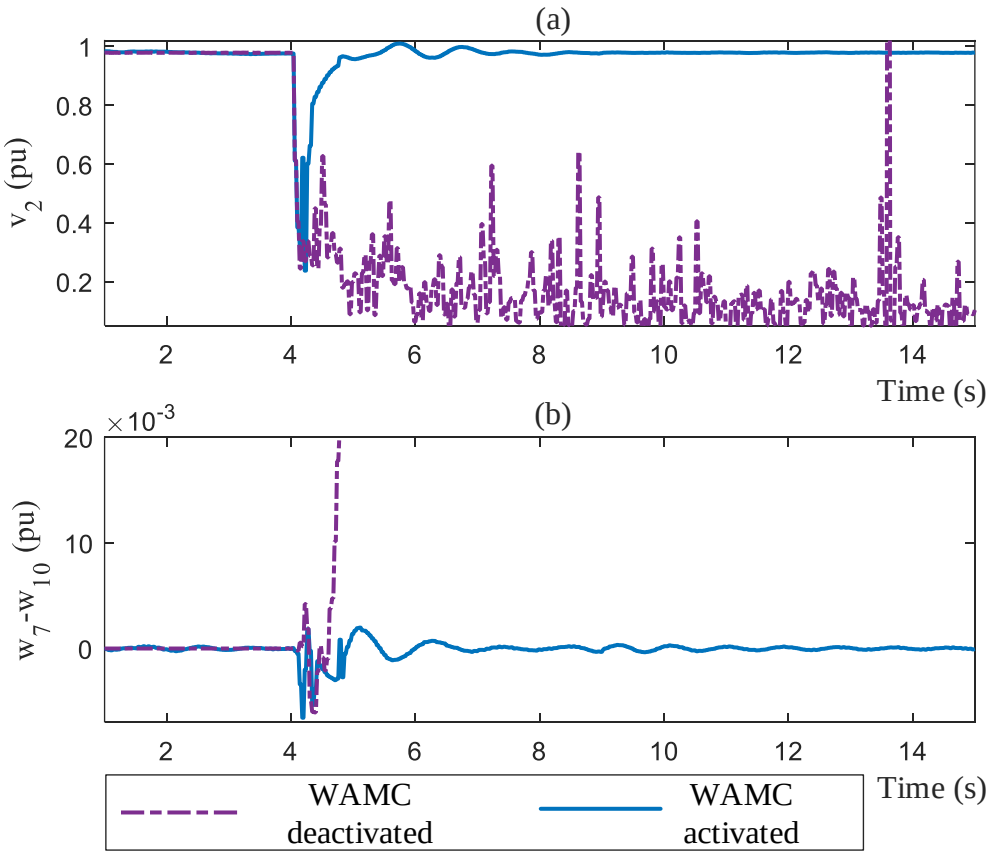

Fig. 8.18 Real-time simulation results showing the system response when the WAMC scheme is activated and deactivated considering the compensation of local (a) and inter-area (b) modes.

realistic operation for the WAMC application, a separate third core is used which holds the WAMC system and it operates in a much higher time step (Tp=40 ms).

The performance of the WAMC scheme is evaluated under the occurrence of a 5-cycle three-phase fault. More specifically, the fault takes place at t=4 s on the line which connects bus 2 to bus 3 and it is followed by a line tripping at t=4.1 s while it recloses at t=4.7 s (Fig. 8.17). Once again, dynamic loads are included in the simulation in order to consider a more realistic and highly dynamic behavior of the system during transient conditions. Thus, exponential dynamic loads (according to the parameters of [130] in TABLE 5.7) are placed on buses 8, 15, 21, 23, 25, 27 and 29. The performance of the novel WAMC scheme is evaluated by comparing the system's response when the WAMC is activated and when it is deactivated. The graphical results of the real-time simulation (Fig. 8.18) illustrate clearly the performance enhancement offered by the WAMC system in damping effectively all the local and inter-area oscillations. In particular, the system remains stable only in the case where the proposed WAMC scheme is activated. This outcome is further confirmed through the Prony analysis result of TABLE 8.9.

8.5.3 WAMC implementation and validation in a real-time Hardware-In-the-Loop configuration

Although the real-time simulation results (shown previously) illustrate the effective operation of the advanced wide area controller when the WAM system is also considered, its further validation under almost actual conditions can be achieved. More specifically, this subchapter aims to utilize real equipment for developing the WAMC system in a real-time HIL configuration. This is a necessary and important procedure, since it is actually one-step before the realization of the WAMC system and its application to a real field test. Fig. 8.19 illustrates the laboratory setup considered for implementing the WAMC system in a real-time HIL configuration. The required components which are described here are the real-time simulator, the PMUs, the Global Positioning System (GPS) antennas and the PDC:

1) Real-time simulator: The OPAL-RT OP5700 real-time simulator is considered here, along with the eMEGASIM software package. The OP5700 holds the test system in one of its cores. More specifically, the IEEE 9-bus dynamic test system is used and modified accordingly in order to generate and provide through its analog outputs all the necessary three-phase voltages and currents to the PMUs. The optimal PMU placement on the IEEE 9-bus dynamic test system is shown in

Fig. 8.19, where three PMUs are placed on buses 4, 7 and 9. Note that the WAMC scheme is developed in a second separate core of the real-time simulator, in order to utilize its high computational power for running this kind of algorithms in near real-time conditions.

2) Phasor Measurement Units: Two PMUs of Arbiter (model 1133A) are employed to take the analog signals of the three-phase voltages and currents (provided by the real-time simulator) and derive their respective phasors. It is worth mentioning here that due to the availability of only two PMUs and furthermore, due to the limitation on the output analog ports, the third PMU is implemented virtually into the real-time simulator. Note that all three PMUs satisfy both, measurement requirements and real-time data transfer requirements of the IEEE Std. C37.118.

3) GPS antennas: The provision of synchronized PMU measurements is a crucial procedure for the implementation of near real-time applications. For this reason the GPS is utilized, which provides a precision signal for time synchronization with an accuracy of ±0.2 μs [99]. Furthermore, all the PMU measurements need to be synchronized to the Coordinated Universal Time (UTC). Therefore, GPS antennas are installed into the laboratory setup (Fig. 8.19) to operate as time sources for the synchronization of the actual and virtual PMUs.

4) Phasor Data Concentrator: A PDC is responsible for gathering and time aligning the synchrophasor data provided by more than one PMU [102]. Therefore, the laboratory setup considers also a PC where a python script is developed for executing the PDC functions (data gathering and time alignment) and for transferring the aligned measurements to the WAMC system.

Before proceeding to the evaluation of the WAMC performance, it is important to ensure that the WAM is providing sufficient and acceptable results. Fig. 8.20a illustrates the voltage magnitude of bus 5, while Fig. 8.20b the current magnitude of the line connecting bus 9 to bus 3. More specifically, each subplot presents a comparison between the ideal measured value and the result of the linear state estimator. It is worth noting here that the latter is based only on actual PMU measurements deriving from three buses (buses 4, 7 and 9). As shown, all the estimated signals are extremely close to the actual ones, indicating the successful operation of the state estimator.

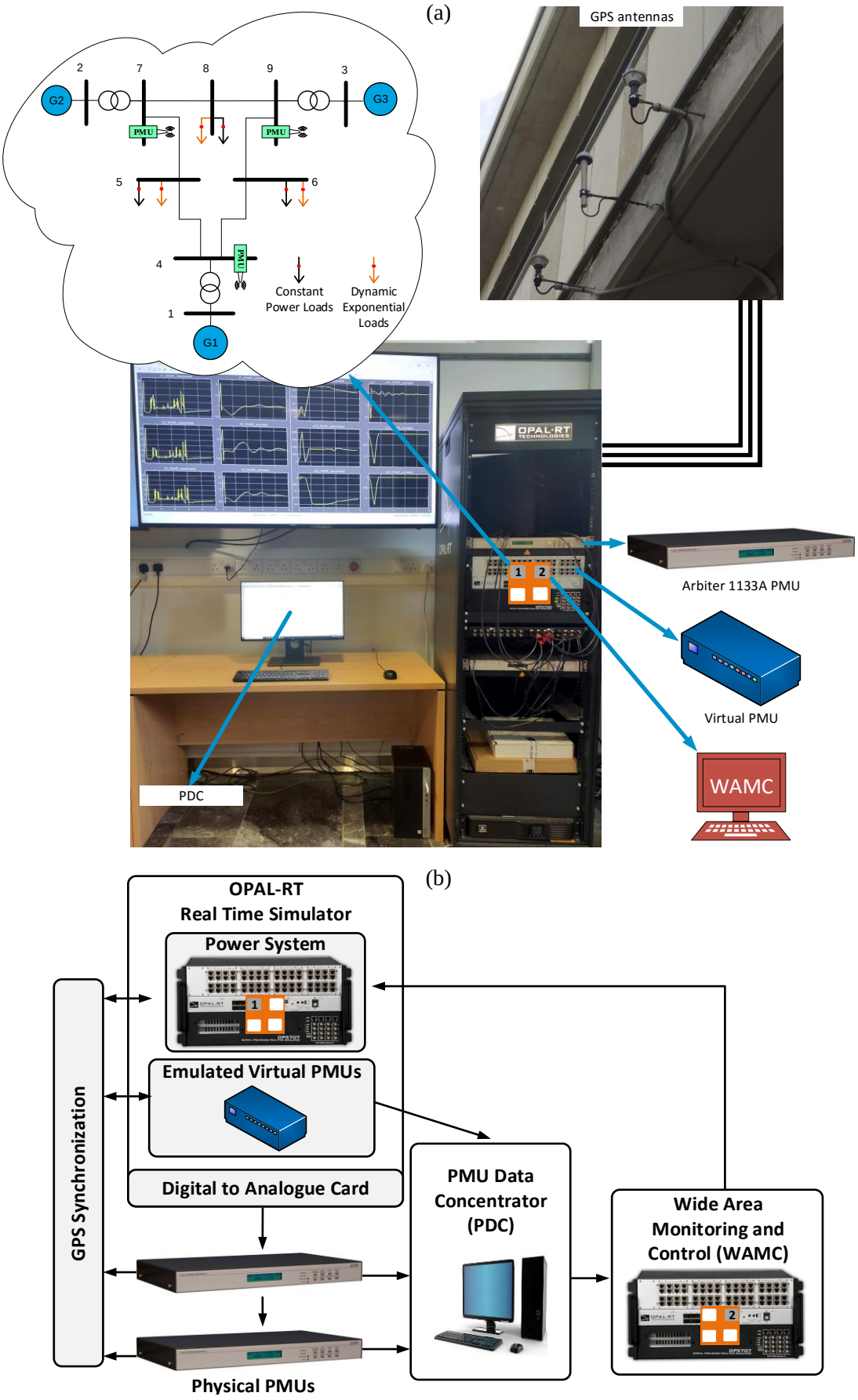

Fig. 8.19 (a) Laboratory setup for testing the proposed WAMC scheme in actual conditions, which is consisted by the real-time simulator, actual and virtual PMUs, GPS antennas and a PDC. Core 1 of the real-time simulator holds the IEEE 9-bus dynamic test system, while core 2 runs the WAMC application. Optimal PMU placement is also shown along with the locations of the dynamic loads. (b) Schematic diagram illustrating the components of the laboratory setup.

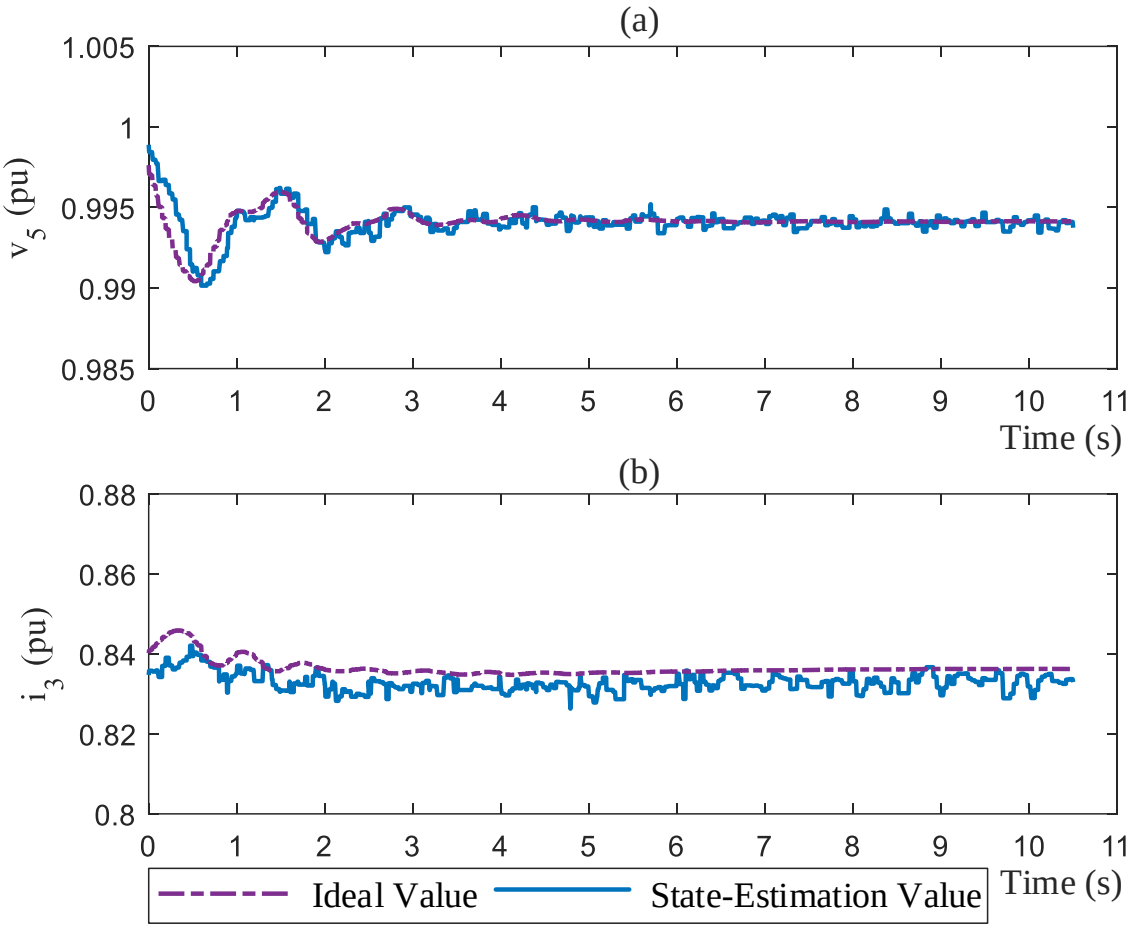

Fig. 8.20 Comparison between ideal and state-estimation values of (a) voltage and (b) current measurements resulting from the HIL laboratory setup.

To illustrate the enhanced damping capability achieved through the utilization of the proposed WAMC scheme, the system's response when the WAMC is activated is compared to the response when the WAMC is deactivated. Both scenarios consider the occurrence of a three-phase fault on bus 7, which is cleared after 0.18 s. In addition, it is worth mentioning here that as Fig. 8.19 illustrates, all the loads of the system are replaced by a combination of a constant power load and a dynamic load (while preserving the total power equal to the initial one) in order to include more realistic and intense conditions during the fault. Fig. 8.21 and TABLE 8.10 present the experimental results of the real-time HIL configuration. Based on these results, one can note the significantly better damping performance of the system when the WAMC scheme is activated. More specifically, as Fig. 8.21 denotes, by deactivating the WAMC scheme the system goes to instability during the disturbance. Prony analysis results of TABLE 8.10 confirm all the aforementioned remarks. It is worth mentioning that the outcomes derived here validate the performance of the proposed scheme in almost realistic and actual conditions, ensuring its effective operation.

TABLE 8.10: PRONY ANALYSIS RESULTS OF WAMC INTO A HIL LABORATORY SETUP

Type	WAMC DEACTIVATED		WAMC ACTIVATED	
	ζ(%)	*f(Hz)*	*ζ(%)*	*f(Hz)*
Local mode	Instability		8.18	1.9
Inter-area mode	Instability		9.4	0.96

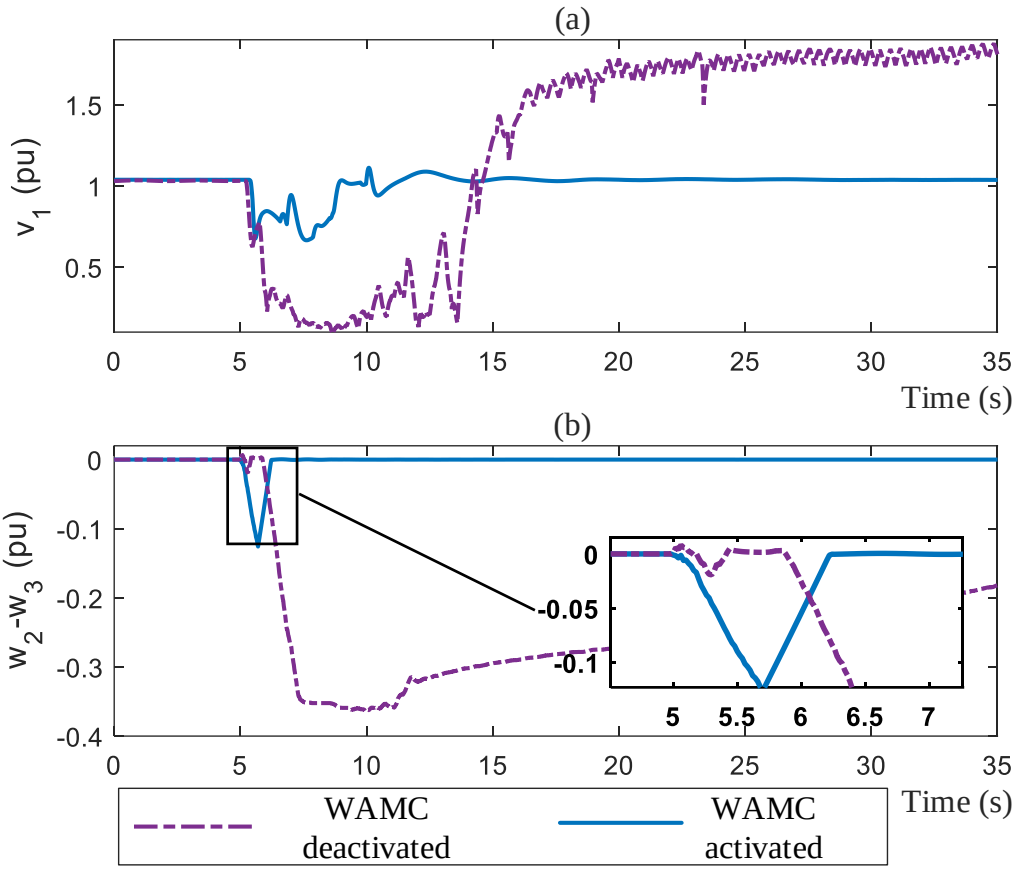

Fig. 8.21 Experimental real-time simulation results of HIL laboratory setup showing the system response when the WAMC scheme is activated and deactivated considering the compensation of local (a) and inter-area (b) modes.

8.6 Conclusion

The primary objective of this chapter was the development of highly effective and novel WAC methods, for the effective coordination of all the synchronous generator local controllers. More specifically, advanced techniques have been introduced aiming at the enhancement of the exciter operation and the simultaneous coordination of the governor and PSS (through their common input signal). The former is realized by adopting the synchronous generator model with one damper winding in the *q*-axis and the transient saliency neglected, while the latter became feasible through the use of the multi-machine power system dynamic model. Both methodologies are combined forming that way an advanced WAC scheme. The high performance of these methods enable the effective compensation of the impact of the non-linear dynamic loads, which has been found to be a threat to the WAC operation.

In addition, the identified drawbacks of the conventional wide area controller are also addressed here, enhancing in this way its robustness. This includes the development of a method for estimating the rotor angle based on synchronized measurements, the appropriate utilization of the coherency concept for ensuring scalability of the wide area controller, and the WAM-WAC integration for considering an optimal PMU placement. However, the most crucial drawback is the utilization of a constant weighting factor for the tuning of the WAC contribution which can affect directly the performance of the wide area controller. To address this issue, an adaptive tuning methodology has been implemented (through the electric connectivity concept) for regulating on-line the contribution of the coordination signals, based on synchronized measurements.

Finally, all the proposed methodologies presented in this chapter are tested and evaluated in real-time and realistic conditions. The latter is achieved through the use of realistic simulation environments applied into a real-time simulator in order to be as close as possible to the actual operating conditions. For evaluating the performance of the advanced wide area controller in actual conditions, a laboratory setup is developed where the proposed scheme is integrated into a WAMC system. The setup considered a real-time simulator, actual PMUs, GPS antennas and a PDC, all connected in a common HIL configuration. All the simulations and tests have illustrated through graphical and numerical results the enhanced performance of the advanced wide area controller in damping effectively all the local and especially the inter-area oscillations.

CHAPTER 9
CONCLUSIONS AND FUTURE WORK

9.1 Conclusions and impact

The future power system has to be able to cope with the new emerging challenges, while its reliability and stability should be not compromised under any circumstances. WAC is a promising application which is capable of reinforcing the system by addressing major threats to its stability, such as the appearance of inter-area oscillations. However, up until now the wide area controller's robustness to various conditions (which can take place) is not properly considered during its design and testing phase, limiting that way its widespread utilization. Therefore, this Ph.D. dissertation focuses on the development of robust and highly effective WAC methodologies, aiming to preserve and enhance the system's stability under any condition. For the implementation of a robust wide area controller, it is essential to identify firstly all the factors that can have an impact to its performance and then propose methods to compensate them. For this reason, realistic simulation environments have been developed which provide accurate representation of the power system behavior, especially during transient conditions. The procedure to derive realistic simulation environments was presented in Chapter 3 of this Ph.D. dissertation, where available standards (e.g., steady-state and dynamic measurement errors, data delays) and published studies (system parameters uncertainty, dynamic loads) are properly considered.

A conventional wide area controller is utilized for evaluating the impact of several factors on its performance. The formulation of the adopted scheme is presented in detail in Chapter 4, where several disadvantages which need to be addressed have been highlighted as well. In addition, an introduction to the Prony analysis tool is also shown in Chapter 4, which is used in this Ph.D. dissertation for evaluating the WAC damping performance. The investigation of the potential threats to the WAC damping capability took place in Chapter 5, which considered the presence of measurement errors, data delays/dropouts, system parameter uncertainties, unreported topology changes and dynamic loads. For the case of measurement errors, the overall error introduced by the whole measurement chain has been taken into consideration, which consist of both steady-state and dynamic PMU measurement errors. The data delays include both the measurement infrastructure delays and the feedback control delays of a two-level communication infrastructure, where various combinations of

three different distributions (uniform, Beta and Gamma) are used to simulate them. The system parameter uncertainties tested in this chapter are separated into the generator and the transmission line parameters that are stored in the databases of the control centers. Unexpected topology changes are simulated by removing a transmission line, changing that way the topology of system which in turn affects its modes. Finally, the modelling of the dynamic loads considered static and dynamic non-linear load models, such as the exponential, exponential dynamic, ZIP and ZIP-Induction Motor (ZIP-IM) load models. The investigation has determined that the main threats which can compromise the WAC performance and the system's stability are the data delays/dropouts, the unreported topology changes and the presence of dynamic loads (specifically, exponential dynamic loads). In addition to these, the increasing introduction of renewables into the system is also considered here as a factor which must be addressed as well, since under high penetration levels it can deteriorate the system's stability.

This Ph.D. dissertation has presented novel methodologies for addressing the impact of all the identified threats. Considering the data delays/dropouts, two model-free and fast predictors are proposed in Chapter 6 in order to ensure the availability of measurements to the wide area controller input at all times, even in the cases of severe delays and data dropouts. Both methods are implemented based on the Autocorrelation LPC and require only measurement signals as inputs, while no information of the system's model is needed. The results indicated that by including the proposed linear predictors into the WAC scheme the performance of the latter is substantially improved, even at the event of severe delays which if left undamped they could lead the system to instability. Furthermore, as it was shown by testing the first linear predictor-WAC combination in the presence and absence of measurement errors, it was concluded that measurement errors could actually affect the WAC performance indirectly, through their impact on the operation of the linear predictor. Therefore, all the measurement signals should be treated accordingly before utilizing them in the WAC application, in order to minimize their error. Furthermore, this result actually illustrates the necessity of utilizing realistic simulations for the design and evaluation of WAC methodologies, where factors which do not seem to have a direct impact on the performance (thus they are commonly neglected) could be identified to affect the operation of the WAC indirectly. The sensitivity of the first linear predictor to the presence of measurement errors is addressed by proposing an advanced predictor which results to a more robust solution. The advanced predictor was compared also to conventional predictive schemes for better illustrating its superior performance and enhanced capabilities. The

outcome which derives from Chapter 6 is the importance of incorporating an effective prediction scheme in the WAC architecture, which is capable of compensating both the measurement infrastructure delays and feedback delays.

The impact of the high penetration of RESs on the system's stability is addressed by proposing two novel coordination methodologies in Chapter 7. While the second methodology is actually advancing the first one, the two schemes have a different approach since the former does not consider the renewables to be coordinated by the wide area controller, while the latter integrates the RESs into the WAC scheme. More specifically, the first method suggests a cooperation between the wide area controller and the renewables, where there is no need to derive WAC signals for the control of RESs. Therefore, the renewable integration into the WAC scheme is not required to improve the dynamic stability of the system. This became feasible by making the synchronous generators "aware" of the dynamic operation of the RES (through the WAC signals) and by modifying the RES local controller to properly utilize the available reactive power of the renewable in order to damp out any local oscillations. The second methodology allows the two-way "awareness" between the generators and RESs. Actually, it makes both the generators "aware" of the RES oscillations and vice versa, the RESs "aware" of the generator oscillations. More specifically, it proposes a hierarchical WAC scheme that coordinates all the generator and renewable local controllers, improving considerably the power system dynamic stability under a high penetration of renewable energy sources. Note that adjustments where applied to the renewable's WAC signals so that minor modifications will be required on the RES local controllers to become compatible for coordination. Considering the unreported topology changes, the WAM-WAC integration is proposed in Chapter 8 for updating in real-time the system topology (i.e. bus admittance matrix) which is utilized by the WAC scheme. Finally, the impact of the exponential dynamic loads is addressed through the implementation of novel and advanced methods for the effective coordination of the synchronous generator local controllers.

Apart from compensating the threats to the WAC operation, the identified drawbacks of the adopted wide area controller are addressed as well in order to enhance its robustness. More specifically, the considered drawbacks are: 1) the assumption that PMUs provide also the generator's rotor angle δ as a synchronized measurement, 2) scalability issues due to the substantial increase of the required inputs and the derived output signals when moving to larger systems, 3) the utilization of a constant weighting factor for the tuning of the WAC contribution, and finally 4) the assumption of having PMUs installed on all the generator

buses. For addressing the first drawback, a method is proposed for the estimation of the rotor angle based only on synchronized measurements. Furthermore, the scalability of the wide area controller is achieved by utilizing appropriately the coherency concept. The disadvantage of using a constant weighting factor for regulating the WAC contribution is overcome by proposing a novel adaptive tuning methodology which is based on synchronized measurements and the electric connectivity concept. Finally, the optimal PMU placement is achieved through the integration of the WAM with the WAC scheme.

This Ph.D. dissertation considers along with the WAC robustification, the development of a highly effective wide area controller. Therefore, novel methodologies are proposed for the effective coordination of all the local controllers of the system. The aim is to increase the local controllers' performance in damping effectively all the local and inter-area oscillations by overcoming their lack of global observability. The proposed advanced techniques intend to enhance the operation of the exciter, the governor and PSS. This is achieved by adopting the synchronous generator model with one damper winding in the *q*-axis (transient saliency neglected) and the multi-machine power system dynamic model. For the WAC of the governor and PSS, a simultaneous coordination scheme is proposed which became feasible through the interaction of the wide area controller with their common input signal (i.e., rotor speed deviation). The combination of the proposed novel techniques results to the appearance of an advanced wide area controller, which has high performance in damping effectively all the local and inter-area oscillations even under extreme conditions (i.e. high penetration of dynamic loads).

Finally, it is important to emphasize that this Ph.D. dissertation considered cutting-edge simulation technology for evaluating the advanced controller's robustness and performance under real-time and realistic conditions. More specifically, a real-time simulator is combined with the proposed realistic simulation environments forming that way a suitable testbed for deploying and validating WAMC methodologies. It is also important to highlight that this Ph.D. dissertation has proposed the development of a novel laboratory setup that consists of real equipment (i.e. PMUs, PC, GPS antennas) and a real-time simulator, for evaluating the WAMC performance and robustness in almost actual conditions.

As a conclusion, this Ph.D. dissertation significantly contributes to the development of a robust and highly effective wide area controller for enhancing the stability of the system. Realistic, accurate and real-time simulation models are implemented for identifying and

mitigating properly all the threats to the WAC operation. In addition, the procedure to derive novel and advanced coordination schemes is illustrated, in order to ensure the complete and effective compensation of all the local and especially the inter-area modes under any condition. Therefore, all the methodologies proposed in the context of this Ph.D. dissertation are essential to achieve robustification and damping performance enhancement of the wide area controller, increasing substantially the stability of the system. However, it is important to emphasize here that as expected there is also a tradeoff involved with obtaining robustness and high effectiveness. This tradeoff actually arises from the increased processing times which are associated with the proposed WAC side applications such as, the linear predictors, the state estimation, the adaptive tuning, the near real-time update of the system's topology and the implementation of additional coordination signals for the RESs coordination. Therefore, an increased processing power is required in order to execute all these actions promptly while ensuring the robustness and enhanced damping performance of the wide area controller. Furthermore, the high dependence of the proposed wide area controller on the aforementioned side applications, could be also a tradeoff for the WAC reliability.

9.2 Future work

This Ph.D. dissertation focuses on deriving a robust and highly effective wide area controller. As a result, all the threats to the WAC operation are identified, methods to mitigate their impact are proposed and advanced coordination techniques for enhancing the WAC performance are developed. However, there is still area for improvement especially on the wide area controller side. An obvious future work is to obtain a universal coordination architecture, which considers all the types of fast-acting resources for contributing to the increase of the system's small signal stability. In other words, a wide area controller will be developed which can coordinate all the local controllers of the system, having as an objective to compensate faster and more effectively all the inter-area oscillations. Therefore, methodologies must be implemented for integrating along with the synchronous generators and RESs, the HVDCs and FACTSs into the WAC scheme.

In addition to this, the universal coordination scheme should be able to improve the system operation in several ways while keeping always the compensation of inter-area oscillations as a high priority. More specifically, since the coordination of all the local controllers will be taking place, a well-known issue which can be addressed in this context is the appearance of sub-synchronous oscillations. These oscillations can lead to shaft fatigue or even failure and they are associated with the interaction of the generators with FACTSs

or HVDCs. Therefore, the universal coordination scheme can be considered for coordinating accordingly adjacent components (e.g. synchronous generators and HVDC/FACTS) at the event of these subsynchronous phenomena for their prompt and total compensation. Another issue that was aforementioned is the significant reduction of the system's inertia as the penetration of the renewables is increasing significantly into the grid. Although novel coordination schemes were presented in Chapter 7 for addressing the impact of the high penetration of RESs on the system's stability, the inertia reduction is still an open issue. The introduction of virtual inertia into the renewables is a very attractive solution to address this problem. In this context, the wide area controller could be enhanced in taking also decisions considering the required virtual inertia which needs to be added to the system, based on system inertia estimation methodologies.

Apart from the coordination of the local controllers, the system loads can also be utilized by the wide area controller for enhancing significantly the system damping performance. Up until now, loads are treated as passive components, the demand of which cannot be modified. However, the installation of smart appliances into the households and the introduction of the demand-side control concept have provided the means to obtain more responsive and controllable loads. The load controllability is even more enhanced due to the growing introduction of inverter-based loads into the system, which allows their easy integration into coordination schemes. To illustrate the effect of considering such interactive loads into the WAC architecture, a novel dynamic test system must be implemented which considers all the power system levels (transmission and distribution). This test system will be used for developing a hierarchical control scheme which can coordinate actuators from the transmission and distribution systems. Therefore, the WAC scheme will derive coordination signals which can be passed down to the medium-voltage and low-voltage levels. More specifically, coordination signals (similar to the ones derived for the renewables in Chapter 7) will be directed to the high-voltage level feeders, which will operate as regional supervisory systems. This means that upon receiving the WAC active and reactive power deviation signals (ΔP and ΔQ) the high-voltage level feeders will decide which medium-voltage level feeders will participate into the coordination scheme. In turn, the medium-voltage level feeders will define which of the available loads of the low-voltage distribution system (i.e. household appliances) will be activated/deactivated at each time step, forming that way a hierarchical structure. However, a challenging task is to perform this procedure in near real-time conditions (in which the WAC scheme operates), where delays and data dropouts take place.

The integration of loads into the WAC scheme has a limitation similar to the one presented in the case of the RES integration with the wide area controller. More specifically, in subchapter 7.2 it has be noted that the lower bound of the renewable's active power can be as much as the WAC needs it to be, but the upper bound is limited by the available active power. In the case of the loads, the wide area controller can deactivate and re-activate loads which are already available, but it cannot activate loads which were initially turned off by the user. Therefore, it is very interesting to integrate into the WAC architecture a combination of a renewable and a load. In this way, the limitation for increasing the renewable power can be overcome by reducing the load demand and vice-versa, the constraint of increasing the power consumption of the loads can be compensated by applying a curtailment on the RES output power.

In the near future, the laboratory setup of Chapter 8 needs to be upgraded in order to comprise larger real-time dynamic test systems into the HIL configuration. This includes the utilization of IEEE dynamic test systems such as the 39-bus and 68-bus, but the actual objective is to develop and consider also a realistic real-time model of the Cyprus power system in this setup. To achieve this though, a significantly larger number of PMUs will be required, which will be implemented virtually into the real-time simulator (since there is a limitation on the number of actual PMUs that can connect externally). Due to the substantial increase of the synchronized measurements, an industrial PC might be also needed to operate as a PDC in real-time conditions. Furthermore, an important upgrade of the existing laboratory setup is the addition of an external controller dedicated for WAMC applications, instead of utilizing a core of the same real-time simulator that represents the power system. Another task related to the laboratory setup is to introduce large delays and dropouts by simulating and including also into the HIL configuration the network communication system. This addition will allow to test and evaluate in actual conditions the integration of the linear predictors (Chapter 6) into the WAC scheme. In this context, it is important to emphasize here that even by considering almost delay-free communication networks (e.g. 5G networks), data latencies will still exist in the communication infrastructure due to the operational/processing delays occurring from the real-time applications, the PMUs and the PDC.

A very interesting topic to examine in future work is the development of an advanced wide area controller for contributing in both, positive and negative sequence components. This novel concept is based on the fact that currently the WAC is operating and contributing only on the positive sequence. This is mainly due to the development of the wide area

controller to coordinate primarily all the synchronous generators which are positive sequence sources. Note that the positive sequence component is directly connected to the balanced conditions of the system. This means that the WAC scheme has high performance under balanced symmetrical conditions, but its damping capability reduces in unbalanced conditions since it is unable to "sense" and properly "act" on these oscillations. The presence of unbalances into the system results to the appearance of the negative sequence component. Although, synchronous generators cannot take any actions against the negative sequence oscillations, other types of energy sources (such as the renewables) are able to contribute to it. Furthermore, considering the detection of the unbalanced conditions, the PMUs have the capability of providing also negative sequence measurements. Therefore, the aim of this novel concept is the creation of positive sequence (WAC^{+}) and negative sequence (WAC^{-}) wide area controllers. The former will utilize all the synchronous generators for damping any oscillation on the positive sequence component, while the latter will coordinate appropriately all the RESs to compensate the disturbances on the negative sequence component.

One can argue here that a more decentralized approach is more desirable instead of a centralized structure. However, the issue here is that the application of distributed control on each one of the energy sources which participate into the WAC scheme will require the availability of remote signals from all the remaining energy sources, since these are required for the detection of inter-area oscillations. This means that a more expensive and complex communication infrastructure will need to be developed for the purposes of decentralized WAC. Once again, the coherency concept can be considered here in order to develop a hybrid approach. More specifically, coherency concept can be used for identifying in near real-time the coherent groups in a centralized manner and drive only the necessary measurements to each energy source, which is equipped with a distributed wide area controller.

Finally, another task for future work is to evaluate and derive methods to detect and compensate the impact of cyber-attacks on WAMC architecture. Cyber-attacks are increasingly becoming a critical threat to the WAMC operation, mainly due to its heavy dependence on the communication infrastructure. More specifically, cyber-attacks can degrade the WAC operation to the point where it can lead the system to instability. One type of cyber-attack was described in subsection 2.2, namely the denial of service, where the aim of this attack is to cause data dropouts to occur on the communication between the PMUs and the WAMC application. Apart from the data dropouts, attacks which aim to increase the

communication delays also exist. In addition, other types of cyber-attacks on the power system can take place and need to be addressed as well, such as the alteration of the synchronous measurement time stamp through GPS spoofing on the PMUs. This kind of attack can actually affect the time alignment of the PDC and also the estimated angles. Another type of cyber-attack which can take place in the power system is the so-called Man-In-The-Middle (MITM) attack, where in this case the attacker secretly gets between the PMU and PDC communication and it alters the synchronized measurements. In addition to these, indirect attacks in other parts of the WAMC scheme, are crucial to the WAC performance. As an example, by affecting the system topology or the state-estimator through cyber-attacks will deteriorate the WAC operation, since it is highly depended on them. For the evaluation, detection and compensation of the cyber-attack impact, the laboratory setup needs to be considered where actual attacks will take place.

Robustification and damping performance enhancement of the wide area controller is an on-going procedure, since new challenges and threats emerge as the power system is heading towards to the realization of the smart grid concept.

REFERENCES

[1] S. Chakrabarti, E. Kyriakides, T. Bi, D. Cai, and V. Terzija, "Measurements get together," *IEEE Power and Energy Magazine,* vol. 7, no. 1, pp. 41-49, 2009.

[2] A. R. Messina, Inter-area Oscillations in Power Systems: A Nonlinear and Nonstationary Perspective (Power Electronics and Power Systems), Guadalajara: Springer, 2009.

[3] F. Bai, Y. Zhu, X. Wang, K. Sun, Y. Ma, M. Patel, E. Farantatos, and N. Bhatt, "Design and implementation of a measurement-based adaptive wide area damping controller considering time delays," *Electric Power Systems Research,* vol. 130, pp. 1-9, Jan. 2016.

[4] J. Lian, R. Huang, S. Wang, R. Fan, M. A. Elzondo, H. Kirkham, J. Hansen, L. D. Marinovici, D. Schoenwald, and F. Wilches-Bernal, "Universal Wide-area Damping Control for Mitigating Inter-area Oscillations in Power Systems," Pacific Northwest National Laboratory, Washington, 2017.

[5] X. Wu, F. Dörfler, and M. R. Jovanović, "Input-output analysis and decentralized optimal control of inter-area oscillations in power systems," *IEEE Trans. Power Systems,* vol. 31, no. 3, pp. 2434-2444, 2016.

[6] M. Jonsson, M. Begovic, and J. Daalder, "A new method suitable for real-time generator coherency determination," *IEEE Trans. Power Systems,* vol. 19, no. 3, p. 1473–1482, 2004.

[7] D. N. Kosterev and C. W. M. W. A. Taylor, "Model validation for the August 10, 1996 WSCC system outage," *IEEE Trans. Power Systems,* vol. 14, no. 3, pp. 967-979, 1999.

[8] ENTSO-E, "Analysis of CE inter-area oscillations of 19 and 24 February 2011," ENTSO-E, Brussels, 2011.

[9] ENTSO-E, "Analysis of CE inter-area oscillations of 1st December 2016," ENTSO-E, Brussels, 2017.

[10] S. Mohagheghi, G. Venayagamoorthy, and R. Harley, "Optimal wide area controller and state predictor for a power system," *IEEE Trans. Power Systems,* vol. 22, no. 2, pp. 693-705, 2007.

[11] M. E. Raoufat, K. Tomsovic, and S. M. Djouadi, "Virtual actuators for wide-area damping control of power systems," *IEEE Trans. Power Systems,* vol. 31, no. 6, pp. 4703-4711, 2016.

[12] S. Roy, A. Patel, and I. N. Kar, "Analysis and design of a wide-area damping controller for inter-area oscillation with artificially induced time delay," *IEEE Trans. on Smart Grid,* vol. 10, no. 4, pp. 3654-3663, 2019.

[13] C. Lu, Y. Zhao, K. Men, L. Tu, and Y. Han, "Wide-area power system stabiliser based on model-free adaptive control," *IET Control Theory & Applications,* vol. 9, no. 13, pp. 1996-2007, 2015.

[14] W. Yao, L. Jiang, J. Wen, Q. Wu, and S. Cheng, "Wide-area damping controller for power system interarea oscillations: A networked predictive control approach," *IEEE Trans. Control Systems Technology,* vol. 23, no. 1, pp. 27-36, 2015.

[15] D. Cai, P. Wall, M. Osborne, and V. Terzija, "Roadmap for the deployment of WAMPAC in the future GB power system," *IET Generation, Transmission & Distribution,* vol. 10, no. 7, pp. 1553-1562, 2016.

[16] V. Terzija et al., "Wide-area monitoring, protection, and control of future electric power networks," *Proceedings of the IEEE,* vol. 99, no. 1, pp. 80-93, 2011.

[17] W. Yao, L. Jiang, J. Wen, S. J. Cheng, and Q. H. Wu, "Networked predictive control based wide-area supplementary damping controller of SVC with communication delays compensation," in *Proc. IEEE PES General Meeting*, Vancouver, 2013.

[18] S. Wang, X. Meng, and T. Chen, "Wide-area control of power systems through delayed network communication," *IEEE Trans. Control Systems Technology,* vol. 20, no. 2, pp. 495-503, 2012.

[19] D. Roberson and J. F. O'Brien, "Loop shaping of a wide-area damping controller using HVDC," *IEEE Trans. Power Systems,* vol. 32, no. 3, pp. 2354-2361, 2017.

[20] A. S. Musleh, S. M. . Muyeen, A. Al-Durra, I. Kamwa, M. A. S. Masoum, and S. Islam, "Time-delay analysis of wide-area voltage control considering smart grid contingences in a real-time environment," *IEEE Trans. Industrial Informatics,* vol. 14, no. 3, pp. 1242-1252, 2018.

[21] C. Huang, F. Li, D. Zhou, J. Guo, Z. Pan, and Y. Liu, "Data quality issues for synchrophasor applications Part I: a review," *Journal of Mod. Power Syst. Clean Energy,* vol. 4, no. 3, pp. 342-352, 2016.

[22] D. Gautam, V. Vittal, and T. Harbour, "Impact of increased penetration of DFIG-based wind turbine generators on transient and small signal stability of power systems," *IEEE Trans. Power Systems,* vol. 24, no. 3, pp. 1426-1434, 2009.

[23] L. Zacharia, M. Asprou, and E. Kyriakides, "Measurement errors and delays on wide-area control based on IEEE std C37.118.1-2011: impact and compensation," *IEEE Systems Journal (Early Access).*

[24] L. Zacharia, M. Asprou, and E. Kyriakides, "Investigation of the factors influencing wide area control," in *Proc. IEEE PES General Meeting,* Chicago, 2017.

[25] L. Zacharia, M. Asprou, and E. Kyriakides, "Design of a data delay compensation technique based on a linear predictor for wide-area measurements," in *Proc. IEEE PES General Meeting*, Boston, 2016.

[26] L. Zacharia, L. Hadjidemetriou, and E. Kyriakides, "Cooperation of wide area control with renewable energy sources for robust power oscillation damping," in *Proc. IEEE PowerTech*, Manchester, 2017.

[27] L. Zacharia, L. Hadjidemetriou, and E. Kyriakides, "Integration of renewables into the wide area control scheme for damping power oscillations," *IEEE Trans. Power Systems,* vol. 33, no. 5, pp. 5778-5786, 2018.

[28] L. Zacharia, M. Asprou, and E. Kyriakides, "Wide area control of gevernors and power system stabilizers with an adaptive tuning of coordination signals," *IEEE Open Access of Power and Energy (Accepted).*

[29] D. Dotta, A. S. e Silva, and I. C. Decker, "Wide-area measurements-based two-level control design considering signal transmission delay," *IEEE Trans. Power Systems,* vol. 24, no. 1, pp. 208-216, 2009.

[30] B. Chaudhuri and B. C. Pal, "Robust damping of multiple swing modes employing global stabilizing signals with a TCSC," *IEEE Trans. Power Systems,* vol. 19, no. 1, pp. 499-506, 2004.

[31] H. Wu, K. S. Tsakalis, and G. T. Heydt, "Evaluation of time delay effects to wide-area power system stabilizer design," *IEEE Trans. Power Systems,* vol. 19, no. 4, pp. 1935-1941, 2004.

[32] I. Kamwa, R. Grondin, and Y. Hebert, "Wide-area measurement based stabilizing control of large power systems-a decentralized/hierarchical approach," *IEEE Trans. Power Systems,* vol. 16, no. 1, pp. 136-153, 2001.

[33] T. Surinkaew and I. Ngamroo, "Hierarchical co-ordinated wide area and local controls of DFIG wind turbine and PSS for robust power oscillation damping," *IEEE Trans. Sustainable Energy,* vol. 7, no. 3, pp. 943-955, 2016.

[34] M. Beiraghi and A. M. Ranjbar, "Additive model decision tree-based adaptive wide-area damping controller design," *IEEE Systems Journal,* vol. 12, no. 1, pp. 328-339, 2018.

[35] L. Zhu, H. Liu, Z. Pan, Y. Liu, E. Farantatos, M. Patel, S. McGuinness, and N. Bhatt, "Adaptive Wide-Area Damping Control Using Measurement-Driven Model Considering Random Time Delay and Data Packet Loss," in *Proc. IEEE PES General Meeting*, Boston, 2016.

[36] X. Zhang, C. Lu, X. Xie, and Z. Y. Dong, "Stability analysis and controller design of a wide-area time-delay system based on the expectation model method," *IEEE Trans. Smart Grid,* vol. 7, no. 1, pp. 520-529, 2016.

[37] B. P. Padhy, S. C. Srivastava, and N. K. Verma, "A network delay compensation technique for wide area SVC damping controller is power system," in *Proc. IEEE PES T&D Conference and Exposition*, Chicago, 2014.

[38] M. Hadjikypris, O. Marjanovic, and V. Terzija, "Damping of inter-area power oscillations in hybrid AC-DC power systems based on supervisory control scheme utilizing FACTS and HVDC," in *Power Systems Computation Conference (PSCC)*, Genoa, 2016.

[39] F. Okou, L.-A. Dessaint, and O. Akhrif, "Power system stability enhancement using a wide area signals based hierarchical controller," *IEEE Trans. Power Systems,* vol. 20, no. 3, pp. 1465-1477, 2005.

[40] J. Zhang, C. Y. Chung, C. Lu, K. Men, and L. Tu, "A novel adaptive wide area PSS based on output-only modal analysis," *IEEE Trans. Power Systems,* vol. 30, no. 5, pp. 2633-2642, 2015.

[41] R. Yousefian, R. Bhattarai, and S. Kamalasdan, "Transient stability enhancement of power grid with integrated wide-area control of wind farms and synchronous generators," *IEEE Trans. Power Systems,* vol. 32, no. 6, pp. 4818-4831, 2017.

[42] A. Thakallapelli, S. J. Hossain, and S. Kamalasadan, "Coherency and online signal selection based wide area control of wind integrated power grid," *IEEE Trans. Industry Applications,* vol. 54, no. 4, pp. 3712-3722, 2018.

[43] M. Li and Y. Chen, "A Wide-Area Dynamic Damping Controller Based on robust H∞ control for wide-area power systems with random delay and packet dropout," *IEEE Trans. Power Systems,* vol. 33, no. 4, pp. 4026-4037, 2018.

[44] F. Okou, L.-A. Dessaint, and O. Akrhrif, "Smith predictor approach for the design of a robust wide-area measurements based hierarchical controller," in *Proc. IEEE PES General Meeting*, San Francisco, 2011.

[45] T. Zabaiou, F. A. Okou, and L. A. A. O. Dessaint, "Time-delay compensation of a wide-area measurements-based hierarchical voltage and speed regulator," *Canadian Journal of Electrical and Computer Engineering,* vol. 33, no. 2, pp. 77-85, 2008.

[46] D. Ke and C. Y. Chung, "Design of probabilistically-robust wide-area power system stabilizers to suppress inter-area oscillations of wind integrated power systems," *IEEE Trans. Power Systems,* vol. 31, no. 6, pp. 4297-4309, 2016.

[47] Y. Liu, S. You, and Y. Liu, "Study of wind and PV frequency control in U.S. power grids—EI and TI case studies," *IEEE Power and Energy Technology Systems Journal,* vol. 4, no. 3, pp. 65-73, 2017.

[48] R. Yousefian, A. Sahami, and S. Kamalasadan, "Hybrid transient energy function-based real-time optimal wide-area damping controller," *IEEE Trans. Industry Applications,* vol. 53, no. 2, pp. 1506-1516, 2017.

[49] B. J. Pierre et al., "Design of the Pacific DC Intertie wide area damping controller," *IEEE Trans. Power Systems,* vol. 34, no. 5, pp. 3594-3604, 2019.

[50] R. L. Cresap, W. A. Mittelstadt, D. N. Scott, and C. W. Taylor, "Operating experience with modulation of the Pacific HVDC Intertie," *IEEE Trans. Power Apparatus and Systems,* Vols. PAS-97, no. 4, pp. 1053-1059, 1978.

[51] D. Trudnowski, D. Kosterev, and J. Undrill, "PDCI damping control analysis for the western North American power system," in *Proc. IEEE PES General Meeting*, 2013, 2013.

[52] C. Lu, X. Wu, J. Wu, P. Li, Y. Han, and L. Li, "Implementations and experiences of wide-area HVDC damping control in China Southern Power Grid," in *Proc. IEEE PES General Meeting*, San Diego, 2012.

[53] D. Cai, L. Ding, X. Zhang, and V. Terzija, "Wide area inter-area oscillation control system in a GB electric power system," *The Journal of Engineering,* vol. 2019, no. 16, pp. 3294-3300, 2019.

[54] A. Vahidnia, G. Ledwich, and E. W. Palmer, "Transient stability improvement through wide-area controlled SVCs," *IEEE Trans. Power Systems,* vol. 31, no. 4, pp. 3082-3089, 2016.

[55] P. Mahish, A. K. Pradhan, and A. K. Sinha, "Wide area predictive control of power system considering communication delay and data drops," *IEEE Trans. Industrial Informatics,* vol. 15, no. 6, pp. 3243-3253, 2019.

[56] T. Zabaiou, L.-A. Dessaint, F.-A. Okou, and R. Grondin, "Wide-area coordinating control of SVCs and synchronous generators with signal transmission delay compensation," in *Proc. IEEE PES General Meeting*, Minneapolis, 2010.

[57] T. Zabaiou, L. Dessaint, F. Okou, and R. Grondin, "Wide-area measurements based coordination of SVCs and synchronous generators," in *Proc. IEEE PES General Meeting*, Pittsburgh, 2008.

[58] D. A. Halamay, T. K. A. Brekken, A. Simmons, and S. McArthur, "Reserve requirement impacts of large-scale integration of wind, solar, and ocean wave power generation," *IEEE Trans. Sustainable Energy,* vol. 2, no. 3, pp. 321-328, 2011.

[59] C. Liu, G. Cai, W. Ge, D. Yang, C. Liu, and Z. Sun, "Oscillation analysis and wide-area damping control of DFIGs for renewable energy power systems using line modal potential energy," *IEEE Trans. Power Systems,* vol. 33, no. 3, pp. 3460-3471, 2018.

[60] M. Mokhtari and F. Aminifar, "Toward wide-area oscillation control through doubly-fed induction generator wind farms," *IEEE Trans. Power Systems,* vol. 29, no. 6, pp. 2985-2992, 2014.

[61] A. Yogarathinam and N. R. Chaudhuri, "Wide-area damping control using multiple DFIG-based wind farms under stochastic data packet dropouts," *IEEE Trans. Smart Grid,* vol. 9, no. 4, pp. 3383 - 3393, 2016.

[62] A. Yogarathinam and N. R. Chaudhuri, "Wide-area damping control using reduced copy under intermittent observation: A novel performance measure," *IEEE Trans. Control Systems,* vol. 27, no. 1, pp. 434-442, 2019.

[63] A. E. Leon and J. A. Solsona, "Power oscillation damping improvement by adding multiple wind farms to wide-area coordinating controls," *IEEE Trans. Power Systems*, vol. 29, no. 3, pp. 1356-1364, 2014.

[64] Y. Xu, F. Li, Z. Jin, and M. Hassani Variani, "Dynamic gain-tuning control (DGTC) approach for AGC with effects of wind power," *IEEE Trans. Power Sysems,* vol. 31, no. 5, pp. 3339-3348, 2016.

[65] D. Apostolopoulou, P. W. Sauer, and A. D. Domínguez-García, "Balancing authority area model and its application to the design of adaptive AGC systems," *IEEE Trans. Power Systems,* vol. 31, no. 5, pp. 3756-3764, 2016.

[66] M. Benasla, T. Allaoui, and M. Brahami, "Coherency concept to increase the effectiveness of wide-area damping controller," in *8th International Conference on Modelling, Identification and Control,* Algiers, 2016.

[67] P. Demetriou, L. Hadjidemetriou, A. Kyriacou, E. Kyriakides, and C. Panayiotou, "Real-time identification of coherent generator groups," in *IEEE PowerTech*, Eindhoven , 2015.

[68] M. Naglic, M. Popov, M. A. M. M. van der Meijden, and V. Terzija, "Synchronized measurement technology supported online generator slow coherency identification and adaptive tracking," *IEEE Trans. Smart Grid (Early Access).*

[69] A. Thakallapelli, S. J. Hossain, and S. Kamalasadan, "Coherency based online wide area control of wind integrated power grid," in *IEEE International Conference on Power Electronics, Drives and Energy Systems,* Trivandrum, 2016.

[70] B. P. Padhy, S. C. Srivastava, and N. K. Verma, "A coherency-based approach for signal selection for wide area stabilizing control in power systems," *IEEE Systems Journal,* vol. 7, no. 4, pp. 807-816, 2013.

[71] J. W. Stahlhut, T. J. Browne, G. T. Heydt, and V. Vittal, "Latency viewed as a stochastic process and its impact on wide area power system control signals," *IEEE Trans. Power Systems,* vol. 23, no. 1, pp. 84-91, 2008.

[72] Y. Wang, C. Lim, and P. Shi, "Adaptively adjusted event-triggering mechanism on fault detection for networked control systems," *IEEE Trans. Cybernetics,* vol. 47, no. 8, pp. 2299-2311, 2017.

[73] Y. Wang, P. Shi, C. Lim, and Y. Liu, "Event-triggered fault detection filter design for a continuous-time networked control system," *IEEE Trans. Cybernetics,* vol. 46, no. 12, pp. 3414-3426, 2016.

[74] W. Yao, L. Jiang, Q. H. Wu, J. Wen, and S. J. Cheng, "Design of wide-area damping controllers based on networked predictive control considering communication delays," in *Proc. IEEE PES General Meeting,* Minneapolis, 2010.

[75] F. Zhang, Y. Sun, L. Cheng, X. Li, J. H. Chow, and W. Zhao, "Measurement and modeling of delays in wide-area closed-loop control system," *IEEE Trans. Power Systems,* vol. 30, no. 5, pp. 2426-2433, 2015.

[76] F. Wilches-Bernal et al., "Time delay definitions and characterization in the pacific DC intertie wide area damping controller," in *Proc. IEEE PES General Meeting*, Chicago, 2017.

[77] M. Long, C. Hwa, and J. Y. Hung, "Denial of service attacks on network-based control systems: impact and mitigation," *IEEE Trans. Industrial Informatics,* vol. 1, no. 2, pp. 85-96, 2005.

[78] N. R. Chaudhury, S. Ray, R. Majumder, and B. Chaudhury, "A new approach to continuous latency compensation with adaptive phasor power oscillation damping controller (POD)," *IEEE Trans. Power Systems,* vol. 25, no. 2, p. 939–946, 2010.

[79] B. P. Padhy, S. C. Srivastava, and N. K. Verma, "A wide-area damping controller considering network input and output delays and packet drop," *IEEE Trans. Power Systems,* vol. 32, no. 1, pp. 166-176, 2017.

[80] M. K. Jena, S. R. Samantaray, and B. K. Panigrahi, "A new wide-area backup protection scheme for series-compensated transmission system," *IEEE Systems Journal,* vol. 11, no. 3, pp. 1877-1887, 2017.

[81] F. Aminifar, M. Shahidehpour, M. Fotuhi-Firuzabad, and S. Kamalinia, "Power system dynamic state estimation with synchronized phasor measurements," *IEEE Trans. Instrumentation and Measurement,* vol. 63, no. 2, pp. 352-363, 2014.

[82] M. Asprou, E. Kyriakides, and M. Albu, "The effect of variable weights in a WLS state estimator considering instrument transformer uncertainties," *IEEE Trans. Instrumentation and Measurement,* vol. 63, no. 6, pp. 1484-1495, 2014.

[83] "IEEE guide for synchronization, calibration, testing, and installation of Phasor Measurement Units (PMUs) for power system protection and control, IEEE Std C37.242™-2013," IEEE Power and Energy Society, NY, USA, 2013.

[84] K. V. Khandeparkar, S. A. Soman, and G. Gajjar, "Detection and correction of systematic errors in instrument transformers along with line parameter estimation using PMU data," *IEEE Trans. Power Systems,* vol. 32, no. 4, pp. 3089-3098, 2017.

[85] A. Pal, P. Chatterjee, J. S. Thorp, and V. A. Centeno, "Online calibration of voltage transformers using synchrophasor measurements," *IEEE Trans. Power Delivery,* vol. 31, no. 1, pp. 370-380, 2016.

[86] R. F. Nuqui, M. Zarghami, and M. Mendik, "The impact of optical current and voltage sensors on phasor measurements and applications," in *Proc. IEEE PES T&D*, New Orleans, 2010.

[87] S. Chakrabarti, E. Kyriakides, and M. Albu, "Uncertainty in power system state variables obtained through synchronized measurements," *IEEE Trans. Instrumentation and Measurement*, vol. 58, no. 8, pp. 2452-2458, 2009.

[88] "IEEE standard for synchrophasor measurements for power systems, IEEE Std C37.118.1™-2011," IEEE Power & Energy Society, NY, USA, 2011.

[89] B.-K. Choi, H.-D. Chiang, Y. Li, Y.-T. Chen, D.-H. Huang, and H. G. Lauby, "Development of composite load models of power systems using on-line measurement data," in *Proc. IEEE PES General Meeting*, Montreal, 2016.

[90] B. Genet and J. Maun, "Dynamic load parameter assessment based on continuous recorder measurements," in *IEEE PowerTech*, Bucharest, 2009.

[91] E. Polykarpou, M. Asprou, E. Kyriakides, C. Hadjilaou, A. Petoussis, and Z. Achillides, "Effect of load composition on the frequency response of the cyprus power system," in *2018 ICSEE International Conference on the Science of Electrical Engineering*, Eilat, 2018 (Accepted).

[92] P. Demetriou, M. Asprou, J. Quiros-Tortos, and E. Kyriakides, "Dynamic IEEE test systems for transient analysis," *IEEE Systems Journal*, vol. 11, no. 4, pp. 2108-2117, 2017.

[93] P. M. Anderson and A. A. Fouad, Power System Control and Stability, 2nd Edition, Wiley-IEEE Press, 2002.

[94] M. Asprou, S. Chakrabarti, and E. Kyriakides, "A two-stage state estimator for dynamic monitoring of power systems," *IEEE Systems Journal*, vol. 11, no. 3, pp. 1767-1776, 2017.

[95] "Instrument transformers-Part 2: Additional requirements for current transformers," IEC 61869-2:2012, 2012.

[96] "Instrument transformers-Part 3: Additional requirements for inductive voltage transformers," IEC 61869-3:2011, 2011.

[97] "Model 1133A Power Sentinel GPS-Synchronized Power Quality/Revenue Standard, Operation Manual," Arbiter Systems Inc., Paso Robles, CA, USA, 2014.

[98] C. Huang, F. Li, T. Ding, Y. Jiang, J. Guo, and Y. Liu, "A bounded model of the communication delay for system integrity protection schemes," *IEEE Trans. Power Delivery,* vol. 31, no. 4, pp. 1921-1933, 2016.

[99] "IEEE standard for synchrophasor data transfer for power systems, IEEE Std C37.118.2™-2011," IEEE Power & Energy Society, NY, USA, 2011.

[100] Y. Wang, M. Haenggi, and Z. Tan, "The meta distribution of the SIR for cellular networks with power control," *IEEE Trans. Communications,* vol. 66, no. 4, pp. 1745-1757, 2018.

[101] G. Huang, D. Akopian, and C. L. P. Chen, "Measurement and characterization of channel delays for broadband power line communications," *IEEE Trans. Instrumentation and Measurement,* vol. 63, no. 11, pp. 2583-2590, 2014.

[102] "IEEE guide for Phasor Data Concentrator requirements for power system protection, control, and monitoring, IEEE Std C37.244™-2013," IEEE Power and Energy Society, NY, USA, 2013.

[103] L. Hadjidemetriou, E. Kyriakides, and F. Blaabjerg, "A robust synchronization to enhance the power quality of renewable energy systems," *IEEE Trans. Industrial Electronics,* vol. 62, no. 8, pp. 4858-4868, 2015.

[104] L. Hadjidemetriou, E. Kyriakides, and F. Blaabjerg, "A grid side converter current controller for accurate current injection under normal and fault ride through operation," *Proc. Industrial Electronics Society, IECON,* pp. 1454-1459, 2013.

[105] L. Hadjidemetriou, E. Kyriakides, and F. Blaabjerg, "An adaptive tuning mechanism for phase-locked loop algorithms for faster time performance of interconnected renewable energy sources," *IEEE Trans. Industry Applications,* vol. 51, no. 2, pp. 1792-1804, 2015.

[106] L. Hadjidemetriou, P. P. Demetriou, and E. Kyriakides, "Investigation of different fault ride through strategies for renewable energy sources," in *Proc. IEEE PES PowerTech*, Eindhoven, 2015.

[107] WG C4.605, "Modelling and Aggregation of Loads in Flexible Power Networks," CIGRE, 2014.

[108] P. E. S. N. Raju, A. Nechifor, M. M. Albu, J. Yu, and V. Terzija, "Development and validation of a new oscillatory component load model for real-time estimation of dynamic load model parameters," *IEEE Trans. Power Delivery (Early Access).*

[109] P. Regulski, D. S. Vilchis-Rodriguez, S. Djurović, and V. Terzija, "Estimation of composite load model parameters using an improved particle swarm optimization method," *IEEE Trans. Power Delivery,* vol. 30, no. 2, pp. 553-560, 2015.

[110] A. P. Tellez, "Modelling aggregate loads in power systems," KTH, Stockholm, 2017.

[111] D. Karissson and D. J. Hill, "Modelling and identification of nonlinear dynamic loads in power systems," *IEEE Trans. Power Systems,* vol. 9, no. 1, pp. 157-166, 1994.

[112] I. R. Navarro, "Dynamic load models for power systems: Estimation of time-varying parameters during normal operation," Lund University, Lund, 2002.

[113] P. W. Sauer and M. A. Pai, Power System Dynamics and Stability, Prentice Hall, 1998.

[114] M. Eremia and M. Shahidehpour, Handbook of Electrical Power System Dynamics, Wiley-IEEE Press, 2013.

[115] V. Terzija, D. Cai and J. Fitch, "Monitoring of inter-area oscillations in power systems with renewable energy resources using Prony method," in *CIRED 2009 - The 20th International Conference and Exhibition on Electricity Distribution - Part 2*, Prague, 2009.

[116] S. Chitturi, S. Chakrabarti, and S. N. Singh, "Comparing performance of Prony analysis and matrix pencil method for monitoring power system oscillations," in *Proc. IEEE Innovative Smart Grid Technologies - Asia (ISGT ASIA),* Kuala Lumpur, 2014.

[117] D. P. Wadduwage, U. D. Annakkage, and K. Narendra, "Identification of dominant low-frequency modes in ring-down oscillations using multiple Prony models," *IET Generation, Transmission & Distribution.,* vol. 15, no. 9, pp. 2206-2214, 2015.

[118] V. S. Patel, F. S. Bhil, F. S. Kazi, and S. R. Wagh, "Energy-sorted Prony analysis for identification of dominant low frequency oscillations," in *Proc. Australian Control Conference*, Fremantle, 2013.

[119] D. Cai, P. Regulski, M. Osborne, and V. Terzija, "Wide area inter-area oscillation monitoring using fast nonlinear estimation algorithm," *IEEE Trans. Smart Grid*, vol. 4, no. 3, pp. 1721-1731, 2013.

[120] S. Nabavi, J. Zhang, and A. Chakrabortty, "Distributed optimization algorithms for wide-area oscillation monitoring in power systems using interregional PMU-PDC architectures," *IEEE Trans. Smart Grid*, vol. 6, no. 5, pp. 2529-2538, 2015.

[121] "IEEE standard for synchrophasor measurements for power systems, Amendment 1: Modification of selected performance requirements, IEEE Std C37.118.1a™-2014," IEEE Power and Energy Society, NY, USA, 2014.

[122] M. Asprou and E. Kyriakides, "Estimation of line parameters using the hybrid state estimator," in *Proc. IEEE PES PowerTech*, Grenoble, 2013.

[123] M. Bockarjova and G. Andersson, "Transmission line conductor temperature impact on state estimation accuracy," in *Proc. IEEE PES PowerTech*, Lausanne, 2007.

[124] V. Milojević, S. Čalija, G. Rietveld, M. V. Ačanski, and D. Colangelo, "Utilization of PMU measurements for three-phase line parameter estimation in power systems," *IEEE Trans. Instrumentation and Measurement*, vol. 67, no. 10, pp. 2453-2462, 2018.

[125] S. S. Mousavi-Seyedi, F. Aminifar, and S. Afsharnia, "Parameter estimation of multiterminal transmission lines using joint PMU and SCADA data," *IEEE Trans. Power Delivery*, vol. 30, no. 3, pp. 1077-1085, 2015.

[126] M. Asprou, E. Kyriakides, and M. M. Albu, "Uncertainty bounds of transmission line parameters estimated from synchronized measurements," *IEEE Trans. Instrumentation and Measurement*, vol. 68, no. 8, pp. 2808-2818, 2019.

[127] A. Abur and A. G. Exposito, Power System State Estimation: Theory and Implementation, Basel: Marcel Dekker, 2004.

[128] E. Kyriakides, Innovative Concepts for On-line Synchronous Generator Parameter Estimation, Arizona: Arizona State University, 2003.

[129] P. Agnihotri, A. M. Kulkarni, A. M. Gole, B. A. Archer, and T. Weekes, "A robust wide-area measurement-based damping controller for networks with embedded multiterminal and multiinfeed HVDC links," *IEEE Trans. Power Systems*, vol. 32, no. 5, pp. 3884-3892, 2017.

[130] P. Ju, E. Handschin and D. Karlsson, "Nonlinear dynamic load modelling: model and parameter estimation," *IEEE Trans. Power Systems*, vol. 11, no. 4, pp. 1689-1697, 1996.

[131] L. Cheng, G. Chen, W. Gao, F. Zhang, and G. Li, "Adaptive time delay compensator (ATDC) design for wide-area power system stabilizer," *IEEE Trans. Smart Grid*, vol. 5, no. 6, pp. 2957-2966, 2014.

[132] F. Zhang, L. Cheng, and W. Gao, "Prediction based hierarchical compensation for delays in wide-area control systems," *IEEE Trans. Smart Grid,* vol. 9, no. 4, pp. 3897-3899, 2018.

[133] R. Liu, M. Mohanpurkar, M. Panwar, R. Hovsapian, A. Srivastava, and S. Suryanarayanan, "Geographically distributed real-time digital simulations using linear prediction," *International Journal of Electrical Power & Energy Systems,* vol. 84, pp. 308-317, 2017.

[134] C. Dufour and J. Bélanger, "On the use of real-time simulation technology in smart grid research and development," *IEEE Trans. Industry Applications,* vol. 50, no. 6, pp. 3963-3970, 2014.

[135] M. S. Almas and L. Vanfretti, "RT-HIL implementation of the hybrid synchrophasor and GOOSE-based passive islanding schemes," *IEEE Trans. Power Delivery,* vol. 31, no. 3, pp. 1299-1309, 2016.

[136] L. Bottaccioli et al., "A flexible distributed infrastructure for real-time cosimulations in smart grids," *IEEE Trans. Industrial Informatics,* vol. 13, no. 6, pp. 3265-3274, 2017.

[137] OPAL RT Technologies, "Hardware-In-the-Loop," OPAL-RT Technologies, 2019. [Online]. Available: https://www.opal-rt.com/hardware-in-the-loop/. [Accessed 23 10 23].

[138] OPAL RT Technologies, "Power Hardware-In-the-Loop," OPAL-RT Technologies, 2019. [Online]. Available: https://www.opal-rt.com/power-hardware-in-the-loop/. [Accessed 23 10 2019].

[139] M. Naglic, M. Popov, M. A. M. M. van der Meijden, and V. Terzija, "Synchro-measurement application development framework: An IEEE Standard C37.118.2-2011 supported MATLAB library," *IEEE Trans. Instrumentation and Measurement,* vol. 67, no. 8, pp. 1804-1814, 2018.

[140] I. Tyuryukanov, M. Popov, M. A. M. M. van der Meijden, and V. Terzija, "Discovering clusters in power networks from orthogonal structure of spectral embedding," *IEEE Trans. Power Systems*, vol. 33, no. 6, pp. 6441-6451, 2018.

[141] M. Asprou, E. Kyriakides, and S. Chakrabarti, "The use of a PMU-based state estimator for tracking power system dynamics," in *IEEE PES General Meeting*, National Harbor, 2014.

[142] Siemens, "Selection of PMU functionality," Siemens AG, Nuremberg, 2016.

LIST OF PUBLICATIONS

Refereed Archival Journal Publications

1. **L. Zacharia**, M. Asprou, and E. Kyriakides, "Wide area control of gevernors and power system stabilizers with an adaptive tuning of coordination signals," *IEEE Open Access of Power and Energy (Early Access).*
2. **L. Zacharia**, M. Asprou, and E. Kyriakides, "Measurement errors and delays on wide-area control based on IEEE std C37.118.1-2011: impact and compensation," *IEEE Systems Journal (Early Access).*
3. **L. Zacharia**, L. Hadjidemetriou, and E. Kyriakides, "Integration of renewables into the wide area control scheme for damping power oscillations," *IEEE Trans. Power Systems*, vol. 33, no. 5, pp. 5778-5786, 2018.
4. A. Charalambous, L. Hadjidemetriou, **L. Zacharia**, A. D. Bintoudi, A. C. Tsolakis, D. Tzovaras, and E. Kyriakides, “Phase Balancing and Reactive Power Support Services for Microgrids”, Applied Sciences, vol. 9, no. 23, pp. 5067.
5. A. D. Bintoudi, L. Zyglakis, A. C. Tsolakis, D. Ioannidis, L. Hadjidemetriou, **L. Zacharia**, N. Al-Mutlaq, M. Al-Hashem, S. Al-Agtash, E. Kyriakides, C. Demoulias, and D. Tzovaras, "Hybrid multi-agent-based adaptive control scheme for AC microgrids with increased fault-tolerance needs," *IET Renewable Power Generation*, vol. 14, no. 1, pp. 13-26, 2020.

Refereed Archival Conference Proceedings

1. **L. Zacharia**, M. Asprou, and E. Kyriakides, "Investigation of the factors influencing wide area control," in *Proc. IEEE PES General Meeting*, Chicago, 2017.
2. **L. Zacharia**, L. Hadjidemetriou, and E. Kyriakides, "Cooperation of wide area control with renewable energy sources for robust power oscillation damping," in *Proc. IEEE PowerTech*, Manchester, 2017.
3. **L. Zacharia**, M. Asprou, and E. Kyriakides, "Design of a data delay compensation technique based on a linear predictor for wide-area measurements," in *Proc. IEEE PES General Meeting*, Boston, 2016.

4. **L. Zacharia** *et al*., "Optimal Energy Management and Scheduling of a Microgrid in Grid-Connected and Islanded Modes," *2019 International Conference on Smart Energy Systems and Technologies (SEST)*, Porto, Portugal, 2019, pp. 1-6.

5. **L. Zacharia** *et al*., "Islanding and Resynchronization Procedure of a University Campus Microgrid," *2018 International Conference on Smart Energy Systems and Technologies (SEST)*, Sevilla, 2018, pp. 1-6.

6. L. Hadjidemetriou, **L. Zacharia,** and E. Kyriakides, "Flexible power control scheme for interconnected photovoltaics to benefit the power quality and the network losses of the distribution grid," 2017 IEEE 3rd International Future Energy Electronics Conference and ECCE Asia (IFEEC 2017 - ECCE Asia), Kaohsiung, 2017, pp. 93-98.

7. L. Hadjidemetriou, **L. Zacharia**, E. Kyriakides, B. Azzopardi, S. Azzopardi, R. Mikalauskiene, S. Al-Agtash, M. Al-hashem, A. Tsolakis, D. Ioannidis, and D. Tzovaras, "Design factors for developing a university campus microgrid," in Proc. IEEE ENERGYCON2018, Limassol, Cyprus, Jun. 2018, pp. 1-6.

8. L. Hadjidemetriou, A. Charalambous, **L. Zacharia,** and E. Kyriakides, "A Sensor-less Control Scheme for Grid Tied Inverters to Provide Phase Balancing Services to the Distribution Grid," *2019 21st European Conference on Power Electronics and Applications (EPE '19 ECCE Europe)*, Genova, Italy, 2019, pp. P.1-P.10.

9. D. Monoyios, L. Hadjidemetriou, **L. Zacharia**, E. Kyriakides, "Cost-Effective Optimization for an Energy Efficient Design of the Electrical Installation of Buildings," in Proc. IEEE ENERGYCON2018, Limassol, Cyprus, Jun. 2018, pp. 1-6.

10. D. Bintoudi, L. Zyglakis, A. C. Tsolakis, D. Ioannidis, M. Al-Hashem, S. Al-Agtash, L. Hadjidemetriou, **L. Zacharia**, E. Kyriakides, C. Demoulias, and D. Tzovaras , "An improved decentralised coordinated control scheme for microgrids with AC-coupled units," 2018 International Conference on Smart Energy Systems and Technologies (SEST), Sevilla, 2018, pp. 1-6.